HYPERGLYCAEMIA AND ITS IMPLICATION ON THE PANCREATIC ISLET MICROVASCULATURE IN DIABETIC RAT MODELS

By

Eleonore Ngounou

BMedScHon (Human Anatomy); MSc (Anatomy)

Dissertation presented in fulfilment of the requirements for the degree of Doctor of Philosophy in Morphological Sciences in the Faculty of Medicine and Health Sciences at Stellenbosch University

December 2020

Supervisor: Dr A Alblas
Co-supervisors: Ms ML Greyling
Prof KJ Baatjes
Prof BJ Page

DECLARATION

By submitting this thesis electronically, I declare that the entirety of the work contained therein is my own, original work, that I am the sole author thereof (save to the extent explicitly otherwise stated), that reproduction and publication thereof by Stellenbosch University will not infringe any third party rights and that I have not previously in its entirety or part submitted it for any qualification.

Signed:

Date: 30-07-2020

SUMMARY

BACKGROUND: Despite the considerable progress made in the treatment of diabetes mellitus, vascular damage remains the leading cause of patient death. The mechanisms underlying vascular abnormalities in obesity and diabetes mellitus remain to be elucidated and may be the main cause of β-cell death. In addition, the detailed description of islet microvasculature in the pancreas is lacking in the literature; therefore, a better understanding of the characteristics of the blood vessel and the factors that maintain β-cell function is needed in clinical practice.

OBJECTIVE: To describe the spatial distribution and histomorphology of islet microvasculature under the effect of hyperglycaemia in two experimental diabetic models.

METHODS: Eight week old male Wistar rats (n=50) were divided into two groups that received either a standard diet (RAC) (n=20) or a high-fat diet (HFD) (n=30) for two weeks. By the end of the two weeks, altered glucose uptake was confirmed in the HFD group by an oral glucose tolerance test (OGTT). A subgroup (RAC / STZ) of the RAC group (n=10) and another (HFD / STZ) of the HFD group (n=10) then received 50 and 35mg/kg of body weight (BW) of streptozotocin (STZ) to induce type I diabetes mellitus and type II diabetes mellitus, respectively. They were kept diabetic for an additional eight weeks. The body weight and blood glucose (BGL) of the animals were recorded throughout the experimental period (88 days).

Blood was collected for flow cytometry and Luminex assay before half the number of animals were sacrificed for pancreatic tissue collection for histological procedure. The remaining half was used to replicate (cast) the pancreatic vasculature by perfusion with polyurethane-based casting resin (PU4ii). Haematoxylin and Eosin (H&E) stained sections were used to assess the general morphology of pancreatic tissue. Methenamine silver and immunostaining using CD34 antibody, delineated the basement membrane and endothelial cells, respectively, of islet microvasculature. A digital camera and a nano-computed tomography (nano-CT) scanner made it possible to generate digital and 3D images. Quantitative evaluation of topographic morphometric parameters of the pancreatic vascular network in the duodenal and splenic regions of the pancreas in each experimental condition was performed using the imageJ and Volume Graphics VGStudioMax 3.0®. Reconstruction of the pancreatic vascular network was attempted using the vascular tree scale laws.

RESULTS: A significant increase in the mean body weight was accompanied by a slight increase in mean BGL within 2 weeks in HFD. Streptozotocin caused the development of two diabetic models with all clinical symptoms (polyuria, polyphagia, high BGL (> 28mmol/L) and a significant decrease in body mass in both diabetic groups (26.68% and 15.54% in RAC / STZ and HFD /

STZ respectively). The results of the flow cytometry and the Luminex assay validated the presence of islet vascular lesions in animals, which also justified the significant necrosis of endothelial cells, a decrease ($p<0.05$) in the mean percentage of the stained area of CD34 pixels in islets, and thickening of the basement membrane. The scaling law was used to obtain the relationships between 1) the length and volume of the pancreatic vascular tree up to capillary level ($R2=0.693\pm0.053$), 2) the diameter of the lumen and the blood flow in each pancreatic vascular branch ($R2=0.988\pm0.055$), and 3) the diameter and length of the branches of the vessels ($R2=0.838\pm0.0123$).

CONCLUSION: This investigation has established detailed morphological features of the vasculature of the pancreas in the duodenal and splenic regions in normal and diabetic rat models. There were large differences in the structure of the pancreatic vasculature between the two regions appearing to be dictated by metabolic demand. However, there are still challenges in 3D visualisation of the capillary networks of the pancreatic vascular tree, which was the main limitation of this study.

OPSOMMING

AGTERGROND: Ten spyte van aansienlike vooruitgang in behandeling van diabetes mellitus, bly vaskulêre skade die hoof oorsaak van pasiënt sterftes. Die meganismes onderliggend aan vaskulêre abnormaliteite in vetsugtigheid en diabetes mellitus moet uitgelig word, want dit mag die hoof oorsaak van afsterwing van β-selle wees. Tesame hiermee, is daar ook ‘n gebrek aan ‘n breedvoerige beskrywing wat handel oor die mikrovaskulatuur in die pankreas in die literatuur; met ander woorde, verbetering in kennis van die eienskappe van die bloedvate en die faktore wat β-sel funksie handhaaf, word in die kliniese praktyk benodig.

DOELWIT: Om die effek van hiperglisemie op die ruimtelike verspreiding en histomorfologie van eiland mikrovaskulatuur in twee eksperimentele diabetiese modelle te beskryf.

METODES: Agt weke oue manlike Wistar rotte (n=50) is vir twee weke volgens die rotte se diëte, onderskeidelik ‘n standaard (RAC) dieët (n=20), en ‘n hoë vet (HFD) dieët (n=30). ‘n Verminderde glukose opname is na twee weke in die HFD groep bevestig deur gebruik te maak van ‘n orale glukose toleransie toets (OGTT). ‘n Subgroep van die standaard dieët (RAC/STZ) (n =10) en die hoë vet dieët (HFD/STZ) (n=10), het daarna 50 en 35mg/kg liggaamsgewig (BW) Streptozotocin (STZ) ontvang om tipe I diabetes mellitus en tipe II diabetes mellitus, onderskeidelik, te induseer. Die rotte is vir ‘n verdere agt weke in ‘n diabetiese toestand gehou. Daar is deur die eksperimentele periode (88 dae), rekord gehou van die liggaamsmassa en bloedglukosevlakke (BGL) van die diere.

Bloed is vir sitometrie en Luminex bepaling getrek voor die helfte van die aantal diere geoffer is vir verkryging van pankreasweefsel vir histologiese prosedures. Deur gebruik van perfusie met ‘n poliuretraan gebaseerde giet hars (PU4ii) is weefselafgietsels van die bloedvate van die pankreas in die oorblywende helfte gemaak. Hematoksillien en Eosien (H&E) kleuring is gebruik om die algemene morfologie van die pankreasweefsel te bepaal. Met behulp van Methenamine silver, en immunositochemiese kleuring met behulp van CD34 teenliggame, is die basaalmembraan en endoteelselle van die eiland mikrovaskulatuur, onderskeidelik, geïllustreer.

‘n Digitale kamera en nano-CT skandeerder het dit moontlik gemaak om digitale en 3D beelde te skep. Met behulp van ImageJ en Volume Graphics VGStudioMax 3.0® is kwantitatiewe evaluering van topografiese morfometriese kenmerke van die vaskulêre netwerk in die duodenale - en spleniese areas van die pankreas in elke eksperimentele toestand gedoen. Vaskulêre boom skaaltoepassings is gebruik vir rekonstruksie van die vaskulêre netwerk van die pankreas.

RESULTATE: In diere met ‘n hoë vet dieët (HFD) is binne 2 weke ‘n betekenisvolle toename in gemiddelde liggaamsmassa, asook ‘n geringe toename in gemiddelde bloedglukosevlakke

(BGL), waargeneem. Na toediening van Streptozotocin is twee diabetiese modelle wat alle kliniese simptome insluit (poliurie, polifagie, hoë bloedglukosevlakke (>28mmol/L) ontwikkel, asook ‘n betekenisvolle afname in liggaamsmassa in beide diabetiese groepe (26.68% en 15.54% in RAC / STZ en HFD / STZ, onderskeidelik). Resultate na vloeisitometrie en Luminex bepaling het die teenwoordigheid van vaskulêre letsels in die eilande van die diere, asook betekenisvolle nekrose in endoteelselle, ‘n afname ($p<0.05$) in die gemiddelde persentasie in die area met CD34 kleuring in die eiland, en verdikking van die basaalmembraan, bevestig. Skaaltoepassings het die verhouding tussen 1) die lengte en vaskulêre volume van die vaskulêre boom van die pankreas tot op kapillêre vlak ($R2=0.693\pm0.053$), 2) die deursnit van die lumen en bloedvloei in elke vaskulêre tak in die pankreas ($R2=0.988\pm0.055$), en 3) die deursnit en lengte van die takke van die bloedvate ($R2=0.838\pm0.0123$), bevestig.

KONKLUSIE: Hierdie navorsing het gedetailleerde morfologiese eienskappe van die vaskulatuur van die pankreas in beide die duodenale en spleniese gedeeltes in normale en diabetiese rotmodelle bevestig. Daar bestaan groot verskille in die struktuur van die bloedvate tussen die twee gebiede in die pankreas, wat klaarblyklik metaboliese aanvraag weerspieël. Daar is egter nog uitdagings in 3D beelding van die kapillêre netwerke in die vaskulêre boom van die pankreas. Laasgenoemde was dan ook die grootste beperking van die studie.

ACKNOWLEDGEMENT

I would like to express my deep gratitude to the following people:

To my supervisors Dr A Alblas, Ms ML Greyling, Prof KJ Baatjes and Prof BJ Page, all academic staff in the Division of Clinical Anatomy for their consistent support, patience and guidance needed to make this research work a success.

To Dr R van Wijk, my PhD research colleague of the Division of Clinical Anatomy for all her constructive advice and editing work. Thank you, dear Rochelle.

To all the staff of CT Facility Unit, Mrs T.Reid of the flow cytometry unit, Dr C Manirafasha, PhD student in the division of Physiology, Stellenbosch University who contributed enormously during the data collection.

To the authorities of the University of Buea for facilitating my enrollment in this program

To Prof G. Enow Orock, pathologist and Head of Department of Biomedical Sciences, the University of Buea for his continuous support and his assistance in reading histological slides.

To Mr N Markgraaff and all the staff of the Animal Unit of the Faculty of Health Sciences for their assistance in handling animals during data collection.

To Mr R Williams for his technical and moral support in all stages of this project. Thank you, Reggie!

To the Schlumberger Foundation *(Faculty of the Future)* for the financial assistance that made this project feasible.

To my late parents, papa and mama Djossi, my brothers and sisters for their moral and financial support.

To my ex-husband RM Tcheptang Noucha, for the care he lavished on our children during my absence for research work.

Above all to Almighty God who continuously protected and guided me throughout this work.

.

TABLE OF CONTENTS

ABBREVIATIONS

%	Percent
γ	Empirical exponent
µm	Micrometre
µL	Microliters
2D	Two dimensional
3D	Three dimensional
ACCU-CHEK	A proprietary blood glucose measuring system
ACs	Acinar cells
ACS	Activated cells
AF700	Alexa Fluor
AFr	Area fraction
AGE	Advanced glycation end-product
Akt	Serine/threonine protein kinase
AMP	5'Adenosine monophosphate-activated protein
APC	Allophycocyanin
au	Arbitrary Units
ATP	Adenosine triphosphate
BM	Basement membrane
BMI	Body mass index
BW	Bodyweight
C	Crown
CD	Cluster of differentiation
CD133	Cluster of differentiation 133
CD31	Cluster of differentiation 31
CD34	Cluster of differentiation 34
CD45	Cluster of differentiation 45
CEC	Circulating endothelial cell
CEPC	Circulating endothelial progenitor cells
C-KIT	Tyrosine-protein kinase kit
Cp	Capillary
CT	Computer tomography
CTGF	Connective tissue growth factor

Cx	Connexion
CXC	Chemoreceptor
CXCR4	Chemoreceptor type 4
DAB	3,3′-Diaminobenzidine
DM	Diabetes mellitus
DME	Diabetes macular edema
DMEM	Dulbecco's modified eagle medium
DMSO	Dimethyl sulfoxide
DNA	Deoxyribonucleic acid
DR	Diabetes retinopathy
EC	Endothelial cell
ECD	Endothelial cell density
ECM	Extracellular matrix
EDHF	Endothelium-derived hyperpolarising factor
eNOs	Endothelial nitric oxide synthase
EPC	Endothelial progenitor cell
ES	Electronic system
ET	Endothelin
EV	Extracellular vesicles
FAK	Factor adhesion kinase
FF	Flow fraction
FI	Fatty infiltration
FBS	Fetal bovine serum
FITC	Fluorescein isothiocyanate
FTS	Fluid transportation system
g	Gram
G	Gravity
GE	General electric
GK	Goto-Kakizaki
H&E	Haematoxylin and eosin
HFD	High fat diet
HFD-SSC	High fat diet and sodium citrate buffer
HFD-STZ	high fat diet and Streptozotocin
HG	High glucose

HGF	Hepatic grow factor
i	Branching level
ID	Inner diameter
IDF	International diabetes federation
IL-6	Interleukin 6
IPDA	Inferior pancreaticoduodenal artery
IRMA	Intraretinal microvascular abnormalities
IRS	Insulin receptor substrate
ISF	Interstitial fluid
ITSA	Islet total surface area
K	Average capillary flow
KDR	Kinase insert domain receptor
KG	Kilogram
KOH	Potassium hydroxide
KTL	Proportionality constant in unit of time/area
L	Length
Lc	Length of capillary
LCs	Lymphocytes
Mag	Magnification
MAPC	Mesenchymal stem cell
min	Minute
mL	Milliliter
mm^2	Millimeter square
mMol/L	Millimole per liter
MNC	Mononuclear cells
MSA	Methanemine stained surface area
ms	Milliseconds
MVD	Microvascular density
n	Number of vessels
N	Number of capillary
Nc,max	Number of capillaries in a vascular system
NADPH	Nicotinamide adenine dinucleotide phosphate
ND	Numerical density
NFkβ	Nuclear factor kappa β

NO	Nitric oxide
NPDR	Non-proliferative diabetes retinopathy
OD	Outer diameter
OGTT	Oral glucose tolerance test
OS	Optical system
PAS	Periodic acid Schiff
PBMC	Peripheral blood mononuclear cells
PBS	Phosphate buffered saline
PDGF	Platelet-derived growth factors
PDR	Proliferative diabetes retinopathy
PE	Phycoerythrin
pg/mL	Pictograms per milliliter
PI3k / Akt	Phosphatidic inositol 3 kinase/ protein kinase B
PI3K	Phosphoinositide - 3 kinase
PKC	Protein kinase C
PP	pancreatic polypeptide
PTF1	Pancreas specific transcription factor
PU4ii-	Polyurethane resin
Pdx1	Homeodomain transcription factor pancreas duodenal homeobox 1 or insulin promoter factor 1
Q	Blow flow
RAC	Standard rat chow
RAC-SSC	Standard rat chow and sodium citrate buffer solution
RAC-STZ	Standard rat chow-Streptozotocin
RAGE	Receptor for advanced glycation end products
RNA	Ribonucleic acid
rpm	Revolution per minute
ROI	Region of interest
ROS	Reactive oxygen species
s	Second
SCID	Severe combined immune deficiency
SPCA	Society for the Prevention of Cruelty to Animals
SPDA	Superior pancreaticoduodenal artery
SPA	Splenic artery

SSC	Sodium citrate
SST	Serum separator tubes
St	Stem
STZ	Streptozotocin
SU	Stellenbosch University
T1DM	Type 1 diabetes mellitus
T2DM	Type 2 diabetes mellitus
TGF	Transforming growth factor
THBS	Thrombospondin
THBS1	Thrombospondin 1
TIFF	Tagged image format file
TIMP-1	Tissue inhibitor of metalloproteinase 1
TNFα	Tumor necrosis factor-alpha
Tsg	Mean transit time to a specific segment
V	Volume
Vc	Volume of the crown
Vcap	Volume of the capillary
VEGF	Vascular endothelial growth factor
VEGF-A	Vascular endothelial grow factor-A
VPF	Vascular permeability factor
VSM	Vascular smooth muscle
vWF	von Willebrand factor
WT	Wall thickness
α	Alpha
β	Beta
δ	Delta
ε	Epsilon

LIST OF FIGURES

LIST OF TABLES

CHAPTER 1: INTRODUCTION

1.1 BACKGROUND

Diabetes mellitus (DM) is a metabolic disease that affects millions of people around the world, regardless of age, gender, and social background (Mbanya et al., 2010). A recent report by the International Diabetes Federation (IDF) postulated that Africa would experience the largest increase in the prevalence of diabetes over the next 20 years (Peer et al., 2014). It is calculated that up to 69.2% of diabetes cases in Africa remains undiagnosed in 2015 alone (Pheiffer et al., 2018). In 2009, more than two million South Africans were diagnosed with diabetes, representing one of the highest incidences in the sub-Saharan region (Pheiffer et al., 2018).

Governments have developed several strategies to alleviate this burden. These range from preventive methods (Manyema et al., 2015), early diagnostic techniques (McLennan, 1998) to therapeutic and basic care systems for patients (McDuffie et al., 2001). Despite remarkable progress in the treatment of DM, vascular complications such as vascular neuropathies (Sowers, Epstein & Frohlich, 2001; Nathan et al., 2005) have been associated with long-term diabetic conditions (Sowers et al., 2001; Nathan et al., 2005). The high mortality rate associated with cardiovascular complications accompanying diabetes underscores the need to strengthen understanding of the main causes and progression of the disease (Bhupathiraju & Hu, 2016).

Type 1 (T1DM) and Type 2 (T2DM) DM are the two most common types of DM in Africa (Mbanya et al., 2010). In T1DM, the lack of insulin production is due to the autoimmune destruction of beta cells (β-cells) (Cao & Wang, 2014), whereas, in T2DM, the non-responsiveness of body tissues to insulin action leads to high blood glucose levels. Both diabetes types are characterised by a high fasting blood glucose level (hyperglycaemia) (Van Belle et al., 2011) which is thought to be deleterious to the endothelial capillaries within the islets of Langerhans (Li et al., 2006; Tal, 2009). The intra-islet capillaries, which are the interface between blood and the islet cells, play an important role in the physiology and pathology of the endocrine pancreas (Favaro et al., 2005). Beta cells are important cellular components of the endocrine pancreas and its functions are highly dependent on blood perfusion through its microvasculature (Nyman et al., 2010), governed by the vascular networking, structure and haemodynamic forces within the micro-organ.

Despite the link between cardiovascular diseases and DM, studies aiming at improving outcomes of diabetic patients have devoted most effort to effective insulin production and sensitivity (Herold et al., 2009; Kars et al., 2010; Keenan et al., 2010), and β-cell replacement therapy (Johnson, 2016; Wallner et al., 2018). The studies of parameters that maintain the integrity of the islet

microvascular system under normal and pathological conditions have been neglected. The prompt availability of insulin in the blood, when secreted by pancreatic β-cells and its action on the peripheral tissues, is notable in the physiological state compared to slower exogenous insulin injected subcutaneously (Sanlioglu et al., 2013). Questions about the pattern and physico-mechanical properties of islet blood flow under diabetic conditions remain unanswered.

1.2 ROLE OF ISLET STRUCTURE AND CELLULAR INTERACTIONS

Glucose is one of the metabolites that accumulate rapidly in the blood after digestion and its levels must be regulated. Immediately after a meal, the level of digested food end-products such as monosaccharides, short peptides, amino acids and triacylglycerols begin to increase in the blood. This activates β-cells to secrete insulin that acts on other organs to absorb these metabolites from the bloodstream (Suckale & Solimena, 2008). At the same time, the increased level of insulin in the blood rapidly reduces the release of these metabolites from storage organs such as the liver and adipose tissues. In humans, the level of glucose in the blood must be maintained between 3.5 and 7 mmol/L and each time this concentration is radically altered, several cell types, especially the endothelial cells (ECs) are destroyed (Brownlee, 2005). However, to maintain the regulation of these metabolic processes and manage the environmental changes appropriately, islet cells must communicate with each other and with other cells.

In addition to β-cells, the islet is composed of several other cell types and their distribution varies within regions of the pancreas (Mattsson, 2004; Longnecker, 2014). Most metabolic processes in the body require good intercellular communication and the endocrine pancreas is one of the best examples of tissue whose function depends entirely on the type of intercellular communication that occurs (Samols & Stagner, 1990).

The inter-islet cells communication and the communication between islet cell and other distant cells are made via the microvasculature of the islet of Langerhans (Samols & Stagner, 1990; Brunicardi et al., 1996). These communications have a direct impact on the function and regulation of endocrine hormones (Stagner & Samols, 1986). The type, volume and direction of blood perfusion within the islet themselves are key factors in determining the individual islet cell function (Kawamori et al., 2009).

In tissues of vertebrates, cells are located from one another within a radius of 50–100 micrometres (μm) of a capillary. The mechanism that ensures that the system of blood vessels ramifies to maintain this principle is not well understood (Alberts et al., 2007). Under certain physiological and pathological conditions such as in obesity and DM, tissue components are altered, resulting in tissue hypertrophy (Venkatesan et al., 2013) or hyperplasia (Linnemann et al., 2014). Blood

vessel networking and structure adjust to cater for the new physico-spatial environment. Factors determining the flux of blood to the tissue must therefore be looked at, to evaluate how the body system adjusts when facing these physiological shifts (Dai et al., 2013).

It is worth noting that vascular function such as tissue perfusion and peripheral resistance reflect continuous structural remodelling of blood vessels in response to several stimuli in an attempt to replenish oxygen and nutrient supply under diabetic and obese conditions. For example, an increase in vessel diameter with increased wall shear stress and an increase in wall mass with increased circumferential stress is required to ensure stable vascular adaptation. Several studies have been conducted to validate these changes in other tissue vascular networks under different physiological and pathological conditions (Aiello & Wong, 2000; Folkman, 2002; Alberts et al., 2007; Duh et al., 2017). However, little work has been done on the pancreas (Dai et al., 2013), one of the body's most important organs for its role in glucose metabolism and its implication in the development of DM.

1.3 STRUCTURAL AND PANCREATIC REGIONAL DIFFERENCES ASSOCIATED WITH BLOOD SUPPLY

Macroscopically, the pancreas is divided into three main regions, the head, the body and the tail. The islet distribution and size differs in each region of the pancreas (Gray, 1989). The duodenal part of the pancreas (head) is more vulnerable to pancreatic diseases such as DM (Wang, et al., 2013) and cancer (Daniel et al., 2010). A recent study identified two types of islets within the pancreatic tissue: islets that are more vascularised and vulnerable to β-cell death induced by the inflammatory cytokines or hypoxia *in vitro*, and those with less proliferative β-cells (Olsson & Carlsson, 2011). These findings reveal for the first time, the other side of the vascularisation coin (In't Veld & Lammert, 2015). However, whether this islet vascularisation difference is associated with regions of the pancreas is yet to be clarified. In addition, the origin and source of blood supply of the pancreas differ embryologically from one region to the other (Gray et al., 1989). Also, there is a direct correlation between vascular density and islet function that can be explained by the fact that the metabolism of glucose by β-cells is exclusively aerobic and depends on the continuous supply of oxygen (In't Veld & Lammert, 2015).

1.4 THE INTEGRITY OF THE ENDOTHELIAL CELLS

Diabetes and obesity cause serious structural changes to islets in particular, and in the pancreatic tissue in general (Canzano et al., 2019, Dai et al., 2013, Favero et al., 2014). Studies on changes in islet cytoarchitecture under these conditions are well documented (Tal 2009, Folli et al., 2018).

However, vascular morphological adjustments associated with these transformations have not yet been clarified.

The vascular endothelium remains the only structure in direct contact with blood. This endothelium is highly specialised and well equipped for the strategic role played between blood and tissue. Recent studies have shown a direct relationship between the endothelial cells (EC) dysfunction and angiogenesis in organs such as the eyes (Duh & Aiello, 1999; Aiello & Wong, 2000), and the kidneys (Duh & Aiello, 1999). Similar studies on the pancreas tried to replicate that relationship (Li et al., 2006; Dai et al., 2013): these studies reported less description on the overall changes in the structure and features of the islet microvasculature.

The important role of the vascular endothelium in cardiovascular biology is increasingly appreciated (Drexler & Hornig, 1999). Mature ECs have limited regenerative capacity (Shantsila et al., 2007). The scientific community is therefore interested in circulating endothelial progenitor cells (CEPCs), and in particular, their presumed role in maintaining endothelial integrity and function, as well as in postnatal neovascularization (Rafii & Lyden, 2003). It has been suggested that these cells could not only be responsible for the continuous recovery of the endothelium after injury or damage but could also participate in angiogenesis, giving impetus for new vascular damage treatment possibilities (Rafii & Lyden, 2003). Indeed, there is increasing evidence of reduced availability and impaired endothelial progenitor cells (EPCs) function in the presence of cardiovascular disease and associated co-morbidity risk factors (Rafii & Lyden, 2003). Thus, many studies on the potential for the use of EPCs in a clinical setting are in progress (Wang et al., 2013; Keighron et al., 2018).

In conclusion, it remains unclear why endocrine cells exist in the exocrine parenchyma of the pancreas in all species and why these cells coexist in small micro-organs (Gustafsson & Islam, 2007). However, it is believed that this arrangement has profound effects on the intercommunication between the islet cells and the islet microvasculature to ensure precision secretion of the islet hormones.

A clear description of the distribution and morphology of blood vessels in the islet of Langerhans may inform an avenue to management and treatment of DM.

1.5 RESEARCH QUESTION

The structural and functional integrity of the capillary is a key factor in maintaining the health of a body system; a condition such as hyperglycaemia affects the integrity of ECs within the capillaries and has shown to be the main cause of mortality and morbidity in diabetic patients (Giugliano et al., 1996).

During the last decade, several studies aimed to improve the health of diabetic patients (García-Pérez et al., 2013; Vissarion et al., 2014; Shah & Garg, 2015). However, despite the improvement in drug delivery technology, cardiovascular complications remain the main cause of mortality in diabetic patients (Einarson et al., 2018) with the alteration of vascular EC function and the disruption of the histomorphology of the basement membrane (BM) (Skeie et al., 2018). Cardiovascular complications that accompany diabetes have been widely studied in the eye; particularly in the retina (Aiello & Wong, 2000), nervous system (Mooradian, 1988) and kidneys (Duh & Aiello, 1999) with few studies performed on the pancreas, particularly in islets of Langerhans. Drug and β-cell replacement therapy, which aims to maintain normoglycaemia, has been widely investigated (Kulkarni et al., 1999; Ryan et al., 2001; Tuttle et al., 2001; Xu et al. 2008) in diabetic patients and experimental animals; but the description of the structural and the architectural pattern of blood capillaries within the endocrine pancreas in normal and diabetic conditions warrants further investigation.

The incidence of DM may be a consequence of certain structural changes in the pancreatic vessels, atherosclerotic lesions, and disturbances of the haemodynamic response during the patient's life. For example, reduced blood flow has been identified as one of the most persistent physiological deficits of Alzheimer Disease (De la Torre & Mussivand, 1993; Bateman et al., 2006). In this dementia, it is unclear whether the reduced nervous tissues blood flow is a response to neuronal damage or a factor initiating the characteristic neuropathology (De la Torre 2002). Similarly, it can be hypothesised that even before the body enters a prediabetic state, the pancreatic blood vessel structure and distribution are initially made to cause the death of β-cells and that this weakness is specific to the duodenal pancreas.

The duodenal islets are rich in pancreatic polypeptide (PP) cells, with these cells being more vulnerable to pancreatic diseases than the remaining regions in the pancreas (Wang et al., 2013). It is well established that the cytoarchitecture within the islets differs from one region to another (Rahier et al., 2008). This suggests that the microvascular distribution and amount of blood perfusion within the pancreatic tissue under normal circumstances and increased insulin demand may not be the same in all regions of the pancreas. Therefore, a precise regional structural assessment of the distribution of blood capillaries in the endocrine pancreas under normal and diabetic conditions is necessary and may highlight the cause for the vulnerability of duodenal islets to pancreatic diseases. Establishing the correct pathogenesis for DM could, for instance, unravel the exact mechanisms behind the β-cells failure and, in so doing, target specific therapy to adequately overcome or treat this disease.

In view of this scientific gap, this research work attempted to answer to following questions:

- What topographic and structural patterns of blood vessels distribution are found in pancreatic tissue with an emphasis on the islet of Langerhans under normal, obese and diabetic conditions?
- Are there regional pancreatic differences in these patterns that justify the vulnerability of the duodenal islets to pancreatic diseases and therefore the pathophysiology of DM?

1.6 AIMS AND OBJECTIVES OF THE STUDY

1.6.1. Aim

This study aims to describe the key morphological and morphometric characteristics of the pancreatic islet microvasculature under normal and diabetic conditions (Figure 1.1).

1.6.2. Objectives

The following objectives are considered to achieve this aim:

- Develop a T1DM and a T2DM diabetic rat model using a high dose of streptozotocin (STZ) and a combination of a high-fat diet (HFD) and a low dose of STZ, respectively.
- Monitor food and water intake as well as the blood glucose profile of the control and experimental groups of rats throughout the study to determine diabetic success rate and status of diabetes-induced rats. With high blood glucose levels, it is expected that the blood vessels will be affected. Flow-cytometry and magnetic Luminex techniques using peripheral blood mononuclear cells (PBMC) samples and serum respectively will confirm the degree of effect of hyperglycaemia on the blood vessel in general. The effect of hyperglycaemia on the pancreatic vasculature would further be validated by a morphological assessment.
- Detect the percentage of circulating endothelial progenitor cells (CEPC) in the blood samples by using flow-cytometry techniques and four monoclonal antibodies: CD31, CD34, CD45 and CD133. Detect the level of the serum cytokine biomarkers for vascular injury using in a Magnetic Luminex assay multiplex techniques with Luminex MAGPIX CCD imager.
- The distribution of blood vessels in a tissue determines the speed and efficiency of blood flow in this tissue. Compare the angioarchitecture of islet microvasculature between the duodenal pancreatic islets and the splenic pancreatic islets of both the control and diabetic rat models. Using routine Haematoxylin and Eosin (H&E) stain as well as methenamine silver technique to outline features of pancreatic blood vessels and the basement membrane (BM) supporting the endothelial cells (EC). Evaluate the density, integrity and damage of EC of the microvasculature in the islets of different pancreatic regions using

immunohistochemical CD34 antibody as a marker for EC. Generate microvasculature casts (using a low viscosity polyurethane-acrylic (PU4ii) casting resin) and non-destructive 3D images, using an X-ray nano-computed tomography (nano-CT) system, of the duodenal and splenic regions of the pancreas in control and diabetic rats to describe the detailed network of the vascular tree of the pancreas in the different regions.

- Establish the angioarchitecture of the pancreatic tissue (blood vessel structure and distribution) by using the morphometric parameters such as the vascular density, capillary calibre, the inter-branching distances and the branching angles and how this can influence islet cells to function in control and diabetic rat models.

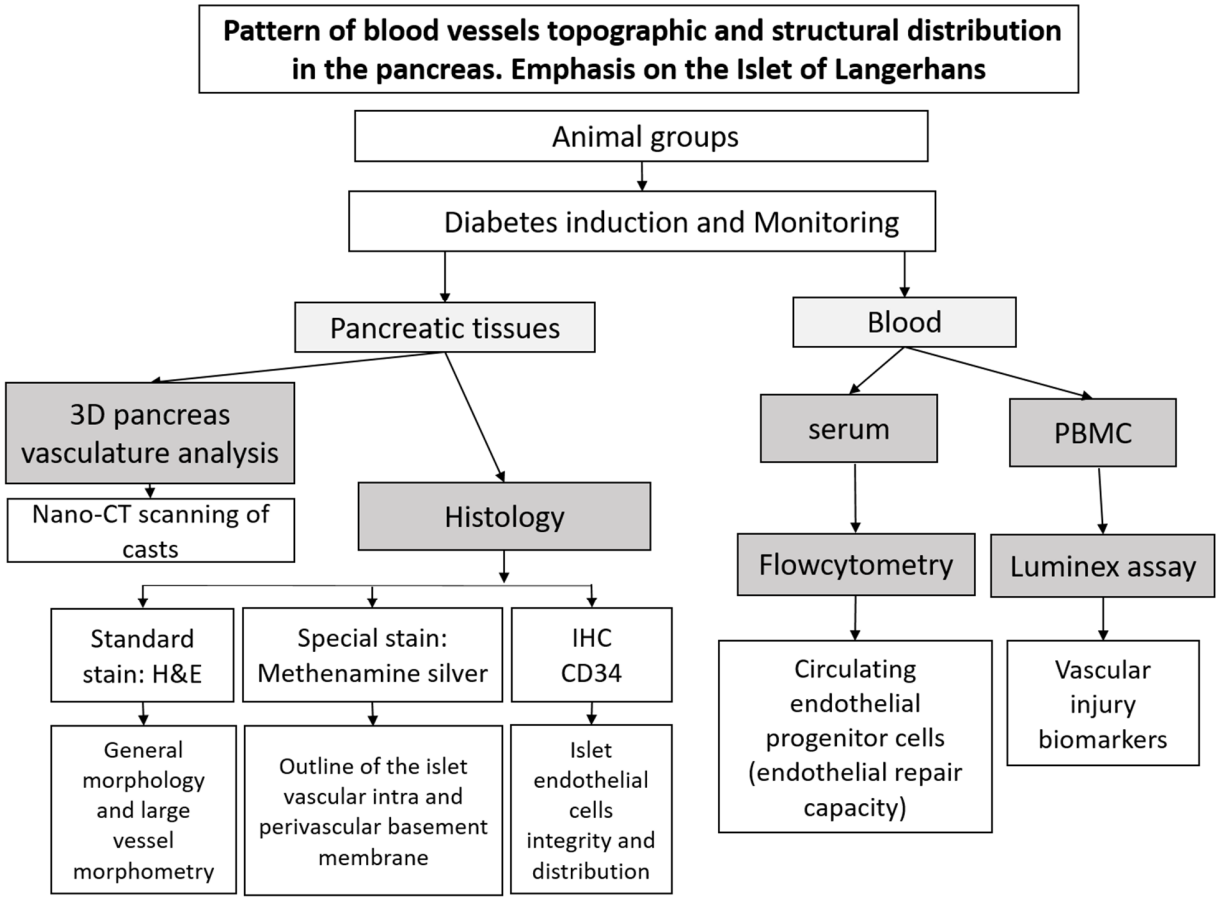

Figure 1.1: Outlines of the objectives of the work.

CHAPTER 2: LITERATURE REVIEW

This chapter highlights the following: firstly, current concepts describing the relationship between the islet cytoarchitecture and its blood vessel distribution and structure, and β-cell function while emphasising the major controversies. Secondly, previous work describing the structure and distribution of the islet microvasculature using various approaches and the effect of diabetes mellitus (DM) will be reviewed, and thirdly, aims to set the scene to address the research question of this study.

2.1 ANATOMY OF THE PANCREAS

An understanding of the general morphology of the pancreas provides a proper foundation for assessing islet function, which is dependent on the integrity and possibly the origin of its blood supply.

2.1.1 Early development of the pancreas

The pancreas develops from two primordia in the distal portion of the embryonic foregut (Edlund, 2002): namely, a dorsal primordium, formed opposite the hepatic bud and a ventral primordium, sometimes bilobed, situated very close to the hepatic bud (In't Veld & Smeets, 2015) (Figure 2.1A). At the 7th week of intrauterine life, the two primordia fuse and the ventral primordium later becomes a part of the head (ventral portion or uncinated process) of the pancreas, while the dorsal primordium develops to become the dorsal head, the body, and tail (In't Veld & Smeets, 2015) (Figure 2.1B).

The importance of ECs in the organogenesis in several organs is well reported in the literature: nervous system (Leventhal et al., l1999), liver (Matsumoto et al., 2001, Jung et al., 1999), lung, kidney, (Gerber et al., 1999) and pancreas (Lammert et al., 2001) with clear coordination between blood vessels growth and the tissues. In humans, at embryonic day eight (e8.5), the development of the pancreatic buds begins with the appearance of ECs close to the gut endoderm, the prospective dorsal bud being also adjacent to the notochord (Jennings et al., 2015). Expression of pancreatic specific transcription factors (Pdx1 and PTF1), which marks the onset of pancreas development, is maintained only in the region where the gut comes into contact with the ECs of the dorsal aorta or the vitelline vein (Ranjan et al., 2009). Endothelial cells not only signal the expression of Pdx1 (insulin promoter factor 1) but also maintain the differentiation of Pdx1-expressing cells into insulin-producing cells around blood vessels

(Lammert et al., 2001; 2003). For example, in the absence of the dorsal aorta, pancreatic development is abolished in *Xenopus* embryo, suggesting that the pancreatic differentiation depends on the presence of ECs in the region of the developing pancreas (Lammert et al., 2001). In addition, ECs have been thought to provide a BM to islet cells because they are unable to generate it themselves (Nikolova et al., 2007). The growth of the pancreatic vascular endothelium is coordinated with the embryonic development of the islet, which is likely guided by the vascular endothelial growth factor (VEGF), in particular, VEGF1 (Lammert et al., 2003; Ranjan et al., 2009).

To summarise, the development of the pancreas is initiated by EC contact with the endoderm of the gut, which also sustains the chain of factors that control the pancreatic progenitor cells differentiation into insulin-secreting cells. An improved understanding of the molecular mechanism of the ECs early role in the development of pancreatic islets in humans may help uncover the causes of β-cell failure in certain physiological and pathological states and hence, expose new solutions for the treatment of diabetes.

2.1.2 Macroscopic anatomy of the pancreas

Although the pancreas is a very loose and diffuse structure in rodents (Longnecker, 2014), the adult human pancreas is a lobulated, digestive gland located in the posterior abdominal wall. Surrounded by a very thin connective tissue capsule, the gland extends transversely between the duodenum on the right side of the body (duodenal pancreas) and the spleen, which is located on the left side of the body (splenic pancreas). The pancreas is divided into four main regions (Figure 2.1C): the head on the right is the widest portion and moulded into the C-shaped concavity of the duodenum, with the posterior part of the head projecting inferiorly to form the wedge-shaped uncinate process (Gray et al., 1989). The pancreatic tail is narrow and directed towards the hilum and gastric surface of the spleen. The neck, which is about 2 cm long, projects anteroposteriorly on the left from the head and merges into the pancreas body, which separates it from the tail (Gray et al., 1989; Moore, 2013). The capsule of the pancreas invaginates at different points around the gland to form septa that divide the pancreatic tissue into lobes and serving as supportive tissues for major blood vessels (Gray et al., 1989).

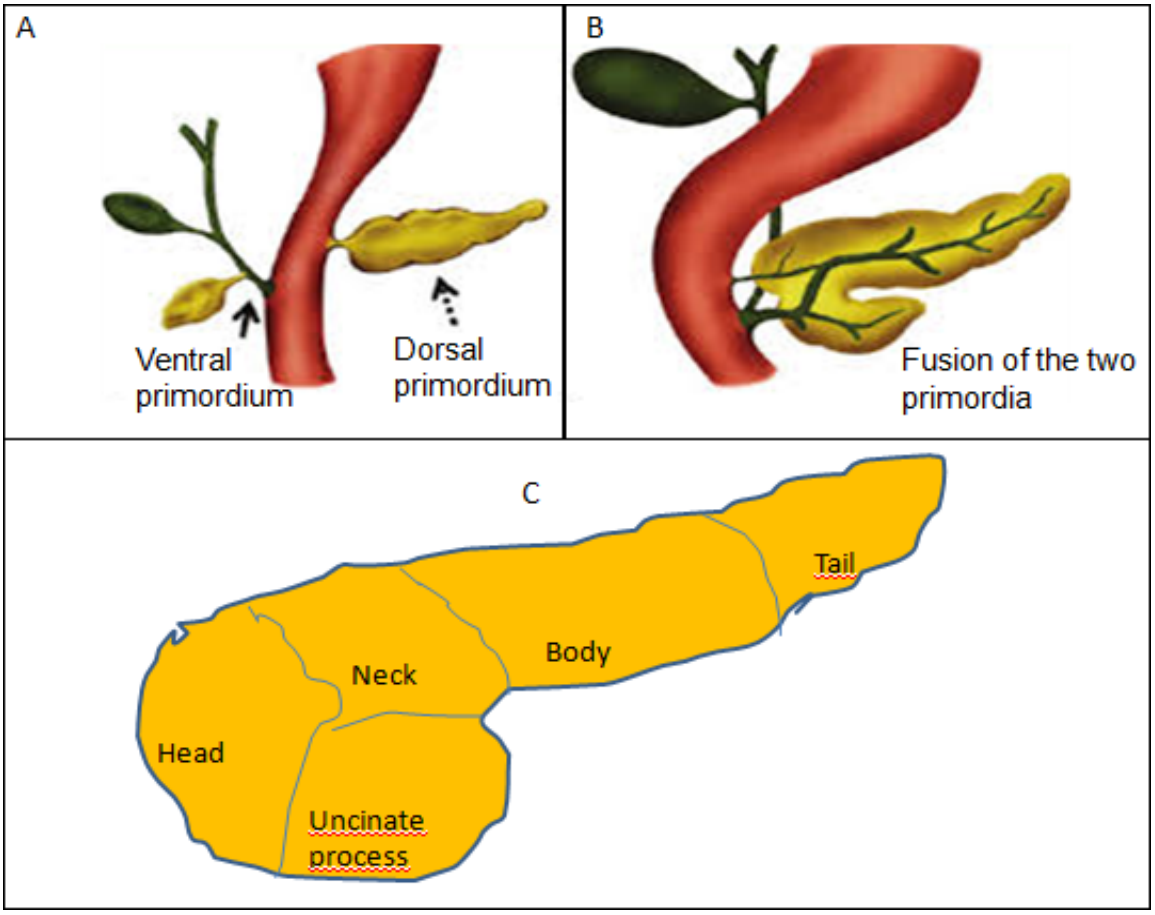

Adapted from Borghei et al., (2013)

Figure 0.1: Schematic representation of the embryology of the human pancreas.

A) Two primitive pancreatic (yellow) and liver (green) outpouchings from the endodermal lining of the distal region of the developing foregut at 4th week of the embryonic development. B) Future pancreas formed from the fusion of the two primitive pancreatic outpouchings at the 7th embryonic week. C) The complete developed pancreatic tissue isolated from the surrounding organs having four major regions.

2.1.3 Microscopic anatomy of the pancreas

Structurally, in humans, the pancreas is a composite gland mainly made up of exocrine and endocrine components (Gray et al., 1989). The exocrine component represents about 98% of the pancreas and is classified as a compound tubulo-acinous gland composed of numerous closely packed acini. The secretions from the acini assist in the digestion of nutrients (Moore, 2013). Acini are a set of pyramid-shaped secretory cells around a central lumen of a blind duct

system separated from each other by a thin layer of connective tissue septa. Acinar cells produce a mixture of digestive enzymes and bicarbonates that are collected by the end ducts (intercalated channels) which gradually drain into the duodenum by the intralobular channels, the interlobular canals and finally, the pancreatic duct. This major pancreatic duct, the duct of Wirsung, receives delicate tributaries as it runs in an increasing diameter from the tail to the head and joins the bile duct at the hepatopancreatic ampulla of Vater before releasing its content into the duodenum (Gray et al., 1989).

The endocrine component, which enshrines the scope of the present study, consists of clusters of cells scattered within the exocrine parenchyma whose secretions are directly secreted into the bloodstream and primarily concerned with glucose homeostasis in the body (Gray et al., 1989).

2.1.4 Blood supply of the pancreas

The pancreas receives its blood supply from the celiac and superior mesenteric arteries (Yousef El-Gohary, 2018). Although the detailed distribution of the microvasculature within the pancreas is yet to be established, the main vascular supply to the neck, body, and tail comes from the tortuous splenic artery, a branch of the celiac trunk. The head of the pancreas receives the superior and inferior pancreaticoduodenal arteries, branches of the gastroduodenal and superior mesenteric arteries respectively (Gray et al., 1989). In the pancreas, these major arteries branch out into the interlobar arteries, which in turn, branch into intralobular arterioles before supplying a capillary network to acini and islets. The capillaries supplying the neck, body, and tail terminate in small lobar veins thereafter into the main intralobar veins and eventually into the portal system via the splenic vein. The blood supply from the head drains directly into the portal system and the superior mesenteric vein through the superior and inferior pancreaticoduodenal veins respectively (Gray et al., 1989).

Most of the lymph vessels follow the blood vessels and usually end in the pancreatic splenic lymph nodes lying along the splenic artery (O'Morchoe, 1997). Few vessels drain into the pyloric lymph nodes and then into the celiac, hepatic and finally into the superior mesenteric lymph nodes (Gray et al., 1989).

2.1.5 Nervous system of the pancreas

The pancreas is supplied by parasympathetic, sympathetic and sensory nerve fibres all reaching the gland anchored on the arteries after connection with intrapancreatic ganglia (Ahren et al, 2006, Li et al., 2019). These ganglia were first described by Langerhans in 1869 and have now

been well studied (Sha et al., 1995, Liu & Kirchgessner, 1997; Love & Szebeni, 1999). Their size varies depending on the location and health of the pancreas. They can be oval, round or polygonal and located along or on the nerve trunk in pancreatic connective tissue, acini, and islets. Appearing to be encapsulated (Love & Szebeni, 1999), the largest ganglia are found in the duodenal pancreas and contain more neurons (Sha et al., 1996). In addition, in T2DM, the ganglia are increased in size (Tang et al., 2018).

For several decades, the intrapancreatic ganglia have been considered as a simple parasympathetic relay. However, recent studies suggest that they are similar to the enteric or intrinsic nervous system (a system of mesh-like neurons, an important division of the autonomic nervous system that governs the function of the gastrointestinal tract) and therefore are involved in regulating islet hormone secretions by controlling the activity of smooth muscle fibres and therefore local blood flow (Costa et al., 2000).

The nerve fibres of the preganglionic sympathetic fibres are branches of the vagus (cranial nerve 10)) that synapse with the intrapancreatic postganglionic fibres (Li et al., 2019). The sympathetic and the sensory originate from the splanchnic nerves (Rossi et al., 2005). The sympathetic fibres are vasoconstrictor and derive from the spinal cord segments of the thoracic splanchnic nerves (T6-10). Along with the parasympathetic, sympathetic fibres are also parenchymal, feeding the acini and islets (Gray et al., 1989).

The sensory fibres leave the pancreas along with the sympathetic fibres towards the spinal cord. Although they inhibit insulin secretion, their physiological importance in the pancreas in general and in the islet in particular remains elusive (Ahren et al, 2006). For example, the detailed explanation of the pain pathways that characterize pancreatitis remains obscured and therefore clinical management cannot be specific (Atsawarungruangkit & Pongprasobchai 2015). However, the cause of pain first thought to be due to structural changes in pancreatic tissue now appears to be associated with neurobiological alterations such as neuropathic remodelling and peripheral and central sensitization of pancreatic pain (Pasricha 2012).

2.1.6 The endocrine pancreas

The German pathologist Paul Langerhans (1847-1888) identified the pancreatic islet: clusters of cells scattered within the exocrine parenchyma having different staining properties from the surrounding tissue. Then seen as lymphatic tissues or embryonic remnants, these cells were discovered to be the endocrine component of the pancreas twenty-four years later by the French Histologist Edouard Laguesse (1861-1927). He named them the Islets of Langerhans (Gustafsson & Islam, 2007).

2.1.6.1 Morphology of the endocrine pancreas

In vertebrates, the endocrine pancreas is composed of unevenly scattered groups of special cells (islet cells) representing approximately 1-2% of the total pancreatic parenchyma (Mattsson & Nordin, 2004, Longnecker, 2014). There are roughly one million islets in the human pancreas, each usually made up of five cell types: the alpha (α), the beta (ß), the delta (δ), the pancreatic polypeptide (PP) and the epsilon (ε) cells producing glucagon, insulin, somatostatin, PP and ghrelin hormones respectively (Longnecker, 2014). Each islet is separated from the remaining exocrine tissue by a connective tissue capsule (Mattsson & Nordin, 2004); the extent of which is species-dependent (van Deijnen et al., 1992; Stendahl, Kaufman & Stupp, 2009; Chuet al., 2013; Jansson et al., 2016). The islet size and the number of insulin-secreting cells increase from birth to adulthood (Meier et al., 2008). However, the details on the distribution of islet microvasculatures and its ability to maintain optimal β-cell functions throughout life are yet to be understood and may be different from one individual to another, thus making some humans more predisposed to DM than others.

Each adult islet is a rounded mass of about 50-600 μm in diameter and is made up of 50 to 3000 cells of which β-cells represent about 60% in human (Meda, 2013) and 80% in rodents (Cabrera et al., 2006; Kim et al., 2009). Under the light microscope, islet cells form a structural meshwork separated by a dense labyrinth of capillaries (Brunicardi, et al., 1996). Two types of islets have been recognised and described, namely, diffuse islets which are very large, less demarcated and rich in PP cells with very few other endocrine cells (Wang, et al., 2013), and a smaller, compact and well-circumscribed islet, predominantly found in the body and the tail regions of the pancreas (Islam, 2010).

2.1.6.2 Distribution, size and cell types in the islet

The number and size of islets in the pancreas vary not only from one individual to another but, in addition, by factors such as one's body mass index (BMI) and pregnancy (Slavin et al., 2010; Steiner et al., 2010). In addition, the concentration of the islets is lower in the head than in the tail region of the pancreas (Savari et al., 2013). Smaller islets contain predominantly β-cells, while large islets contain mainly non-β-cell types (Jansson et al., 2016). Conversely, α-cells and the glucagon hormone content of the ventral islets (head region of the pancreas) are significantly smaller in size than those of the dorsal islets (tail region pancreas), which is associated with higher levels of insulin secretion in response to glucose (Kelly, et al., 2011). In contrast, the pancreatic head (part of the ventral pancreas) is very rich in PP cells (55-99%), the highest percentage being limited to the uncinate process (~100%) (Rahier et al., 2008; Wang et al., 2013). The high percentage of PP cells in this region of the pancreas may be associated with

the pancreatic ontogenesis, particularly the "double" vascular arcades, unlike other marginal intestinal vessels that surround the gland head (Jin et al., 2010). These speculations are not yet elucidated, and more work on the pancreatic vasculature is needed to clarify this question.

The distribution of cell types within the islet differs from one species to another and between different members of the same species (In't Veld & Marichal, 2010) (Figure 2.2). In rodents, the β-cells form the core of the islet and is surrounded by a mantle of non-β-cells, whereas in humans, the cells are intermingled (Orci et al., 1975; Cabrera et al., 2006). Similar to that of the human pancreas, islet cells types in the adult guinea pig (Caviaporcellus) are intermingled, but with the islet predominantly made up of β-cells (95%) (Crowther et al., 1989). In some species of monkeys and horses, the non-β-cells form the core and β-cells the mantle (Brunicardi et al., 1996).

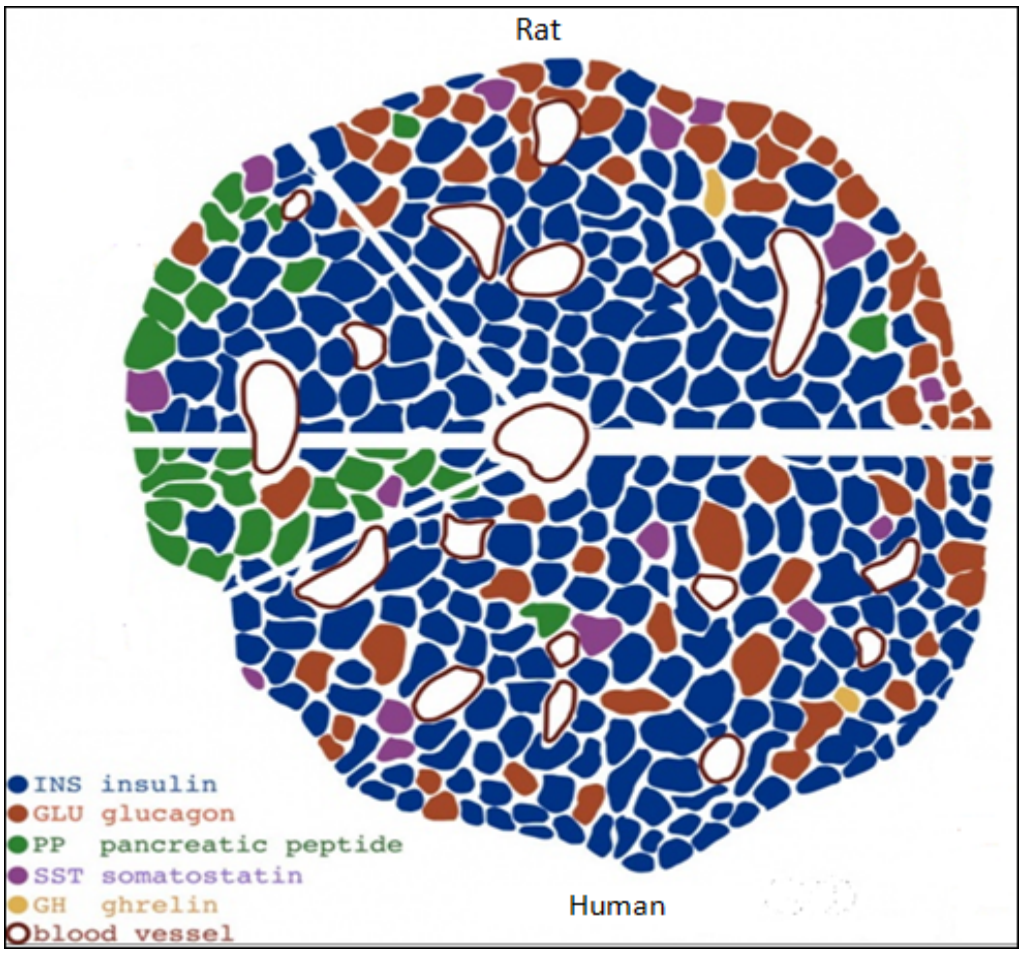

Adapted from Suckale & Solimena (2008)

Figure 0.2: Schematic representation of different types of islet cells in human and rat.

This representation shows the different types of islet cells and their distribution in the ventral and dorsal islet comparing human and rat respectively. Different cell types are colour-coded. Rodent islets, unlike human islets, present a characteristic insulin core (blue).

The structure and architecture of the islets in the rodent are well described with congruence on the core to mantle organisation within the islet (Orci et al., 1975; Cabrera et al., 2006; Cirulli, Halban & Rouiller, 1993) (Figure 2.2). However, the organisation of islet cell types in humans remains controversial. Eberhard, Kragl and Lammert (2010) described the human islet as having a cauliflower appearance with α-cells forming the mantle but folding inside the core towards the β-cells. A 3-dimensional (3D) analysis of consecutive sections through the entire human islet revealed a more comprehensive cellular architectural pattern where the islets cells are arranged in a continuous folded epithelial plate (Bosco et al., 2010). The epithelial plate is organised into three laminae: the central portion, consisting of β-cells and bounded on both sides by non-β-cells and more externally, lined by vascular channels. In other words, a layer of β-cells sandwiched between two enriched non-β-cells (Figure 2.3). The special architecture of the human islet maintains all the cell types close to vessels and, simultaneously favours a heterologous contact between α-cell and β-cell; and a homologous contact between β-cells. This architecture is observed in all the regions of the pancreas and seems to have a functional significance (Bosco et al., 2010). The porcine islet is composed of numerous mouse-like islets, similar in structure to that of the mouse and human (Bosco et al., 2010). Therefore, the murine animal model appears to be the most appropriate model for islet research.

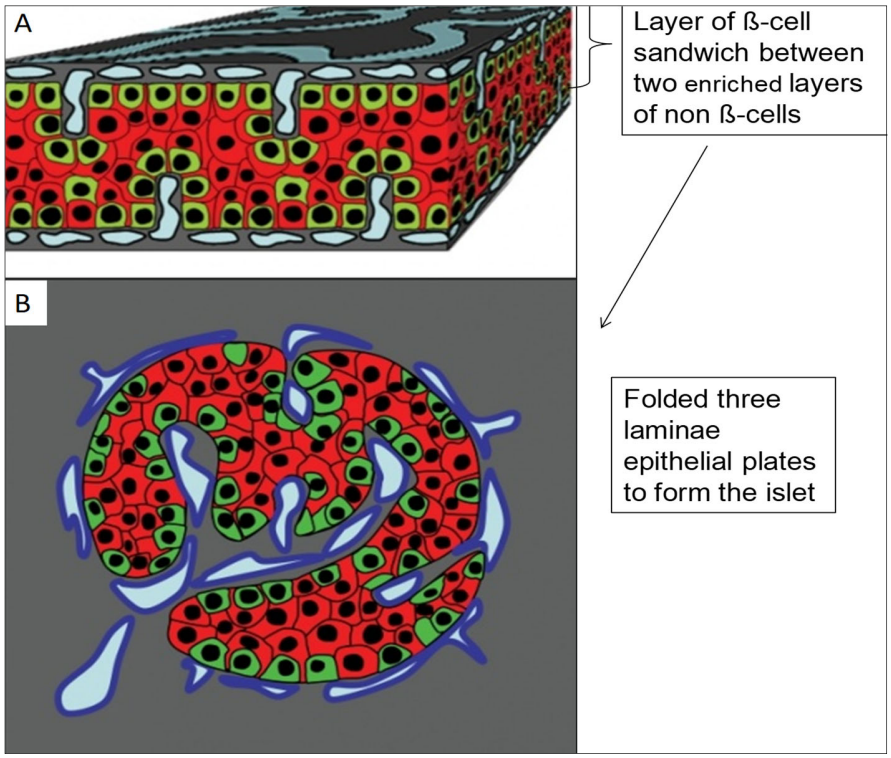

Adapted from Bosco et al., (2010)

Figure 0.3: Human islet topographical organisation of cells types around the blood vessels.

A) Epithelial plate made up β- (red) cells, non-β- (green) cells and blood vessels (light blue). B) Folded plate to form a round shape islet.

Precise anatomical organisation and the proximity of islet cells are essential for effective and normal insulin hormone secretion (Kelly et al., 2011). Isolated β-cells aggregate into pseudo-islets in culture, similar to that of the native islets; thereby suggesting that islet architecture induction may lie within the islet cells themselves (Cirulli et al., 1993). Whenever β-cells are separated and cultured in the presence of α-cells, the α-cells attract the β-cells, (Cirulli et al., 1993). However, with the complexity of human islet architecture, cells within the islet are not independent regarding cellular organisation but may depend on more complex mechanisms. A disturbance of normal islet cell architecture in murine models is caused by a decrease in insulin secretion. In this instance, β-cells intermingle with non-β-cells, indicating that in addition to cell-to-cell interactions, various metabolic and neuronal factors may modify islet cellular architecture for enhanced functionality (Gannon et al., 2000).

2.1.7 Islet cell-to-cell communication

Metabolic processes in the body require good intercellular communication. The endocrine pancreas is one of the best examples of tissue where function depends entirely on the type of intercellular communication.

2.1.7.1 Beta-to-beta cell intercommunication

A β-cell communicates with another β-cell through several cells and neuronal adhesion molecules, and even by insulin itself. The functional importance of islet cell and connexion (Cx) adhesion molecules have been extensively studied using pseudo-islets developed from clonal lineages (Squires et al., 2000; Serre-Beinier & Caille 2003; Kelly et al., 2011). Of all, N and E-cadherins play a major role in β-cell aggregation during development (Jain & Lammert, 2009). The dominant-negative R-cadherin used to replace the N and E cadherins in β-cells of the mouse embryo has been shown to significantly interfere with β-cell clustering and islet formation. That alteration possibly interferes with the automatic increase in insulin secretion, following the state of postprandial hyperglycaemia in the body (Jaques, et al., 2008). On the other hand, gap junctions mediate the spontaneous secretion of basal insulin release, which depends on the oscillation in the membrane potential of intracellular free calcium (Benninger & Piston, 2014). Gap junctions are specialised tubular structures called connexon composed of six connexins that pair with the connexon of the neighbouring cell to create intercellular channels. The channels are used to exchange cytoplasmic ions and secondary messengers (Benninger & Piston, 2014) from one cell to another (Jain & Lammert, 2009). However, it appears that the biophysical property of gap junctions in the insulin-secreting cell is directed to the connexon 36 (Cx 36) in such a way that murine models lacking the Cx 36 gene have reduced first-phase and pulsatile insulin secretion leading to glucose intolerance and later on, DM (Benninger & Piston, 2014).
Insulin was thought to have a negative feedback mechanism on β-cells, but it is now well known that it significantly interferes with β-cell metabolism concerning β-cell proliferation (Otaniet al., 2004).

2.1.7.2 Alpha-to-alpha cell intercommunication

Alpha cells are specialised in the secretion of glucagon during low blood glucose levels in the body. The α-cells retain a very low level of secretion, even during an increase in blood glucose, and glucagon exerts a feedback effect through a complex mechanism involving glutamate, a co-glucagon secreting substance (Jain & Lammert, 2009).

2.1.7.3 Delta cell to other cell intercommunication

Somatostatin is secreted not only by the δ-cells in the pancreas but also by neural and gastrointestinal cells (Hauge-Evans et al., 2009). The low dose of somatostatin in the islet is thought to exert a local inhibitory effect on α- and β-cells within the islet via the microcirculation and/or the interstitial tissue (Bonner-Weir & Orci, 1982). However, out of multiple studies describing the activity of somatostatin (Pace & Tarvin, 1981; Carroll & Carroll, 2007), none has shown whether its action in the islet is ascribed to general circulating somatostatin, or to the local release portion by the δ-cell until Hauge-Evans et al. (2009) confirmed the importance of local somatostatin hormone on islet function using transgenic animals with a knockout somatostatin-expression gene. The local somatostatin has an inhibitory effect on insulin and glucagon secretion. Importantly, an increase in blood glucose levels stimulates both insulin and somatostatin secretions to limit the β-cell response (Mann & Bellin 2016).

2.1.8 Non-endocrine cells of the islet of Langerhans

Although the following section focuses on the current knowledge about islet microvasculature and its contributions to islet function by using previous reports, the description and the role of the non-endocrine cells associated with these vessels are important. Structures situated between the endocrine cells in the pancreatic islet are mainly connective tissue (stroma) surrounding blood vessels (In't Veld & Smeets, 2015). However, other types of non-endothelial cells are embedded within the islet; namely connective tissue cells, immune cells, predominantly macrophages (De Koning et al., 1998), and neuronal elements (Jansson et al., 2016).

2.1.8.1 Connective tissue cells

The stromal cells of the islet are mainly fibroblasts. These fibroblasts make up the main reticular network and collagen fibres of the islet and contribute abundantly to the formation of the islet capsule (Ohtani, 1987). The other stromal cells are stellate, these characterised by cytoplasmic lipid droplets and representing 4 to 7% of all parenchymal cells in the islet (Li et al., 2016). Although the function of the stellate cells within the islet is poorly understood, these cells interact with the vasculature and penetrating macrophages by facilitating EC migration (Fransson et al., 2015). On the other hand, the increase in their numbers (stromal cells or stellate cells) is well known to be associated with chronic pancreatitis and in pancreatic adenocarcinomas, thus contributing to pancreatic fibrosis that characterises these diseases (Zha, et al., 2014; Apte, et al., 2015).

Reticular fibres encircle the islet capillaries which form pericapillary spaces inside the capsule. Intra-islet capillary channels thus formed continue with those in the surrounding acini gland

thereby confirming the existence of the insulo-acinar portal system in human pancreas (Ohtani et al., 1987). Cajal cells are another group of stromal cells in the islet originating from neural cells. In humans, these cells are found mainly in the intestine (Liu et al., 2015) closely situated next to the microvessels (Liu et al., 2015). In the intestine, Cajal cells act as pacemaker cells helping in the regulation of intestinal motility (Lammers, 2015). In the pancreas, it remains unclear whether a similar effect is noted on the vasculature. However, the proximity of Cajal cells to the microvessels is thought to have a functional significance in the pancreas (Liu et al., 2015).

2.1.8.2 Immune cells

Immune cells are normally very rare in the islet but increase during inflammatory conditions such as insulitis. These cells appear to affect the islet microvasculature predominantly during islets' transplantation (Christoffersson et al., 2010; Vågesjö et al., 2015); a topic which is beyond the scope of this study.

2.1.8.3 Neural cells

There are two types of neural elements in the islet namely, axons with a cell body, known as neuro-insular complexes type I, and type II, with no cell body. Nerve supply to the endocrine pancreas is mainly from the parasympathetic system accompanied with few sympathetic fibres (Rodriguez-Diaz et al., 2011). The parasympathetic fibres appear as preganglionic fibres from the dorsal motor nucleus of the vagus nerve and connect to ganglia only in the islet. It is believed that feeding stimulates the parasympathetic pathway and facilitates the secretion of insulin (cephalic phase) (Ahren & Holst 2001) and in hypoglycaemia glucagon (Taborsky et al., 1998) and pancreatic polypeptide hormone (Schwartz et al., 1978). The sympathetic system inhibits this process (Ahren, 2000). In the human endocrine pancreas, sympathetic nerve fibres regulate the islet cell function indirectly by modulating the intra-islet blood flow by vasoconstriction (Rodriguez-Diaz et al., 2011). Sensory nerve endings are also present in rat islets and impact on the regulation of blood flow (Carlsson et al., 1996). There is a difference in the distribution of nerve fibres in human and rodent pancreata. Human islets contain fewer, relatively large nerve fibres while rodent islets have an extensive network of fine nerve fibres (Rodriguez-Diaz et al., 2011; Vågesjö et al., 2015). Intra-islet Schwann cells support the nerve cells and surround islets as if they were attempting to delineate the islet parenchymal from the exocrine portion. Although Schwann cells are known to be activated in islet lesions in non-obese diabetic rats (Teitelman et al., 1998) and are involved in islets post-transplantation regenerative processes (Lammers, 2015), their role in the gland function remains an enigma and is awaiting further investigations.

2.1.8.4 Vascular elements

The vascular system of the islet of Langerhans is formed by capillaries and arterioles, and in turn, consists of ECs making the endothelium, pericytes, vascular smooth muscle and adventitia (already discussed belonging to the stromal component). The following section examines details of the various elements that make up the microvascular system of the islet while emphasising the structure of the endothelium, the main barrier between surrounding islet cells and blood.

Pericytes

Pericytes, also called mural cells, are elongated multi-branched contractile cells located between the endothelium and BM (Brissova et al., 2014; Gökçinar-Yagci et al., 2015). Pericytes surround microvascular ECs (Berg, Chernavvsky-Sequeira et al., 2013) and are rare in pancreatic islets (Morikawa et al., 2002). The functions of these cells are not well defined but are considered important for the production of matrix components as well as angiogenesis (Bergers & Song, 2005). In addition, pericytes and EC interactions are required for the assembly of the vascular BM (Kragl & Lammert, 2010; Armulik et al., 2011), the major support of β-cell proliferation and function in the islet (Nikolova et al., 2006). Consequently, when the vessels lose their pericytes, they (the vessels) become haemorrhagic and hyper-dilated (Bergers & Song, 2005), a condition which remains the hallmark of early diabetic retinopathy (Ejaz et al., 2007). Unfortunately, not much is known on the function of the pericytes in the islets.

Vascular smooth muscle cells

Vascular smooth muscle (VSM) cells in blood vessels play a key role in controlling vascular tone and vascular diameter; the main haemodynamic determinants in the circulatory system (Fray, 1980; Busse & Fleming, 2003). The presence of VSM cells in the arterioles of the islet is the basis for separate regulation of blood flow (Jansson et al., 2016). Islet nerve fibres for the maintenance of effective blood perfusion (Carlsson et al., 1996) may control vascular smooth muscle cells. Endothelial cells are one of the most important components among non-endocrine cells in the islet and are discussed in detail in the following section.

2.2 GENERAL CONCEPTS OF THE ENDOTHELIUM AND THE ENDOTHELIAL CELLS

Endothelial cells form a continuous monolayer barrier (endothelium) controlling the movement of biomolecules and cells between the lumen and the perivascular space (Bennet et al., 1959; Favero et al., 2005). Until recently, the endothelium was perceived as a “cellophane wrapper” around the vascular tree whose sole function was to selectively allow water and electrolytes through (Rajendran et al., 2013). In 1980, with the discovery of nitric oxide (NO), the epithelial

lining of blood vessels revealed an array of homeostatic, hormonal and metabolic functions; one of the most important being the regulation of blood flow (Sandoo et al., 2010, Durand & Gutterman, 2013; Rajendran et al., 2013).

In general, three main types of endothelia are described (Bennet et al., 1959). Firstly, endothelia associated with secretory and filtration of organs and impregnated with fenestrae surrounded by a discontinuous BM. The fenestrae are trans-cellular pores, approximately 50-60nm wide covering a diaphragm of 5 to 6nm thick. Secondly, endothelia associated with vessels of the skin, heart, lung and muscle (Aird, 2007) which are firmly attached to a continuous BM, and thirdly, the 'discontinuous' endothelia, so-called due to their characteristic large fenestrations (from 100 to 200 nm wide), lacking a diaphragm and having a poorly structured BM (Aird, 2007; Favero et al., 2014).

The isolation of ECs was first performed by Jaffe (1973), which helped researchers understand extracellular environment control and learn about cell biology (Aird, 2007). Currently, the concept of vascular ECs as a simple physical barrier between blood and tissues has changed, and cardiovascular researchers should bear in mind the notion of endothelium heterogeneity (Galley & Webster, 2004). A good understanding of this concept in the pancreas will certainly improve the multi-pronged search into the mechanism that leads to the destruction of β-cells in pathology such as diabetes.

2.2.1 Endothelial cell ultra-structure

A typical EC is a squamous epithelial cell with a thickness ranging from less than 0.1μm in capillaries to 1μm in veins and arteries, and having a centrally placed nucleus supported by a basal lamina less than 500 nm wide which, in the pancreas, separates them from the islet cells (Aird, 2007). The morphology of an EC depends on the vessel to which it belongs. Endothelial cells are very sensitive to changes in intravascular tension. When intravascular tension increases, the stiffness of the EC also increase and the cells become flattened and aligned in the direction of the blood flow. When intravascular tension is decreased, ECs swell and lose their alignment and have a cobblestoned paving appearance (Nerem et al., 1981; Favero et al., 2014). For example, in the aorta where there is higher intravascular pressure, ECs are long and narrow, with their long tails pointed towards the direction of the blood flow (Sumagin & Sarelius, 2006). In the pulmonary artery, the pressure is very low, hence ECs are broader and shorter (Kibria et al., 1980).

Each EC is enclosed in a double layer of phospholipids membrane. The layers are separated from each other by a water chamber traversed by complex protein molecules. These protein

molecules act either as receptors or as channels for numerous molecules including proteins, lipids, and hormone and adhesion molecules (Sung et al., 1994; Ranjan et al., 2009). Adhesion molecules help maintain cell-to-cell and matrix intercommunication. Importantly, about 84% of these vascular receptors on islet ECs are specific to islet vascularisation and therefore cannot be found on the ECs of surrounding exocrine tissues (Yao et al., 2005). Examples of these receptors are the proteinase inhibitor and the α1-antitrypsin angiostatic factor (Lou et al., 1999). Endothelial cell heterogeneity of the microvasculature is therefore not only different between organs, but also between distinct regions of the same organ (Kuzu et al., 1992, Aird, 2007).

Each EC membrane has three surfaces: 1) the cohesive surface which connects ECs and is made up of specialized intercellular junction such as adherent junctions (gap junction) or syndesmosis (tight junction) which facilitate the transport processes (Pasyk & Jakobczak 2004; Dejana & Orsenigo 2013); 2) the adhesive surface of ECs which is attached to the basal lamina and, 3) the luminal surface carrying specific binding proteins regulating the transport of circulating blood cells (Pasyk & Jakobczak 2004).

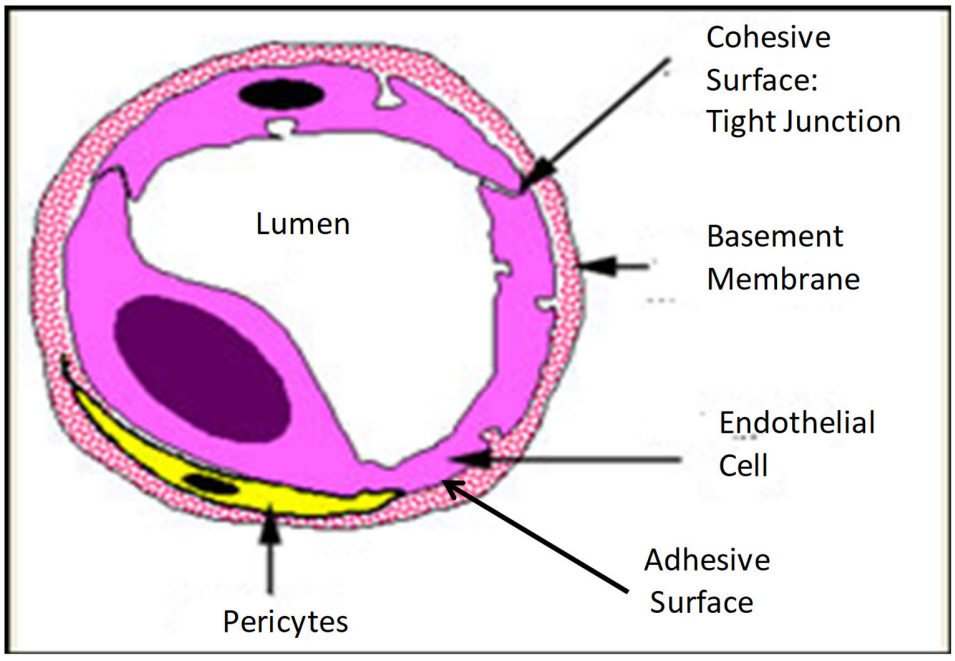

Adapted from https://www.histology.leeds.ac.uk/circulatory/capillaries.php

Figure 0.4: Schematic representation of a cross-section of a capillary showing endothelial cells supported by the basement membrane and pericytes around the lumen.

The immunostaining technique applied on tissue sections and cell culture has made it possible to identify and quantify several ECs surface markers such as Cluster of Differentiation 31 and

34 (CD31, CD34), von Willebrand factor (vWF) (Lou et al., 1999; Favero et al., 2014) and vasoactive substances (Olsson & Carlsson, 2006).

Many other (growth) factors involved in the regulation of angiogenesis, such as pro-angiogenic factors, vascular endothelial growth factor (VEGF) and angiostatic factors, endostatin, and pigment epithelial-derived factor can be produced by EC (Mattsson et al., 2006). In human adults, the islet ECs mass is stable and the turnover rate very low; indicating that the amount of pro-angiogenic and angiostatic factors produced is maintained in close equilibrium (Olsson & Carlsson, 2006).

Islet ECs present a large number of fenestrae (Figure 2.4), thus facilitating trans-endothelial transport of hormones (Aiello & Wong, 2000). The fenestrations are induced and maintained by the high level of the local production of vascular endothelial growth factor-A (VEGF-A) by the pancreatic β-cells (Aiello & Wong, 2000; Vasir, et al., 2001; Lammert et al., 2003; Zhang et al., 2004). The luminal surface of ECs carries a negatively charged mucopolysaccharide layer, which is an integral part of the vascular barrier (Reitsma et al., 2007). This carbohydrate-rich layer (also known as glycocalyx) forms a platform in which plasma and endothelial-derived molecules are incorporated, acting as the gatekeeper of the endothelium, and subsequently the determinant of vascular permeability (Reitsma et al., 2007).

2.2.1.1 Endothelial cell function: emphasis on the islet

The endothelium plays an important role in day-to-day islet life and tissue function (Mai et al., 2013). In addition to its physical barrier role, under normal physiological conditions, the endothelium has several other functions that can be characterised according to three main categories, namely, trophic, tonic and trafficking (Davidson, 2010). In the body, ECs are the main regulator of 1) vascular homeostasis through the release of many vasoactive substances and growth factors (trophic function) (Michiels, 2003; Eberhard et al., 2010; Brissova et al., 2014) 2), vascular haemodynamic (tonic function) (Cines et al., 1998; Mai et al., 2013), and 3) vascular permeability, coagulation, and cellular extravasation (trafficking) (Claesson-Welsh, 2015). The following section highlights the major functions of the ECs.

2.2.1.2 Regulation of permeability

The term "vascular permeability" traditionally refers to the natural sieve that allows substances and small molecules to pass through the capillary wall to the surrounding tissues (Claesson-Welsh, 2015). The circulating blood is under the hydrostatic pressure that pushes the water out of the vessels (Adamson et al., 2004). In addition, blood vessels normally let most ions pass so that no difference in hydrostatic pressure would exist between the blood and the tissues. The

hydrostatic pressure is maintained when blood retains a high concentration of protein to develop oncotic pressure and thus draws water into the vessels (Adamson et al., 2004). Endothelial cells, therefore, can prevent the diffusion of proteins out from the vessels. Plasma contains three major proteins: albumin, globulin, and fibrinogen (Adkins et al., 2002). In the event of a loss of protein from the circulation, the oncotic pressure decreases and allows the diffusion of fluid into the surrounding tissues, causing oedema. Eighty percent of the oncotic pressure is generated by albumin (Darwish & Lui 2019). However, some proteins such as antibodies and proteins associated with hormone secretion must exit the circulation and enter the surrounding tissues to improve the body's immune system (Strell. & Entschladen 2008). The molecular mechanism that controls vascular leakage depends on the organ, vessel type, and kinetics. However, two major models have been proposed to explain this: some models depend on the formation of transendothelial canals from vesicles or vacuoles, while others involve endothelial junctions that can transiently be dissociated and allow extravasation (Claesson-Welsh, 2015). Cell membrane dissociation is attributed to the retraction of ECs (Majno et al., 1969) due to the action of the motor proteins (provide molecular motion in the cells by interacting with rigid cytoskeleton) of the cell to open the paracellular junctions. However, the hypothesis of cellular retraction has been challenged and the change in cellular form has been attributed to the natural recoil process that occurs whenever the cell junction is disassembled (Adamson et al., 2003).

The regulation of the vascular permeability is thus directly influenced by molecules that cause the disintegration of the barrier or indirectly by the pressure, the blood flow and the nature of what is transported through the vascular wall (Claesson-Welsh, 2015). Molecular regulators of vascular permeability include growth factors such as VEGF, abundant in the islet and inflammatory cytokines (histamine and bradykinin) (Claesson-Welsh, 2015).

2.2.1.3 Regulation of the immune response

The extravasation of leukocytes across blood vessels to the tissues is vital for the functioning of the immune system. The early phase of this process is well understood but details of its terminal phase where leukocytes migrate through the junctions between adjacent ECs while preserving the barrier function of the endothelium are still poorly understood (Johnson-Léger et al., 2000). However, like some specific proteins, immune cells also pass through ECs to the surrounding tissues. Because the size of these immune cells is larger than that of proteins, the extravasation of leukocytes across blood vessels seems to be a difficult task. Endothelial cells thus have two major roles in this process (cellular extravasation): they first attract immune cells to the site of the infection and secondly allow the immune cells to pass through their membrane to the surrounding tissues (Johnson-Léger et al., 2000). The second function has three distinct steps:

1) immune cells roll along the surface of ECs mediated by a set of proteins called selectins expressed by ECs whereas erythrocytes pass directly. 2), Immune cell adheres to the surface of ECs; in response to infection, cells in the tissue release chemokines and chemoattractants which trigger the expression of integrins on the surface of immune cells. The integrins bind proteins on the surface of ECs and lock the immune cell to the surface of the endothelium. 3) The immune cell then migrates to enter the surrounding tissue by squeezing itself through the endothelium (endothelial cells and BM) (Johnson-Léger et al., 2000).

2.2.1.4 Initiation of growth and the formation of new blood vessels

Endothelial cells also initiate the growth of new vessels. During vessel formation, a remarkable degree of coordination is required between different transforming cell types.

Generally, hypoxia (Chen et al., 2009; Blanco & Gerhardt, 2013) and wounds initiate the development of new vessels (Hong et al., 2014). In response to these conditions, tissue cells express several proteins, the most important of which is VEGF. Vascular endothelial growth factor plays a unique role in this process because it radically changes the morphology of an EC subtype, namely, the tip cell (Cines et al., 1998; Blanco & Gerhardt, 2013). First, the tip cell reverses polarity in the cell, so that the apical surface that normally faces the lumen becomes tissue-directed (Gerhardt et al., 2003). Secondly, the complex joint between a tip cell and the neighbouring cell is impaired, and ultimately, the tip cell invades the surrounding tissue by extending filopodia (Phng et al., 2013). Notably, only tip cells respond to VEGF; because if all cells do so, the entire vessel would degenerate. At the same time, tip cells prevent the response of neighbouring cells to VEGF.

A group of molecules called semaphorins, expressed by the surrounding tissue, guide the direction of the crawling of tip cells. Semaphorins also dictate the development of neurons (Marín et al., 2010). Following the tip cells in the surrounding tissue, specialised cells called stalk cells which divide to produce more ECs and can surround the lumens of the newly formed vessels. During this process, while VEGF acts as the driving force behind vasculogenesis and sprouting, angiopoietins (Ang 1) and ephrin subsequently intervene in this process of remodelling and maturation of the initial immature blood vessel (Holash et al., 1999). After blood vessel maturation, the maintenance and stability seem to be under the control of Ang 1 (Gale & Yancopoulos, 1999).

Increased levels of such restructure cytokines as TNF (tumour necrotic factor) and IL-1 (interleukin-1)and IL-6 (interleukin-6) in addition to VEGF promotes abnormal vascular growth as in early atherogenesis (Ikeda et al., 1990, Sprague & Khalil 2009). Assessment of these cytokine levels in the blood circulation using a technique such as Luminex assay has helped to

predict early vascular dysfunction which may occur well before the structural manifestations (Sprague & Khalil 2009).

2.2.1.5 Detection and response to changes in blood pressure and flow

In a quiescent state, ECs balance the production of a vasodilator (NO, prostacyclins, endothelium-derived hyperpolarising factor (EDHF)) and vasoconstrictor (endothelin and angiotensin) factors to ensure that vascular tone, blood pressure, and optimal blood flow are maintained (Widlansky et al., 2003). The ECs lining the blood vessels can detect shear stress generated by the blood flow and transmit signals to the inside of the cell. In the cell, the increase in shear stress causes ECs to produce more vasodilator substances such as NO on their cell membrane (Kunnen et al., 2018). The impact of shear stress also extends to the genetic level and may cause an increase or reduction in the expression of several genes through the activation of the transcriptional factors or the stabilisation of mRNA (Kunnen et al., 2018). The morphology and function of the vessels are altered in response to changes in blood flow (Ando & Yamamoto, 2013): a mechanism called "flow-induced remodelling" resulting from the interplay between vasodilator factors, inflammation and factors that alter the intercellular matrix (Heil & Schaper, 2004; Silver & Vita, 2006).

The absence of EC response to shear stress will lead to the development of vascular diseases such as hypertension, thrombosis, aneurysms, and atherosclerosis, to name but a few (Heo, Fujiwara & Abe, 2014). As a result, studies have made some progress in elucidating how ECs perceive shear stress and transmit the information into the cell (Bodin, Bailey & Burnstock, 1991; Bodin & Burnstock, 2001; Wang et al., 2016). Thus, mechanotransduction of shear stress in the cell is characterised by the simultaneous activation of several intracellular signalling pathways mediated through different types of molecules and micro-domains associated with the cell membrane (Resnick et al., 1993; Tarbell et al., 2014). However, the details of the mechanism responsible for ECs characteristic response to shear stress remain poorly understood (Tarbell et al., 2014).

2.2.1.6 Regulation of clotting

The role of the endothelium is crucial in the regulation of the mechanism of coagulation using both anticoagulants and pro-coagulants. Under normal physiological conditions, ECs express the tissue-inhibitory factor pathway and thrombomodulin that prevents the activation of pro-coagulation molecules such as Stuart Power factor (factor X), thrombin and fibrin. However, as soon as the endothelium is injured, the surface of the ECs quickly turns into a pro-coagulant

state by inducing the tissue factors that will initiate the extrinsic coagulation cascade (Cines et al., 1998).

2.2.2 βeta-cell and endothelial cell communication

Apart from the pivotal role played by islet ECs, ECs in general also have endocrine functions. They produce numerous factors that mediate the proliferation, survival, and expression of multiple genes consistent with good physiology and β-cell function (Figure 2.5) (Gregersen et al., 1996; Johansson et al., 2006; Nikolova et al., 2006).

2.2.2.1 Islet Vascular endothelial growth factor

Originally, referred to as vascular permeability factor, VEGF constitutes a group of proteins, a subfamily of the platelet-derived growth factor, secreted by most cells including islets cells (Narayanan et al., 2017). The family of VEGF is made up of seven secreted glycoproteins: VEGF-A, VEGF-B, VEGF-C, VEGF-D, VEGF-E, VEGF-F and placental growth factor (Narayanan et al., 2017). In most tissues, VEGF acts on the EC membrane via a VEGF receptor (there are 3 types of VEGF receptors: VEGFR-1, VEGFR-2 and VEGFR-3), a specific angiogenic factor receptor tyrosine kinase, by transphosphorylation to firstly, promote angiogenesis. In the islet, VEGF provides a unique dense vascular niche to optimise the function and secondly, affect proliferation of the endocrine pancreas during the intrauterine life (Otonkoski et al., 2008; Eberhard & Lammert, 2009). Thirdly, promote endothelial pores in all the fenestrated capillaries (Roberts & Palade, 1995). The absence of the VEGF secretion in experimental studies showed capillaries with less fenestration (Lammert et al., 2003). Finally, VEGF-A is essentially required for the fine-tuning of body glucose regulation (Brissova et al., 2014).

In rodents, hypoxia and islet isolation increases the expression of VEGF-A via hypoxia-inducible factor-1 found expressed in cells (Gorden et al., 1997; Vasir et al., 2001). However, VEGFR-2 appears to be the major receptor of the proangiogenic effects of VEGF-A (Suto et al., 2005; Narayanan et al., 2017).

In summary, VEGF expression is increased in all conditions where blood or oxygen delivery to the islet is reduced and this action is antagonised by thrombospondin (Jiménez et al., 2000).

2.2.2.2 Angiopoietins, ephrin, and extracellular vesicles

In addition to VEGF, other angiogenic factors have also been reported to be involved in the integrity and maintenance of blood vessels: this includes angiopoietins, ephrins and extracellular vesicles (EVs), to name but a few (Narayanan et al., 2017). Angiopoietins made up of Ang-1, Ang-2 and Ang-4 ligands and their receptors, Tie-1 and Tie-2 tyrosine kinase (Lammert et al.,

2003; Brissova et al., 2006; Jabs et al., 2008; Eberhard & Lammert, 2009) are all expressed by islet and perivascular cells in mice and humans (Brissova et al., 2006). The activation of Ang-1 prevents cytokine-mediated apoptosis in ECs via a complex signalling pathway involving phosphoinositide 3-kinase/protein kinase (pI3k / Akt) (Su et al., 2007) and facilitates cell-cell contact and contact with extracellular matrix (Scharpfenecker et al., 2005).

Ephrin ligands, on the other hand, bind to tyrosine kinase receptors to intervene in various aspects of cellular communication (Himanen & Nikolov, 2003), resulting in improved pancreatic function (Dorrell et al., 2011).

Recent reports show that EVs play an important role in the communication between islet cells (Camussi et al., 2010) in humans (Figliolini et al., 2014) and experimental mouse models of islet xenotransplantation in severe combined immune deficiency (SCID) (Cantaluppi, et al., 2012). Extracellular vesicles are involved in intercellular communication through the transfer of proteins and nucleic acids. These vesicles are secreted by membrane nanoparticle circular fragments released into the microenvironment by various cell types and can directly stimulate target cells and thus play a pivotal role in cell-to-cell communication (Figliolini et al., 2014).

2.2.2.3 Endothelial cells and islet basement membrane

Basement membranes are thin layers of special extracellular matrix that separate the islet cells from the ECs (Otonkoski et al., 2008). Endothelial BMs stand as the only structural support of pancreatic cells and are very important in the physiological microenvironment of the islet (Nikolova et al., 2007). The ECs are usually firmly attached to the BM via integrins which provide elastic support and selective filtration of molecules and cells between the vessel and the perivascular space (Korpos et al., 2013). In addition, the BM also prevents the diffusion of proteins because it carries a strong negative charge (Suh & Miner, 2013).

Islet BM is mainly made up of collagen IV, fibronectin and laminin (Timpl & Brown, 1996; Eberhard & Lammert, 2009; Cao & Wang, 2014). While collagen IV remains the major structural component of the BM, laminins sustain the regulation of organ cellular function by affecting specific signals to cells attached or moving through the BM (Otonkoski et al., 2008, Durbeej, 2010). The composition of laminin subtypes of the BM varies not only from one species to the other, but also from one organ to another, and even within the same organ. For example, laminin 211 and 411 have been identified in the mouse pancreas instead of the 332 and 511 found in most glandular tissues (Otonkoski et al., 2008).

On the other hand, mouse β-cells express several β-1 integrins, a type of receptor for laminins, which is very important in the mediation of cell-to-cell and cell-matrix interactions (Jiang et al., 2002). The human insulin-secreting cells, in contrast, express a different receptor for laminin

named Lutheran (Otonkoski et al., 2008). The relationship between β-cells and ECs established during pancreatic development is maintained throughout adult life (Eberhard & Lammert, 2009). Insulin gene protein expression and glucose-stimulated insulin secretions are highly dependent on the BM. The loss of BM and the disruption between BM and pancreatic endocrine cells result in the death of islet cells (Wang et al., 2001; Nikolova et al., 2006; Irving-Rodgers et al., 2008), thus, emphasising that the integrity of the BM must be maintained in conditions such as diabetes. Recently, it has been discovered that the BM in the human islet consists of two layers which act as the double-layered blood-brain barrier in the central nervous tissue (Otonkoski et al., 2008). The potential tissue space between the two BM sheets could be involved in the regulation of the trafficking of inflammatory cells such as in autoimmune insulitis. Otonkoski et al., (2008) established that the only laminin isoform that is specific to human islet BM was laminin 511 (earlier known as laminin 10).

Pericytes are embedded within the BM (Clee et al., 2006) and are recruited by EC-derived platelet-derived growth factors (PDGF) (Eberhard & Lammert, 2009) to help stabilise the islet microvasculature (Clee et al., 2006).

2.2.2.4 Thrombospondin-1 secreting endothelial cell and islet function

Thrombospondin 1 (THBS1) is a multi-domain matrix adhesive glycoprotein that is highly expressed in pancreatic endothelium (Dubois et al., 2010; Olerud et al., 2008; Olerud et al., 2011). Thrombospondin 1 naturally regulates cell proliferation, migration and apoptosis in healthy tissues and curtails tumorigenesis by limiting vessel density. Thrombospondin 1 can modify the islet morphology and plays a major role in the modulation of β-cell function by activating the transforming growth factor (TGF-β1) (Crawford et al., 1998) (TGF-β1 activation in adult inhibits Smad6 and Smad7 molecules causing the downstream gene expression in the nucleus (Yinan Jiang et al., 2018)). In severe DM (Type 1 and 2), one of the therapeutic approaches is the transplantation of isolated islets either in the liver or beneath the kidney capsule (Stokes et al., 2017). Unfortunately, the marked decrease of vascular density and subsequently an impaired EC function has rendered this therapeutic approach ineffective (Mattsson et al., 2004). However improved pancreatic islet revascularisation is achieved after transplantation in a partial or total THBS1 deficient mouse (Olerud et al., 2008). More work should focus on the therapeutic value of the two antagonistic factors (VEGF and THBS) in diabetes.

2.2.2.5 Endothelins

Endothelin (ET) is a powerful vasoconstrictor derived from the endothelium that stimulates insulin production (Lai et al., 2007) by calcium receptor mechanisms (De Carlo et al., 2000). While ET-1, a predominant isoform of the family of ET which includes ET-2, ET-3, ET-4, (Lüscher & Barton, 2000) appears to have a potent effect on the microvasculature of native islets, ET-3 directly stimulates insulin secretion (Gregersen et al., 1996). Hypoxia regulates the expression of ET-1 in pancreatic endocrine cells and ECs (Kourembanas et al., 1991; Kugelmeier et al., 2008). Similarly, insulin also stimulates the expression and secretion of ET-1 from bovine ECs and in humans and can thus regulate the concentration of circulating ET-1 (Cheifetz et al., 1992).

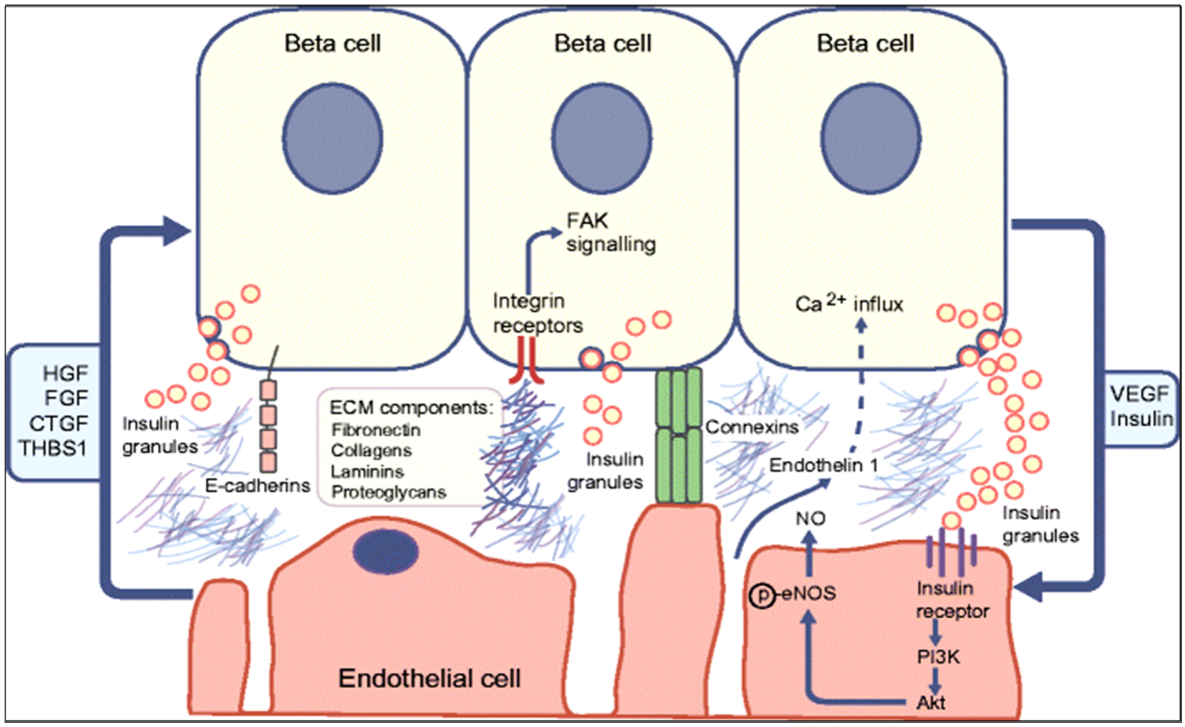

Adapted from Hogan & Hull (2017).

Figure 0.5: Schematic representation of the major factors that regulate the beta-cell endothelial cell axis.

Under normal physiological conditions, islet ECs produce several factors (HGF, CTGF, ET and THBS1) regulating the β-cell proliferation, -survival and function. Extracellular matrix (ECM) molecules like fibronectin, collagens, and laminins affect insulin expression and release from β-cells, mainly via integrins and activate signalling pathways such as focal adhesion kinase (FAK).

2.3 ISLET MICROVASCULATURE AND ISLET CELLS FUNCTION

The islet houses a rich vascular network that morphologically resembles the renal glomerulus (Jansson et al., 2016; Olsson & Carlsson, 2006). The network is continued with the blood supply of the exocrine pancreas (Cao & Wang, 2014). However, vessels in the islet are more tortuous, and have greater volume (width 8-10 µm vs. 4-6 µm) and density (Brissova et al., 2006; Favaro et al., 2005), and provide no less than the 10% of the total pancreatic blood flow through a highly fenestrated capillary (5 to 10 fold) compared to that of the exocrine pancreas (Cao & Wang, 2014; Henderson & Moss, 1985; Kuroda et al., 1995; Marichal, 2010). A difference exists between the islet microvasculature in the rodents (Figure 2.6A), and in humans (Figure 2.6B) (Bonner-Weir, 1993; Olsson & Carlsson, 2006). In humans, islet capillaries are larger and significantly less dense (Brissova el al., 2015; Carlsson et al., 2002), than in rodent islet capillaries (Jansson et al., 2016).

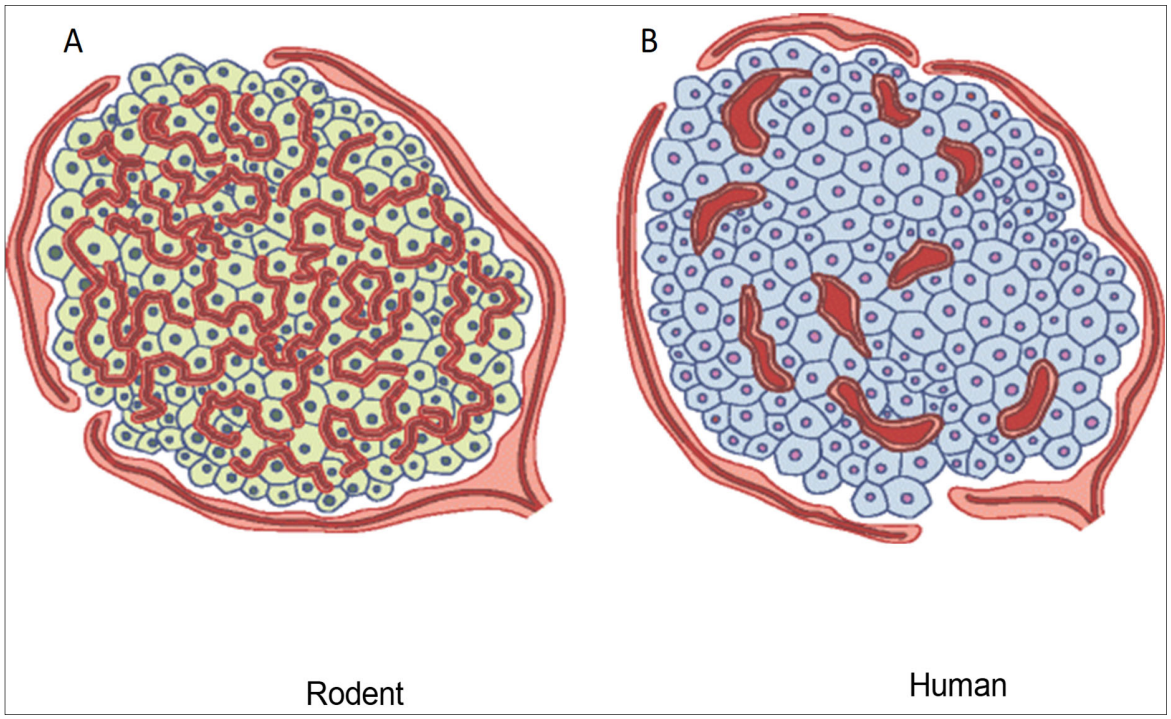

Adapted from Hogan & Hull (2017).

Figure 0.6: Schematic illustration of the significant difference in the islet microvasculature architecture between rodents and humans.

A) The rodent islets contain an extensive network of fine, tortuous capillaries. B) In contrast, human islets contain fivefold fewer, but larger vessels, which are less tortuous.

In either case, in humans, two to three arterioles supply larger islets branching from the closest exocrine intralobular arteries, which are sometimes tributaries to exocrine acini (Bonner-Weir,

1993). These arterioles have a diameter of about 20 to 30 µm and consist of one or (rarely) two layers of smooth muscle fibres, all surrounded by adventitial tissues containing fibroblasts and occasionally, adipose tissue (Lai et al., 2007). However, small islets are usually supplied directly by a capillary network serving the exocrine tissues (Bonner-Weir, 1993). Capillary walls consisting of a single layer of endothelial cells, thus, shortening the diffusion pathway between the blood and tissue fluid achieve this. The efficiency of diffusion is further enhanced by the slow blood flow in the islet, which helps to increase the time available for diffusion (Jacob et al., 2016). The anatomy of islet veins depends on the species and the size of the islet. Nevertheless, these veins remain very similar to those found in other regions of the body. Small islets as mentioned above, drain with exocrine cells whereas the large ones empty directly into one to four basket-like networks of one to four veins lying in the connective tissue between the exocrine tissues. The islet capsule drains into the intralobular veins and finally in the portal vein (Jansson et al., 2016). No valve or evidence of blood flow control has been described (Jansson et al., 2016). The largest islet in human and rodents has a so-called 'insuluno-acinous' portal system, which is a series of connected capillary systems that appear to be important in humans and primate islets, although not extensively studied (Bonner-Weir, 1993).

Islets themselves have no lymphatic vessels (O'Morchoe, 1997; Rubbia-Brandt et al., 2004, Källskog & Jansson, 2011; Korsgren & Korsgren, 2016). The protein-rich lymph collected from intercellular space is drained by peri-islet lymph vessels, which in turn drain into larger vessels, before returning into the systemic blood circulation (Korsgren & Korsgren, 2016). A lymphangiogenesis stimulator induces a marked increase in the number of lymph vessels, but still only on the periphery of the islets (Mandriota et al., 2001). This is also confirmed in the islet after transplantation (Källskog et al., 2006).

2.3.1 The function of islet cells controlled by the pattern of blood flow

Although there is a clear correlation between islets' endocrine activity and blood flow (Jansson et al., 2016), it does not provide a good explanation for paracrine islet interaction. When it was discovered that glucagon was required for the stimulation of insulin secretion (Samols et al., 1966) and insulin for the suppressing of glucagon secretion (Samols et al., 1969; 1971), the hypothesis of an intra-islet negative and positive insulin-glucagon feedback mechanism was proposed.

The close anatomical location of the two cells within the islet led to the hypothesis that the interaction between the cells types (Samols et al., 1966) may be via the inter-cellular fluid, a concept that was quickly rejected when somatostatin was observed to be a strong inhibitor of

both α- (Goodner et al., 1974) and β-cell secretions (Alberti et al., 1973). However, this hypothesis could be extended by considering that α-, β- and δ-cells mutually regulate the secretion of one another to maintain homeostasis of the body via the interstitial fluid (ISF). If one assumes that the above hypothesis is true, it is still not enough to explain how the three cell types could interact to maintain glucose homeostasis under particular metabolic needs. In states of hypoglycaemia, increasing glucagon and decreasing insulin secretions are essential for normalising blood glucose levels. However, this association could not be achieved when glucagon was accepted as an insulin secretion promoter (Samols & Stagner, 1988). The possible explanation for this assumption is that: 1) the glucose concentration alone in the local islet milieu could dictate cell-type activities, and 2) neurotransmitters, locally released may control cell-types that function in such a way that during an emergency, adrenergic and normal postprandial cholinergic supply is maintained (Samols et al., 1972).

To support the paracrine theory, it was postulated that there could be a physical barrier between cells to prevent α- and β-cell somatostatin receptors being overwhelmed by the high local concentration of the somatostatin hormone (Kawai & Rouiller, 1981). Although this hypothesis was accepted, questions remained unanswered about the preference or prevention of islet cell-type interactions (Samols & Stagner, 1988). The islet cell architecture triggers the idea of a potential blood flow pattern within the islet, which over the past decade has also shown serious controversy (Nyman et al., 2008).

2.3.2 Islet blood flow pattern controversies

It remains clear that consistent data on islet microvasculature is lacking (Ballian & Brunicardi, 2007). During a symposium on the *Microvasculature of the Islet* in 1995 (Brissova et al., 2006), no less than three models were presented, and researchers were still unable to provide definitive answers to the question around islet microvasculature (Brissova et al., 2006; Zanone et al., 2005). So far, no work has resulted in establishing the correct pattern of the islet microcirculature that could explain the supposed paracrine role (Stagner et al., 1989; Brunicardi et al., 1996; Samols & Stagner, 1990). However, investigators all support the hypothesis that the intra-islet capillaries are designed to maintain close contact with islet cells, with insulin-secreting cells having their apical side toward the endothelial fenestrae. Bosco et al. (2010) discussed the three proposed intra-islet microvasculature pattern models published to date (Figure 2.7).

The first model (Figure 2.7A) is based on the concept that hormones which are secreted by non-β cells affect insulin secretion by β-cells, which in turn cannot influence other secretions of islet hormones (Murakami et al. 1992; Murakami et al. 1993; Brunicardi, et al., 1996).

This model possibly occurs only in the islet phenotype with a special cellular arrangement where cell types are clustered in different regions, as seen in mice, rats and rabbits, having a β-cell core and a non-β-cells mantle region (Orci & Unger, 1975). Thus, afferent arteries close to the islet divide into several capillaries as they penetrate the islet by the mantle which is first supplied, this before continuing towards the core centre where they are converted into venules and exit the islet. Blood from the core then drains into larger pancreatic veins (insulo-venous drainage). These veins branch into capillaries that supply the exocrine pancreas, forming the insulo-acinar portal system. (Murakami et al., 1993; Ballian & Brunicardi, 2007). In some monkey species and horses, the perfusion is, however in the opposite direction to maintain the flow of blood from non-β-cells to β-cells in conformity with their cellular architecture (Brunicardi et al., 1996).

In contrast to the first model, the second model (Figure 2.7B) presents blood flowing from the β-cells rich core of the islet, to the non-β cell-rich mantle. This suggests that insulin secreted in the core by the β-cells affects the other islet cell types as capillaries run towards the surface of the islet while forming venules. In humans and some primates, the arrangement of islet cells is intermingled, especially in large islets making the blood pattern difficult to describe. Still, these islets could be considered as being formed by a fused smaller typical core-mantle islet, in which blood is perfused as mentioned above, in different units and form venules outside the unit before leaving the islets. In all cases, the capillaries of the islets eventually form venules and flow into larger veins. These veins branch again into capillaries to supply the exocrine glands, thus forming the insulo-acini portal system just like in the first model. Several isolated studies on pancreas perfusion have been used to evaluate the pattern of islet microvasculature. These investigators using immunoglobulins against pancreatic endocrine hormones used anterograde and retrograde perfusion and concluded that, in most of the species, the order of perfusion is from β-to-α-to-δ-cells (Stagner et al., 1989, Samols & Stagner, 1990).

In the third model (Figure 2.7C), the islet blood flow is described as feeding arterioles that penetrate one pole of the islet, branching into capillaries, supply cells and exit the islet through the other pole as venules, this before joining the insulo-acini system. In this model, blood flows through the islet regardless of the cell types. However, even though the order of islet cell perfusion is not fixed, in this model, investigators have described the regulation of blood flow through the islets by an external and internal gate (Aharinejad et al., 1993). The external gate controls the blood flow of the entire islet and is located at the terminal pole while the internal gate is located in the proximal capillaries, consisting of vascular ECs, and regulates the flow of the blood to a region of the islet with the same type cells. Here, under the influence of blood glucose levels, the vascular ECs dilate to occlude the lumen of a set of capillaries and thus direct

blood to a specific region of the islet rich in specific cell types. Therefore, in hyperglycaemia, a set of internal gates open and blood is directed towards the region of the islets rich in β-cells while the capillaries to the regions rich in α-cells are occluded. During low blood glucose levels, the opposite mechanism occurs.

In summary, the pattern of islet microvasculature is considered as the basis of the islet cellular intercommunication. Consequently, challenges of drug delivery within the organ remains an enigma, with more work on the matter being required. However, other factors such as haemodynamics are determinants for blood vessel functions (Wootton et al., 1983) and in the islet may play a major role in the pathogenesis of DM in humans.

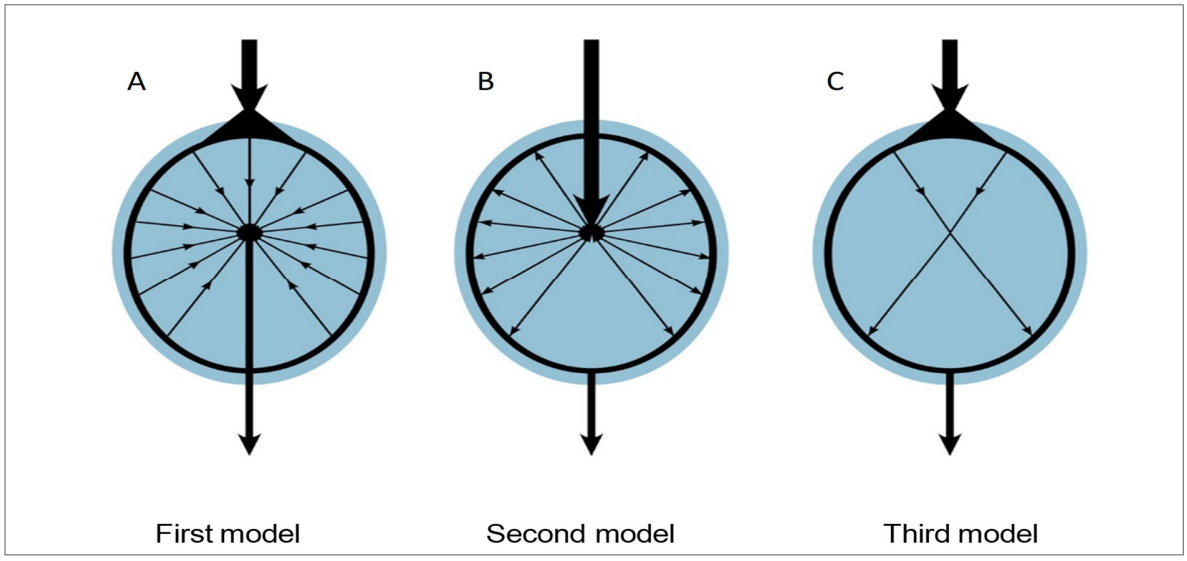

Adapted from Yousef El-Goharyl, (2018)

Figure 0.7: Schematic representation of the three blood flow patterns of islet microcirculation.

A) Secreting hormones from non-β-cells flow to the centre of the islet affecting β-cells. B) Blood carries insulin secreted by β-cells from the centre of the islet to the periphery to influence non-β-cell function at the periphery of the islet. C) Blood flow in the islet independent of cell types.

2.3.3 Islet cell function and haemodynamics

The word haemodynamic signifies the movement of blood and is, therefore, the area of study of the physical properties of the circulatory system (Secomb, 2016). Continuous monitoring and adaptation of the body to its environment are done by the haemodynamic response (Pries et al., 2005). This ensures the transportation of necessary elements such as O2 to the body for the maintenance of metabolism at the cellular level, of pH, osmotic pressure, temperature as well as the immune response (Secomb, 2016). To achieve this objective, the blood flowing in the

vascular tree must be maintained at a specific pressure in different segment levels (Tortora & Derrickson, 2012). The pressure of blood flow is related to the wall tensions and is a function of the topographical distribution and the structural property of the vascular tree. While the vascular tree topography includes parameters such as parent to daughter branching pattern, size (diameter), number of branching nodes per parent vessel, interbranching distances, branching angle and bifurcation indices, the structural property is concerned with characteristics of the wall (individual layer thickness) (Rizzoni et al., 2017).

In the body, all vessels have a wall and a lumen. The lumen is a hollow passage through which blood flows. The amounts of smooth muscle and connective tissue in the vessel wall vary depending on the diameter and function of the vessel, but the endothelial mucosa is always maintained (Alberts et al., 2002). Vessels are categorised into different types based on their histological structure: arteries, veins, arterioles, capillaries and venules. The wall of the artery is thicker than that of the vein. However they are structurally similar, consisting of three main layers: 1) the inner tunica intima, the thinnest of the three-layer made of a single layer of endothelial cells, separated from the media by the basal lamina, 2) the tunica media is the thickest layer in the artery made up mainly of circular smooth muscle fibres, it lies between the intima and tunica adventitia. The adventitia is the external layer, thicker in veins.

Most reports in the literature focused on describing the branching pattern of the pancreatic vasculature (Ebner & Anderhuber, 1985; Peri et al., 1969). Although histomorphological studies of different types of blood vessels have been done in other organs to solve several clinical problems e.g. uterus (AM & EA 2018), lungs (Bshouty 2012), heart (Velican & Velican, 1977; Keelan et al., 2016) to our knowledge, there is a lack of data on the detailed information concerning the pancreatic vessels in normal and diabetic conditions.

2.3.3.1 Principles of haemodynamics

A relationship between the elastic properties of the arteries and the rate of blood flow in the vessel is established. Similar to the circulation of fluids in a tube, the circulation of blood in the vessels is controlled by simple physical factors. Jean Léonard Marie Poiseuille (1797-1869) established the fourth power relationship between the flow rate and the diameter of a tube subjected to a fixed pressure gradient over its entire length. To illustrate this, Ohm's law states that currents in a cable can be calculated by dividing the voltage by resistance. I = U / R. When applied to the cardiovascular system, Ohm’s law is expressed as Q = (P1-P2) / R. Where;

U (voltage) = (P1-P2) (pressure difference)

R (resistance) = R (resistance)

I (current) = Q (blood flow)

The driving force for blood flow in the cardiovascular system is equal to the pressure difference between two given points in the vessel (P1-P2). In the human body, about 5 litres of blood circulate every minute representing about 80mL/kg body weight (BW). In fish, the pressure is lower and the total amount of blood perfused is small. For example, 20mL/kg BW only is perfused in one minute.

Resistance plays a very important role in Ohm's equation. In the equation, the resistance itself is dependent on the diameter and length of the vessel, and the viscosity of the blood (fluid). Normally, the viscosity and length of the vessel can be considered constant. The diameter of the vessel and the pressure difference remain the most important factors in this equation.

The difference in the degree of haemodynamic control and the resulting characteristics of microvasculature from one region of the pancreas to the other influence islet cell function. The development of pancreatic diseases such as insulitis in the region of the pancreatic head can be facilitated by such factors. It should be noted that in conditions of insulitis, which is characterised by the invasion of blood leukocytes into the islet, and which generally precedes the development of T2DM (Roberts et al., 2017), the perfusion of the pancreatic vasculature is very high (Roberts et al., 2017), and may be different from one pancreatic region to another. For example, studies of the brain have shown that there is a strong correlation between different areas of the chinchilla temporal cortex and the level of both vascular density and blood flow (Harrison et al., 2002); a condition associated with differences in metabolic demands. This correlation may be extrapolated in the pancreas which already displays a different regional distribution of cell type in the duodenal and splenic regions. Pancreatic β cells are well known to be metabolically more active than other cells (Farack et al., 2019) and are more numerous in the splenic region than in the duodenal region. (Savari et al., 2013). Factors defining haemodynamics in the rodent islet, for example, may differ between the core and the mantle and this could also be associated with the diseases of the pancreas. Therefore, to understand the factors that lead to the destruction of β-cells in an environment where many other cells are present in diseases such as diabetes, detailed mapping of the physical principles of blood flow is needed.

2.4 DIABETES MELLITUS AND ISLET MICROVASCULATURE

Hyperglycaemia causes multiple alterations of the integrity of the islet microvasculature. These are, the changes of vessel density and diameter (Canzano et al., 2019), the nature of ECs (Li et al., 2003), the amount of smooth muscle around the blood vessel, the number of connective tissues constituting the vascular wall and changes in the vascular functional signalling (Rask-

Madsen & King, 2005). All these hyperglycaemia-induced alterations result from the dysfunctionality of ECs detailed in the following section.

2.4.1 Endothelial dysfunction in diabetes

Diabetes and insulin resistance cause a combination of endothelial dysfunctions reducing the atherogenic role of the vascular endothelium.

2.4.1.1 Manifestations of endothelial dysfunction

The term endothelial dysfunction refers to "*impairment of the ability of the endothelium to properly maintain vascular homeostasis*" (Widlansky et al., 2003). When ECs are continually exposed to high glucose levels (>10 mMol/L) *in vivo* (Simionescu et al., 1996) and *in vitro* (Popov & Simionescu, 2006), they gradually lose their normal quiescent properties to a biosynthetic phenotype termed EC activation. As a result, EC dysfunction is established with the disturbance in the production and activities of multiple biochemical elements, which normally do not occur under physiological conditions (Pober & Min, 2006).

Insulin resistance precedes T2DM and remains the physiological mechanism that characterises the disease. There is a relationship between insulin resistance and endothelial dysfunction (de Jongh et al., 2004; Villela et al., 2006, Li et al., 2011; Ghosh et al., 2017). Endothelial dysfunction also precedes the development of T2DM (de Jongh et al., 2004; Villela et al., 2006). For example, the non-diabetic subjects with diabetic parents exhibit endothelial dysfunction and an increase in markers of endothelial activation in the plasma (Caballero et al., 1999; Balletshofer et al., 2000; Tesauro et al., 2007). Non-diabetic offspring of type 2 diabetic parents with evidence of glucose tolerance test also showed an elevation of systemic inflammation (Meigs et al., 2004; Meigs et al., 2006). A technique such as the magnetic Luminex assay allows for the determination of these markers in the blood serum very early before the onset of DM and hence helps in the prevention of the disease.

Similarly, other multivariable predictors of the occurrence of T2DM are flow-mediated dilation (Rossi et al., 2005) and polymorphisms of endothelial NO synthase (eNOS) (Monti et al., 2003). The fact that endothelial dysfunction precedes the development of DM indicates that there may be a common pathophysiological mechanism of a causal link between insulin resistance and endothelial dysfunction. Clinically, treatments such as resveratrol (Tabit et al., 2010) and Metformin (Nasri & Rafieian-Kopaei 2014) that improve insulin sensitivity automatically enhance endothelial function (Caballero et al., 2003; Tabit et al., 2010).

2.4.1.2 Mechanisms of endothelial cell dysfunction

Obesity and DM, play detrimental roles in the pathogenesis of atherosclerosis and cardiovascular diseases (Ghosh et al., 2017). There is increasing evidence that dysfunction of the vascular endothelium is early events in the pathogenesis of atherosclerosis and T2DM. The following section summarises the roles and underlying mechanisms regarding free fatty acids and glucose-mediated endothelial dysfunction using the literature. Endothelial cell dysfunction is characterised by altered EC signalling leading to increased oxidative stress, elevated expression of pro-inflammatory and pro-thrombotic factors, activation of protein kinase C (PKC), and abnormal vasoreactivity. All these factors decrease the mechanism of intracellular NO bioactivity (Barac et al., 2007; Tabit et al., 2010). Therefore, if the signalling pathways involved in free fatty acid and glucose-induced endothelial dysfunction are well-targeted, this could serve as a preventive approach against endothelial dysfunction and the subsequent complications such as atherosclerosis. These items are further clarified in the indicated paragraphs.

Activation of the eNOs

One of the most important mechanisms of EC dysfunction is an alteration in the intracellular signalling pathway that causes the activation of the eNOs (Tabit et al., 2010). This process is well studied (Figure 2.8): The production of NO in ECs depends on the enzymatic conversion of arginine to NO and cirulline by eNOs (Marletta, 1993; Zweier, et al., 1999). Endothelial NO synthase (enzyme) is normally expressed in caveolae. Caveolae are invaginated plasma membranes, rich in specialised lipids and proteins, for example, caveolin-1 (Shaul, et al., 1996). Normally, eNOS has a very low level of basal activity due to its association with caveolin-1 but becomes activated within seconds after stimulation of ECs by acetylcholine and serotonin. Endothelial NO synthase (enzyme) activation can be enhanced by other protein-protein interactions, oestrogen, bradykinin, shear stress via the activation of the phosphoinositide-3 kinase (PI3 kinase) and Akt (or protein kinase B) system (Dimmeler, et al., 1999; Montagnani, et al., 2001). Once produced, eNOs-derived NO diffuses locally into the arterial walls and activates guanylyl cyclase in smooth muscle (enhancing vessel dilation) (Figure 2.8A), platelet vessels and ECs to induce its biological effects. Insulin stimulates the activation of eNOs in the context of endothelial dysfunction in diabetics. The binding of insulin to its receptor (insulin receptor substrate, IRS) causes phosphorylation and activation of eNOs via PI3 kinase (Muniyappa & Sowers, 2013). Studies demonstrate that inactivation of endothelial-specific knockout of the insulin receptors reduced eNOs expression and caused vasodilatory endothelial insufficiency (Wheatcroft, et al., 2004; Duncan et al., 2008).

Increased oxidative stress

Another important mechanism by which the development of endothelial dysfunction is established in diabetes and associated conditions is the increase of oxidative stress. The exposure of the arterial tissue to high glucose and fatty acid levels cause the production of superoxide and a failure in the bioactivity of NO in the vascular walls (Inoguchi et al., 2000).

The increase in oxidative stress has a potential effect on the failure of eNOs bioactivity in several ways. The first reaction may be between superoxide and NO to produce peroxynitrite, a strong reactive oxygen species (ROS) and that of guanylyl cyclase in the smooth muscle of the vascular wall; a reaction which automatically does not only reduce the formation of NO but also that of the responsiveness of target tissues to NO (Zou, et al., 2002, Munzel, et al., 2005). Secondly, the cellular redox status of critical eNOs cofactors such as tetrahydrobiopterin is also influenced by ROS that uncouples eNOs and causes the production of superoxide rather than NO (Guzik, et al., 2002). Reactive oxygen species can also increase lipid peroxidation products that interfere with the receptors of the activation of eNOs leading to the inactivation of NO and a reduction of the responsiveness of target tissues to NO (Tong, et al., 2010).

Several sources of superoxide have been identified in the vascular tissue. One of them is the nicotinamide adenine dinucleotide phosphate-oxidase (NADPH oxidase), a membrane subunit highly involved in the cellular inflammatory process and normal EC signalling (Stocker & Keaney, 2004). Nicotinamide adenine dinucleotide phosphate-oxidase and superoxide are highly increased in pathological conditions such as in DM. Antioxidant treatments such as alpha-tocopherol restore the endothelial function under these conditions (Beckman, et al., 2003).

Even though oxidative stress contributes to endothelial dysfunction and that antioxidants can improve endothelial function in certain situations, large-scale treatment with alpha-tocopherol has failed to show the expected beneficial effects. A strategy prepared to inhibit the enzymatic source of ROS will be able to bring a greater relief in the treatment of endothelial dysfunction associated with DM.

Pro-inflammatory induced activation of endothelial cells

Pro-inflammatory factors such as tumour necrosis factor-alpha (TNF-α) and C-reactive protein activate the ECs to express adhesion molecules (Huang & Vita, 2006). Expression of adhesion molecules associated with other factors accelerates the inflammatory process of the EC leading to the reduction of eNOs cellular expression and the loss of NO bioactivity (Zhang et al, 1997; Verma et al., 2002).

Hyperglycaemia causes a systemic inflammation which impairs EC function and contributes to atherosclerosis (Beckman et al., 2002), which is why the level of circulatory inflammatory markers (TNF, interleukin intercellular adhesion molecule and C-reactive protein) is very high in diabetic patients (Dandona et al., 1998; Festa et al., 2000; Vozarova et al., 2001 Keaney et al., 2004).

One of the key regulators of endothelial activation is the transcription nuclear factor kappa B (NFκB), also linked to the pathogenesis of insulin resistance (Read, et al., 2006). Nuclear factor-kappa B is activated by inflammatory cytokines, free fatty acids, and the receptor for advanced glycation end products (RAGE) (Bierhaus et al., 1997; 2001; Kim et al., 2001). Hence, NFkB knockout prevents insulin resistance (Shoelson et al., 2006).

Activation of protein kinase C

Protein kinase C is a family of serine/threonine kinases with a crucial role in signal transduction of a wide variety of cell types (Nishizuka, 1984). The serine/threonine kinases family is formed by several isoforms, the most important being the PKCβ isoform which can be activated by the accumulation of diacylglycerol (Inoguchi et al., 1992) leading to the reduction of eNOs phosphorylation (Tesfamariam et al., 1991). During hyperglycaemia and elevated fatty acids in the blood (Figure 2.8B), diacylglycerol accumulates due to an alteration of mitochondrial substrates utilisation (Morino et al., 2006). On the other hand, PKCβ activates NFkB (Itani et al., 2002; Rask-Madsen & King, 2005). The bioactivity of NO is enhanced by inhibiting PKCβ (Kouroedov et al, 2004) thus preventing the development of endothelial dysfunction (Beckman et al., 2002). The link between inflammation, endothelial dysfunction and insulin resistance in DM can be explained by the activation of protein kinases (Dasevcime & King, 2007)

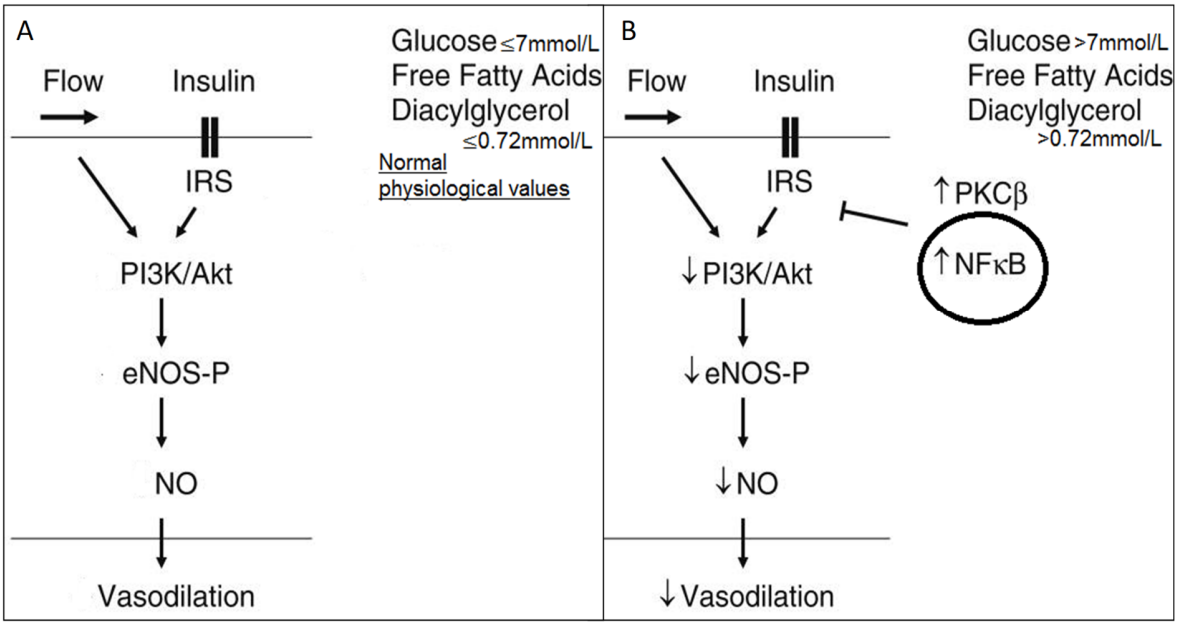

Adapted from Tabit et al., (2010)

Figure 0.8: Insulin-mediated activation of eNOS pathway.

A) In healthy condition (normal glucose and free fatty acid level), insulin binds to the insulin receptor in tissues leading to the production NO via a chain of a complex mechanism involving the phosphorylation of endothelial nitric oxide synthase (eNOS). B) Hyperglycaemia and obesity, on the other hand, causes the activation of PKCβ leading to the activation of NFκB, which blocks the insulin signalling and reduces the synthesis of nitric oxide (NO) and thus the vasodilatation.

Mitochondrial dysfunction

Recent studies have demonstrated proximity between mitochondrial dysfunction and the mechanism of increased formation of superoxide and activation of PKCs in the diabetic vascular system (Kim et al., 2008, Sergi et al., 2019). Under normal physiological conditions, the main function of mitochondria is to use oxygen to produce adenosine triphosphate (ATP), the main source of energy in the cell. However, 1 to 2% of the total amount of oxygen used by the mitochondria is devoted to the formation of superoxide (Chance et al., 1979). Superoxide is very important in cell growth, differentiation and programmed cell death (Bancroft & Gamble, 2008). Increase of ROS derived from mitochondria enhances the activation of a central regulator of cellular energy, AMP (5' Adenosine monophosphate-activated protein) kinase (Quintero et al., 2004), and leading to mitochondrial dysfunction. This abnormality is prevented by mitochondria-directed antioxidants, such as lipoic acid, and therefore improves insulin sensitivity, Akt-activation and NO-mediated vasodilation (Heitzer et al., 2002).

The mitochondrial dynamics that govern the formation of new mitochondria depend on eNOs and NO bioactivity (Nisoli, et al., 2003). The mechanism is altered in pathological conditions such as DM and is characterised by an accumulation of dysfunctional mitochondria. As a result, there is an increase in ROS and impaired ATP production (Twig, et al., 2006).

Increase circulating endothelial cell

Endothelial cells exposed to chronic hyperglycaemia may experience senescence and apoptosis (Piconi, et al., 2006, Liu, et al., 2014). This condition causes ECs to be detached from their BMs and released into the circulation. In the circulation, they are either detected as circulating mature endothelial cells (CEC) if detached as an entire cell or microparticles when the detachment is partial (Avogaro, et al., 2011). Circulating endothelial cell levels are therefore higher in Type 2 diabetic patients, irrespective of the level of glucose control. Coronary heart disease is predicted by elevated EC-derived endothelial microparticles in the blood, which is an even more significant independent risk factor than the presence of diabetes, hypertension or lipid levels. Endothelial cell apoptosis causes arterial denudation that induces a cascade of proatherosclerotic processes (Nomura, 2009).

The next section reviews studies highlighting morphological changes in the vascular structure under conditions of diabetes with the focus on the endocrine pancreas.

2.4.2 Examples of the implication of hyperglycaemia on the vasculature of tissue organs

2.4.2.1 The pancreatic environment

High blood sugar level causes dysfunction of ECs which lead to severe vascular structural changes. The morphology of the islet capillary in humans with T2DM presents with the following main changes: cell enlargement, in which about 36% is an increase in vascular density (Brissova et al., 2015; Shah et al., 2016), thickening and/or dilated and fragmented capillaries, irregular capillary morphology, thickening of capillary BM and increased abnormal endothelial permeability (Li et al., 2006; Roy et al., 2010). These changes are well documented in humans and a variety of rodents (Li et al., 2006; Shao et al., 2006; Lacraz et al., 2009). Recently, it has been shown that acute and long-lasting hyperglycaemia is associated with reduced glycocalyx dimensions, which may play a major role in ECs dysfunction under this condition (Cheng et al., 2016).

In combination, the phenotypes that characterise the EC under the insult of high glucose (HG) level demonstrate noticeable cell plasticity, associated with an alteration in specific molecules and intracellular biomechanical pathways. However, a common pathway leading to these

vascular dysfunctions has not been established. It has been observed that these vascular transformations are more pronounced in specific organs in the body such as the eye (retinopathy), kidney (nephropathy) and nervous system (neuropathy). Unfortunately, studies on the structure of the islet microvascular system on which the survival and function of β-cells depend under normal and pathological conditions have been neglected. In the next section, the pattern of the structural changes described in the eye in patients with retinopathy, as an example of an organ affected by DM, will be discussed.

2.4.2.2 The retina

Diabetic retinopathy (DR) is characterised by damage to small vessels of the retina. The disease affects about 100 million people worldwide and has become a huge burden in society (Antonetti et al., 2012; Duh et al., 2017; Leasher et al., 2016). The effects of hyperglycaemia on non-vascular tissues have been identified in the eye region and are very important in the development and progression of DR, albeit in unison with the vasculature (Duh et al., 2017). Diabetic retinopathy is classified into two main categories: 1) the non-proliferative diabetic retinopathy (NPDR) classified according to some visible features such as intraretinal microvascular abnormalities (IRMA), changes in venous size, microaneurysms and retinal haemorrhages and 2) the advanced stage of PDR, characterised by growing new blood vessels from the pre-existing retinal vasculature (also called pathologic preretinal neovascularization). Until recently, all visible features have been the mainstay for the detection and diagnosis of DR but with improved technology, the evaluation of more subtle pathology such as altered retinal function and neural layer abnormalities in patients is possible.

Diabetic macular oedema (DME) is a feature common to both NPDR and PDR (Duh, Sun & Stitt, 2017). The DME remains the primary cause of visual blindness in patients with DR and is a consequence of rupture in the blood-brain barrier. Blood-brain barrier rupture results in a leakage of intravascular fluid and circulating proteins that invade the neural retinal tissue (Frey & Antonetti, 2011). The extravasation of fluid into the neural retina causes an abnormal retinal thickening and sometime cystoid oedema of the macula (Duh et al., 2017).

Characterised histologically in certain long-term preclinical models and human post-mortem eyes, retinal vascular lesions are always preceded and/or accompanied by an early loss of pericytes and vascular BM thickening and eventual death of ECs, which are the main characteristics of vasodegenerative in early DR (Curtis et al., 2009; Mizutani et al., 1996). Notably, most processes leading to a vascular lesion in DR have a direct impact on vision. Loss of vessel integrity results in the progressive nonperfusion of the retinal vascular bed in NPDR, which eventually leads to occlusion or degeneration of capillaries with the development of some

localised ischemia (Stitt et al., 2016). Ischaemia results in an alteration in normal oxygenation levels, the driving force behind the origin of the expression of pro-angiogenic growth factors. The increase in growth factor production stimulates angiogenesis and leads to the formation of new vessels. The newly formed vessels protrude into the preretinal space, which can result in vitreous haemorrhage or retinal detachment resulting in severe vision loss (Stitt et al., 2016).

Basement membranes in the human retinal vasculature undergo diabetes-dependent alterations (To et al., 2013). It has been postulated that BM thickening in hyperglycaemia is associated with the following events: 1) formation of “advanced glycation end products” of BM proteins (Stitt et al., 1997; Degenhardt et al., 1998; King, 2001); 2) a strong increase of cross-linking and a decreased rate of BM protein degradation; and finally 3) an up-regulation of BM protein synthesis (Kuiper et al., 2008; Roy, et al., 2010).

However, research is still not clear on why and how BMs thicken and why such structural changes result in the chronic conditions associated with diabetes, such as diabetic retinopathy. Postulating that a too thick BM can prevent the passage of metabolic molecules and immune cells is a possible answer to this question. For example, impaired oxygen diffusion across the vascular wall contributes to hypoxia-induced uncontrolled angiogenesis in the retina and vitreous body, leading to delayed wound healing and peripheral nerve damage, (Kuiper et al., 2008). Thickening of the BM may also cause a reduction in vascular elasticity, thus inducing high blood pressure (Curtis et al., 2009; Zatz et al., 1986).

If retinopathy describes the standard structural pattern of the effect of hyperglycaemia on body tissues, then what are the factors or mechanisms that prevent this standard process to occur in nephropathy and neuropathy as the literature do not report these pathologies to be a consequence of excessive angiogenesis (Reidy et al., 2014)? Although the early stage of these pathologies (retinopathy, nephropathy neuropathy and other vascular diseases associated with high blood glucose level) always starts with the activation of ECs (excessive channelling of glucose intermediaries into various metabolic pathways with the generation of AGEs and ROS followed by tissue ischaemia), the mechanism that causes the later stage of these diseases in different tissues seems to take different directions. Few studies on the effect of insulin resistance and hyperglycaemia on the islet microvasculature are reported in the literature. Just as in the eyes, EC dysfunction in the pancreas causes thickening of BM but with less reported further events that finally may lead to β-cell death in the pre-diabetic state (Li et al., 2006; Roy, et al., 2010). However, assuming that unknown factors lead to insulin resistance in T2DM, for example, which associates islet microenvironment more often with higher sugar levels, how do beta cells remain extremely vulnerable to the condition?

2.5 VASCULAR REPAIR

It was thought that mesodermal cell differentiation into angioblasts and subsequent endothelial differentiation occur exclusively during embryonic development (Urbich & Dimmeler 2004). This dogma was reversed in 1997 with the publication of Asahara (1997) and peers who showed that purified CD34 and haematopoietic progenitor cells obtained from adult humans, differentiated *ex vivo* into cells possessing the properties of ECs. Investigators termed these cells "EPCs" and found that they expressed many other EC markers. At the site of ischaemia and wounds, these cells were being incorporated into neovessels.

The discovery of EPCs has given hope to scientists dedicated to research into the biological mechanisms that can replace mature and/or damaged ECs in the body. However, several studies support the idea that EPC alterations are involved in the pathological process of cardiovascular disease in diabetes, but several questions remain unanswered. In this section, the link between endothelial progenitor cells and vascular diseases in DM is discussed.

2.5.1 Endothelial progenitor cells

The origin and definition of EPCs have been controversial since their discovery (Asahara et al., 1997). Based on the selection of cell surface antigen expression, Asahara et al. (1997) isolated EPCs or angioblasts from human peripheral blood using magnetic grains. Endothelial progenitor cells are now known to be a distinct population of cells that can differentiate and promote vessel repair in adults (Urbich & Dimmeler 2004). However, no unique or specific protein marker can be used to isolate EPCs from the peripheral blood (Hirschi et al., 2008). Three general approaches of EPCs identification have been described in humans (Yoder, 2012).

One of the first and simplest methods is to collect low-density mononuclear cells (MNCs) from the peripheral blood and plant them in petri-dishes coated with fibronectin and covered with a culture medium enriched in foetal serum and endothelial factors (Asahara et al., 1997). Four to five days after culture, the cells floating in the culture medium are removed; cells adhering to fibronectin are examined morphologically for consideration as EPCs. However, this method lacks specificity and therefore cannot be recommended for either isolation or enumeration of EPCs (Yoder, 2012). Blood platelets, for example, are known to contaminate MNC preparations in this method (Prokopi et al., 2009).

The second approach in EPC identification is based on the particular pattern of cell surface antigen expression on the cell (Asahara et al., 1997). The fact that no specific marker for EPC is defined has rendered the isolation of EPCs over time very difficult. The use of CD34 and fetal liver kinase or kinase insert domain-containing receptor (KDR) in human subjects as markers

for EPCs were instituted and have continued to be used as substitute markers for the presence of a circulating cell lineage showing vascular reparative properties (Yoder, 2012). In addition to haematopoietic and progenitor cells, CD34 is also expressed on many other cell types such as mature ECs, epithelial, mesenchymal, and even cancer stem cell populations, and is therefore inadequate as a single marker for the discrimination of all putative cell lines.

Kinase insert domain receptor, on the other hand, is a VEGFR, also widely expressed on endothelial, cardiac and blood cells, and therefore not useful for discriminating between cell lines expressing CD34. Additional markers are certainly needed for the identification of functional EPCs (Peichev et al., 2000). Peichev et al. (2000) used adenosine phosphate 133 (AP133), a novel 120 Kd glycosylated polypeptide to separate peripheral blood cells as this cell marker is not expressed by mature ECs. Thus, co-expression of KDR and AP133 on CD34-positive cells phenotypically identifies a unique population of functionally CEPCs.

The third approach used to identify human circulating EPCs is based on the colony-forming ability of *in vitro* plated MNC (Ito et al., 1999). This method was an expanded form of the first method (Asahara et al. 1997) in that blood cells were isolated and plated in fibronectin-coated petri dishes twice: first for 24 hours and then for 7 days. The reason for the pre-planting was to remove any circulating monocytes, macrophages or mature endothelial cells from the MNC fraction that could contaminate the putative EPC test system. While commendable, the impact of the method was diminished because investigators could not prove that all of these cells were depleted. The method was then improved by Hill et al. (2003) who brought pre-planting to 48 hours and the test has been commercialised since then.

2.5.2 Origin of endothelial cell during tissue repair

Endothelial progenitor cell lines are derived from different precursors cells. During tissue repair, ECs ($CD14^{++}$, $CD34^{+++}$, CD133) may be formed from several possible sources of EPCs (Figure 2.9) and other circulating progenitor cells and circulating mature ECs; the bone marrow-derived haematopoietic (CD34, CD45, $CD133^{++}$) (Jackson et al.,2001) and mesenchymal (C-kit, CD34) (Sabry et al.,2016) stem cells and the non-bone marrow tissue-resident (C-kit) (Beltrami et al., 2003) stem cells (Urbich & Dimmeler 2004, Mutin et al., 1999). Although haematopoietic stem cells (CD14+, CD45) are the direct precursor of EPCs, EPCs may also be generated from their myeloid differentiated cells in the process of monocytes and macrophages formation.

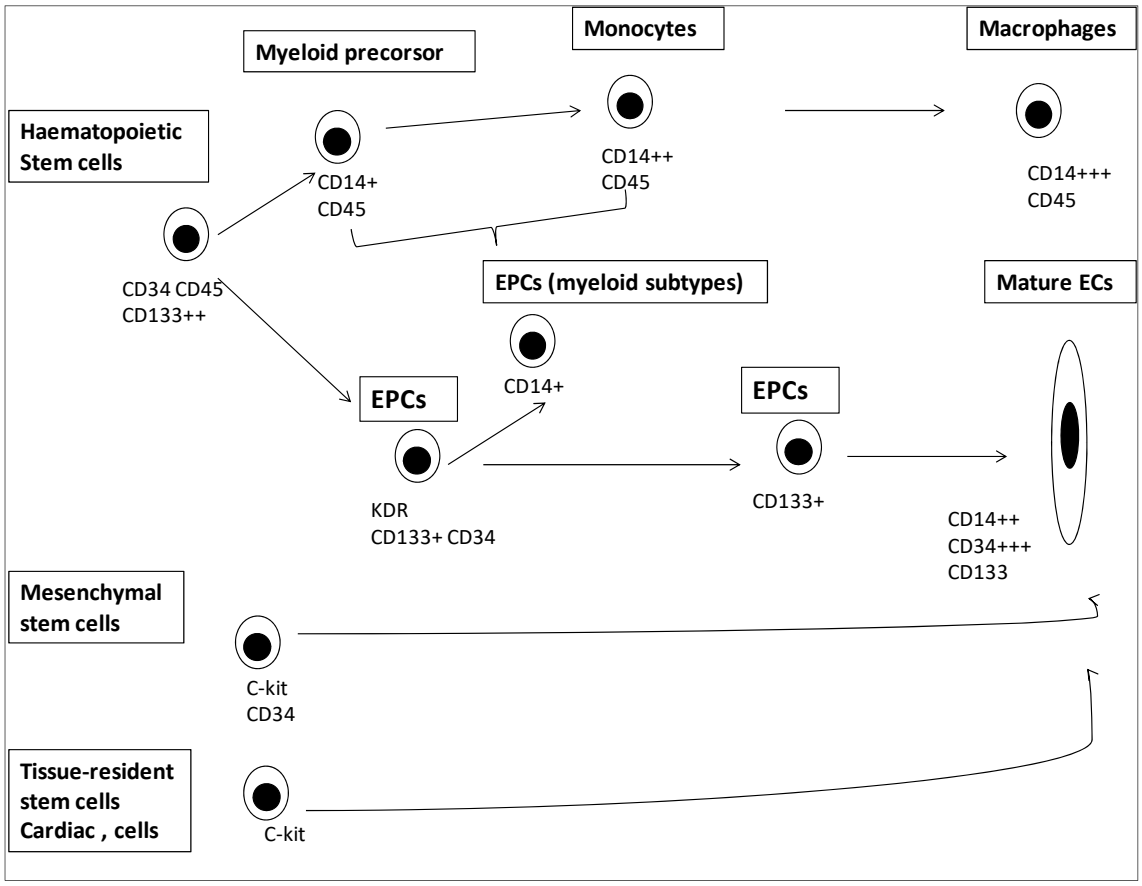

Adapted from Urbich & Dimmeler 2004

Figure 0.9: Schematic representation of an overview of the potential origin of endothelial progeny and their specific biomarkers within the circulating blood.

2.5.3 Role of endothelial progenitor cells

Defining the role of EPCs remains complicated because so many different EPCs definitions have been used (Rafii & Lyden, 2003). A growing consensus is emerging that many circulating blood cells are involved in the process of forming new blood vessels as well as remaining novel therapeutic targets for disease of the cardiovascular system (Yagihashi et al., 2011). The controversy exists as to whether cells that have many characteristics of the haematopoietic lineage but participate in the formation of new blood vessels should be called EPCs or not. In clinical practice, circulating EPCs concentrations have been used as a biomarker for detection and disease staging (Alaiti et al., 2010). Patients with DM have impaired EPC function and therapeutic measures to restore EPC function have been proposed (Fadini et al., 2007). However, higher levels of CEPCs detected in the circulation of patients, predicted a better health outcome (Kusuyama et al., 2006).

2.5.4 The mobilisation of endothelial progenitor cells and mechanism of vascular repair

The number and function of EPCs appear to be inversely related to the severity and degree of atherosclerosis (Tepper et al., 2002; Loomans et al., 2004). In addition, growth factors and cytokines such as VEGF, SDF-1(stromal cell-derived factor-1), erythropoietin, and oestrogens may also stimulate the mobilisation of EPCs from their various sources in the body (Zampetaki, et al., 2008; Cubbon et al., 2009).

Endothelial progenitor cells in the circulation are directed towards the injured endothelium by chemokine signalling such as tissue hypoxia-induced increased expression of SDF-1. Facilitated by the interactions between SDF-1 and chemokine receptor CXC 4 (CXCR4), EPCs adhere to the injured site and begin to proliferate and to form new ECs or to release pro-vasculogenic cytokines (Ceradini et al., 2004). Once integrated into the injured site, EPCs intervene in endothelial repair either by proliferation or by the formation of new ECs or by releasing growth factors and pro-vasculogenic cytokines. These molecules are essential for the proliferation of local mature ECs or other EPCs (Rennert et al., 2012). Recent research has suggested that cardiovascular risk factors such as obesity and DM impede not only the differentiation and function of EPCs but also the recruitment of these cells (McClung et al., 2005; Avogaro et al., 2011; Lee & Poh, 2014; Stitt et al., 2016).

2.6 METHODS OF ASSESSMENT OF VASCULAR STRUCTURE AND FUNCTION

The primary method used to assess macrovascular structure is by means of ultrasound ('B-mode' imaging) with the focus on the carotid artery. The carotid artery is widely imaged as it is accessible, easy to measure and associated with cardiovascular events in adults (O'Leary et al., 1992). The intima and media thickness is reported in a combined fashion because ultrasound results of the intima cannot be separated from that of the media (Järvisalo et al., 2001).

On the other hand, microvasculature at the cellular level is very important and can reveal the global changes of an organ in a disease condition. However, the study of these tiny structures is challenging (Schatten, 2012). Several techniques have been used to demonstrate the microvascular system in humans and animals. These attempts were made to obtain the precise microvascular architecture of system organ but with controversial results (Aharinejad & Lametschwandtner, 1992). Despite the development of electron microscopy imaging, vascular corrosion cast techniques have remained the best choice in studying the 3-D topography of small blood vessels (Verli, et al., 2007). This technique started in a gross anatomy laboratory where the pursuit was to find a substance that could fill the major body space and vessels (Schatten, 2012). A few decades ago, methyl methacrylate and related compounds were used to obtain

replicas of blood vessels followed by their investigation under scanning electron microscopy. This achievement opened a new era in micromorphological research (Aharinejad & Lametschwandtner, 1992). This technique of exposing blood vessel patterns attracted the interest of numerous scientists endeavouring to solve several unanswered medical and biological challenges (Verli et al., 2007).

Several techniques have been used to study the endothelial function in humans which often evaluate NO-dependent vasodilatation. Otherwise stated, the evaluation of endothelial function involves the analysis of EC reactivity to vasodilator or vasoconstrictor stimuli, thus contributing to the advancement of the understanding of cardiovascular diseases and possible therapeutic targets (Verma, 2003), such as flow dilatation, venous occlusion plethysmography, and serum marker measurement. However, none of these methods has been applied in the clinical setting, due to the invasiveness, high costs and difficulty in standardisation of techniques (Brocq et al., 2008).

2.7 THE USE OF ANIMAL MODELS IN VASCULAR RESEARCH ASSOCIATED WITH DIABETES MELLITUS

Of all the living beings, humans are the most affected by DM and thus several investigations have been conducted to alleviate this disease burden (Mbanya et al., 2010). Unfortunately, for ethical reasons, humans are excluded in basic diabetic research, with the use of animals filling this void. Several animal species have been used for this purpose, with rodents being the most utilized because of their high availability, fast reproduction, both easy to house and maintain. In addition, rodent anatomy and physiology which shares many similarities with human anatomy, are well understood by researchers, thus making results easily applicable for clinical purpose if necessary (Dolenšek et al., 2015). Diabetic animal models are developed by different methods, namely, chemical (King, 2012), genetic (Drel, 2011), spontaneous autoimmune (Wei et al., 2011) and surgical models (partial pancreatectomy) (Brendle, 2010) to name a few. Chemical methods using diabetogenic compounds have been extensively used in diabetes research because they are inexpensive and easy to use (Tesch & Allen, 2007). Streptozotocin (STZ) has been one of the most frequently used as a compound that can selectively destroy β-cells leading to hyperglycaemia (Kwon et al., 1994; Chaudhry et al., 2013, Eleazu et al., 2013). In the past, STZ has been used mainly to generate T1DM. However, recently, Reed (2000) combined a high-fat diet (HFD) and a low dose of STZ to develop a diabetic animal model mimicking human T2DM. Note that STZ internalises in the β cells through the low-affinity GLUT2 transporters on their cell membranes (Eleazu et al., 2013; Lenzen, 2008; Narasimhan et al., 2015). Normally in humans,

the transporters are very reduced (1 to 2% in rats) on the β cell membrane (Eizirik et al., 1994, Tyrberg et al 2001). However, in malignant cells, the transporters are very high. Hence STZ has been administered to a human to selectively destroy malignant pancreatic cells (Flatt et al., 1987, Ledoux & Wilson 1984). Recently human β-cells transplanted into rodents were not destroyed in animals treated with high doses of STZ (Tuomilehto et al., 2001).

The use of animals in cardiovascular diseases associated with DM is well reported in the literature (Dufrane, Goebbels & Gianello, 2010; Thomas et al., 1999). However, little work has been done to quantitatively and qualitatively assess the characteristics of the islet microvasculature, which may be the leading cause of DM. For this reason, rodents have become a convenient model for such investigations when researching DM.

In conclusion, interesting work on the understanding of the genesis, pathophysiology and treatment of DM has led to the development of several strategies for the management of the disease. Today, in our society, sophisticated techniques and the high quality of drug delivery has helped to control the blood glucose level in patients with DM. However, cardiovascular disorders associated with high blood glucose levels remain the main cause of death in these patients, conditions which appear to begin even before the onset of the disease, triggering an alarm on the integrity of the pancreatic vascular system from which insulin is secreted. The title covered in this chapter is displayed below (Figure 2.10).

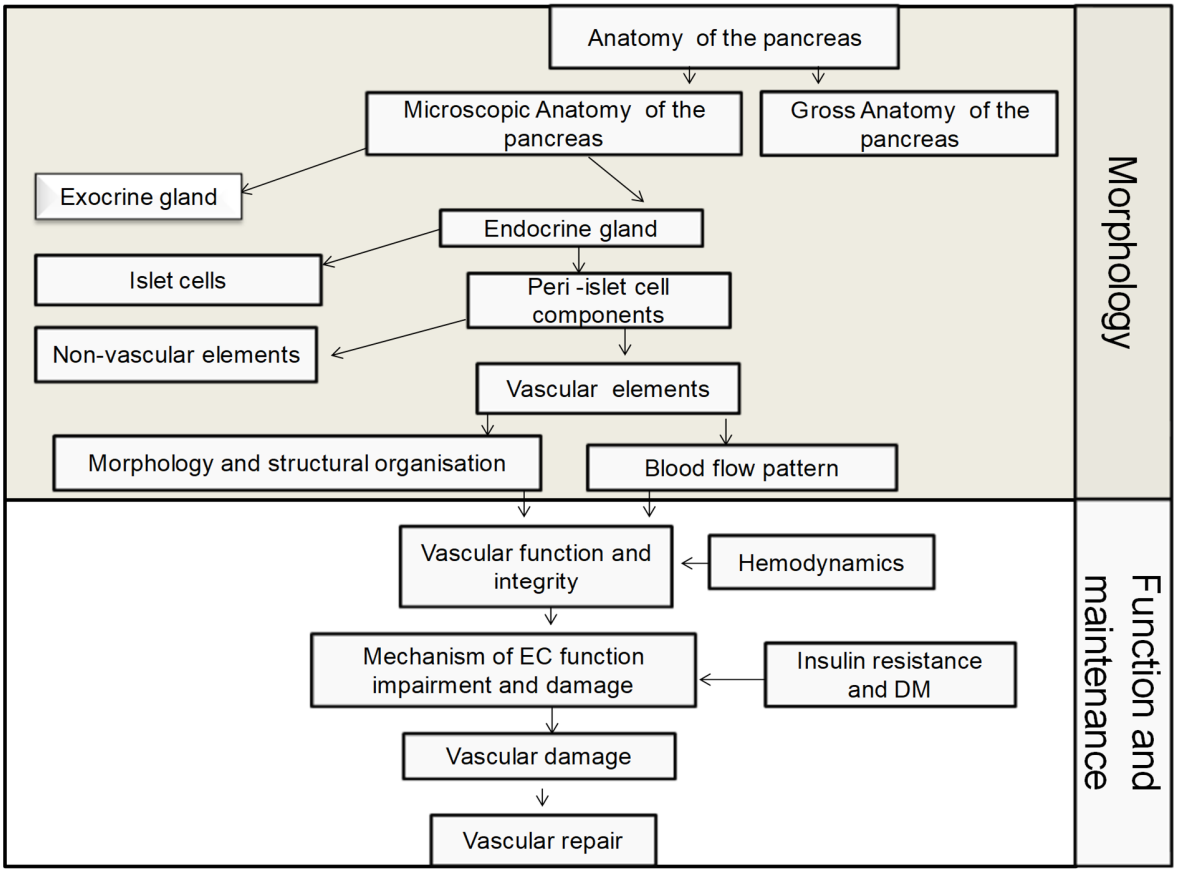

By E. Ngounou

Figure 0.10: Flowchart presenting the chapter headlines.

CHAPTER 3: MATERIALS AND METHODS

3.1 MATERIALS

Human and rodent pancreases have minor morphological differences but are similar in function (Dolenšek et al., 2015). However, Wistar rats (*Rattus norvegicus*) were used in this study because they were readily available and their large size (in contrast to mice, which are smaller) favours easy access to their organs. On the other hand, oestrogens reportedly prevent the full diabetogenic effects of STZ (Le May et al., 2006); therefore females were not included in this study. The details of the ethical clearance, animal sampling, treatment, and experimental procedures used to test the study hypothesis are the focus of this chapter.

3.1.1 Ethics

Ethical approval (Reference number: SU-ACUD 15-00009) was obtained from the Stellenbosch University (SU), Research **Ethics Committee**: **Animal** Care and Use (REC: ACU). The experiment complied with the guiding principles laid down by the Animal Welfare Organisation and the Society for the Prevention of Cruelty to Animal (SPCA), and all the recommendations of the declaration in accordance with the Animal Unit Guidelines for Use of Animals.

Individual animal records and daily monitoring sheets (Appendix 1 & 2 respectively) adapted from those in the Animal Unit of the Faculty of Medicine and Health Sciences, Stellenbosch University were used to track the well-being of the animals during the whole period of the experiment (88 days). All the animal treatments and the laboratory procedures were performed at Stellenbosch University by the principal investigator under the supervision of a qualified veterinarian.

3.1.2 Source and condition of the animals

The Animal Unit of the Faculty of Medicine and Health Sciences, Stellenbosch University sourced and housed all the animals used in the study. Adult male Wistar rats (n=50) aged six to eight weeks (Wistar rats older than twelve weeks are highly vulnerable to STZ) (Wang-Fischer & Garyantes, 2018) were randomly selected and transferred 5 per cage from the source room to the experimental room, prepared for this purpose. Each cage is a large rectangular plastic container (58 x 28 x 29cm) which was lined with sterilised absorbent corncob bedding (Cobtech, Harrismith, South Africa) to improve animal comfort. Before data collection, individual animal's ear punch was used for animal identification; the animals were allowed to acclimatise to their new surrounding for a period of 10 days, while baseline bodyweights and fasting blood glucose

levels were monitored every 3 days. For further study, only the animals weighing between 200-300g and proven normoglycaemic during the 10 consecutive days were used.

The animals were kept in a room with a controlled temperature of 24–26°C and on a normal 12 hours light / dark cycle for the duration of the experiment. The experimental period was considered to be 88 days, starting on the day the animals were collected from the source room to the last day of the diabetic period and was split into 1) an acclimatisation period (10 days), 2) a pre-diabetic period (14 days), 3) a non-diabetic post-STZ injection period (4 days) and 4) a diabetic period (60 days) (Figure 3.1).

The rat's body weight (BW) and fasting blood glucose level (BGL) were recorded every 3 days using an electronic scale and an ACCU-CHEK Aviva blood glucose meter (Roche Diagnostic, South Africa) respectively. Blood used for the testing of glucose level was always obtained by pricking the animal tail with a sterile needle (Guerreiro et al., 2013) (Appendix 3). Food and clean water were provided *ad libitum.* However, the night prior to BW and BGL assessments, food was retrieved from each cage (animals were fasted overnight (12 hours). Because rodents are coprophagic (eating faeces) (Torrallardona et al., 1996), to obtain accurate fasting BGL results, animals were transferred into clean anti-coprophagic cages a night before the day of the blood glucose test, with no food but with clean water.

The daily food and water intakes per rat were recorded throughout the period of the experiment: every morning food was weighed before being supplied to each cage. The next morning, the remaining volume of food was weighed and the difference considered as daily food consumption per cage. The daily food consumption per rat was then calculated by dividing the daily consumption of each cage by the number of animals (five rats) in the cage.

This study had two distinct phases. While the first phase had two major experimental procedures aiming to induce DM and monitor the animals, the second phase consisted of three main experimental procedures conducted to obtain, treat and analyse the samples collected from the animals.

3.2 EXPERIMENTAL DESIGN AND DIABETES INDUCTION

The experiment was designed to develop the T1DM and T2DM animal models using STZ. These two models were to mimic human T1 and T2DM. Human T2DM is known to be preceded by a prediabetic period with insulin resistance (Skovsø, 2014). Therefore, insulin resistance was induced in animals using HFD before the injection of STZ.

3.2.1 Induction of insulin resistance

After ten days of acclimatisation, animals were divided into two main groups (Figure 3.1): the first group named RAC (n=30) continued to be fed with the standard rat chow (RAC) (Atlas Animal Feed, Cape Town) (Appendix 4), while the second group, named HFD (n=20) was exposed to a diet with a high-fat content (HFD). The two groups were maintained for 14 days under their respective diets before undergoing an oral glucose tolerance test (OGTT). After the OGTT, the RAC and the HFD groups were further divided into two and three subgroups of 10 animals each, respectively. The three subgroups from the RAC were named NC (Normal Control, n=10), C-SSC (Control to STZ induced T1DM, n=10) because they received the sodium citrate buffer solution (SSC) and RAC / STZ (STZ induced T1DM; n=10) as they received STZ solution.

The two subgroups from the HFD group were named C-HFD / SSC (Control to HFD / STZ induced T2DM n=10) and HFD / STZ (STZ induced T2DM n=10) (see Figure 3.1 below). The NC, C-SSC and C-HFD / SSC subgroups served as control animals: NC (healthy untreated subgroup) control to all the subgroups, C-SSC control to RAC / STZ and C-HFD / SSC control to HFD / STZ (see Figure 3.1). An evaluation of the pre-diabetic state of the RAC / STZ and HFD / STZ animals subgroup was conducted prior to diabetes induction (STZ injection) using an OGTT.

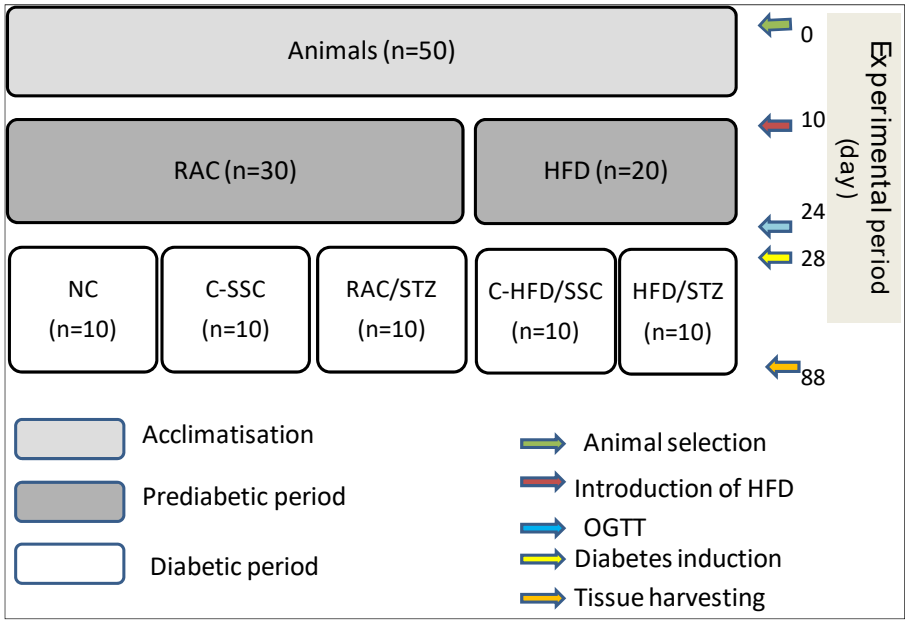

By E. Ngounou

Figure 0.1: Animals' distribution, treatment regimen and monitoring.

Day 0 marked the first day of the experiment when the animals were collected from the source room for acclimatisation, day 10 the introduction of HFD for the induction of insulin resistance, day 24 the administration of STZ for the induction of T1DM and T2DM, day 28 the confirmation of diabetes (BGL > 15 mMol/L) and hence marking the first day of the diabetic period. Finally, day 88 marked the day of sample (blood and tissues) collection.

The HFD consisted of 33% RAC supplemented with 7% sucrose (Illovo, SA), 33% condensed milk (Nestlé, SA) and 15% cooking fat (Hudson & Knight Ltd, SA) by weight, the remainder being added water (Salie et al., 2014) (Figure 3.2). In other words, to obtain 100g of the HFD, 33g of RAC, 33g of condensed milk, 15g of cooking fat, 7g of sucrose and 12g of water were mixed in a plastic container. 400-600g of HFD was prepared and kept in the refrigerator (4°C) to feed both HFD groups (C-HFD / SSC and HFD / STZ) for three consecutive days. The amount of the food to be given to the animals each morning was weighed, and allowed to warm at room temperature for 30 min before being supplied. If after the 3 days there was any remaining food left, it was discarded and a new one prepared.

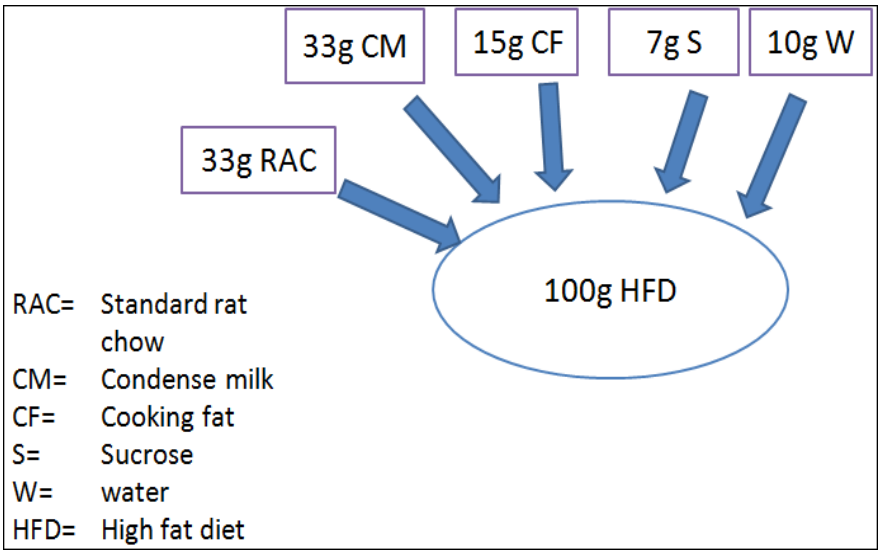

By: E Ngounou

Figure 0.2: Schematic representation of the percentage by mass of each component present in the high-fat diet (HFD).

3.2.1.1 Oral glucose tolerance test

A day before the oral glucose tolerance test (OGTT), each animal subgroup (RAC / STZ, HFD / STZ) fasted overnight. The following morning, after recording the baseline BW and BGL (as described in section 3.1.2), a dose of 3g/kg BW of a 30% Dextrose (D-glucose) solution was

administered orally to each animal via a gavage needle (Appendix 5) (Yessoufou et al., 2011). The oral route was chosen in the study because it remains the best physiological route of glucose absorption in the body (Pacini et al., 2013). Immediately after the gavage, a timer was set at 0:00 seconds to start timing. Subsequently, blood glucose levels were recorded at the following time intervals: 3 minutes (min), 5min, 10min, 20min, 30min, 45min, 60min, 90min and 120min. Animals were returned to the experimental cages for diabetes induction.

3.2.2 Diabetes induction

Previous studies revealed that a high dose of 45-65mg/kg BW is the common doses of STZ used for the induction of T1DM (Litwak et al., 1998; Zarros et al., 2009; Wang-Fischer & Garyantes, 2018) and a low dose of 35mg/kg BW is the best dose for T2DM induction (Skovsø, 2014, Srinivasan et al., 2005). Therefore doses of 50 and 35mg/kg BW were chosen to be administered to RAC / STZ and HFD / STZ subgroup respectively.

3.2.2.1 Type I diabetes mellitus: Streptozotocin-induced diabetes mellitus

Upon completion of the OGTT, each animal in the RAC / STZ subgroup (n=10) received an intraperitoneal injection of a single dose of 50mg/kg BW of STZ solution (Appendix 6). A 2% sucrose solution in addition to clean water was supplied to the animals for 48 hours immediately after STZ injection to prevent sudden hypoglycaemia (Litwak et al., 1998; Tesch & Allen, 2007). Streptozotocin (Sigma-Aldrich, Missouri, USA) was dissolved in SSC 100mM, pH 4.5 (SABAX, Port Elizabeth, South Africa) to obtain a solution of 10mg/mL. The solution was administered to each rat within 5min of being dissolved because, in the SSC, STZ is not stable and degrade within 15-20min (Litwak et al., 1998). Three to four days later only animals with fasting BGL ≥ 15mMol/L (Vella et al., 2017; Lotfipour & Smith, 2018), and maintained for 60 days (Lai & Lo, 2013), were considered diabetic.

Control animals to streptozotocin-induced diabetes mellitus

The animals (n=10) of this subgroup (C-SSC) received an intraperitoneal injection of a corresponding volume of SSC solution and were considered as the age-matched control group for the RAC / STZ group.

3.2.2.2 Type II diabetes mellitus: High Fat Diet-Streptozotocin-induced diabetes mellitus

After OGTT, each animal in the HFD / STZ subgroup received an intraperitoneal injection of a single dose of 35mg/kg BW of STZ solution (Mahmoud et al., 2012). These animals did not receive an additional sucrose solution because their food was already very rich in sucrose. Only

animals with fasting blood glucose levels ≥ 15mMol/L, and maintained for a period of 60 days were considered to be diabetic.

Control animals to the High Fat Diet-Streptozotocin-induced diabetes mellitus

The animals (n=10) of this subgroup (C-HFD / SSC) were administered an intraperitoneal injection of a corresponding volume of SSC solution. These animals were considered as the age-matched control group to the HFD / STZ group.

The developed diabetic animal groups were intended to remain diabetic throughout the remaining duration of the study and hence the level of blood glucose in the body was the determining factor of all other assessment. We also calculated and recorded the success rate of the diabetogenic effects of STZ during the 60 diabetic days on the treated animals.

3.3 BLOOD AND TISSUE SAMPLES COLLECTION, PROCESSING AND STORAGE

Vascular changes under the insult of hyperglycaemia were assessed using whole blood and pancreatic tissue samples from all subgroups. The samples were collected at the end of the experimental period (day 88), processed and stored (details are discussed later in this chapter) The blood samples were intended for the isolation of the CEPCs, using flow-cytometry and detection of cytokines associated with vascular injury using the Luminex assay. Tissue samples were used for routine histological and immunohistochemistry investigations, as well as for corrosion cast techniques.

3.3.1 Blood sample collection

A day before the day of tissue collection, animals from all groups were anaesthetised for blood collection. Serum and peripheral blood mononuclear cells (PBMC) were isolated, collected and stored for further analysis. The details of blood collection are described below.

On the day of blood sample collection (diabetic day 60), each animal was removed from the experimental cage, the BW recorded and the animal placed in a transparent container containing 3% isofluorane vaporised in oxygen for anaesthesia. Complete anaesthesia was confirmed by pedal reflex, and the animal was subsequently positioned on its back to expose the jugular vein running midway between the shoulder and the superior edge of the sternum. A 5mL syringe equipped with a 25cc gauge needle was inserted obliquely and slowly into the blood vessel. A 4ml blood sample was withdrawn from each animal. Light pressure was applied to the site of the puncture wound immediately with a cotton-tipped applicator as the syringe was withdrawn to prevent haemorrhaging before the animals were returned to their cages. Thereafter, the animals were monitored for any sign of hypovolemic shock after the blood sample collection. The blood

obtained was immediately transferred into two separate labelled tubes: 1) 2mL in a serum separator tube (SST) stored at room temperature for 15-30min (Tanner et al., 2008) and used for the analysis of serum biomarkers (Appendix 7) associated with vascular injuries, and 2) 2mL in a heparinised tube, kept at room temperature for 24 hours or more (Betsou et al., 2019). This portion was used for the PBMCs isolation (Appendix 8) from which the CEPCs were to be detected and isolated using the flow-cytometric technique.

3.3.1.1 Serum separation and storage

Blood (2mL) in the serum separator tube (SST) was allowed to clot undisturbed at room temperature for 15-30min. The tubes were then centrifuged at 1,000–2,000xg for 10 min in a refrigerated centrifuge to separate the liquid fraction of the whole blood from the clotted fraction (blood cells). The resulting supernatant (serum) was pipetted and transferred to a polypropylene tube, apportioned into 0.5mL aliquots (serum), stored in cryovial, and transported at –80°C for 4 months without freezing-thawing until analysis. The remaining portion of the blood was discarded.

3.3.1.2 Peripheral blood mononuclear cell isolation and storage

Peripheral blood mononuclear cells include all cells in the peripheral blood circulation with a single distinct nucleus. Circulating endothelial cells (CECs), CEPCs, lymphocytes and monocytes belong to this group. Platelets and erythrocytes have no nucleus, while granulocytes have multilobed nuclei. Hyperglycaemia is known to cause the reduction and dysfunction of CEPC leading to impaired vascular repair in diabetic patients (Yu et al., 2016). Therefore in this study, the determination of the percentage of CEPCs in the blood was to confirm whether or not hyperglycaemia caused any disturbance of the vascular integrity in the diabetic animal models. PBMCs were isolated from the whole blood and the percentage of CEPCs determined in all the animal groups. The isolation of PBMC was done according to the manufacturer's protocol found in the booklet (Abcam).

Diluent, phosphate-buffered saline (PBS), wash buffer foetal bovine serum (FBS) and the freezing solutions used in this procedure were prepared and stored in the refrigerator (4°C), before the PBMC isolation. On the day of PBMC isolation, all solutions were removed from the refrigerator and warmed to room temperature (25°C). Thereafter, 1mL of heparinised whole blood from individual animals was gently diluted with 1mL of PBS plus 2% FBS in a different tube. Because each cell type had a specific density, a density gradient centrifugation process was used to separate the different cell populations. Thus 1mL of density medium (Ficoll-paque plus, density 1.077g/mL (Pharmacia, New Jersey, USA)) was loaded in a 15mL labelled

centrifuge tube. The diluted blood from each tube was layered over the density medium, with care taken not to mix the two fluids (Figure 3.3A). The tubes were then centrifuged at 400xg for 30min at room temperature (25°C).

After centrifugation, the upper plasma layer was aspirated and discarded, then the PBMC layer was collected (Figure 3.3B). The PBMCs were transferred into another 15mL centrifuge tube and resuspended in 10mL Dulbecco's Modified Eagle Medium supplemented with glucose, optimised for EC culture (DMEM X1 + GlutaMAX-1; Gilbco, Thermo Fisher Scientific, USA). The cells were then centrifuged at 200xg for 20 min at room temperature. The supernatant was aspirated and the cells again suspended to ensure that the density medium was completely removed from the sample.

After the supernatant was aspirated, 1.5mL of the freezing medium (10% Dimethyl sulfoxide (DMSO), 40% DMEM, 50% FBS) was added dropwise to the cells before being transferred into a 1.5mL cryovial (Bio-Lab). The cryovials were then placed in a controlled-rate freezer (-1°C per min) at -80°C for 24 hours and thereafter stored in liquid nitrogen until flow-cytometry analysis.

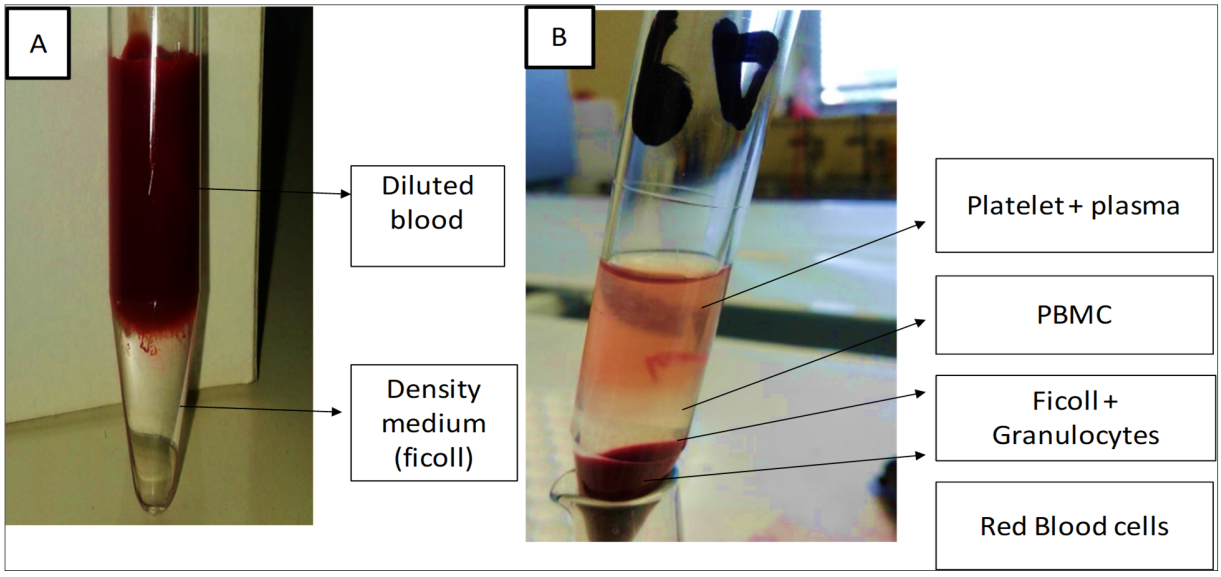

By: E. Ngounou

Figure 0.3: Peripheral blood mononuclear cells isolation:

A) Diluted blood gently superimposed on the density medium (Ficoll-paque plus) already at the bottom of the tube. B). Isolated PBMC is found between the plasma layer containing platelets above and ficoll suspending granulocytes layers below after centrifugation at 400xg for 30.

3.3.2 Surgery and tissue sample collection, treatment and storage

A day after blood sample collection, surgery was performed to harvest the pancreatic tissues for histological (histomorphology and immunohistochemistry) and vascular corrosion cast studies. Of the ten rats of each subgroup, five were considered for histology. The remaining five rats were used to obtain the pancreatic vascular corrosion cast.

3.3.2.1 Tissue harvesting for histomorphology and immunohistochemistry

On the day of tissue collection, the rats were placed in a transparent container and anaesthetised using 3% isofluorane vaporised in oxygen; complete anaesthesia was confirmed by the lack of pedal reflex and the anterior abdominal wall was shaved with an electric shaver before a midline laparotomy incision was made to gain access into the abdominal cavity. After reflecting the liver against the diaphragm, the segment of the duodenum in relation to the pancreatic head was sectioned and removed, along with the entire pancreas and the spleen (Figure 3.4A). The pancreas was immediately dissected as described by Tchokonte-Nana, (2011), weighed, the duodenal (head) and splenic (tail) portions isolated and stored in separate labelled bottles containing 10% formalin fixative (Figure 3.4B). The pancreatic tissue was stored in the fixative for more than 48 hours for proper fixation. Fixation provides the mechanical toughness to the tissue and prevents cell autolysis and tissue putrefaction (Singh et al., 2019). Once fixed, the tissues were moved into 50% ethanol until the time of routine histological procedures (Appendix 9).

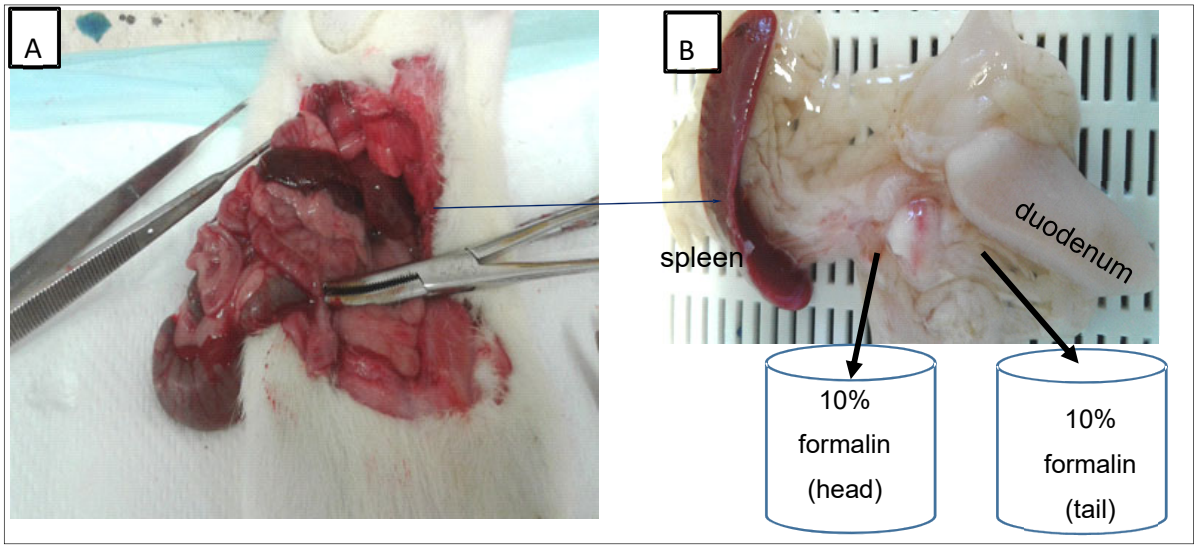

By: E. Ngounou

Figure 0.4: Pancreatic tissue harvested and method of preservation.

A) Pancreatic tissue just harvested with C-portion of the duodenum and the spleen. (B) Preservation of the duodenal and splenic portions in separate glass containers filled with 10% formalin for at least 48 hours to ensure proper fixation before the routine histological procedure.

Tissue sample preparation

Smaller pieces of properly fixed tissue samples were placed into labelled plastic embedding cassettes. The cassettes were then placed in an automated tissue processing machine (Shandon Elliott, OptoLaboratory, Cape Town) for tissue processing. Thereafter the samples were dehydration, clearing and infiltration through a passage in a series of graded alcohol, xylene and hot liquid paraffin (60°C) respectively. Each processed tissue was removed from the cassette and placed (embedded) in an individual metal mould containing melted paraffin wax (60°C) using the embedding machine (Leica Biosystems, Wetzlar, Germany). A properly labelled cassette was placed on top of the mould like a cover while the paraffin was still hot. The mould was allowed to cool and set on an icy surface. The embedding gives mechanical support to the tissue during sectioning. After paraffin solidification, tissue blocks (n=50) were removed from the mould and kept at room temperature until sectioning.

Tissue sectioning

Before tissue sectioning, each tissue block was trimmed to create an even, flat optimal surface area containing the sample and a small paraffin frame (Menon & Fisher 2015). After trimming, three sections were cut from each block using a rotary microtome (Leica RM 2125 RM, Leica Microsystems, Wetzlar Germany). A wet brush was used to gently hold and place the sections in a water bath at a temperature of 40 to 50°C to remove any folds or shrink. The two first sections (5µm thick) were used for routine histological staining (H&E and methenamine silver) while the third one (4µm) was used for immunohistochemical staining. The sections were each mounted on an appropriate microscope slide (BIO-SCAN, ABCAM, UK) and labelled as follows (Figure 3.5): a group name representing a treatment regimen (eg. RAC/ STZ); each one of the five rats in each group was identified by the pre-fix 1 to 5. The three sections representing the staining procedures used were attributed the indices 1 to 3 while the different portions of the pancreas were given a suffix ‘a’ (duodenal or head) and ‘b’ (splenic or tail). Therefore, a slide labelled, for instance, 1RAC / STZa1 mean the first serial section (1) of a duodenal portion of the pancreas (a) of the rat number one (1) in the RAC / STZ group. A total number of 150 slides were labelled and kept in the oven for 60min at 60°C before storage to enhance adhesion of tissue section on the slide. Labelled slides (n=50) carrying the same indices were placed in the

same slide box and underwent the same staining procedure. Boxes containing the slides were kept at room temperature for 2-3 weeks before the staining procedure.

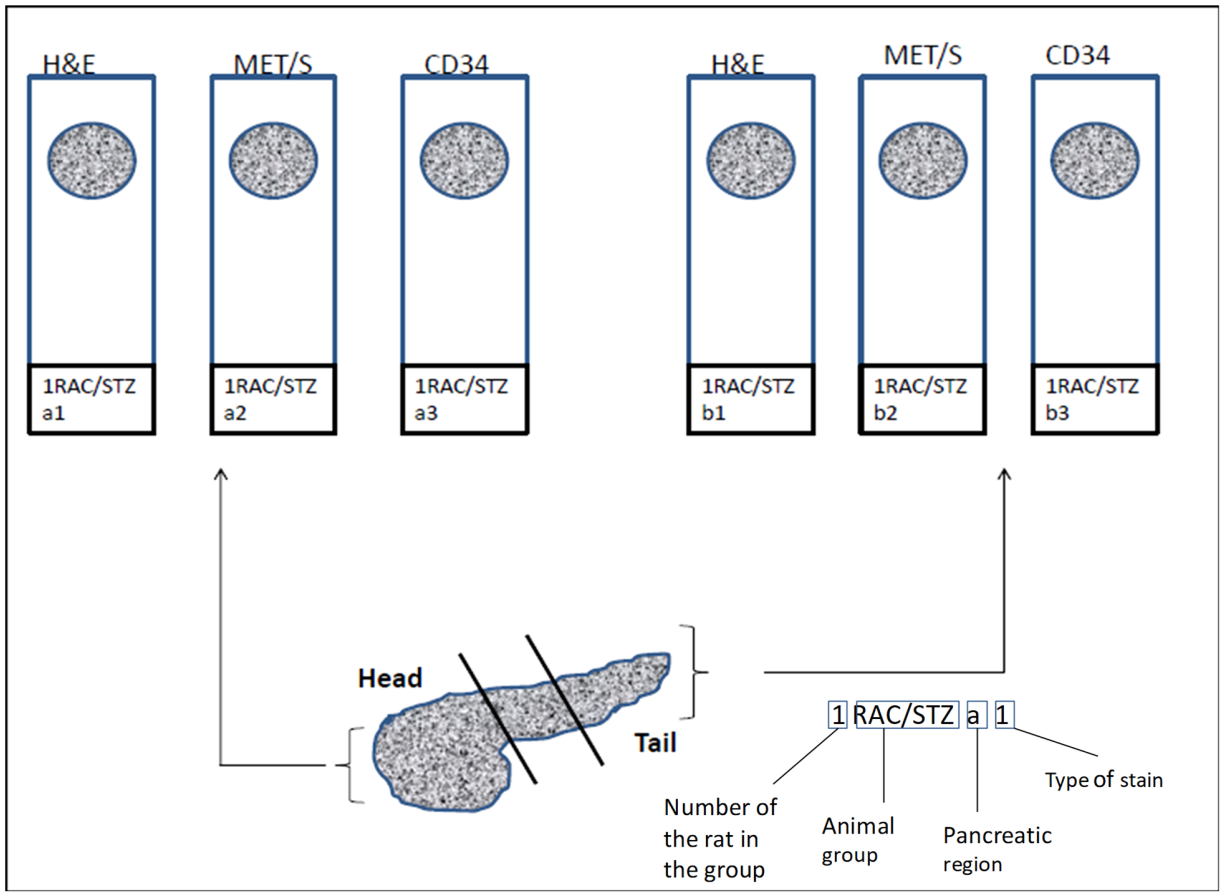

By: E. Ngounou

Figure 0.5: Microscope slide layout and labelling of pancreatic tissue sections.

3.3.2.2 Vascular pancreatic cast preparation

On the day of the casting, the pancreatic vasculature was prepared and perfused with polyurethane-based casting resin (PU4ii) (VasQtec, Switzerland) *in situ*. The vascular corrosion cast preparation involved the pre-casting treatment, the injection of the casting medium proper (Figure 3.6), the corrosion treatment and the drying procedure (Nebuloni et al., 2014, Verli et al., 2007).

Pre-casting treatment

Before the surgery, all perfusates (rising solutions and fixative) required for the pre-casting treatment were prepared and stored in glass bottles at room temperature overnight (Appendix 10). This included the PBS that was used to wash away the contents of the blood vessels and

to rinse the fixative after its use. A 2% glutaraldehyde was used to fix and increase the resistance of the vascular wall, a procedure that prevents the dilatation of the microvasculature during the perfusion of the casting medium. Note that the volume of this solution should just be enough (30mL for each rat for each solution) to clear the blood from the vessels. This is because too high volumes require longer perfusion time and produce tissue ischaemia and oedema (Aharinejad et al., 1993)

The following morning, intraperitoneal injection of 0.5ml sodium heparin (1000U/mL) (ABCAM, UK) was administered to the animal 10min before surgery to prevent the coagulation of blood in the capillaries (Martin-Orti et al., 1999). Animals were anaesthetised in a transparent container using 3% isofluorane vaporised in oxygen. Once anaesthesia was confirmed by the lack of pedal reflex, the animal was placed on the back to expose the anterior thoracic wall. Left and right lateral thoracotomy and a mid-line laparotomy were made to gain access to the thoracic cavity (Figure 3.6B). The left lung was displaced to expose and ligate the thoracic aorta at the level of the sixth thoracic vertebrae (T6) in the posterior mediastinum. An incision was made in the aorta at the seventh thoracic vertebrae (T7) through which a cannula (Fine Bore Polythene Tubing, Smiths Medical, UK, 0.58/0.98 mm ID/OD) was inserted (Figure 3.6C). To maintain constant perfusion and prevent leakage of the solutions, the catheter was ligated to the cut edge of the thoracic aorta. The free end of the cannula was attached to a 50cc syringe barrel containing 40mL of PBS heated at 37°C (Hossler & Douglas 2001, Satomi et al., 2003) (Figure 3.6D). The right atrium was sheared to provide an exit for the perfused fluid. After the perfusion of the phosphate buffer at a rate of 4mL per min, the discolouration of liver from dark red to light pink (because the blood in the liver tissue was replaced by PBS) indicated the effective perfusion, accompanied by the drained perfused fluid turning clear. After clearing blood from the vessels, the syringe containing PBS was removed from the cannula and was immediately replaced by one containing 40mL of 2% glutaraldehyde solution heated to 37°C (Christoffersonm & Nilsson 1988) (Figure 3.6D). The glutaraldehyde was then perfused to fix the vessel wall. Muscular tremor all over the body but mainly in the limbs indicated the effectiveness of the fixation. To clear the excess fixative from the vessels, the second perfusion of PBS was performed. Pancreatic vessels were thus prepared ready to accommodate the casting medium.

Perfusion of the casting medium

As described above, the pre-casting treatment prepared the vessels to receive the casting medium. The casting medium was prepared immediately prior to the perfusion by diluting an acrylic low viscosity PU4ii Resin (VasQtec, Switzerland) in 2-butanone (ACROS Organics

#149670010) and a blue dye (VasQtec, Switzerland) (Figure 3.6A) according to the procedure previously described by Krucker and colleagues (2006) (Appendix 10).

The hardener was added last to initiate the polymerisation (Figure 3.6E). The casting medium was then loaded in a 10cc syringe barrel. The syringe loaded with the casting medium was carefully attached to the free end of the cannula while preventing the entry of air. This was achieved by allowing the casting medium to flow while the syringe is attached to the cannula. The casting media was injected into the blood vessels by light pressure on the syringe barrel. The perfusion pressure of all the three fluids (PBS, 2% glutaraldehyde and the casting medium) was maintained to 110mm/Hg using a manual mercury manometer connected to a T-piece to the injection line. The injection procedure stopped once the excess resin began to extrude from the right atrium (Figure 3.6F). The perfusion time and the resin volume displaced in the syringe were recorded. After injection of the resin, the animal was kept in position for at least 30 min then placed in a hot water bath (60°C) for 12–24 hours to accelerate and complete polymerisation of the perfused casting medium. The immersion in the hot water bath helped reduce the corrosion time and kept the injected specimens in their natural form (Lametschwandtner & Weiger, 1990).

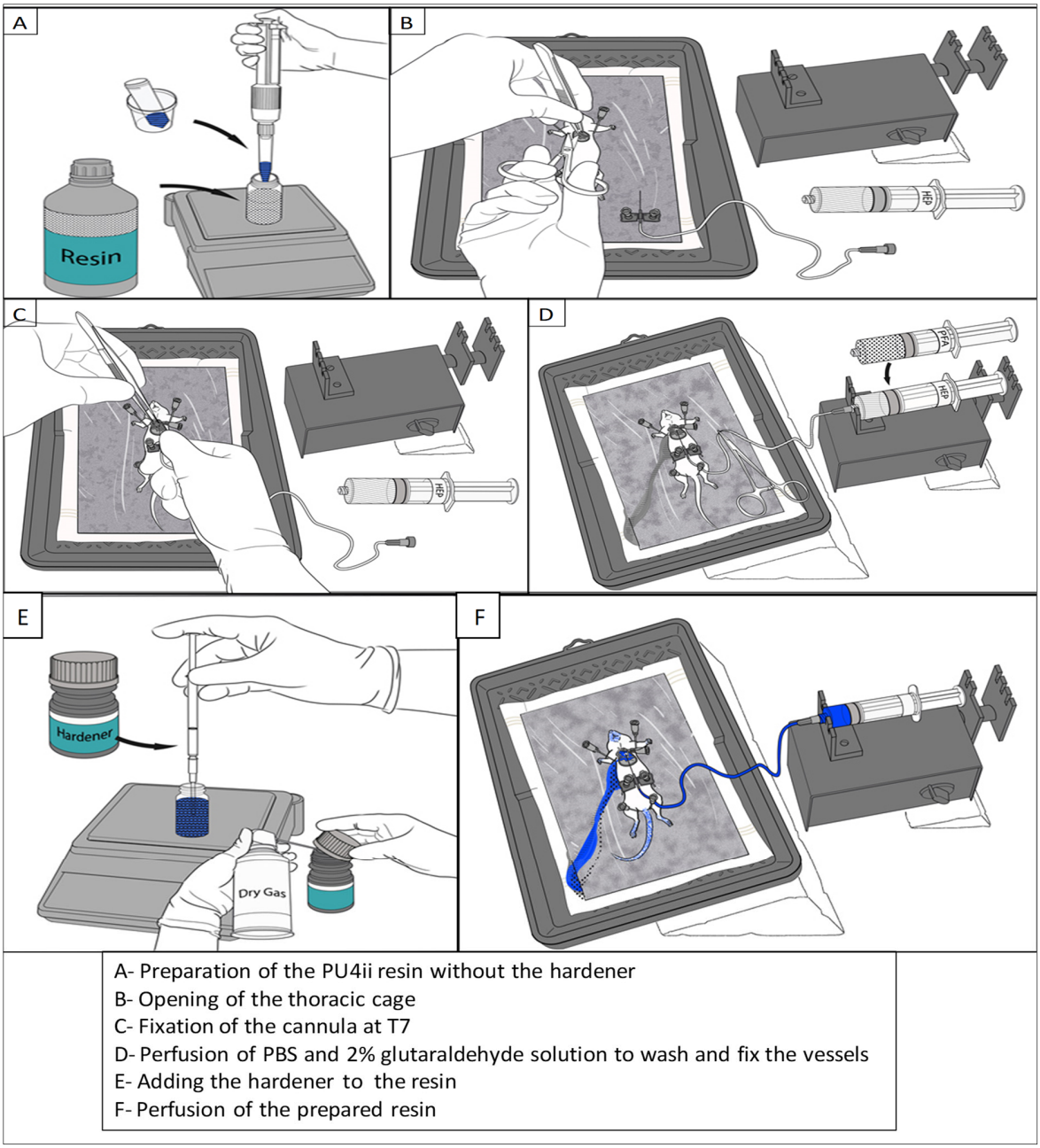

Adapted from http://www:vasqtec.com

Figure 0.6: Steps of the perfusion of the pancreatic tissue

A) Resin + butanone (diluent) + pigment (blue). B) Lateral incision through the thoracic cage and a midline incision of the abdominal cavity to expose the thoracic aorta and the liver respectively. C) Attachment of the needle to the cut edge of the thoracic aorta. D) PBS perfusion for clearing of blood from the vessels followed by the fixative to fix the vessel wall. E) Hardener added to the resin to initiate the resin curing process. F) Resin perfusion.

Tissue cast removal

After complete polymerisation, the resin in the small vessels of abdominal organs could be visualised with the naked eye (Figure 3.7). The liver, stomach, pancreas, intestine and spleen were gently removed from the abdominal cavity after sectioning the vessels attaching these organs to the posterior abdominal wall. The pancreas, as well as the associated duodenum portion and spleen, were detached from the remaining abdominal viscera and placed in a petri dish. Thereafter, the duodenal and splenic portions of the pancreatic gland were identified (Figure 3.7). To avoid tissue distortion during the corrosion procedure, the casted tissues were placed in a perforated embedding cassette and closed before being placed in the corrosive solution.

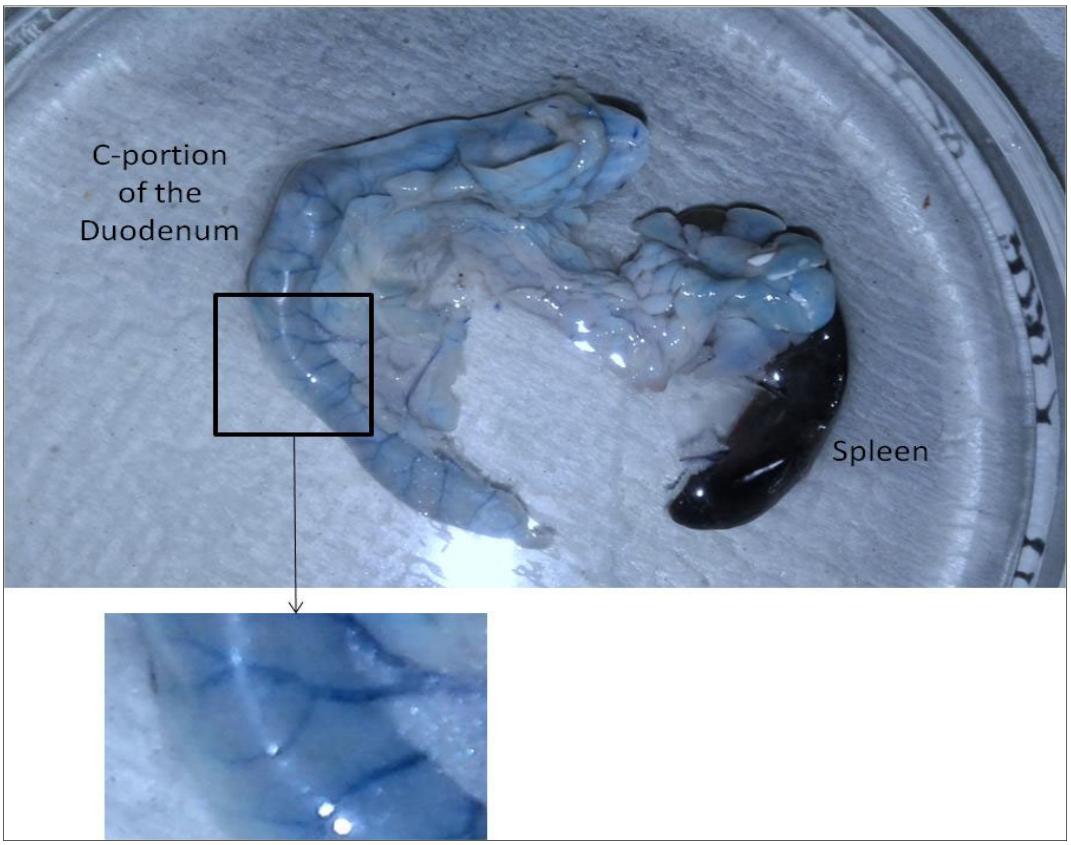

By: E. Ngounou

Figure 0.7: Pancreatic tissue and related duodenal part and spleen.

Below a section of the duodenum well-perfused showing small vessels filled harden resin under the transparent peritoneal covering x10.

Corrosion treatment

The tissue cast enclosed in the embedding cassettes underwent maceration to remove the soft pancreatic tissue surrounding the microvascular cast, using a concentrated solution of 20% potassium hydroxide (KOH), at 60°C overnight or longer (Satomi et al., 2003). After complete maceration of the pancreatic tissues, the resulting structure was the vascular (macro and micro) cast of the C-portion of the duodenum, the pancreas and the spleen. The cast was washed thoroughly and carefully under the running water first, then in 5% formic acid and then again into distilled water (Hossler & Monson 1998) (Figure 3.8).

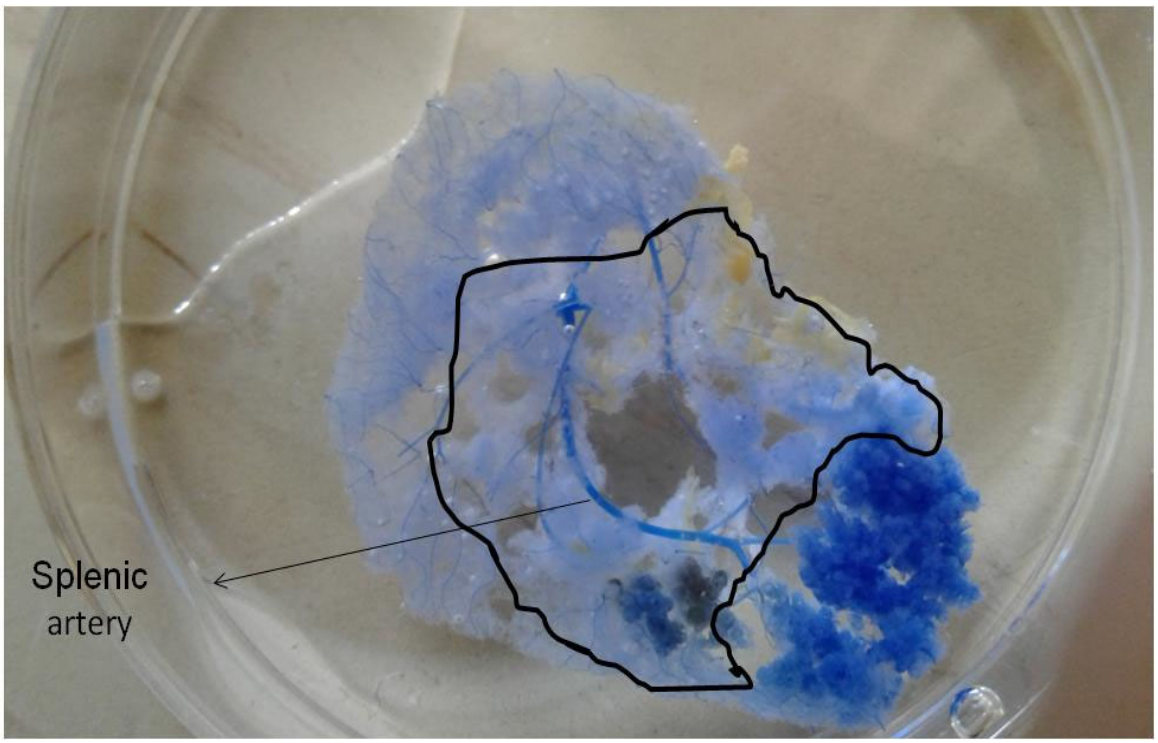

By: E. Ngounou

Figure 0.8: Pancreatic vascular resin cast (encircled).

The cast is showing the vasculature laying between the splenic (lower left) and the proximal portion of the duodenal vascular casts (upper right) respectively.

Drying of cast

The microvascular cast was exposed to ascending grades of ethanol (20, 45, 60, 75 and 100%) to promote low surface tension of the drying water. This prevented the cast from shrinking during drying. After drying, the casts were stored in a dry container at room temperature for visualisation under the Nano computed tomography scanner (nano-CT scan) (General Electric (GE) Phoenix

Nanotom S scanner). After the nano-CT scanning, the C-shape duodenal edge to the splenic tail of the pancreatic vascular casts along the axis of the splenic artery was measured. The length of the cast could give an idea on the width of the pancreatic tissue and the associated vessels. Remember that the pancreatic cast is the replica of the luminal volume of the pancreatic vessel.

3.4 ASSESSMENT OF HYPERGLYCAEMIA ON THE VARIOUS IMMUNODECTECTION PARAMETERS ASSOCIATED WITH THE INTEGRITY OF THE VASCULAR STRUCTURE

Three different immunological detection techniques were used to assess the effect of hyperglycaemia on the integrity of the vascular structure namely:

1) Luminex assay for the assessment of four major serum cytokines associated with vascular injury. This technique is a bead-based immunoassay system which detects multiple analytes during a single experiment,

2) flow-cytometry for the isolation and the evaluation of the percentage of CEPC in the PBMCs. this technique simultaneously analyses multiple parameters of a cell in a heterogeneous group of cells. A single cell is analysed as it passes through a narrow channel and is illuminated by a laser one by one (Figure 3.9) and 3) the immunohistochemistry using CD34 as a marker for endothelial cells on tissue sections.

3.4.1 Serum treatment and analysis for Magnetic Luminex assay

The levels of serum biomarkers for vascular injury were evaluated using Luminex screening assay techniques.

Magnetic Luminex assay multiplex (R&D systems, Bio-techne) with attached Luminex MAGPIX CCD imager was used to measure the level of the vascular injury biomarkers in diabetic animal models. Reagents for assays were developed by R&D System, Inc Minneapolis, MN 55413, USA). Four biomarkers presented in a single vascular injury panel (cat. No. LXSARM-04, Kit No L122445, Microparticle Mixlot No 1482413 and Biotin Antibody Mix No 1482414) were analysed. The panel included the following biomarkers tested at a dilution of 1:3: Interleukin-6 (IL-6), tissue inhibitor of metalloproteinase (TIMP-1), tumour necrosis factor-alpha (TNFα), and VEGF-A. For optimal sensibility, samples were well prepared prior to the assay. Diluents supplied by the manufacturer were used to dilute the unfiltered serum. Washing buffer solutions were all prepared and brought to room temperature before the commencement of the assay procedure.

3.4.1.1 Sample dilution and preparation

Samples thawed overnight at 4°C were brought to room temperature immediately before assay performance. Samples at room temperature were diluted with the assay diluent (calibrator diluent

RD6-52). The assay was strictly performed based on the manufacturer's instruction to Magnetic Luminex cytokine bead-based assays protocol (Figure 3.9) (Luminex High-Performance Assays from R&D systems). In short, diluted serum, a microparticle cocktail (diluted with diluent RD1W), and biomarker standards were added to a 96-well plate, while protecting the beads as much as possible from the light to prevent photobleaching. After two hours of incubation, the plates were washed and the biotin antibody cocktail (a mixture of the four antibodies) was added. Following an hour of incubation, plates were washed and streptavidin-Phycoerythrin (PE) was added for 30min, followed by a final wash and re-suspension in wash buffer. All incubations were carried out in the dark at room temperature on a microplate shaker at 800 rpm.

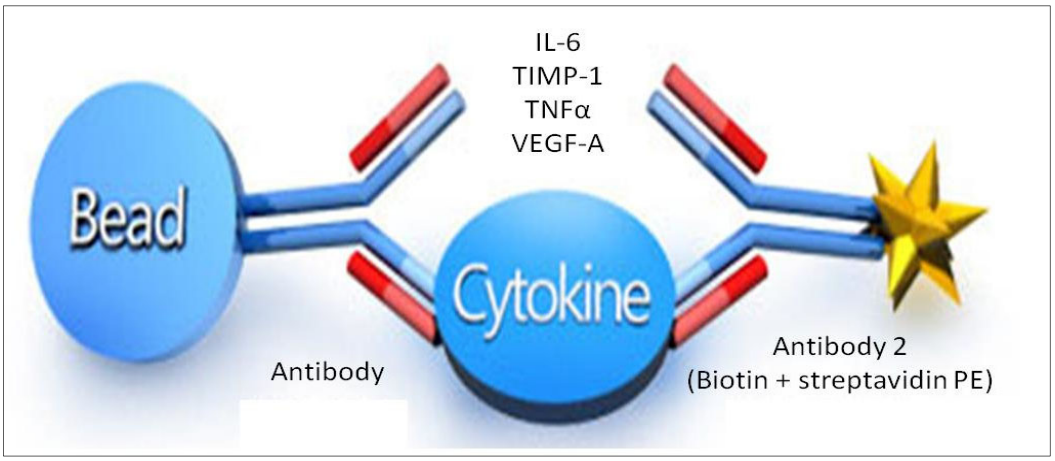

Adapted from Antigenix America.com (2019)

Figure 0.9: Principle of Luminex Assay.

3.4.1.2 Reading of the plate and data analysis

Thirty minutes before the assay procedure, the Bio-plex suspension array system was turned on to heat up, and the reader prepared to read. The vacuum apparatus was calibrated to ensure an optimal bead yield. Well-plates were placed on the Bio-plex® platform (Bio-Rad Laboratories, Hercules, CA, USA) and the vacuum turned with a pressure set to 1-2mm/Hg. Raw data were analysed using the Bio-Plex Manager version 6.0 software.

3.4.2 Isolation of CEPCs from the peripheral blood mononuclear cells using flow cytometry.

3.4.2.1 Cell preparation and labelling

Before the flow-cytometry analysis, the preparation of the cells was performed. Four antibodies CD31, CD34, CD45 and CD133 (Table 3.1) were used to assess the percentage of CEPCs in the

PBMC population (Liao et al., 2010). Antibodies, diluent and wash buffer solutions were all prepared and ready to use before the start of the flow-cytometry procedure (Figure 3.10). The procedure is described below.

A night before the day of analysis, samples were removed from the liquid nitrogen, thawed overnight at 4°C (Appendix 11). The next morning, while the samples were nearly completely defrosted, but were still cold, they were transferred from the cryovial to a 15mL centrifuge tube, and 1mL of warm wash buffer (at 37°C) was added to it dropwise. The samples were then centrifuged at 200xg at room temperature for 5min and after removal of the supernatant, the cells were re-suspended in 100µL Zombie Violet solution and incubated for 10-15min in the dark at room temperature. Zombie Violet is an irreversible cell viability fluorescent dye that is non-permeate to live cells but to those with compromised cell membranes (Paardekooper et al., 2019), and therefore it has been used in flow-cytometry to assess live versus the dead status of mammalian cells. The cells were then stained with pre-optimised volumes of CD133-allophycocyanin (APC), CD31-fluorescein isothiocyanate (FITC), CD34-phycoerythrin (PE) and CD45-Alexa-Fluor 700 (AF700) antibodies) and incubated for 15min in the dark at room temperature. A 1mL wash buffer was added to the samples, which were then centrifuged at 200xg for 5min at room temperature. The supernatant was aspirated, and the cells re-suspended in 500µL PBS. The samples were analysed within 30min on a calibrated 10 colours (3 lasers) Beckman Coulter Navios flow-cytometer, Navios software version 1.3 (Beckman Coulter Inc., California, USA) (Appendix 12) at the Flow-cytometry Unit of Tygerberg Hospital.

Table 3.1: List of antibodies used for CEPC detection using flow-cytometry.

Antibody	Fluorochrome	Clonality	Isotop	Vendor	Volume
Anti-CD31	Fluorescein isothiocyanate	Monoclonal (conjugated)	IgG1	Abcam	0.5µl
Anti-CD34	Phycoerythrin	Monoclonal (conjugated)	IgG1	Abcam	1µl
Anti-CD45	Alexa-Fluor 700	Monoclonal (conjugated)	IgG1	Biolegen	2µl
Anti-CD133	Allophycocyanin	Polyclonal (unconjugated)	IgG1	Abnova	200µl

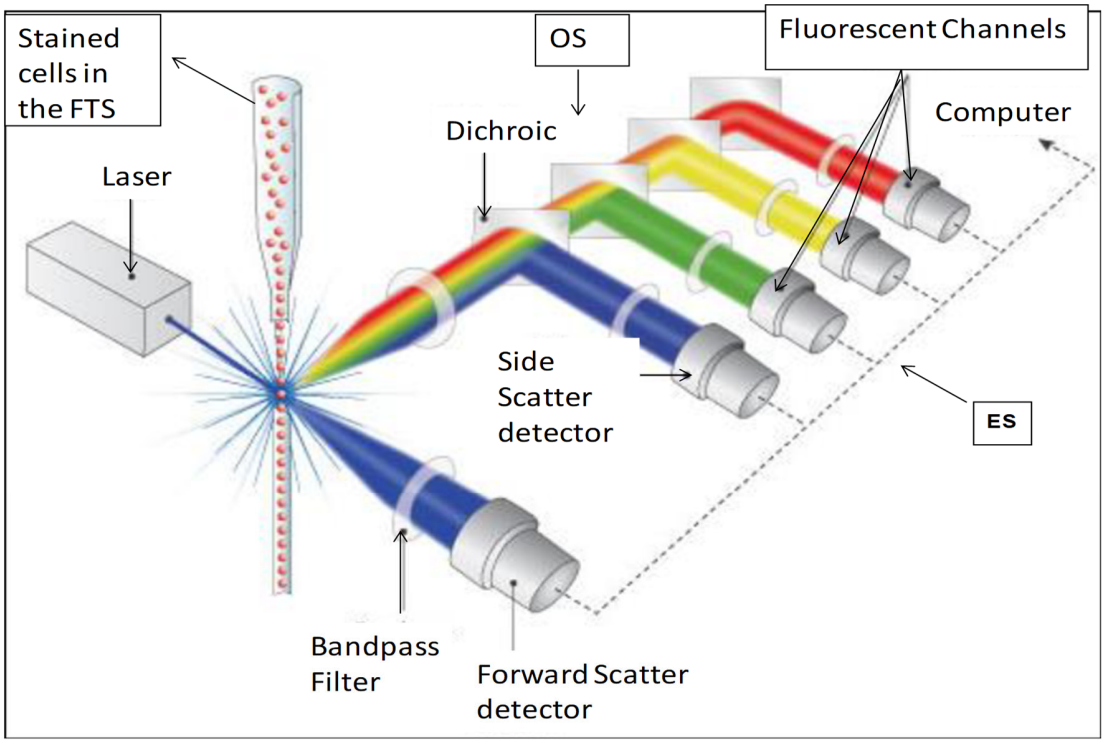

Adapted from https://www.semrock.com/flow-cytometry.aspx (2018)

Figure 0.10: The Basic configuration of a flow-cytometer

The fluid transportation system (FTS), the optical system (OS), the electronic system (ES), and the activated cells (ACS) sorter.

3.4.2.2 Flow-cytometry analysis and data acquisition

In this study, the percentage of viable CEPCs was gradually gated out from the PBMCs (Figure 3.11). Doublets were first eliminated in an FS peak vs FS interval dot plot (Figure 3.11A) followed

by the non-viable cells using Zombie Violet (Figure3.11B) then the lymphocytes and granulocytes using positive to CD45 (Figure 3.11C) and finally cells positive to CD133 (Figure 3.11D), CD34 and CD31 were isolated (Figure 3.11E). Details of each step are described in the following sections.

The flow cytometer was set to acquire either 100 000 total events per sample, or run for 10 min, whichever condition was reached first (Appendix 12). Cells were initially visualised on a density plot of forward scatter (FS) peak vs FS integral, and a gate was drawn around the single-cell population (“Singlet” gate). Following this, single cells were then visualised on a plot of an FS vs Zombie Violet, with a gate drawn around the living cells. On a plot of CD45-AF700 vs FS, a gate was drawn around CD45 positive (+) and CD45 negative (-) cells. On a plot of CD133-APC vs CD45-AF700, the cells were further gated on CD45+CD133+ and CD45-CD133+ populations. Cells were then visualised on a plot of CD31-FITC vs. CD34-PE, where a gate was drawn around the CD45-CD133+CD31+CD34+ cells, therefore gating for CEPC as previously described by Liao et al., 2010.

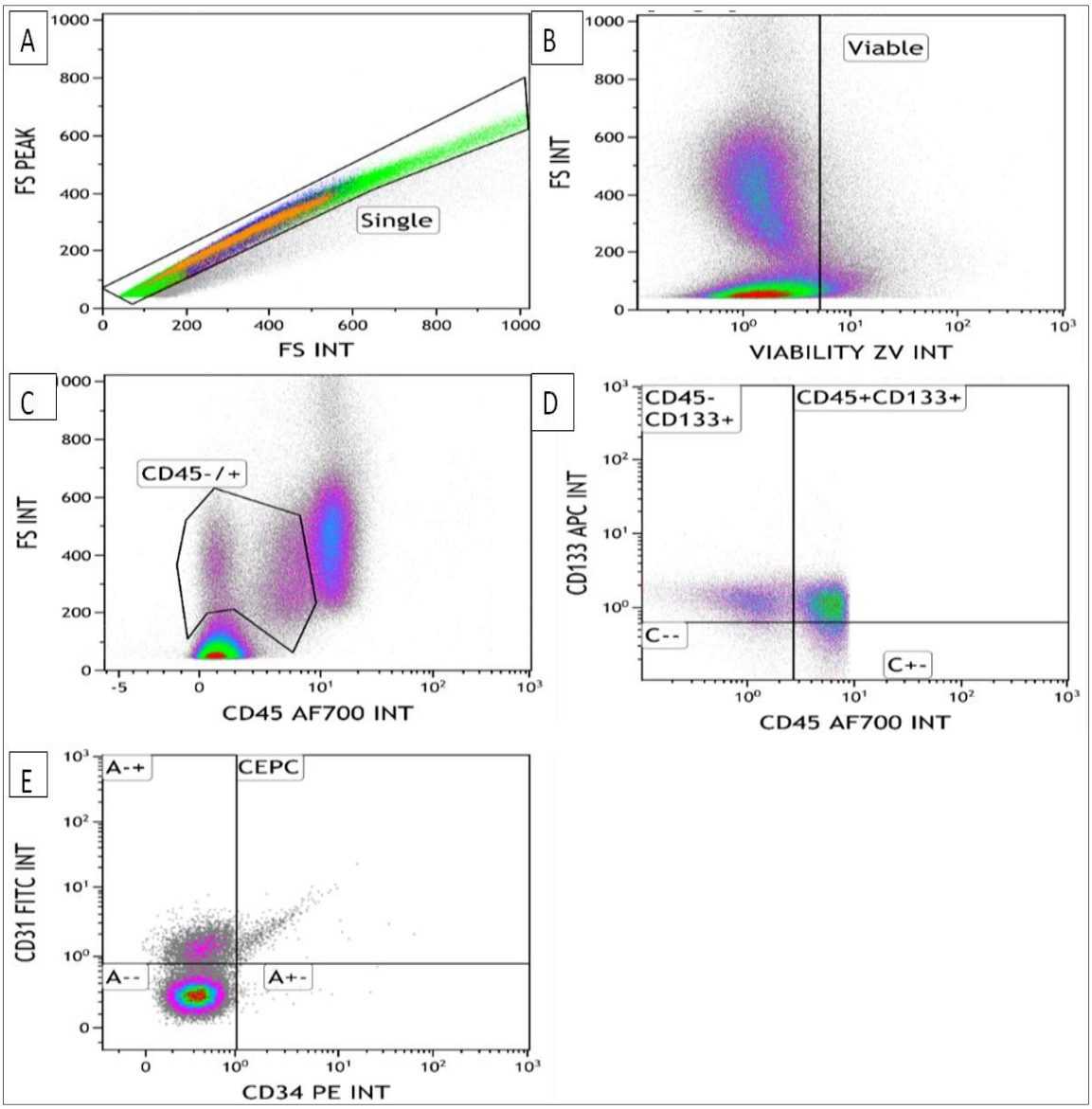

Adapted from Tchokonte-Nana et al., 2017

Figure 0.11: Gating strategies for flow-cytometry.

A) Single cells were separated from doublets on a plot of FS peak vs FS integral. B) Live cells were gated on a plot of FS vs zombie violet. C) Small CD45+ and CD45- cells were gated on a plot of FS vs CD45-AF700 dot-plot. D) CD45+CD133+ and CD45-CD133+ cells were gated on a plot of CD133-APC vs. CD45-AF700. E) A CEPCs were defined as CD45-CD133+CD31+CD34+ and gated on a plot of CD31-FITC vs CD34-PE.

3.4.3 CD34 Immunodetection of the islet endothelial cells, viewing and analysis

Immunohistochemistry (IHC) is a histological technique that was used for the detection of specific protein markers (antigen) inside or on the surface of a cell. Unlike the H&E and methenamine silver stains which were used to show the general morphology of the pancreatic tissue in this study (discussed later in 3.5), the IHC technique was used to better delineate the location of the expression of CD34 antigen on the EC membrane (Lin et al., 1995). To achieve this objective, the monoclonal CD34 antibody ([EP373y] (ab81289) ABCAM, UK) was therefore used as the primary antibody.

Slides with indices 3 (positively charged slides) were taken for immunostaining using a BondMax autostainer for a Bond Polymer Refine detection kit (Code: DS9800) (Leica Biosystems, Wetzlar, Germany). The detection kit contained a peroxide block, post-primary, polymer reagent, DAB chromogen and haematoxylin counterstain. Before the staining process, the protocol was optimised (Appendix 13) and validated using human tonsil sections as positive and negative control. As a result, heat-induced epitope retrieval (HIER) was not applied to the sections and the CD34 antibody was diluted at 1/500 in PBS with 1% bovine serum albumin (BSA). Tissue slide sections underwent the following IHC major steps: 1) The endogenous peroxidase blocking step to reduce the detection of the background proteins, 2) the application of the diluted primary antibody followed, 3) application of the secondary antibody thereafter 4) the polymer built for the secondary antibody was then applied to the slides and washed 5) The CD34 positive cells were finally visualized with the chromogen: DAB (brown) (Appendix 14). After staining, the slides were manually taken for dehydration, clearing, and mounted with a coverslip by a DPX mounting medium and classified according to animal groups (NC, C-SSC, C-HFD / SSC, RAC / STZ and HFD / STZ groups). Digital image viewing and capturing was acquired as described in section 3.4.3.1 of this chapter.

3.4.3.1 Microscopic viewing of the slides, digital image capturing, qualitative data acquisition

Stained slides were classified according to the animal group (NC, C-SSC, C-HFD / SSC, RAC / STZ and HFD / STZ groups). They were viewed and captured with an *Axioskop* microscope (Zeiss, Axioskop 2, Leitz Wetzlar, Germany) equipped with a coloured digital camera (Zeiss HRC microscope camera). The microscope was linked to a computer using ZEN 12 image analysis software.

Viewing and image capturing

A total of 50 slides were viewed. Digital images focused mainly on islets were captured at 10x, 20x and 40x magnification and stored in Tagged Image File Format (TIFF) for endothelial cell morphological and quantitative evaluation.

3.4.3.2 Quantitative assessment

Assessment of the endothelial density

Captured images (tiff file type) focused on the islets (in pixels) were transported in Fiji version of ImageJ software 1.53b and the colourisation plug-in was used to obtain the CD34 % pixel area representing the islet ECs density as described below.

Each digital image presented with ECs stained dark brown (DAB) and the remaining pancreatic tissue light purple (because the nucleus of cells stained with Harris Haematoxylin and cytoplasm remaining unstained) was loaded into the ImageJ software. The aim was to calculate the dark brown (DAB) pixel area in a selected ROI. Because the results were to be reported in percentage, there was no need calibrating the dimension of the images which were loaded in pixel unit to another unit (µm or inch). To measure what was brown and what was not brown, the threshold method was used. On the bar menu of the open ImageJ window, the option **image** was selected and on the drop-down options *adjus*t was chosen, followed by the *colour threshold* option. Another widow opened with a series of sliders and small histograms in a window. At the bottom of the window, under the sliders, the default threshold red colour was selected in the colour space HSB (Hue, Saturation, Brightness) with Hue the colour type such as red. The slider was then adjusted to select the brown colour of the image. This allowed any colour or any series of colour to be selected by their hue saturation and brightness or combination of the three.

The scoring system was based on both the intensity and distribution of deposited CD34 stain per unit area of the islet tissue section as described by Canzano and colleagues in 2019.

Assessment of the islet cells density

In order to evaluate the proximity between each endocrine cell and the blood vessel (stained with CD34), cell density (CD) per unit area of the islet was assessed. Captured images from slides stained for CD34 and focused on the islets were transported in the ImageJ software and the automatic particle counting plug-in was used to count the number of nuclei per unit area of the islet (Appendix 14). Any of the three stained digital images could be used for this evaluation because only the endocrine cell nuclei were taken into account in this process and all slide

sections were counter-stained with haematoxylin. Five islets per tissue section were considered for this evaluation and the mean recorded.

3.5 ROUTINE HISTOLOGICAL STAINING OF THE PANCREATIC TISSUE, VIEWING AND IMAGE CAPTURING

Haematoxylin and eosin stain (Fischer et al., 2008), methenamine silver (Bancroft & Gamble 2008, Churukian 1996) impregnation and CD34 (Kuzu et al., 1992) were used to delineate different levels of the pancreatic tissue morphology, the general structural architecture, the BM and the endothelial cells respectively. After tissue staining, the slide was viewed under the light microscope and morphological and morphometric data collected. The detailed procedures are reported in the following sections.

3.5.1 Routine histological staining for the general histomorphology of the pancreatic tissue

The tissue slides carrying the indices “1” were stained with H&E using a pre-programmed autostainer (Leica Autostainer XL, Wetzlar, UK) (Appendix 15). These stained sections were used for: 1) validation of the general morphology of the pancreatic tissue, and 2) collection of morphometric data of the large pancreatic vessels (diameter, thickness, numerical density area fraction).

3.5.2 Staining of the pancreatic tissue basement membrane

In human and mouse pancreatic islets, β-cell function and survival are dependent on the presence and integrity of the BM around the blood vessel (Nikolova et al., 2006, 2007). Methenamine silver has a high affinity for collagen fibre IV, the main component of most BMs (Nikolova, Strilic & Lammert, 2007; Groulx et al., 2011; Cross et al., 2017) and was therefore used to delineate the pancreatic BM.

The tissue slides carrying the indices “2” were manually impregnated with methenamine silver (Bancroft & Gamble 2008) (Appendix 16). The stained slides were used to assess the intra and peri-islet BMs. The kidney basement membrane from an NC animal was used as the positive control for the Methenamine silver stain.

A total of 50 slides per stain were viewed and digital images captured at 10x, 20x and 40x magnification as described in 3.4.4 (immunohistochemistry) and stored in Tagged Image File Format (TIFF) for quantitative analysis.

When viewing each H&E stained section, the pancreatic tissue general histomorphology was assessed and anatomical abnormalities recorded. In addition, the basic morphometric features

(wall thickness, diameters, numerical density and area fraction) of the large vessels were measured and the results recorded. The captured images from the methenamine silver-stained slides were carried to image J software and the stain density per unit area of the islet assessed.

3.5.2.1. Morphometric assessment of the large vessels of the pancreas

Key parameters that determine the vascular haemodynamic were collected from the large pancreatic vessels: outer diameter (OD), inner diameter (ID], wall thickness (WT), numerical density (ND) and area fraction (Afr). For each parameter, ten different microscopic fields from each slide section were taken into account and the mean value recorded. The OD gave the estimate of the total vessel size, while the ID served to assess the status of the pancreatic vessels' haemodynamics in all groups. When a vessel diameter was deformed by the surrounding tissue, the circularity of the vessel was factored for (Figure 3.12). To evaluate the changes in the abundance of the smooth muscle and the supporting connective tissue forming the wall as a consequence of any form of vascular remodelling, the wall thickness was calculated: 1) as the difference between the OD and the ID divided by two (OD-ID/2) and 2) by drawing a line from the luminal edge of the vessel through the wall to the adventitia and measured. The reason for obtaining the two values was just to improve the accuracy of the results and validate the fact that the wall is maintained uniform in thickness at different points.

The ND was defined as the total number of the cross-sectional edges of blood vessels captured on the pancreatic tissue section per unit area. The area fraction (AFr) of the vessels was defined as the percentage area covered by blood vessels per unit area of the pancreatic tissue section and was therefore calculated as the sum of all the small areas covered by each vessel in a defined ROI. Two values were taken into account in this assessment: the first AFr was measured from the OD (adventitia) for the total area covered by the blood vessel per unit area, and the second from the ID (this gives an account of the blood volume per unit of the tissue at any given time) as described by (Ziemińska et al., 2013). In other words, the total tissue fraction was obtained, namely the wall fraction and the lumen fraction.

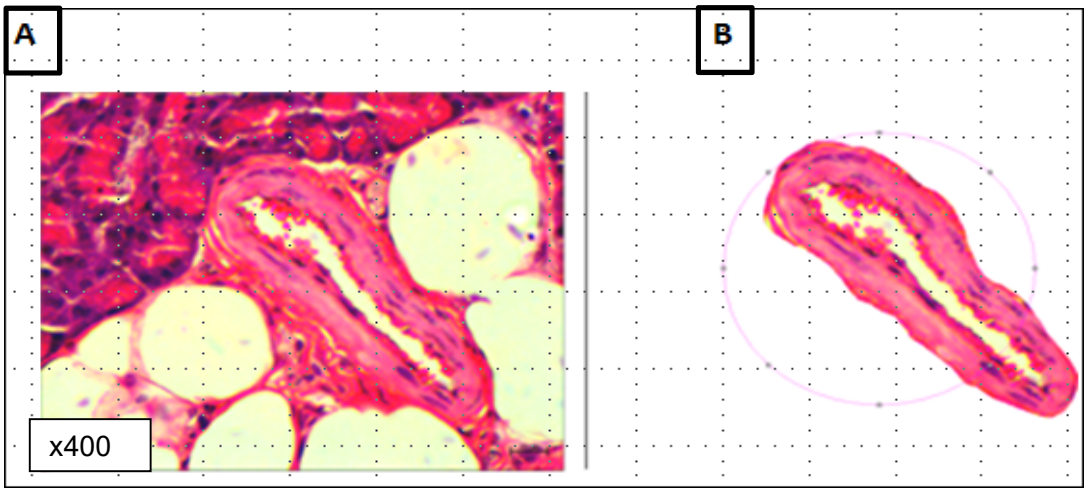

By: E. Ngounou

Figure 0.12: Schematic representation of the methodology used in the evaluation of the total diameter of the compressed (deformed) vessels using ImageJ software.

A) A sample from medium vessel viewed on duodenal tissue section from a rat in the C-HFD/SSC group (x400). B) Blood vessel area selected and surrounding pancreatic tissue cleared off, and then the circularity measured.

3.5.2.2 Quantitative assessment of the Islet basement membrane

The islet BM thickness was simply assessed by threshold of the methenamine silver % pixel area for BM density per unit area on the pancreatic tissue section focused on the islet using ImageJ colourisation method (Figure 3.13) (as described in 3.4.3.2 and other details in Appendix 17).

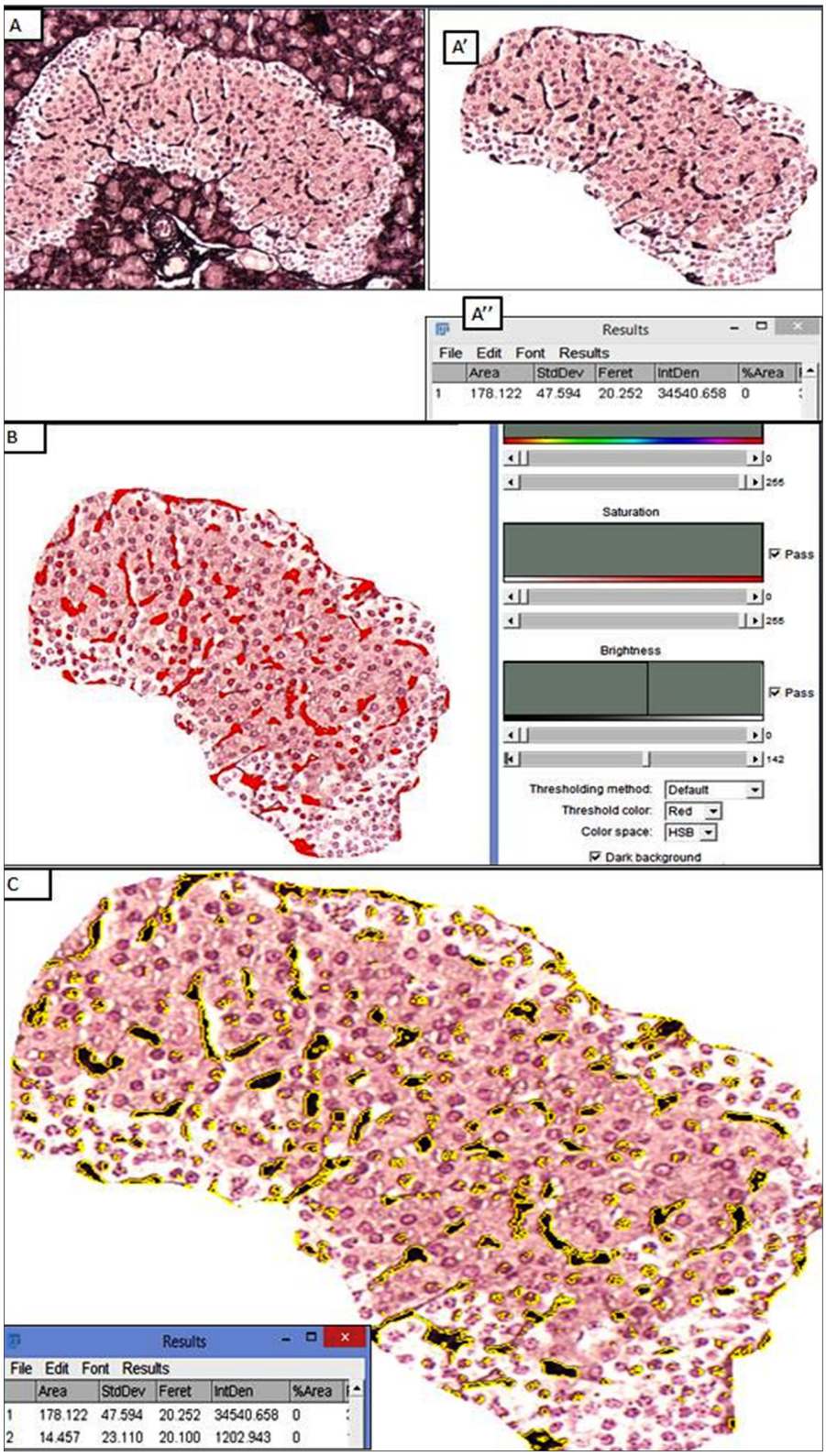

By: E. Ngounou

Figure 0.13: Image of the islet analysis procedure using ImageJ software.

A) A merged image shown from the normal control rat (not treated): the sections were impregnated by the methenamine silver (basement membrane stained dark brown) and counterstained with haematoxylin (cell nucleus stained purple). A') Area of interest selected using the freehand tool and the remaining area clear. The selected area measured (results displayed in the table (A''), 178.122 pixels. B) Methenamine stained pixel area thresholded and coloured by the default threshold colour (red) using the threshold adjustment tool. C) Threshold area delineated (yellow line) and measured.

In this study, at all times, the unit area was 4 mm^2, the sum of 10 small microscopic areas confined within a grid region of interest (ROI) of 0.4 mm^2 each for the islet morphometric analysis. The major components of the islet were assumed to be mainly blood vessels and endocrine cells. Therefore, nerves and other structural elements were considered negligible fractions and should not significantly influence the results. In addition, the digital image was blind-evaluated by another PhD research fellow from the Division Physiology

In summary, the morphometry of the islet microvasculature was assessed first for the BM, secondarily for ECS (the density of the islet ECs). Besides, the endocrine cell density (cell count per unit area) was evaluated. To evaluate the number of blood vessels per islet cell, the ratio between CD34 % pixel stained area per unit area and endocrine cell number was assessed. Islets lack lymphatic vessels (Korsgren & Korsgren, 2016; O'Morchoe, 1997) and therefore were not part of this analysis. Data from the vascular corrosion cast were evaluated alongside these parameters.

3.6 MICROVASCULAR CAST COMPUTER TOMOGRAPHY PROCEDURE

3.6.1 Pancreatic vascular cast viewing and data acquisition

Nano-computed tomography (nano-CT) scans were performed at the Stellenbosch CT Facility using a General Electric V|TomeX L240 system which consisted of a penetrating X-ray source, a sample manipulator, and an X-ray detector as described by Du Plessis et al. (2017). The main difference between a micro-CT and a nano-CT is the resolution. While in micro-CT images are captured in µm or mm, in nano-CT it is in micron using a nano focus. Three major steps help in performing this procedure:

1) Preparation and mounting of the sample

Each vascular cast sample (the pancreas, together with those of the duodenum and spleen) was affixed to an acrylic podium using an epoxy adhesive (Araldite, Huntsman Advanced Materials) and rotated over 360° at angular increments of 0.2° around the vertical axis. No breakage of the

cast was recorded and precautions were taken to ensure that minimal movement of the sample occurred during scanning.

2) Setup of the scanner and parameters

Determining the resolution at which each sample was going to be scanned was very important. Our samples size ranged between 1.8 mm to 2.4 mm for an optimal resolution of approximately 2 to 3.5 nanometers. To reduce the photochromatic of the beam which could cause streaky artefacts, filters (a copper and a tin) were placed between the beam and the sample. Optimized parameters were selected according to the guidelines set out in the manual book. X-ray settings included 220kV and 200µA and copper beam filtration of 1.5mm was used (to reduce the photochromatic of the beam which could cause streaky artefacts), with a voxel size set to 80 µm. X-rays were produced by small X-ray tube which was directed on a specific target.

3) Scanning procedure proper

The procedure was done automatically with frequent supervision to amend errors that could occur, such as X-ray instability or filament burn. From the tube, the X-rays were directed through and around the sample and then collected on a 2D X-ray detector in the form of a projection image composed of thousands of pixels. Image acquisition time was 500 ms per image and images were recorded in 2000 rotation steps during a full 360-degree rotation of the sample.

4) Image reconstitution

Reconstruction was performed on a cluster of PCs using the Datos software that is provided with the system. Data generated were a set of stack images (DICOM) formed by approximately 1000 slides. Each slide was 1000x1000 pixels and the resulting scanned volume contained 109 voxels (volume elements).

Thousands of 2D scanning images from a sample thus obtained were used to reconstruct the 3D data set using a filtered back-projection algorithm. Reconstruction was performed in system-supplied Dato's reconstruction software. Visualization and analysis were performed using the following software: Volume Graphics VGStudioMax 3.0® nano-CT scan for volume rendering and ImageJ for surface rendering.

The reconstituted images obtained were used to assess morphometry and quantitative data concerning the ability of the vessel to supply adequate nutrients and oxygen to the pancreatic tissue in each group.

3.6.2 Morphometry and quantitative analysis

The complete analysis of the pancreatic image was carried out in the Volume Graphics VGStudioMax 3.0® Nano-CT software and ImageJ, but the reading of all the data sets at the same time was prohibitive in terms of calculations. As previously described by Aughwane et al., 2019, to make the analysis feasible on our local computer, the total volume of the circumcised pancreatic plaster was divided into 100 (10 x 10) three-dimensional cubes so that smaller chunks of data could be processed. Each cube and its position in the volume was labelled and then recombined. The following morphometric large data sets from the duodenal and splenic vascular cast were evaluated: the vascular density (number of vessels per mm^2), vascular length density (µm), identification of nodes, count branching nodes (Figure 3.14B), segment length (mm) and associated diameter, branching angle (º) and the diameter distribution (mm) concerning the vessel length. Diameters were measured at the middle of each segment (Figure 3.14A) and throughout the vascular tree until the most distal segment was reached.

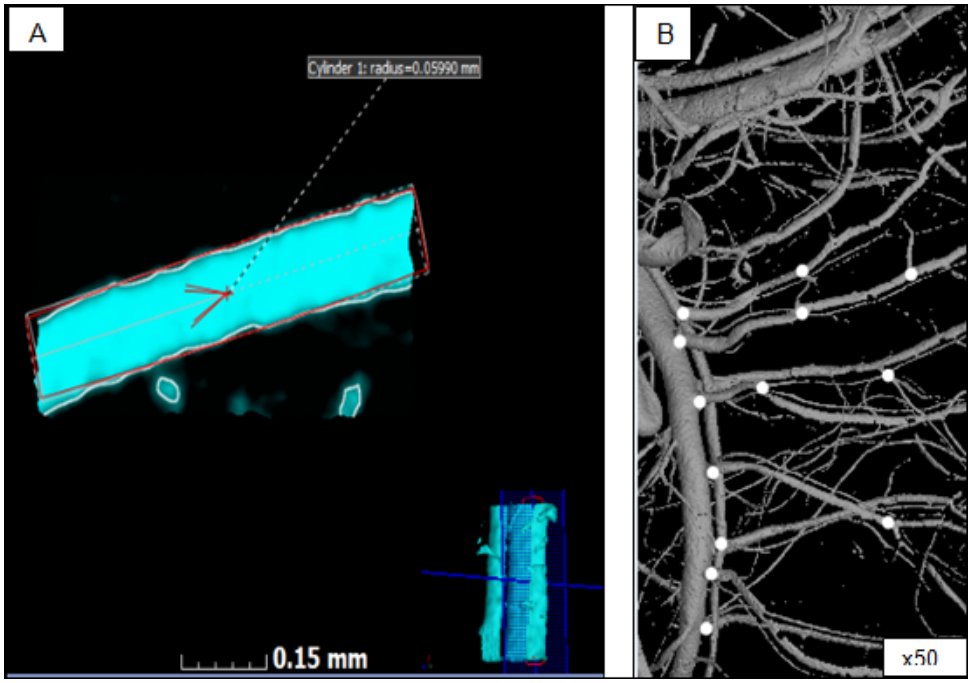

By: E Ngounou

Figure 0.14: Assessment of the diameter of segments of the vessel.

A) Image crop from the splenic vascular cast of a normal control animal and data obtained automatically B) Identification and counting of nodes from the duodenal vascular cast.

A segment was considered to be the portion of the vascular tree between two nodes. The vascular segment of an already measured vessel has been traced to avoid further measurement. A node has been considered to connect three or more segments (Figure 3.15). The terms "mother segment" and "daughter segment" meant the segment immediately proximal and distal, respectively, to the node. In this study, only the node with two daughter vessels was measured. In addition, only the angle between two daughter vessels was taken into account, as it was thought to be related to the efficiency of blood flow, the energy cost of the bulk flow and the distance of diffusion.

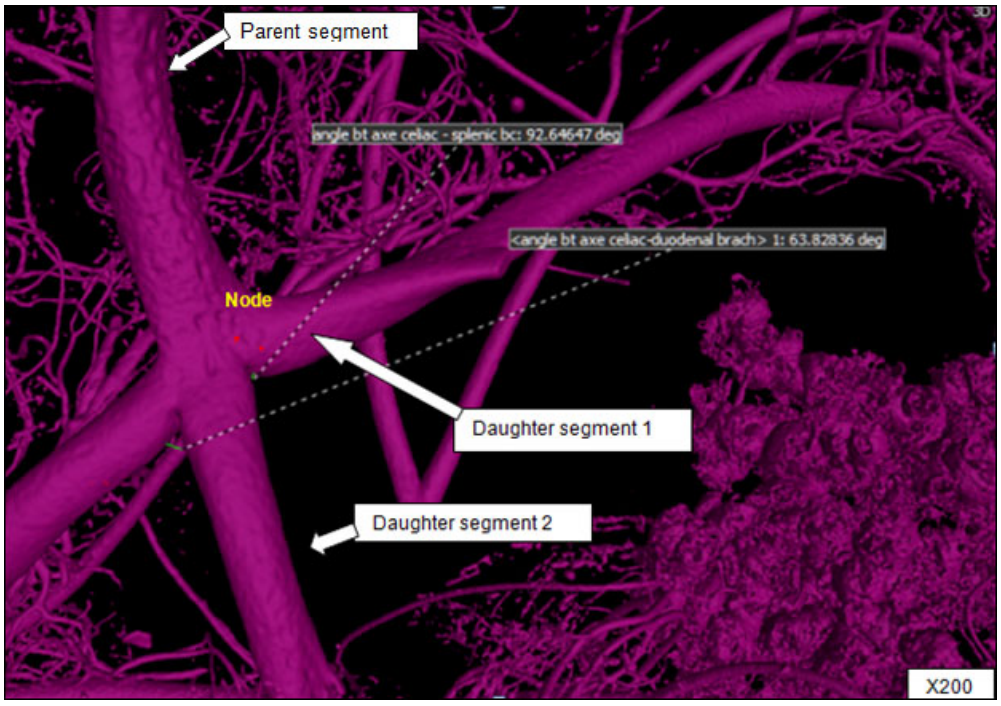

By: E Ngounou

Figure 0.15: Illustration image showing the identification and assessment of node, parent and daughter's segments, branching angle of vessels.

Three-dimensional topology and the pattern of the vascular network was analysed based on the successive arrangement of the types of vessels (arteries/ arterioles, capillaries, venules). The direction of blood flow was identified using the size of the parent vessels (arteries are smaller than veins).

In this study, the intention was not only to attempt to reveal differences in the branching pattern of blood vessels between the two main pancreatic regions (duodenal and splenic) but, more importantly, how the dispersion in local pressure reflect anatomical differences of these regions. The study, therefore, assessed whether there is any difference in the geometry and arrangement

of the vascular tree between the duodenal and the splenic pancreas but more importantly how this showed the link between the vascular anatomy and the function. In the following section, a novel method for the reconstruction of the full pancreatic vascular tree from partial measurements is described.

3.7 PANCREATIC VASCULAR TREE RECONSTITUTION

Several form-function scale relationships such as volume-diameter, length-diameter, flow length and flow diameter have already been previously proposed and validated (Huo & Kassab, 2012) In this study the vascular tree was defined as a network of several "stem" (st) supplying or draining a "crown" (c) as described by (Razavi et al., 2018) (Figure 3.16): in a stem-crown system, the volume of the crown named Vc was defined as the sum of the luminal volume of vessel segments in the entire stem-crown system. The arterial tree of the crown was made up of segments proximal to the capillary while the venous tree segments were regarded as the distal to the capillary (cp). Similarly, the length of the crown named Lc was defined as the cumulative vascular lengths in the entire arterial or venous crown. Blood flow (Q) and the number of capillaries (N) corresponded to the stem and the respective network. Morphometric data based on the entire vascular system were used then derived and tested for the scaling laws or power laws. In this law, the relative structural and functional change of the vascular tree causes the proportional relative change of the other. The entire vascular tree, therefore, consisted of many stem-crown units down to the capillary vessels (Huo & Kassab, 2012). Here the three main arteries supplying the pancreas were considered. Each bifurcation generated a unique stem-crown unit which continues down to the smallest unit. Each smallest unit was an arteriole with two capillaries for an arterial tree or a venule and two capillaries for a venous tree. The pancreatic vascular tree was considered to be formed by the branches of the splenic (SPA), the superior and inferior pancreaticoduodenal (SPDA and IPDA) arteries. Functionally, each stem supplies or collects blood from the crown for an arterial or venous tree, respectively. The present analysis applies strictly to a tree structure (arterial or venous) down to the first capillary bifurcation, the one associated with the islets. As described by the strahler system the capillary was considered order 0. Then when two vessels of order 0 merged the resulting vessel carried the order 1. Vessels of order 1 merged to form vessels of order 2 and so on. Note that when a vessel of order 2 and that of order one merge the resulting vessel is assigned the highest order, in this case, order 2.

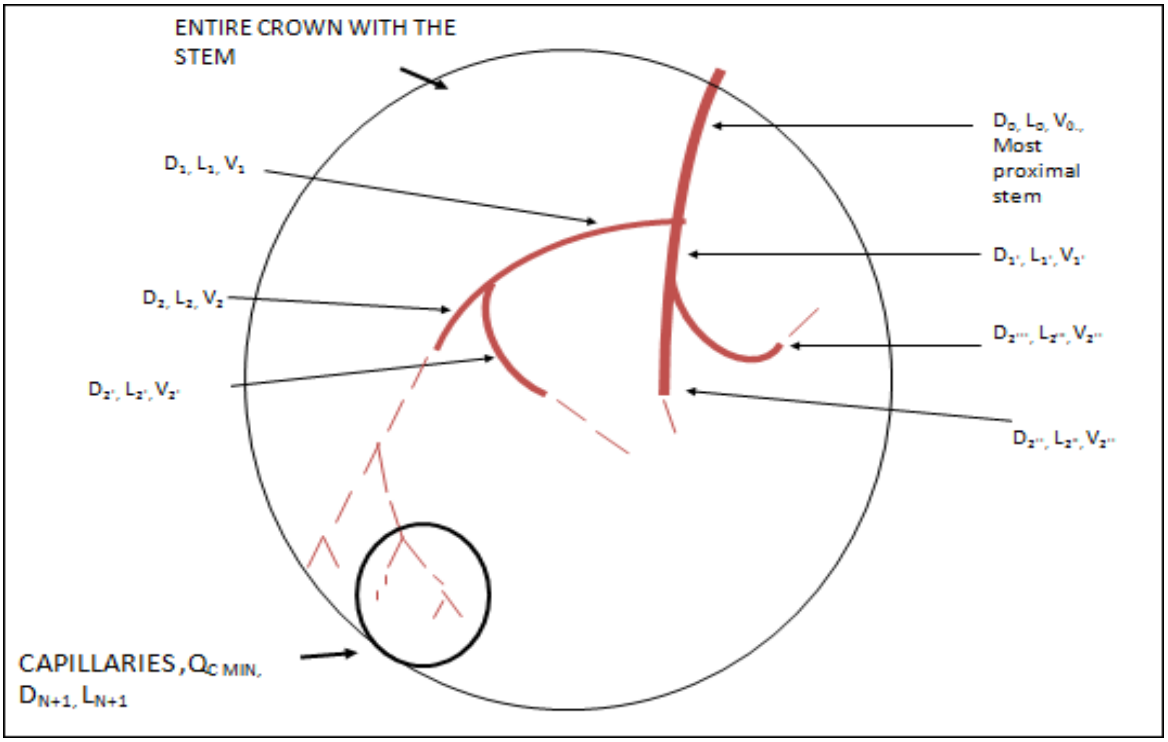

Adapted from (Razavi et al. 2018)

Figure 0.16: A schematic illustration of the definition of stem-crown units

D, L, Q, and V stand for diameter, length, flow rate, and volume, respectively. In a stem-crown unit and subscripts “max” represent the most proximal stem-crown unit in a vascular tree. Three stem-crown unit levels are represented successively in 1, 2 and n.

In this study, the entire arterial network was reconstructed from the main stem down to the first capillaries (<8 μm). Missing data from the cast (such as those of the islet microvasculature) were reconstructed based on histological data (<10 μm) using a computational algorithm as described by Mittal et al., (2005). Based on this assumption, blood vessel resistance was then considered as a function of the vessel's geometry and viscosity that takes into account the Fåhræus effect (stating that there is a decrease in the mean concentration of red blood cells as the diameter of the glass tube in which it is flowing decreases). Boundary conditions were prescribed with an inlet pressure of 120mm/Hg and uniform pressure of 25mm/Hg at the outlet of the first capillary segment (Razavi et al., 2018). Subsequently, a system of simultaneous linear algebraic equations for the nodal pressures was obtained. Once the vessel resistances are evaluated from the geometry, and suitable boundary conditions prescribed, the flow rate was simulated to estimate the transit time within the vascular trees.

Note that at each given time one volume of blood flowing in the exocrine tissue corresponded to ten volumes in the islet and this must be considered in all equations.

3.7.1 Flow perfusion scales with capillary numbers

The hypothesis in this study was that there should be a direct relationship between the blood flowing through the main branch (i.e., stem flow) of a pancreatic vascular tree (like SPNA) and the number of capillaries in the crown formed by the vessel's branches. The formula described by Razavi et al. (2018) was based on the law of mass conservation stipulating that the flow at the inlet of the tree or crown (Qst stem flow) is equal to the sum of the flows at the first capillary segments, Q_{cp} as expressed in the equation (1):

$$Q_{st}=\sum_{i=1}^{N} Q_{cp,i} \qquad (1)$$

In this equation ***N*** was the number of capillaries perfused by a given stem. When considering the average capillary flow rate the formula became**:**

$$Q_{st}=kN_c \qquad (2)$$

with ***k*** being the average capillary flow which is approximately constant across the various stem-crown systems. Therefore, the inlet flow was proportional to the total number of capillary vessels. When normalising the flow and capillarity with respect to an entire pancreatic vascular tree, the following was obtained:

$$\frac{Q_{st}}{Q_{st,max}} = \frac{N_c}{N_{c,max}} \qquad (3)$$

where $Q_{st,max}$ and $N_{c,max}$ stood for the inlet flow and the total number of capillaries in a vascular system, respectively.

3.7.2 Crown volume scales with capillary number

Crown volume was calculated as the sum of volume within the network ($V_c=\sum n_i\,(\pi L_i/D_i^2)$, derived based on the average branching ratio ($n_i = Br^i$, $i = 0, m$; where n was the number of vessels and i the branching level) and the relationship between crown volume and number of capillaries obtained by scaling of vessel diameters and lengths in each branching level results was calculated as follows (equation *4*)

$V_c=K_{VN}(N_c)^{\lambda}$ (4)

where K_{VN} was considered constant. The above equation was normalised with respect to maximum crown volume and number of capillaries in the entire vascular network, and hence the following general formula of scaling relationship was defined as:

$V_cV_{c,max}=(N_cN_{c,max})^{\lambda}$ (5)

3.7.3 Crown length scales with capillary number

The crown length was considered simply as the cumulative length of blood vessels of all branching levels within the network ($L_c=\sum_{ni}L_i$) when considering the mean branching ratio ($n_i = B_{ri}$, $i = 0,., m$; with n being the number of vessels and i the branching level) and scaling of mean length of blood vessels in each level of branching $Li=(Br^{\gamma})^{m-i}L_{cap}$; with L_{cap} being the mean length of capillaries and x an empirical exponent (Huo & Kassab, 2012), resulting in a direct relationship between crown length and number of capillaries (detailed explanation in the supplementary Information, Razavi et al. 2018) expressed in the following equation:

$L_c=K_{LN}N_c$ (6)

where K_{LN}–$Lcap\sum_{i=0}^{m}Br^{(i-m)(1-X)}$

was considered approximately constant. A general form of normalized crown length and number of capillaries with respect to an entire tree was given as:

$$\frac{L_C}{L_{C,max}}=\left(\frac{N_c}{N_{c,max}}\right)X \quad (7)$$

where $L_{c,max}$ and $N_{c,max}$ were the maximum crown length and the number of capillaries in the entire pancreatic tree.

3.7.4 Mean transit time scales with crown volume and length

The structure of the vascular networks is heterogeneous and so is the perfusions of the particles through the different paths of the network. The mean transit time (MTT) was therefore calculated as the average time required for blood to circulate through the vascular network over a period of time. Based on the assumption that blood particles travel with the average speed of the bulk flow

and that the total number of blood particles passing through a vessel segment is proportional to the time-average flow in the segment, the MTT in the network (Tc) could be expressed as follows:

$Tc=\sum_{n=1}^{N} FF_i * T_{gs,i}$ (8)

FF being the flow fraction (equal to the ratio of segment flow to stem flow) and **Tsg* the mean transit time in a specific segment with i = 1,2, n; and 'n' being the total number of segments in the entire pancreatic network. The transit time is well known to be determined by the ratio of blood volume and blood flow (Meier and Zierler, 1954) as follows ($FF_i = Q_i/Q_{max}$) resulting to the equation *(8).* Therefore an elementary derivation by replacing the definition of, transit time in a segment *(Ti = Vi/Qi)* and Equation *(8)* results in:

$Tc*Nc=K_{TN}V_C$ (9)

with K_{TN} being proportionality constant in unit of time/volume. A combination of Equations *(6)* and *(9)* relates mean transit time to crown volume and length, namely:

$T_c * L_c=K_{TL}V_c$ (10)

where the parameter KTL is a proportionality constant in unit of time/area. A general normalized form of the above equation can be written as:

$$\left(\frac{T_c}{T_{c,max}}\right) * \left(\frac{L_c}{L_{c,max}}\right) = +\left(\frac{V_c}{V_{c,max}}\right)^X \qquad (11)$$

where $T_{c,max}$, $L_{c,max}$, *and* $V_{c,max}$ are the crown time, crown length and crown volume in the entire tree, respectively.

3.8 STATISTICAL ANALYSIS

All data in the study were transported and statistically analysed by Prism Graph Pad Prism software (version 5.0a.128 Inc., California, USA). The results are presented as Mean ± Standard Error of the Mean (SEM) with the number of rats each experiment presented in the figure legends. The following tests were used to perform the statistical analysis at the different stages of the study.

1) A Student t-test was used to evaluate the significance between the RAC and the HFD groups in respect to OGTT levels for each time point of the experiment

2). A one-way analysis of variance (ANOVA) followed by Newman-Keuls was used to determine the significant difference between groups with respect to body weight gain or loss, and blood glucose for each time point.

3) Data obtained from Flow-cytometry, magnetic Luminex assay, the percentage pixel area impregnated by methenamine silver and CD34 positive cell and from the large vessels morphometry were analysed using one-way Kruskal-Wallis test to compare the score between two independent groups, followed by a Dunn post-test. The box and whisker graphics generated by the GraphPad Prism represent the median of the mean value as a vertical line passing through the box. The median (average quartile) corresponds to 50% of the scores of the group, the upper quartile, 75%, the 25% lower and the whiskers high and low less than 50%.

4) Two data sets were considered for the asymmetry reconstitution of the pancreatic vascular tree nonlinear regression equation. Firstly, the stem-crown was computed, to begin with, data from the corrosion cast up to the small vessel having diameter <8μm (arterioles). Secondarily the missing data (<8μm) obtained from the histological study was used to complete the vascular tree.

In all tests $p<0.05$ (5% probability level) were considered statistically significant.

CHAPTER 4: RESULTS

This chapter reports on the data obtained from the different experimental procedures performed in this study. This includes the characterisation of two diabetic models followed by the validation of the impact of hyperglycaemia on the integrity of the vascular system using various immunodetection methods. Routine histological techniques were used to assess the general morphology of pancreatic tissue, including the detailed structure of the large vessels (arteries and veins), while the vascular casting technique assessed the volume of blood circulating in the vessel at a given time.

4.1 DIABETES INDUCTION AND ANIMAL MONITORING

The first objective of this study was to develop animal models that mimic the two common types of DM, the T1 and T2DM using STZ. The following sections report data obtained during these procedures.

4.1.1 Effect of a high-fat diet on the animal body weight

Bodyweight changes and BGL profile over time are shown in Figure 4.1. During the 14 days of HFD, both groups (HFD and RAC) had a gradual increase in the mean BW (Figure 4.1A). The HFD group started to have a significant increase in mean BW from day 3 (237.1±6.62 to 246.5±6.62g, $p=0.0366$) and remained so until on day 14 (from 237.1±6.62 to 288.01±5.66g, $p<0.0002$) compared to the RAC group (from 234.85±4.47 to 239.55±6.6g on day 3 and from 234.85±4.47 to 254.21±4.79g on day 14).

4.1.2 Effect of a high-fat diet on the blood glucose level

During the 14 days of HFD, the mean fasting BGL in RAC group remained constant (from 5.47±1.112 on day 0 to 5.7±0.101mMol/L on day 14) while that of HFD group increased significantly over time (from 5.55±0.1037 on day 0 to 7.96±0.34mMol/L on day 14, $p=0.0002$) (Figure 4.1B). However, the significant increase in the mean BGL on day 14 was not sufficient to confirm that the animals in the HFD animals were diabetic (BGL≥15mMol/L).

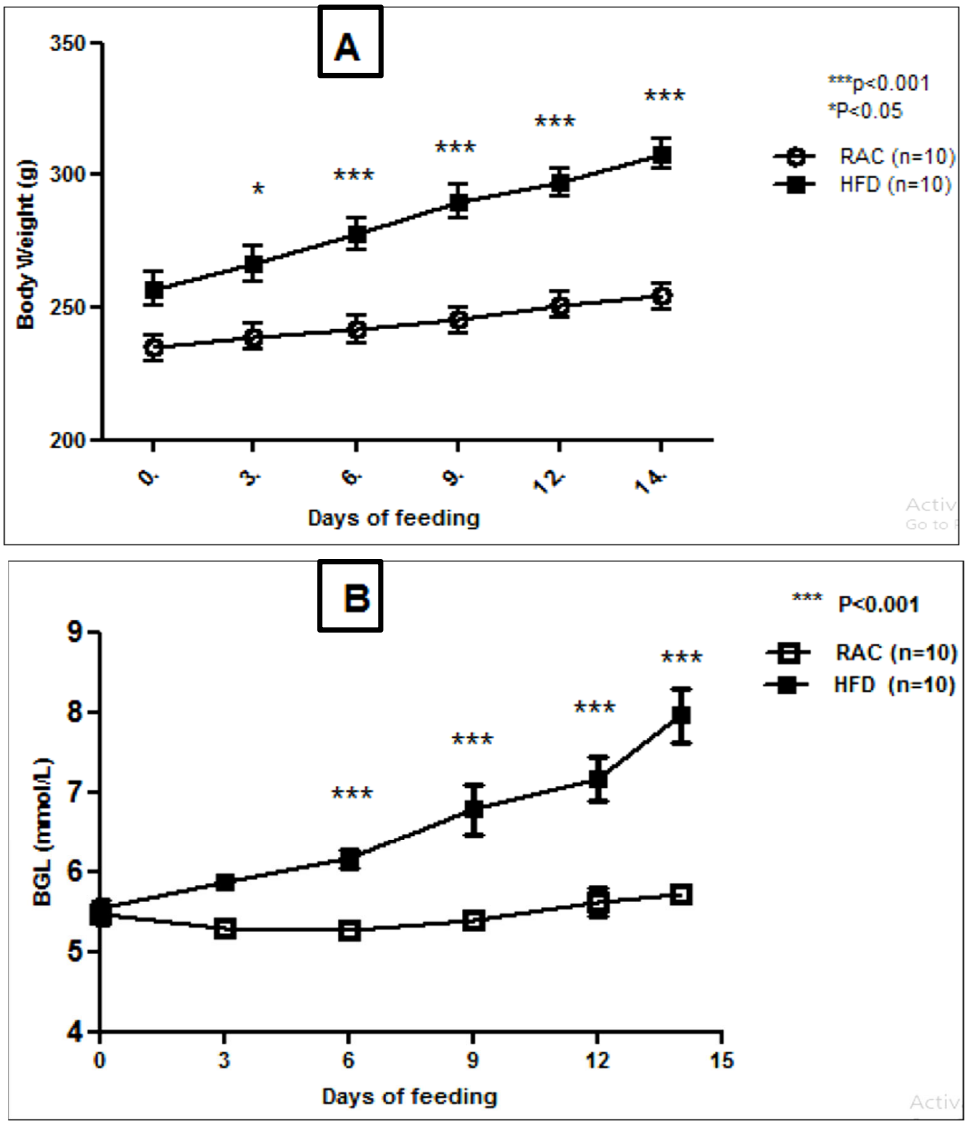

Figure 0.1: Bodyweight (A) and blood glucose level (B) profile during 14 days of a high-fat diet.

Each point on the graph represents mean values ± standard error of the mean (SEM) for the control (RAC) and the high-fat diet (HFD) groups. Statistical significance difference was evaluated using Student's t-test $p<0.05$).

4.1.3 Oral Glucose Tolerance Test (OGTT)

The oral glucose tolerance test shows the body's ability to absorb glucose and therefore the effectiveness of insulin action in the tissues. Blood glucose profiles of the RAC and HFD animals over time (0-3-5-10-20-30-60-90-120min) following an oral bolus of glucose solution (3g/kg BW) are presented in Figure 4.2.

The analysis was done every three days from the animals that were fed on standard rat diet (RAC) and those fed on the high-fat diet (HFD) during the 14 days following the introduction of the high-fat diet.

Before the start of the OGTT test, the reference value of the mean BGL in the HFD group was already significantly higher (p=0.0002) compared to that of the RAC group. Therefore the significant differences between the two groups over time represented in Figure 4.2 are changes from this baseline value. Hence at 0 min, the HFD group had the mean fasting BGL of 7.96±0.349mMol/L and the RAC control group 5.36±0.129mMol/L as reported earlier in 4.1.1. Thereafter a gradual increase in BGL was observed from 5min (7.73±0.165 and 10.78±1.425mMol/L in RAC and HFD groups respectively), with the increase in the HFD group starting to be significantly higher at 10min (p=0.043) compared to the RAC group. The increase in BGL remained significantly higher until 90 min of the OGTT in the HFD group compared to the RAC group (10.79±1.176 vs 6.75±0.137mMol/L, p=0.0146). The highest mean value in the two groups was recorded at 30min (8.49±0.083mMol/L for the RAC group and 15.49±1.758mMol/L for the HFD group (p=0.0001).

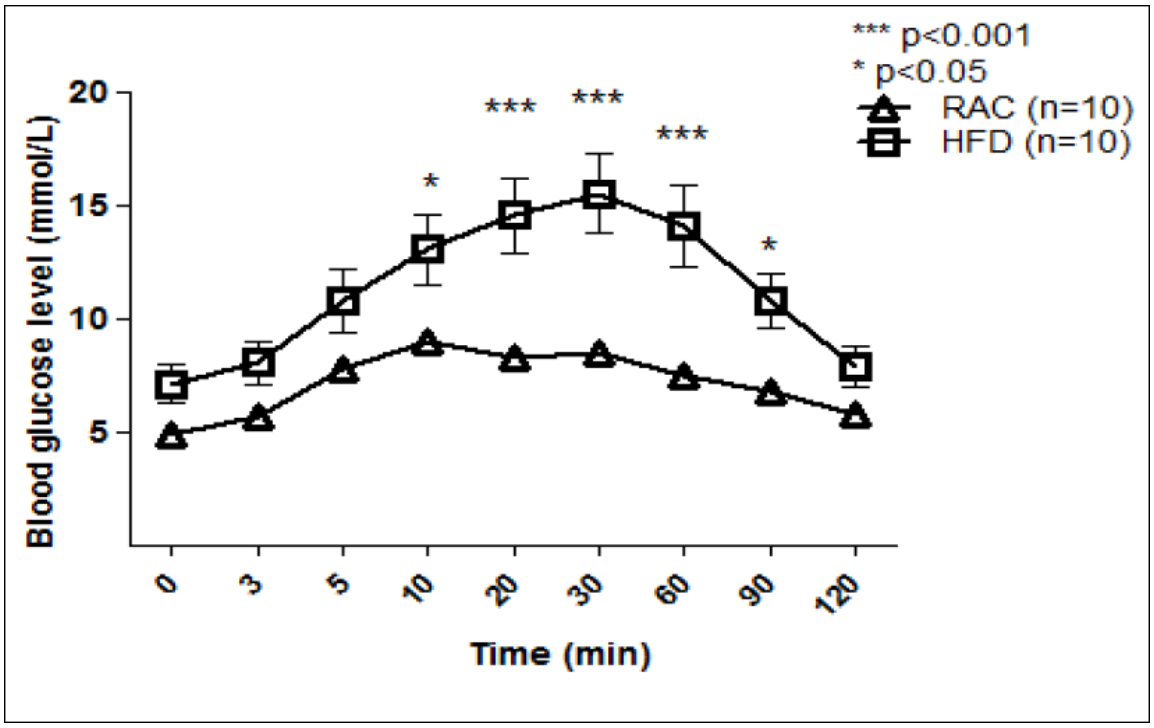

Figure 0.2: Glucose level profile of rats fasted overnight over time during OGTT 14 days after the introduction of a high-fat diet.

Each point on the graph represents mean values ± standard error of the mean (SEM) for the control (RAC) and the high-fat diet (HFD) groups at each time point of the test. The control group (RAC) had a lower glucose excursion over time compared to the HFD group Statistical significant difference evaluated using Student's t-test. Stars (* and ***) indicate different level of significance between the two groups as indicated in the graph.

4.1.4 Diabetic period

The diabetic period began 4 days (corresponding to day 1 of the diabetes period and day 24 of the experimental period) after STZ injection when the BGL in the RAC / STZ and HFD / STZ groups was ≥15mMol/L. Bodyweight, BGL daily food and daily water consumptions .of the animals in all group were recorded.

4.1.4.1 Mean Body weights

The trends of BW of control and STZ treated animals are shown in Figure 4.3. All control (NC, C-SSC and C-HFD / SSC) groups showed a progressive gain in the mean BW (ranging from 5g to 12g every three days) throughout the experiment. At the end of the experiment, the NC group had the lowest mean BW gain of 76.75±6.6g (29.91% increase) followed by the C-SSC group of 88.014±8.45g (34.33% increase). The C-HFD / SSC group achieved the highest and significant mean BW gain (118.94±9.25g for a 42.02% increase, P=0.0006) compared to the other control groups.

Unlike the control groups, the STZ treated groups (RAC / STZ and HFD / STZ) instead of gaining weight, experienced a progressive loss in BW (69.36±5.23g and 44.25±4.53g respectively). At the end of the experiment (diabetes day 60), up to 26.65%, BW loss was recorded (260.26 to 190.9g, p=0.0001) in the RAC / STZ group (Figure 4.3). The HFD / STZ group had a less severe mean BW loss (from 303.05±5.07g to 255.95±6.73g corresponding to a 15.54%, p=0.0005).

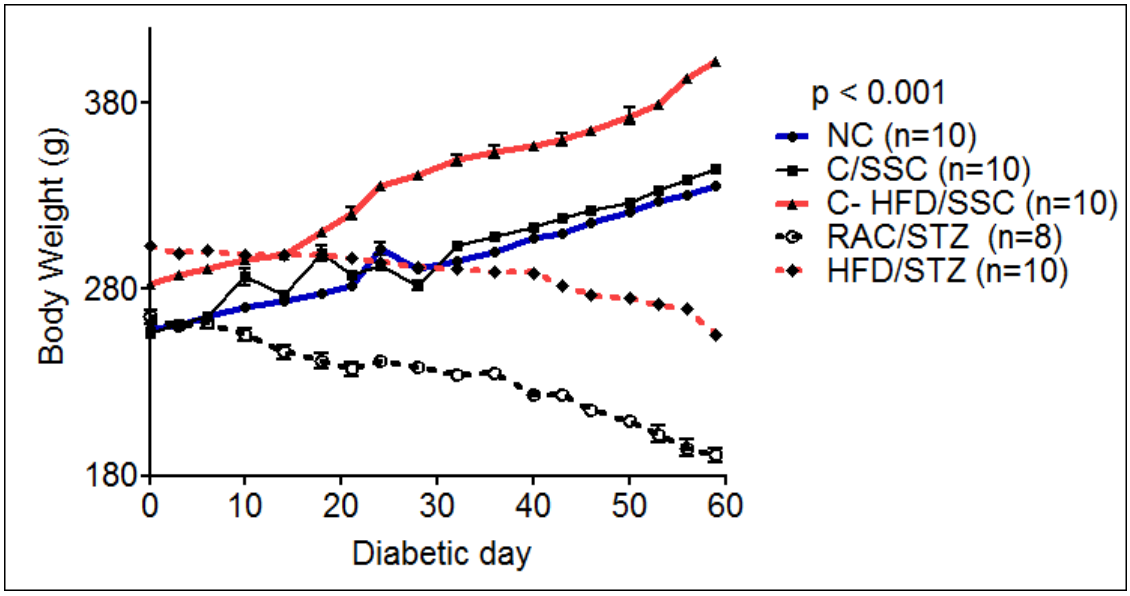

Figure 0.3: Trends in the mean in body weight changes over time in experimental and control groups during the diabetic period.

Each curve in the figure connects points representing the mean body weight of a group of animals measured every three days during the whole diabetic period. All values are expressed as mean±standard error of the mean, statistical difference versus NC, C-SSC and C-HFD / STZ groups using one way ANOVA with the Newman-Keuls post hoc test (P<0.05).

4.1.4.2 Fasting blood glucose level

The trends of mean fasting BGL changes in the experimental and control animals over time are shown in Figure 4.4. A single intraperitoneal injection of 50mg/kg and 35mg/kg BW of STZ significantly increased the mean BGL (>15mMol/L, p=0.0022) within four days post-injection of STZ in RAC / STZ and HFD / STZ groups respectively. These results enable the researchers to declare that these animals were diabetic. Three weeks later (diabetic day 42), the mean BGL of the RAC / STZ animals raised to 30mMol/L and remained above this level until the end of the experiment.

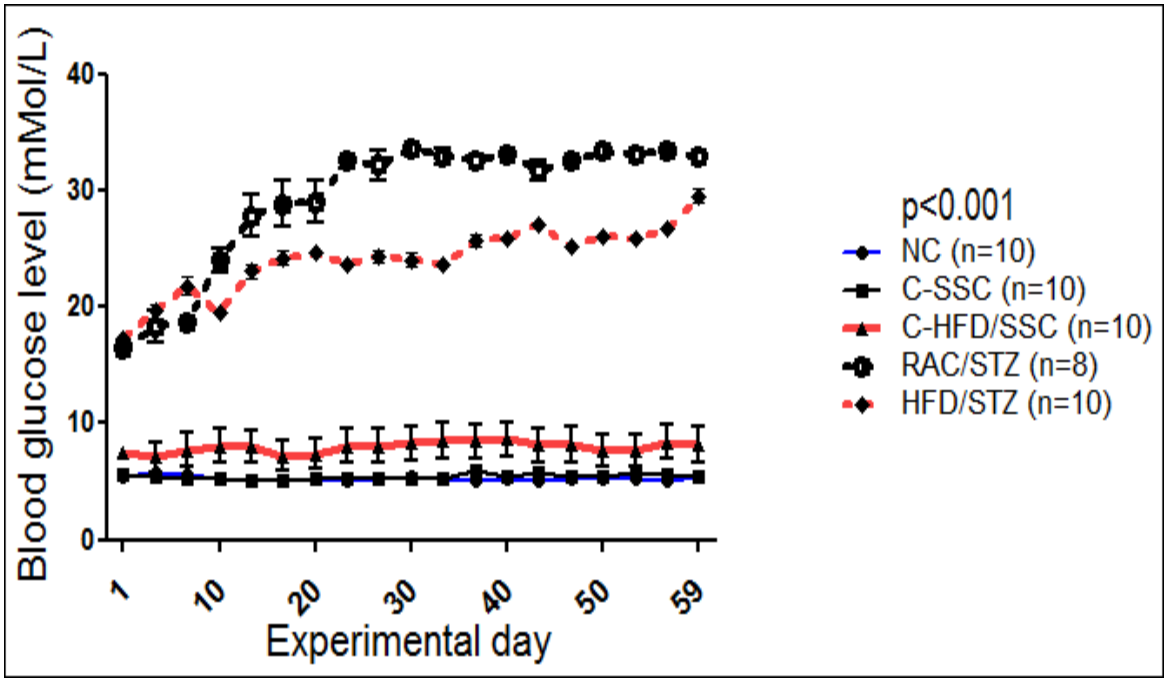

Figure 0.4: Mean blood glucose level profile of experimental and control groups during the diabetic period.

Each curve in the figure connects points representing the mean blood glucose level of a group of animals measured every three days during the whole diabetic period. Each data point is the mean ± standard error of the mean, statistical difference versus NC, C-SSC and C-HFD / STZ groups using one way ANOVA with the Newman-Keuls post hoc test ($P<0.05$).

The significant increase in mean BGL was consistent with the severe loss of mean BW (265.14±9.76 to 190.9±10.47g) as reported earlier, also with the increase in daily food (24.04±1.22 to 43.457±5.80g in Figure 4.5A) and water intakes (36.17±6.34 to 295.375±20.43mL, Figure 4.5B). However, the HFD / STZ group had a lower glucose excursion (19-28mMol/L), accompanied by less severe mean BW loss and a moderate increase in food (21.72±4.22 to 28.01±5.1g) and water (39.34±7.95 to 92.02±8.93mL) intakes (Figure 4.5B). It should be noted that the dose of 35mg/kg BW of STZ would have caused no or only a slight increase (7 to 9mMol/L) in BGL in rats fed with RAC at the end of the experiment (results not reported here). Control animals NC and C-SSC maintained mean BGLs between 4.2 to 5.9mMol/L over time. The C-HFD / SSC groups showed a slight but not significant ($p=0.082$) increase in mean BGL from the tenth diabetic day (from 7.48±0.07 to 8.01±1.23mMol/L) and this remained so until the end of the experiment (diabetic day 60), a characteristic symptom of a prediabetic state.

4.1.4.3 Food and water intake

The daily food (Figure 4.5A) and water (Figure 4.5B) intakes per rat were recorded throughout the prediabetic and the diabetic periods (day 11 to day 88 of the experimental period). Each group maintained its original diet throughout the experiment: RAC for the NC, C-SSC and the RAC / STZ groups and HFD for the C-HFD / SSC and HFD / STZ groups.

Prior to STZ injection, no significant difference in the mean daily food ($p=0.53$) and water ($p=0.123$) intakes per rat between groups was recorded. After STZ injection, both parameters began to increase and became significantly high from the diabetic week 3 in the RAC / STZ ($p=0.00035$) and week 4 for HFD / STZ groups ($p=0.02$) compared to the control ones. The mean values remained high until the end of the experiment ranging between 20.257±3.208g and 47.28±2.91g for the RAC / STZ group and 20.014±3.933g to 31.02±5.436g for the HFD / STZ group. The lowest mean daily food consumption per rat was recorded in week 1 and the highest in week 6 of the diabetic period for both STZ treated groups. The increase in the mean daily food intake in the HFD / STZ animal was moderate compare to that of the RAC / STZ.

Similarly, the mean daily water intake per rat significantly increased ($p<0.001$) for RAC / STZ and HFD / STZ groups, ranging from 182 ± 30mL and 33.771±12.03mL at the end the first diabetic week to 321.02±13.81mL and 102.20±3.428mL in week 6 respectively, typical symptoms of both T1 and T2 DM.

The control animals (NC, C-SSC and C-HFD / STZ, not treated with streptozotocin) had no significant difference in the mean daily food and water intakes per rat throughout the diabetic period. They maintained a relatively constant mean daily food (15 to 24.72±3.93g/day/rat) and water (31.414±5.18 to 42.9±6.68mL/day/rat) intake.

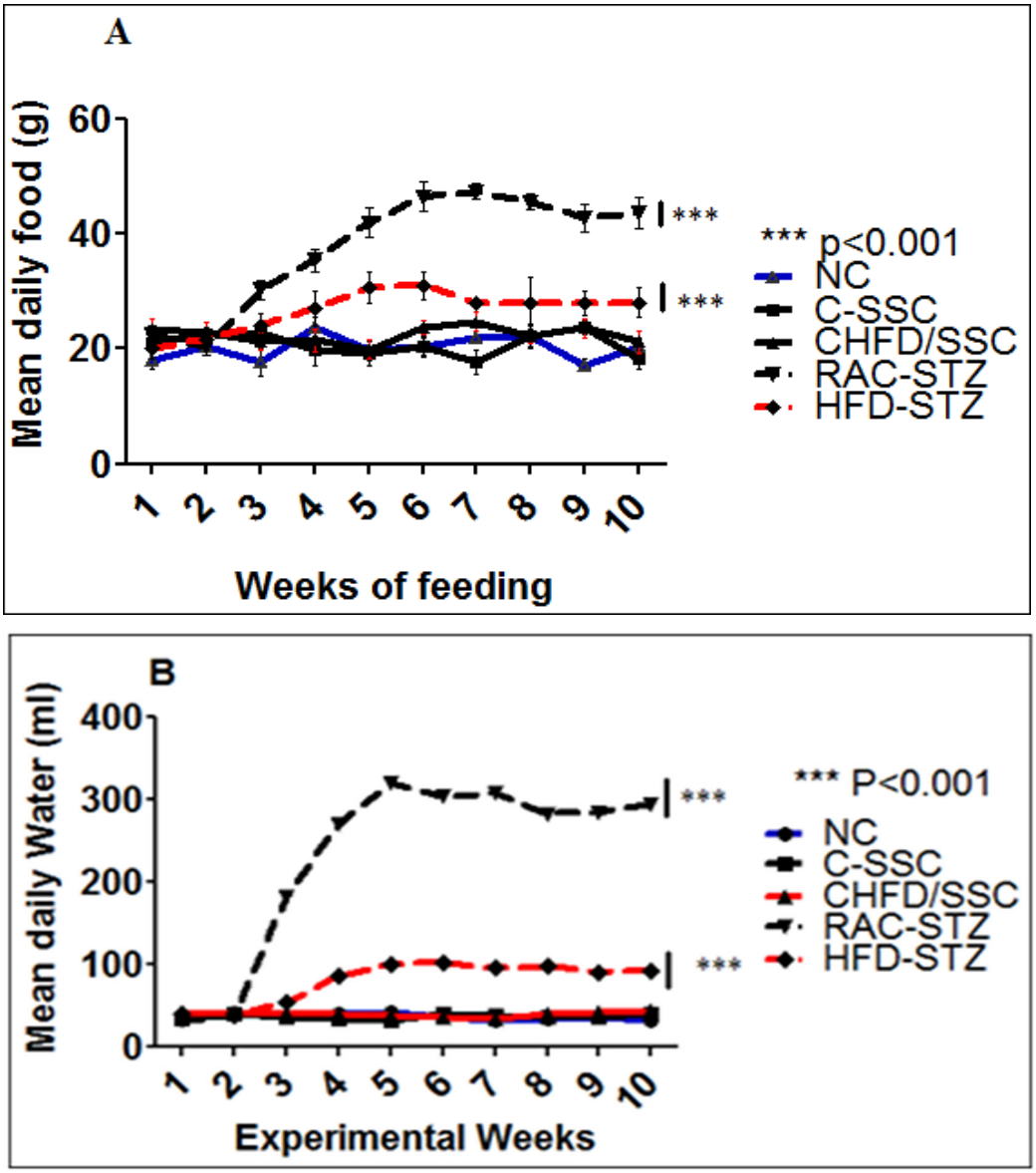

Figure 0.5: Trends of Mean daily food and water intakes under all experimental conditions during the Pre-diabetic (week 1 to 2) and diabetic (week 3 to 10) period.

Each point on the graph represents the mean ± standard error of the mean of daily food intake (A) or water intake (B) per rat each week for 8 (RAC / STZ group) to 10 rats per group; Statistical difference versus NC, C-SSC and C-HFD / STZ groups using one way ANOVA with the Newman-Keuls post hoc test ($p<0.05$).

4.1.4.4 Diabetes induction survival rate

The alteration of the vascular structure is directly associated with the diabetogenic state of an individual. To ensure that hyperglycaemia was induced and maintained in experimental animals

(RAC / STZ and HFD / STZ groups) we examined the survival rate of the diabetogenic effects of STZ (BGL≥15mMol/L) in each diabetic induced group. A success rate of 80% for the RAC / STZ group and 100% for the HFD / STZ group was recorded and maintained during the 60 diabetic days (Figure 4.6). The RAC / STZ group had only 80% survival rate due to the death of two animals on day 34 and 43 of diabetes respectively.

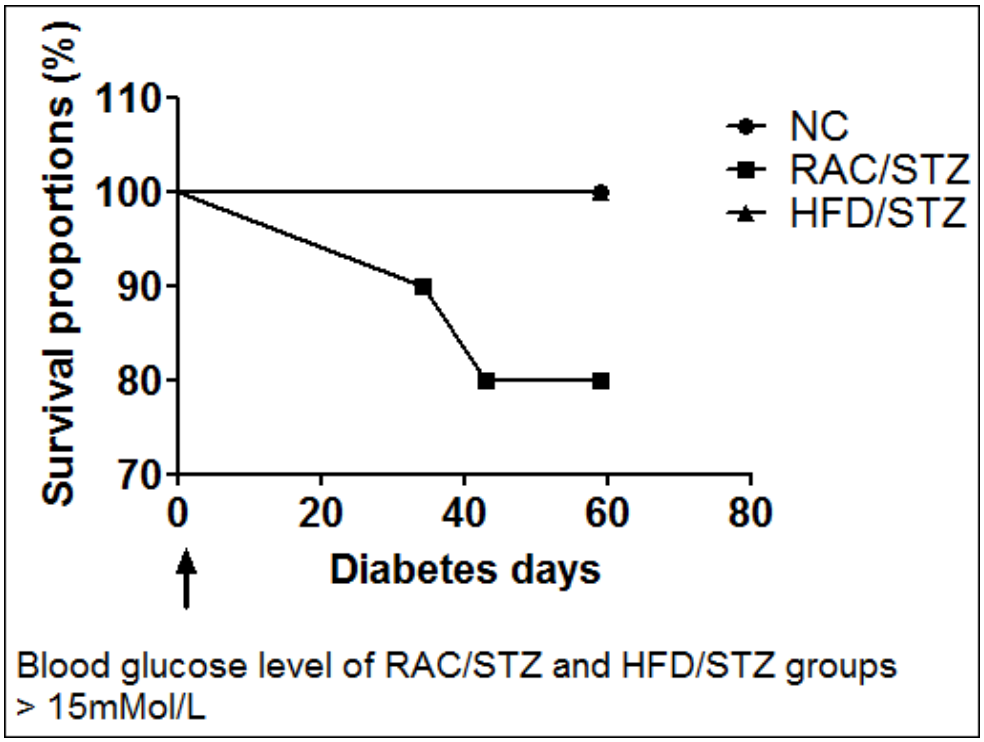

Figure 0.6: Survival rate after streptozotocin administration during the diabetic period.

RAC / STZ and HFD / STZ groups received a dose of 50 and 35mg/kg bodyweight of streptozotocin respectively. Four days later (on diabetic day 1), animals of both groups had a blood glucose level greater than 15mMol/L and were declared diabetic. One rat from the RAC / STZ (n=10) died on the days 34 and another on the day 43 of the diabetic period. Therefore, 80% survival rate was recorded in this group compared to the 100% obtained in HFD / STZ group

4.2 EFFECT OF HYPERGLYCAEMIA ON ANIMALS' IMMUNODETECTION PARAMETERS

The effect of hyperglycaemia on the various animals' immunodetection parameters associated with the vascular damage and repair are discussed here.

The Magnetic Luminex assay and flow cytometry were used to validate the *vascular* damage and *repair* potential of the damage, respectively while CD34 was used as the biomarker for endothelial

cells and discussed later in this chapter under the histomorphology of the pancreatic tissue (4.4.1.1).

4.2.1 Effect of hyperglycaemia on the serum levels of four inflammatory cytokines associated with the vascular damage

The following potential serum biomarkers in response to vascular functional incompetence and injury were analysed in experimental and control animals using Magnetic Luminex assay: IL-6, TNF-alpha, TIMP-1, and VEGF. These cell-signalling molecules are involved in the normal functions of haematopoiesis, the immune system, metabolism, as well as in the pathogenesis of cardiovascular diseases (Qu et al., 2014). The level of IL-6 and TNF characterized as markers for the above-listed disorders were tested to evaluate the degree of the vascular inflammation in this study (Qu et al., 2014). Under the present experimental conditions, serum concentrations of these two cytokines (IL-6 and TNF) were not detectable in all groups because they were out of the range set by the standard protocol. For statistical analysis (one way ANOVA), the fluorescence intensity (FI) was considered as previously justified by Breen, Tan & Khan (2016). The method is considered as a better choice for analysing quantity estimation because it lessens the concern for determining levels of detection. To verify vascular inflammation and injury-induced angiogenesis in diabetic rats, the serum VEGF-A level was evaluated. This is a potent angiogenic factor that has been identified as a primary initiator of proliferative diabetic retinopathy (Aiello & Wong, 2000). TIMP-1, on the other hand, was tested to quantify the increase of the extracellular matrix (collagen and elastin) formation that may be the cause of the increase in the vessel wall thickness (Jacob, 2003).

Although assessing the level of these biomarkers does not specifically indicate whether pancreatic vascular dysfunction has occurred with high blood glucose levels, these tests validate the severity of the effect of hyperglycaemia on the vascular system in general, in the two experimental diabetic models.

4.2.1.1 Mean serum level of Interleukin 6

The mean fluorescence intensity (MFI) of the serum level of IL-6 is shown in Figure 4.7. Mean values ranged from a minimum of 20.05±0.474 in NC group to a maximum of 24.61±1.255a.u. in the RAC / STZ group, with a statistically significant difference ($p=0.0023$) between the 2 groups. No significant difference between NC and the remaining groups was recorded.

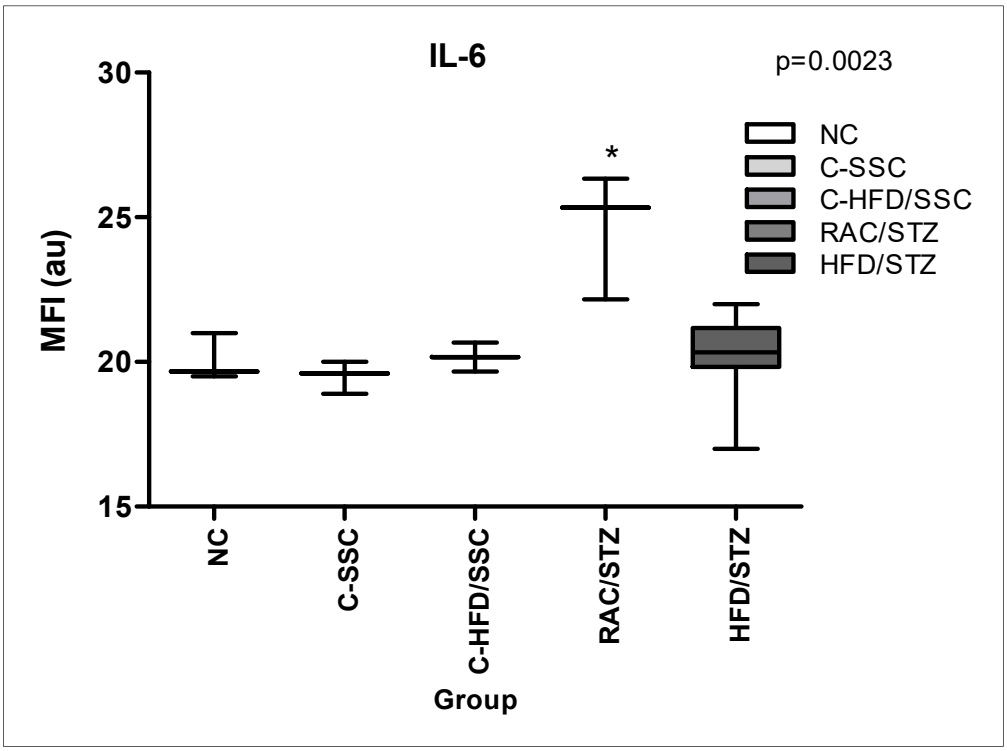

Figure 0.7: Mean serum level of Interleukin-6 after 60 days of diabetes mellitus under all experimental conditions using the Luminex magnetic assay technique.

Interleukin-6 (IL-6) level was significantly higher in RAC / STZ but not in the HFD / STZ group: Box and whisker plot of IL-6 level. The horizontal bars in the box are means of 8-10 rats, the box is the lower and upper quartiles (25-75th percentile) and whiskers are the SEM. All data are expressed in arbitrary unit (au) as mean ± SEM, $p<0.05$. Statistical difference versus NC, C-SSC and C-HFD / STZ groups using the Kruskal-Wallis test followed by post hoc Dunn's test.

4.2.1.2 Mean serum level of the tumour necrosis factor-alpha

The mean fluorescence intensity (MFI) of the serum level of TNF-alpha assay is presented in Figure 4.8. The highest mean value of the TNF- alpha was recorded in the HFD / STZ group (43.05±4.411a.u) followed by the RAC / STZ group (41.666±4.745a.u). The NC group had a mean value of 30.05±3.1a.u. The C-SSC group had the lowest value 29.359±3a.u. which was significantly different (p=0.0065) from the value obtained in the HFD / STZ group. No significant difference was found between NC and the other groups.

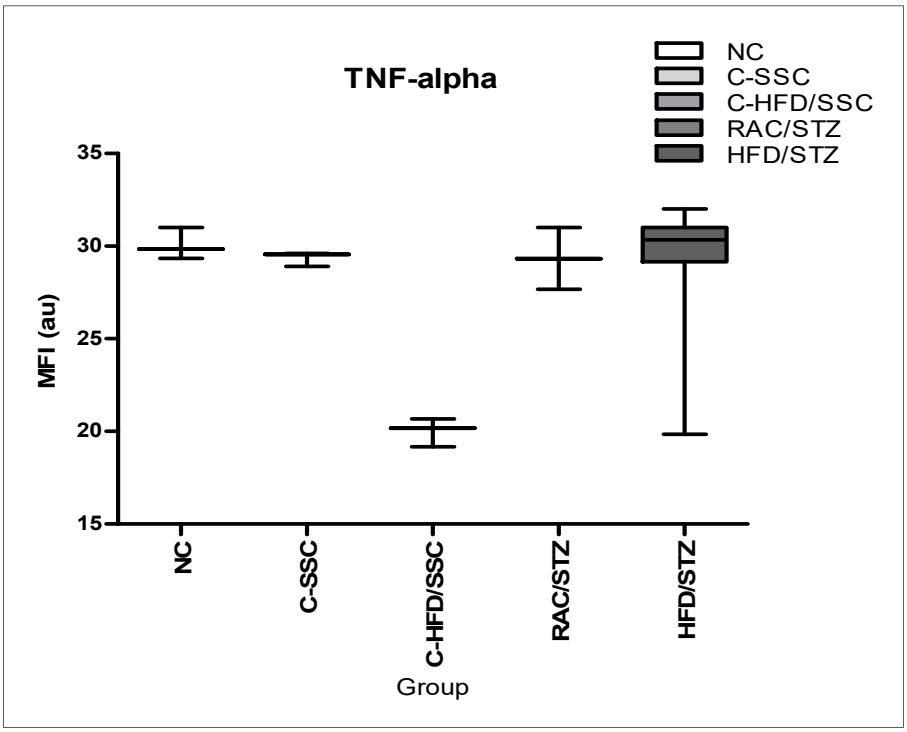

Figure 0.8: Mean serum level of tumour necrosis factor-alpha after 60 days of diabetes mellitus under all experimental conditions using the magnetic Luminex assay technique.

Tumour necrosis factor-alpha (TNF-alpha) serum level was significantly ($p<0.01$) different between the C-SSC group and the HFD / STZ group: Box and whisker plot of TNF-alpha level. The horizontal bars in the box are means of 8-10 rats, the box is the lower and upper quartiles (25-75th percentile) and whiskers are the SEM. All data are expressed in arbitrary unit (au) as mean ± SEM $p<0.05$. Statistical difference versus NC, C-SSC and C-HFD / STZ groups using the Kruskal-Wallis test followed by post hoc Dunn's test

4.2.1.3 Mean serum level of the tissue inhibitor of metalloproteinase 1

Figure 4.9 shows the mean serum level of metalloproteinase 1 (TIMP-1), a tissue inhibitor, under all conditions. The highest mean level was recorded in the RAC / STZ group (3073.665 pg/mL) followed by the HFD / STZ group (1935.593pg/mL, while the lowest was recorded in the C-SSC (1432.3pg/mL) with a significant difference ($p<0.05$) between each of the diabetic groups (RAC / STZ and HFD / STZ) and control groups (NC and C-SSC).

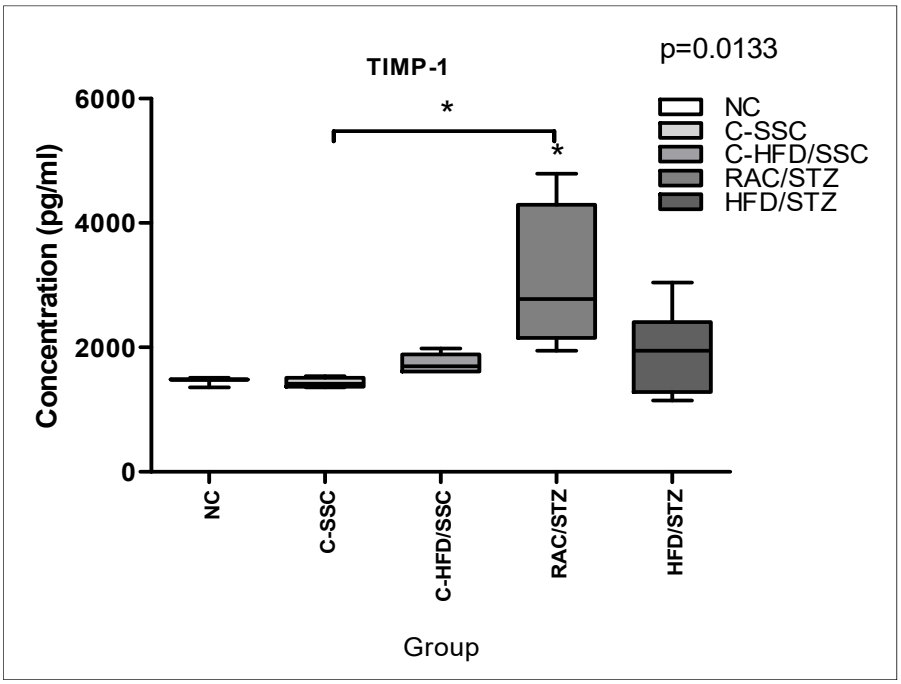

Figure 0.9: Mean serum level of tissue inhibitor of metalloproteinases 1 after 60 days of diabetes mellitus under all experimental conditions using the Luminex magnetic assay technique.

The RAC / STZ group has the highest significantly ($p<0.05$) level of the TIMP-1: The horizontal bars in the box are means of 8-10 rats, the box are the lower and upper quartiles (25-75th percentile) and whiskers are the SEM. All data are expressed in picogramme/millilitre as mean ± SEM, $p<0.05$. Statistical difference versus NC, C-SSC and C-HFD / STZ groups using the Kruskal-Wallis test followed by post hoc Dunn's test.

4.2.1.4 Mean serum level of the vascular endothelial growth factor

Figure 4.10 shows the mean serum vascular endothelial growth factor (VEGF) level in each group. Although there was no significant difference between the groups, an upward trend in VEGF levels (33.3±5.553 and 39.777±6.450pg/mL) was observed in all diabetic groups (RAC / STZ and HFD / STZ respectively) compared to all control groups 14.59±5.095, 14.28±1.573 and 26.27±5.450pg/mL for NC, C-SSC and C-HFD / SSC respectively.

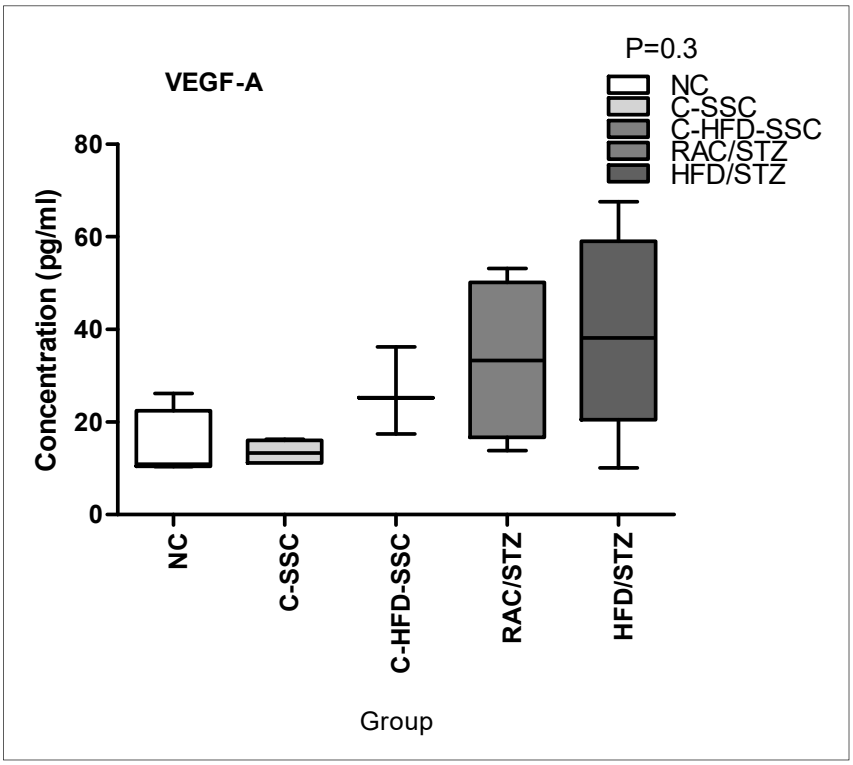

Figure 0.10: Mean serum level of vascular endothelial growth factor after 60 days of diabetes mellitus under all experimental conditions using the Luminex magnetic assay technique.

Vascular endothelial growth factor (VEGF-A) levels were not significantly higher in both diabetic animal groups (RAC / STZ and HFD / STZ group): Box and whisker plot of VEGF-A level. The horizontal bars in the box are means of 8-10 rats, the box is the lower and upper quartiles (25-75th percentile) and whiskers are the SEM. All data are expressed in picogramme/millilitre as mean ± SEM.

4.2.2 Peripheral blood mononuclear cells immunophenotyping by flow cytometry

The effects of hyperglycaemia were examined on the integrity of the endothelium: a flow cytometry technique was used to determine the number of CEPCs in experimental and controls animals. As described in the Materials and Methods chapter (3.4.1.2.), the techniques involved several steps defined by the progressive combination of a series of antibody reactions and a system of gating strategies. All data in the figures below are expressed as mean ± SEM of 8-10 rats, $p<0.05$. Statistical differences versus NC, C-SSC and C-HFD / STZ groups using one way ANOVA with the Kruskal-Wallis post hoc test.

Box and whisker plots show median (central line), upper and lower quartiles (box) and range excluding outliers (whiskers). Data were analyzed using Kruskal–Wallis test followed by the Dunn's multiple comparison test. P≤ 0.05 was considered statistically significant.
Box-plot representation of the circulating endothelial progenitor cells (CEPCs) levels at days 1 and 21. Box-plots show median (middle line), interquartile range (box), 25-75th percentile (whiskers). CR: complete response; VGPR: very good partial remission; PR: partial response; d: day. The paired-samples t-test was used for statistical analyses.

The relationship between serum levels of CEPC and CD34 islets on one hand, and methenamine stained pixel areas and pancreatic vessel thickness, on the other hand, was assessed.

4.2.2.1 Total number of single cells

A gate was drawn around single cells in an FS peak vs. FS interval dot plot. The highest mean of the total event was observed in group C-SSC (635528), followed by groups NC (482363) and then RAC / STZ (352805) (Figure 4.11). The lowest mean (82463.4) was obtained from the HFD / STZ group. There was a significant difference (p<0.01) between the C-SSC group and all the HFD groups.

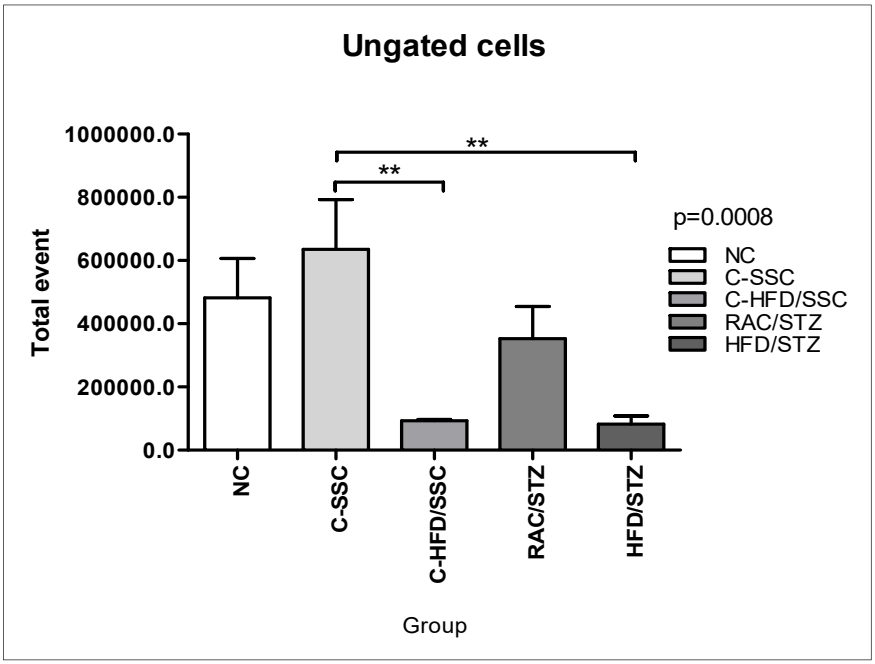

Figure 0.11: Mean total number of cells obtained from the peripheral blood mononuclear cells analysis after doublet elimination in each condition.

Streptozotocin-treated animals (RAC / STZ and HFD / STZ) were maintained diabetic for 60 days before the peripheral blood mononuclear cells isolation. Each column bar is the representation of the mean number of ungated cells in a condition (n=8-10 rats). Data analysed by one way ANOVA Kruskal-Wallis test followed by the Dunn's multiple comparison test. P < 0.05 was considered statistically significant. ** p<0.01

4.2.2.2 The percentage viability

Zombie violet was used to select viable cells from the single ones and data were recorded (Figure 4.12). The NC group showed the highest value of viable cells representing a mean percentage of 91.131%±0.81%, followed by C-HFD / SSC (85.574%±4.212%) and RAC / STZ (77.31%±4). 41%). The HFD / STZ group had the lowest and statistically significant (p<0.05) % viable cells (59.161%±5.79%) compared to the NC group.

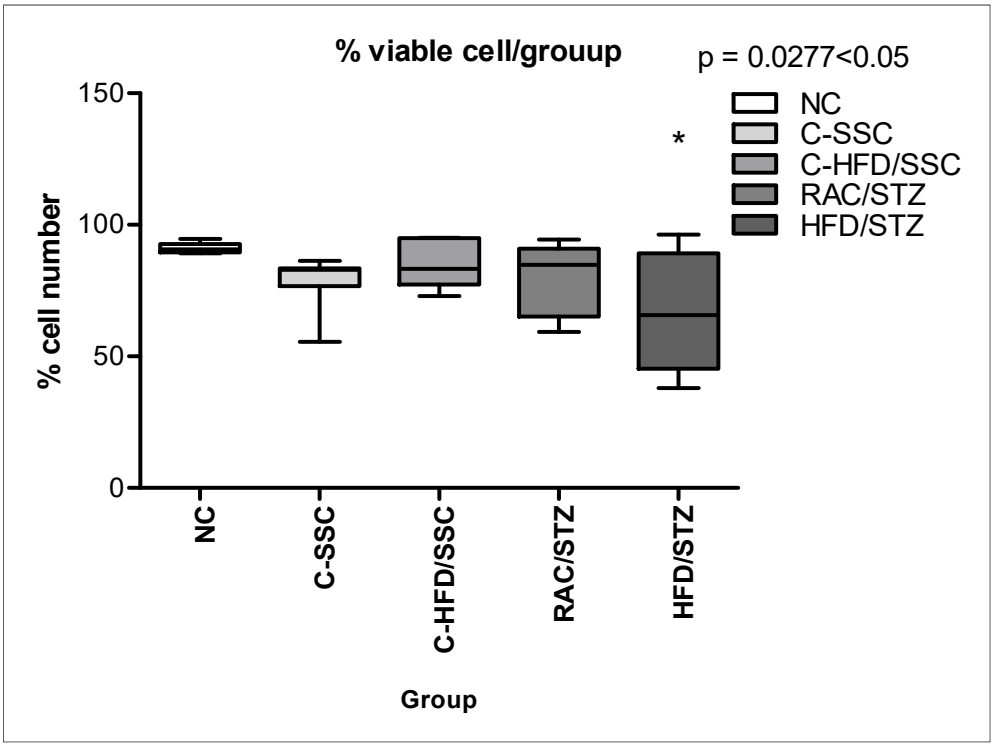

Figure 0.12: Percentage (%) viable cells in each condition.

The Zombie Violet TM solution was used to select viable cells from the total event in each group The horizontal bars in the box are means of 8-10 rats, the box is the lower and upper quartiles (25-75th percentile) and whiskers are the SEM. Results are presented as mean ±SEM. Data

analysed by one way ANOVA "Kruskal-Wallis test" followed by the Dunn's multiple comparison test. P < 0.05 was considered statistically significant. *p<0.05.

4.2.2.3 Expression of CD45 cells

Lymphocytes and granulocytes were selected from the viable cells using the FS vs CD45-AF700 dot plot interval, and the percentages were calculated. There were no significant difference between the groups (NC: 17.5±1.33%, C-SSC: 14.96%, C-HFD / SSC: 18.12±1.45%, RAC / STZ: 15.78±0.96% and HFD / SSC 13.5±2.1%) (p=0.56). The remaining cells were a mixture of smaller CD45+ and CD45- expressing cells.

4.2.2.4 Expression of CD133 cells

The potential fraction of cells containing the CEPCs was further extracted from CD45- / + cells using a CD133-APC vs. CD133-APC dot plot CD45-AF700. All cells expressing CD45+ / CD133+ were separated from CD45- / CD133+ cells without significant statistical difference between the groups for both cell lines. The C-HFD / SSC group had the highest mean percentage of CD45+ / CD133 + cells (2.22±1.02%), whereas the normal control group had the highest mean percentage of CD45- / CD133+ cells. high (1.89±6.03%).

4.2.2.5 Expression of CD45-CD133+CD31+CD34+ (CEPCs yield)

A combination of CD31 and CD34 expressions were then used to assess the level of CEPC from total viable CD45- / CD133 + cells. CEPCs are characterized by CD45- / CD133 + / CD31 + / CD34 + as previously described by (Liao et al., 2010). The normal control group had the highest percentage of CEPC value (1.13±0.373%), followed by the C-SSC group (0.682 ± 0.08%) and then the C-HFD / SSC group (0.360±0.192%) (Figure 4.13, summary in Table 4.1). There was a significant difference (p=0.0325) between the NC and HFD / STZ group which had the lowest percentage CEPCs (0.1213±0.031%). There was no significant difference in the percentage CEPCs value between the control and RAC / STZ groups, as well as between the two types of diabetic rat models.

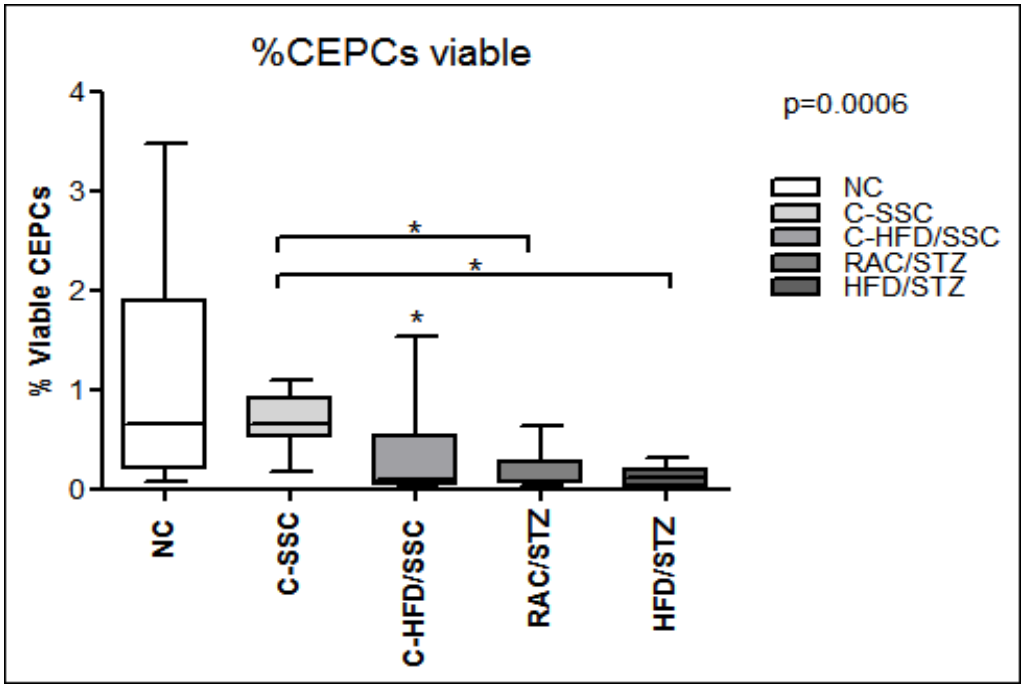

Figure 0.13: Box and whisker plots representation of the percentage CEPCs expression in all conditions.

The horizontal bars in the box are means of 8-10 rats, the box is the lower and upper quartiles (25-75th percentile) and whiskers are the SEM. Results are presented as mean ±SEM. Data analysed by one way ANOVA "Kruskal-Wallis test" followed by the Dunn's multiple comparison test. P < 0.05 was considered statistically significant. *p<0.05.

Table 0.1: Summary of percentage viability of ungated and percentage of total CEPC cells (CD45-CD133+CD31+CD34+) in each condition.

	NC (n=10)	C-SSC (n=10)	C-HFD / SSC (n=10)	RAC / STZ (n=8)	HFD / STZ (n=10)
% Mean Viable cells	89.03 ±1.441	85.57 ± 3.349	68.02 ± 6.392**	78.58 ± 3.085	79.97 ± 4.142
Mean %CEPC (Viab)	1.13 ± 0.373	0.682 ± 0.08	0.360 ± 0.192	0.179 ± 0.066	0.121 ± 0.031*

Results are presented as mean ±SEM. Data analysed by one way ANOVA "Kruskal-Wallis test" followed by the Dunn's multiple comparison test. P<0.05 was considered statistically significant between normal control (NC) and the remaining groups. *p<0.05, ** p<0.01.

4.3 EFFECT OF HYPERGLYCAEMIA ON THE HISTOMORPHOLOGY OF THE PANCREATIC TISSUE

While haematoxylin and eosin successfully stained slide sections of the duodenal and splenic portions of the pancreas and allowed for the evaluation of the general morphology, another set of the sections were impregnated with the silver stain and used to delineate the connective tissue (especially BM) content of the pancreatic tissue in each experimental condition. Finally, the expression of CD34 on the islet endothelial cells helped assess the integrity of the endothelium under all conditions,

4.3.1 The general histomorphology of the pancreatic tissue

The assessment of the general pancreatic tissue morphology using H&E is discussed in this section. The total magnification of the micrographs is reported as the product of the magnification of the eyepiece and the magnification of the objective. That is with a 10X objective, the total magnification is 100X (10X multiplied by 10X).

4.3.1.1 In the normal control group

Micrographs of the duodenal and splenic parts of the pancreatic tissue sections of the NC group stained with H&E are shown in Figure 4.14. The two pancreatic regions showed regular and well-defined islets pale stained areas (encircled) scattered throughout the deeply stained parenchyma (Figure 4.14 A1 and A2). The islets cells had a cord-like cellular arrangement with intervening blood vessels. The duodenal sections displayed larger but less numerous islet than the splenic sections with smaller islets. The parenchyma consisted of pyramidal acinar cells (ACs), having basal nuclei and organized in a cluster around a duct system (D). The duct system was organized into centroacinar cells and intercalated, intralobular, interlobar and main ducts (MD) (Figure 4.14B1 and B2). Each islet was delimited from the surrounding exocrine tissue by a delicate peri-islet capsule (arrow).

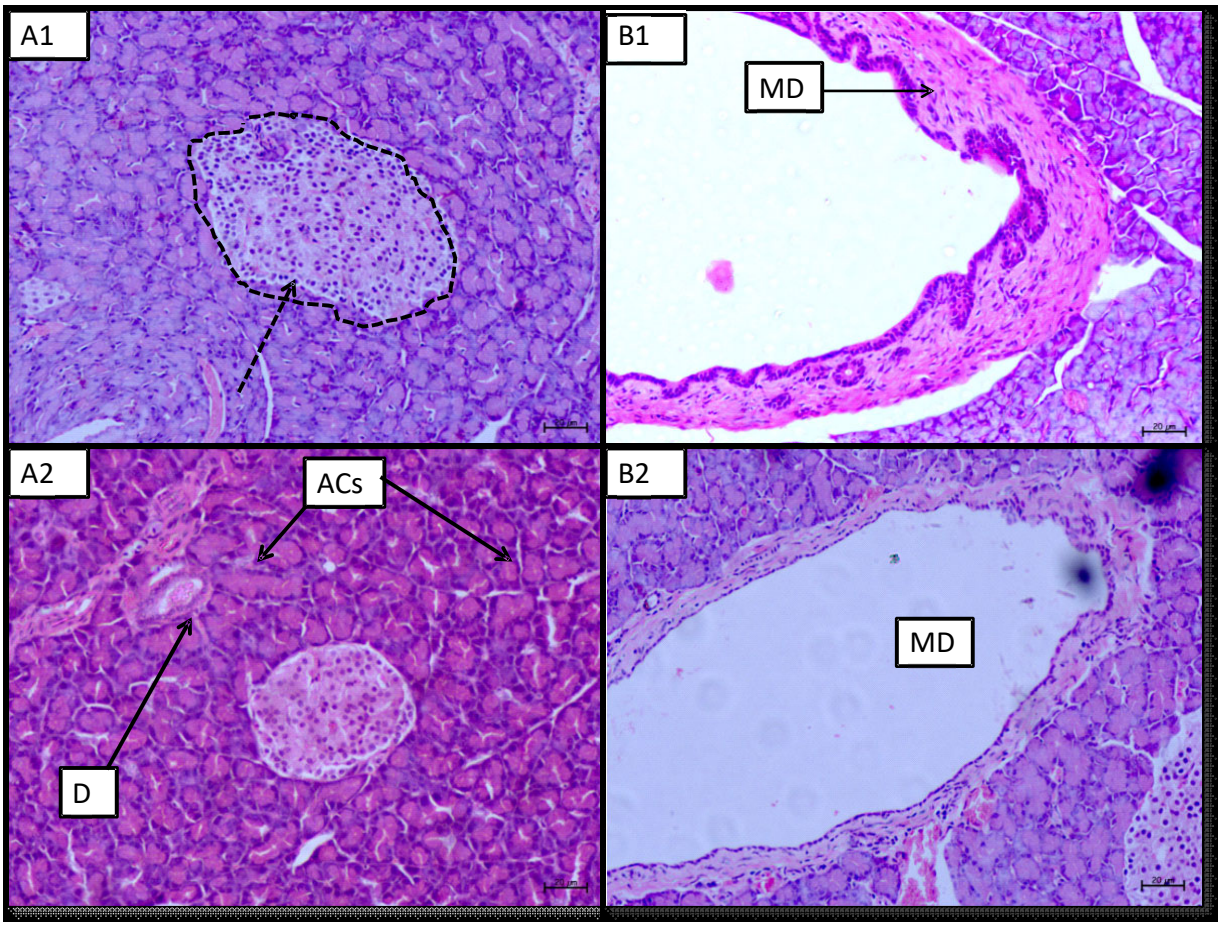

By: E. Ngounou

Figure 0.14: Photomicrograph of the pancreatic sections stained with H&E of normal control animal. Bar:20µm.

A1 and A2 represent sections of the splenic and duodenal pancreas respectively focused on the islet and the surrounding structures: In both cases, at the centre islets with scatter healthy cells stained light purple (encircled) and the acinar cells (ACs) dark blue at their base (because of the presence of nuclei) and pinkish at their apex (luminal aspect). The nuclei of centro-acinar cells are seen within an acinus (arrowhead) as they start the formation of a system of the duct (D) which ends at the main duct (MD) represented in B1 and B2). Mag=200X.

4.3.1.2 In the control to streptozotocin-induced type one diabetic group

Micrographs of the duodenal (Figure 4.15A1 and B1) and splenic parts (Figure 4.15A2 and B2) of the pancreatic tissue sections of the C-SSC group stained with H&E retained the same morphological features as those of the NC tissues with no histological changes.

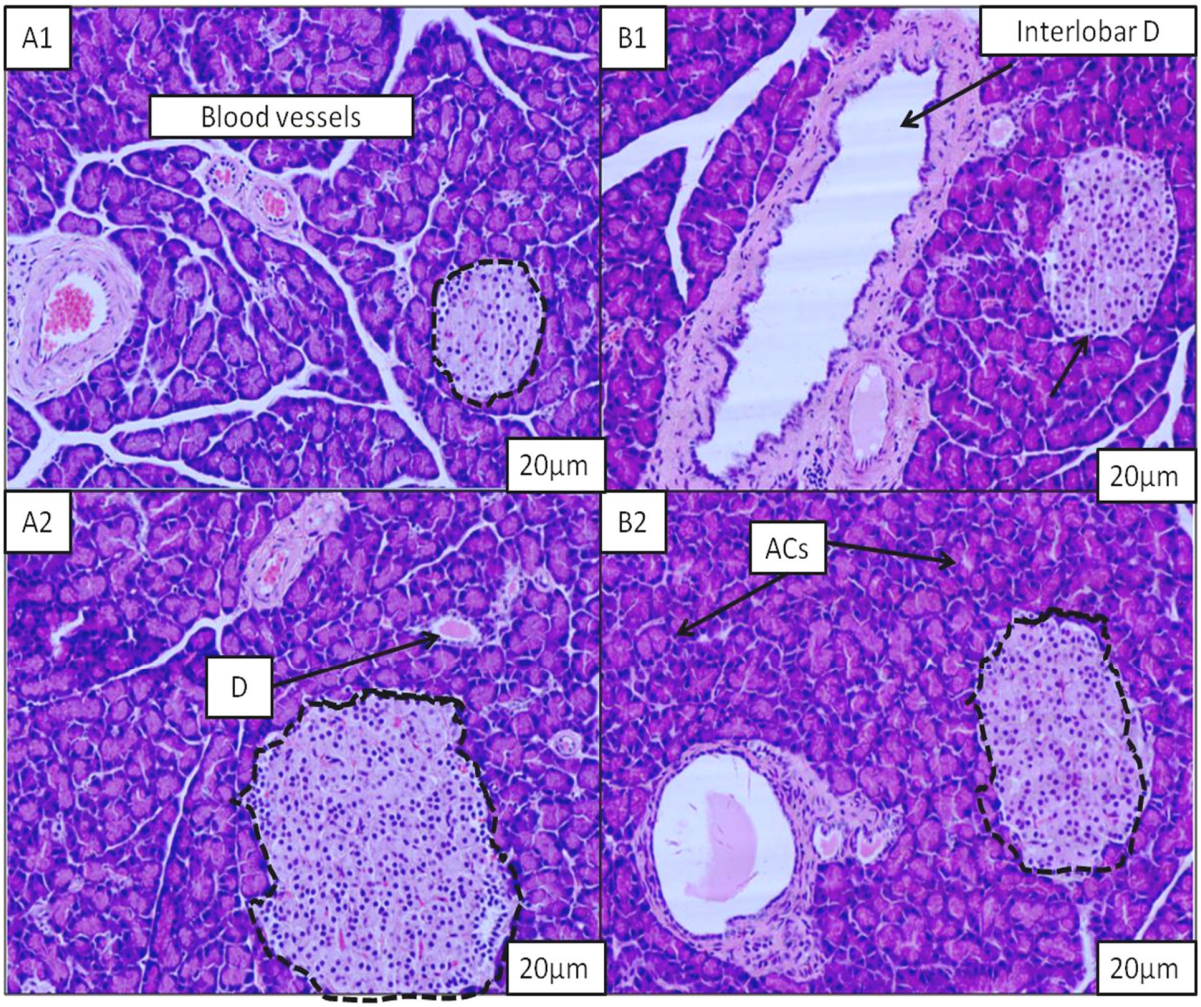

By: E. Ngounou

Figure 0.155: Photomicrograph of the pancreatic sections stained with haematoxylin and eosin of the C-SSC group (control to streptozotocin-induced type one diabetic animal model). Bar: 20µm.

4.3.1.3 In the control to streptozotocin-induced type two diabetic group

Micrographs of the duodenal and splenic portions of the pancreatic tissue sections of the C-HFD/SSC groups stained with H&E are shown in Figure 4.16. The two pancreatic regions (Figure 4.16A1 and B1 for the duodenal part and A2 and B2 for the splenic part) present numerous, large and lightly coloured islets (circled). Each islet was made up of endocrine cells with adjacent clear space (arrowhead) representing fatty infiltrations (FI). The parenchyma as in the normal control group consisted mainly of acinar pyramidal cells (ACs) strongly coloured but associated with a ductal system with moderate cellular hypertrophy. In addition, FI was observed dispersed in the

parenchyma, mainly around ducts (D) and blood vessels (BV). Each islet was delimited from the surrounding exocrine tissue by a peri-islet capsule encumbered (arrow) with fatty deposits.

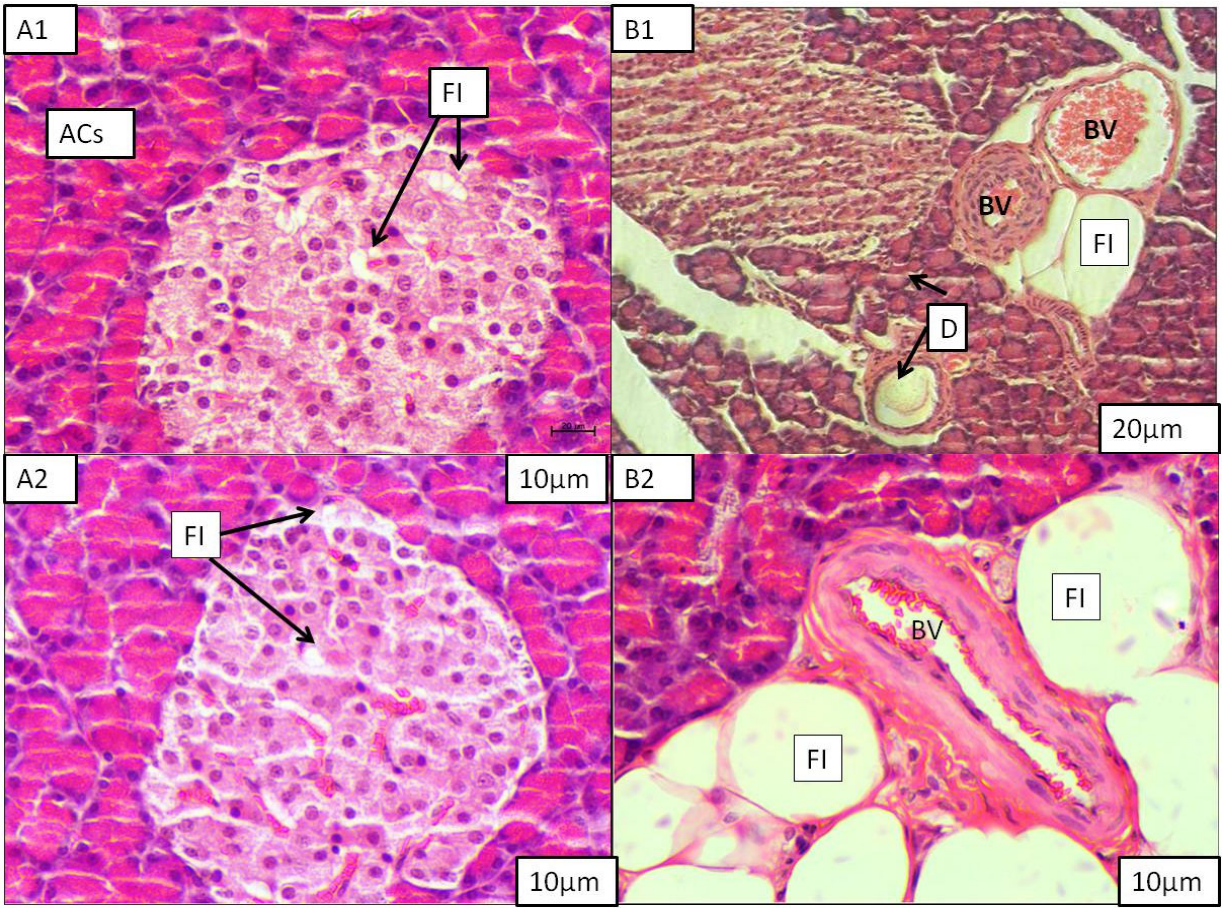

By: E. Ngounou

Figure 0.16: Photomicrograph of the pancreatic sections stained with haematoxylin and eosin of the C-HFD / SSC group (control to streptozotocin-induced type two diabetic model). Bar: 20µm.

A1 and A2 represent sections of the duodenal and splenic pancreas respectively showing islet surrounded by acinar cells (ACs) dark blue at their base and pinkish at their apexes (luminal aspect). Endocrine cells are detached from each other from place to place by intra-islets FI. B1 and B2 show hypertrophied fat cell clustered around medium-sized blood vessels (BV) for the duodenal (B1, Mag 200X)) and splenic (B2, Mag 400X) pancreatic sections respectively. Mag: 200X for A1 and A2, 100X for B1 and 400X for B2.

4.3.1.4 In the streptozotocin-induced type one diabetic group

Micrographs of the duodenal and splenic portions of the pancreatic tissue sections of the RAC / STZ group stained with H&E are shown in Figure 4.17. Examination of the two pancreatic sections

(Figure 4.17 A1 and B1 for the duodenal part and A2 and B2 for the splenic part) showed mainly acinar cells (ACs) because the islets appeared to be smaller in size (circled), shrunk and irregular in shape with a reduced number of endocrine cells, the central region hyalinised and fibrotic (arrow) showing few pyknotic nuclei (PN), focal areas of degeneration and congestion while exhibiting vacuolations (V) with infiltration of mononuclear (MCs) and lymphocytic cells (LCs).

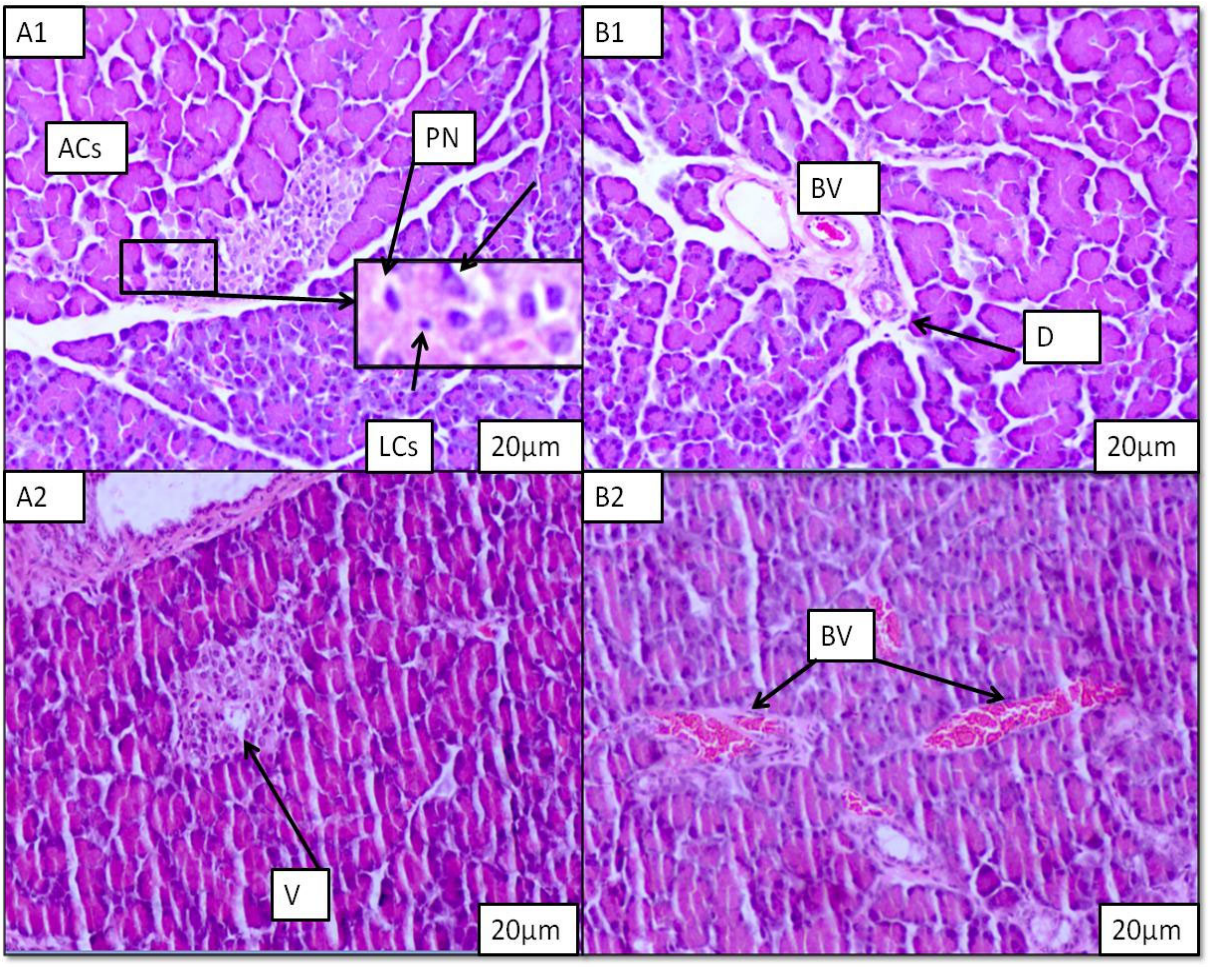

By: E. Ngounou

Figure 0.17: Photomicrograph of the pancreatic sections stained with haematoxylin and eosin of the RAC / STZ group (Streptozotocin-induced type one diabetic model)

A1 and A2 are sections of the duodenal and splenic pancreas: the islet appeared light stained in the centre of the micrograph surrounded by acini. (B1 and B2) show pancreas in this group focused on the islet structures. Islets appeared light purple and shapeless, with less demarcation of the per islet capsule. The acinar cells (ACs) stained dark blue at their base and pink at their apexes (luminal aspect). There are infiltrations of mononuclear (MCs) macrophages and

lymphatic cells within the islet core. Thin-walled blood vessels (B1 and B2) mostly presented in doublet (B2). Mag: 200X.

4.3.1.5 Streptozotocin-induced type two diabetic group

Micrographs of the duodenal (A1 and B1) and splenic (A2 and B2) portions of the pancreatic tissue sections of the HFD / STZ group stained with H&E are shown in Figure 4.18. Regarding the tissue sections of this group, they showed abnormal islet structure similar to that observed in the RAC / STZ sections but with a less degenerative state. These sections still maintained a significant amount of FI in the islet (arrowhead) and around blood vessels (BV) and ducts (D) (B1 and B2) (dotted arrow).

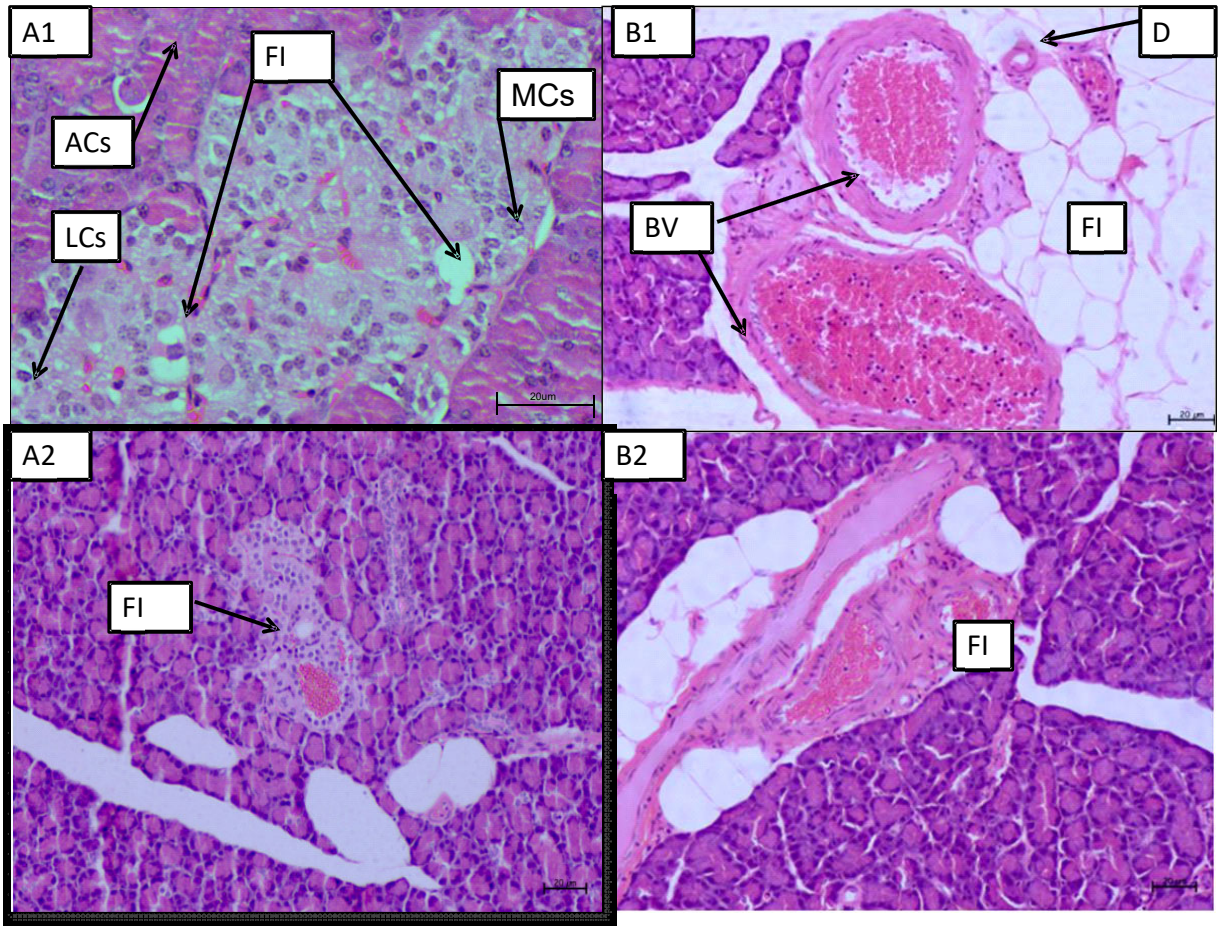

By: E. Ngounou

Figure 0.18: Photomicrograph of the pancreatic sections stained with haematoxylin and eosin of the HFD / STZ group (streptozotocin-induced type two diabetic). Bar: 20µm.

Sections of the duodenal (A1 and B1) and the splenic (A2 and B2) pancreas focused on the islet structures and stained with haematoxylin and eosin. In the two pancreatic regions, the micrographs show light purple and shapeless islets, with less demarcation of the peri-islet capsule. The acinar cells (ACs) stained dark blue at their base and pink at their apexes (luminal aspect). Mononuclear (MCs) macrophage and lymphatic cell (LCs) infiltrations within the islet core. Thin-walled blood vessels (B1 and B2) were usually presented in doublet (B2), this means an artery and its corresponding vein.(A1 Mag: 400X, A2, B1 and B2 Mag: 200X)

4.3.2 Vascular histomorphology

A close microscopic examination of the vascular structure of the two pancreatic regions under all conditions showed the five morphological vessel types normally found in the human body: arteries, arterioles, capillaries, venules and veins. Large pancreatic vessels (arteries >70μm and veins >90μm) were usually embedded within the connective tissue separating pancreatic lobes (interlobar septum). Sections from each group usually exhibited vessels in doublet; an artery and its homologous vein. Under all conditions, arteries (a) (Figure 4.19) were readily identified in the tissue sections because of their smaller luminal diameter, less than half the diameter of the vein (V), and a much thicker wall with distinct smooth muscle layer.

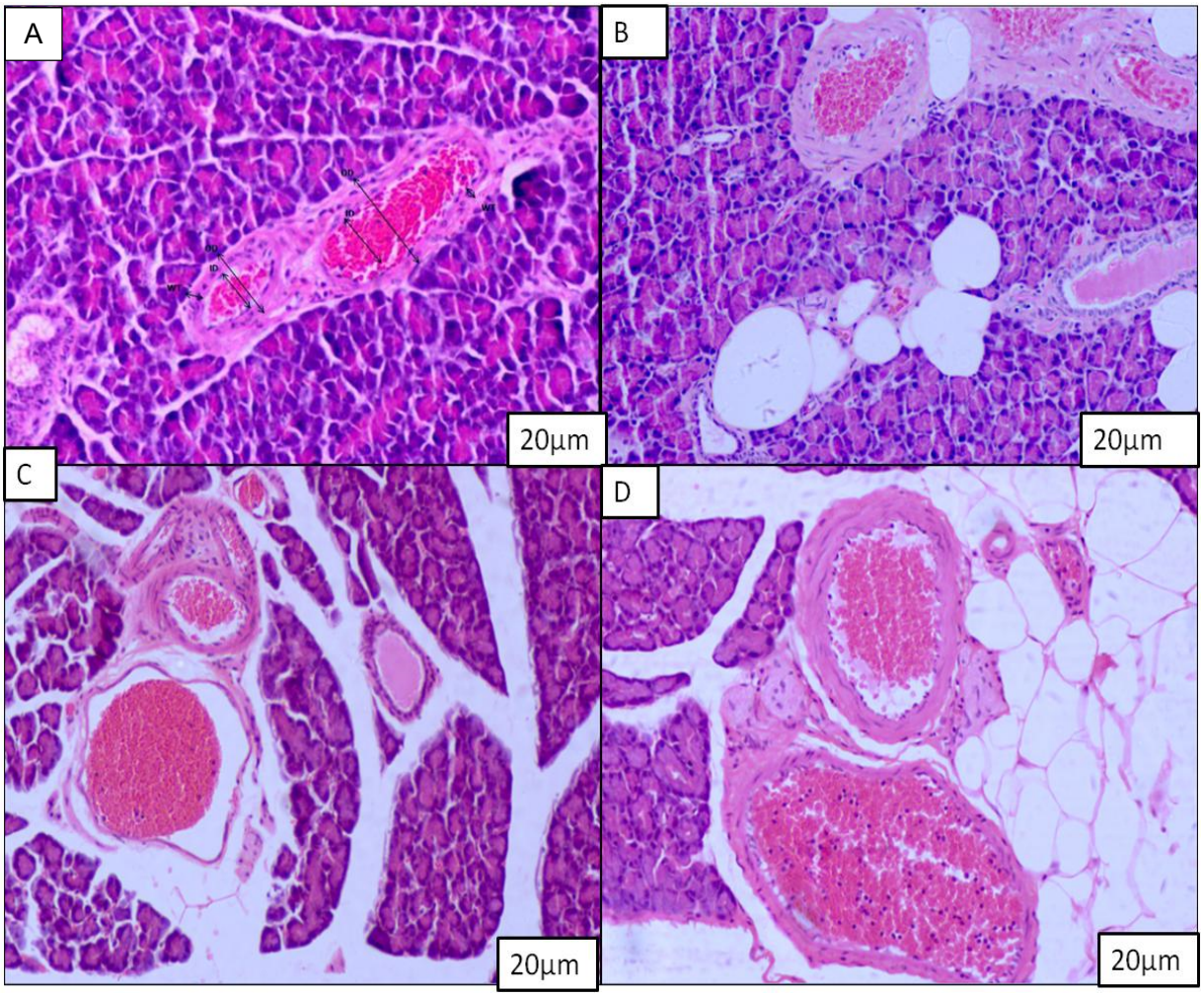

By: E. Ngounou

Figure 0.19: Schematic representation of pancreatic vessels (doublet) illustrating arteries and homologous veins structural differences under all conditions. Bar: 20µm.

Medium size vessels with thick wall and small luminal diameter arteries (a) and thin-walled and large diameter vein (V), A) from normal control, B) From a C-HFD / SSC, C) From a RAC / STZ and D) from an HFD / STZ rats. Detailed structure of the vessel types in each condition is reported in the following sections. Mag=200X.

4.3.2.1 Vascular histomorphology in the normal control group

Histological sections of the NC and C-SSC control groups showed vessels (arteries and veins) with normal anatomical features of in both pancreatic regions. Figure 4.20 represents these features.

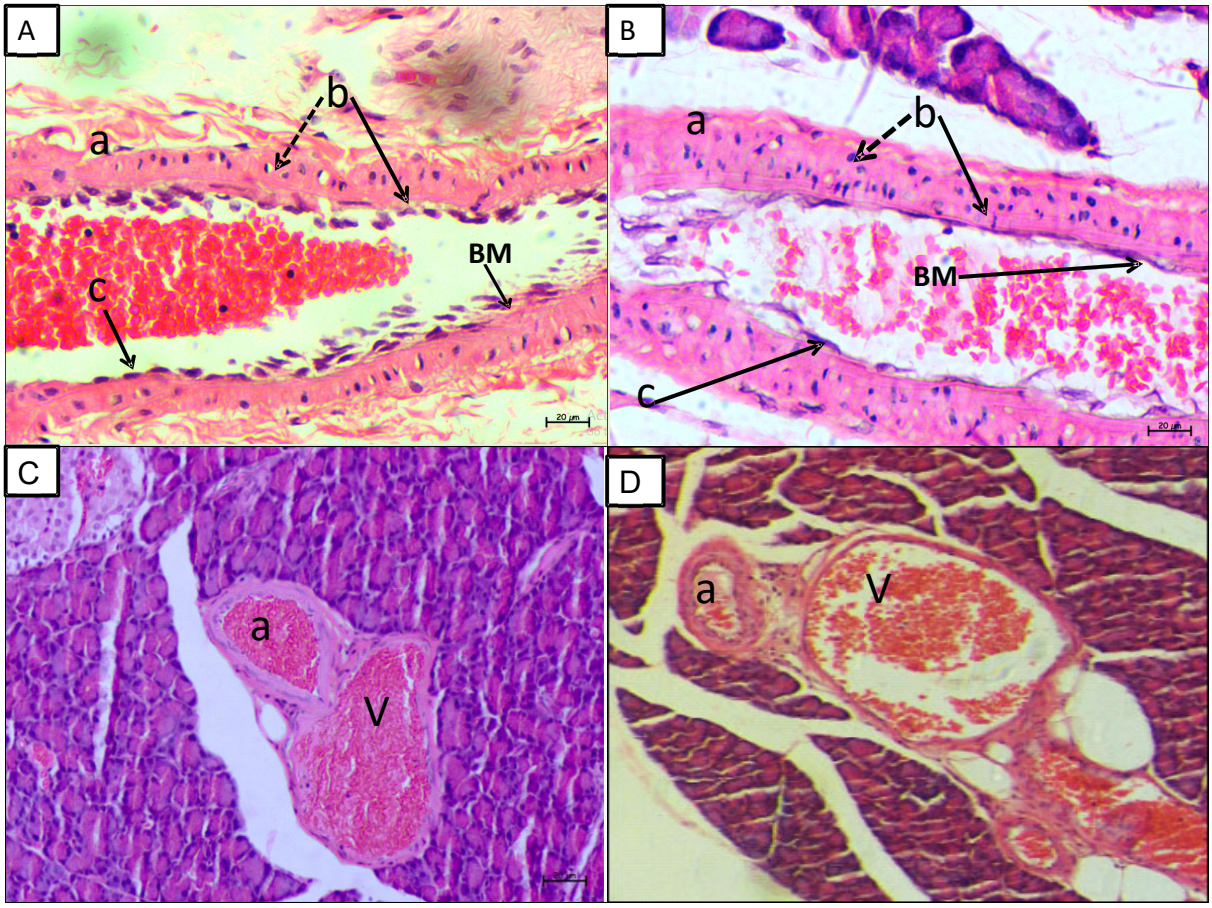

By: E. Ngounou

Figure 0.20: Photomicrograph of histological of H&E-stained pancreatic tissue sections of the normal control animal showing the detailed of the normal anatomical features of the pancreatic vessels. Bar: 20µm.

A and B are longitudinal sections of a large artery from the duodenal and splenic sections respectively. showing a wall made up of three main layers surrounding an elongated lumen containing red blood cells: thin adventitia (a), moderate tunica media with an outer longitudinal (dotted line arrow) and an inner circular (full line arrow) smooth muscle layers (b), a single layer of endothelial cells (a) supported by a moderate thickness of basement membrane (BM) Mag=400X. C and D represent medium vessels (artery (a) smaller and vein (V) larger) from the duodenal and splenic pancreatic tissue respectively with thinner of tunica media. Mag=200X.

The structures of the medium vessels were similar to those of the large vessels, but with less demarcation of the three main layers (Figure 4.20C and D). The smaller vessels (arteries and veins) sizes were abundant Figure 4.21).

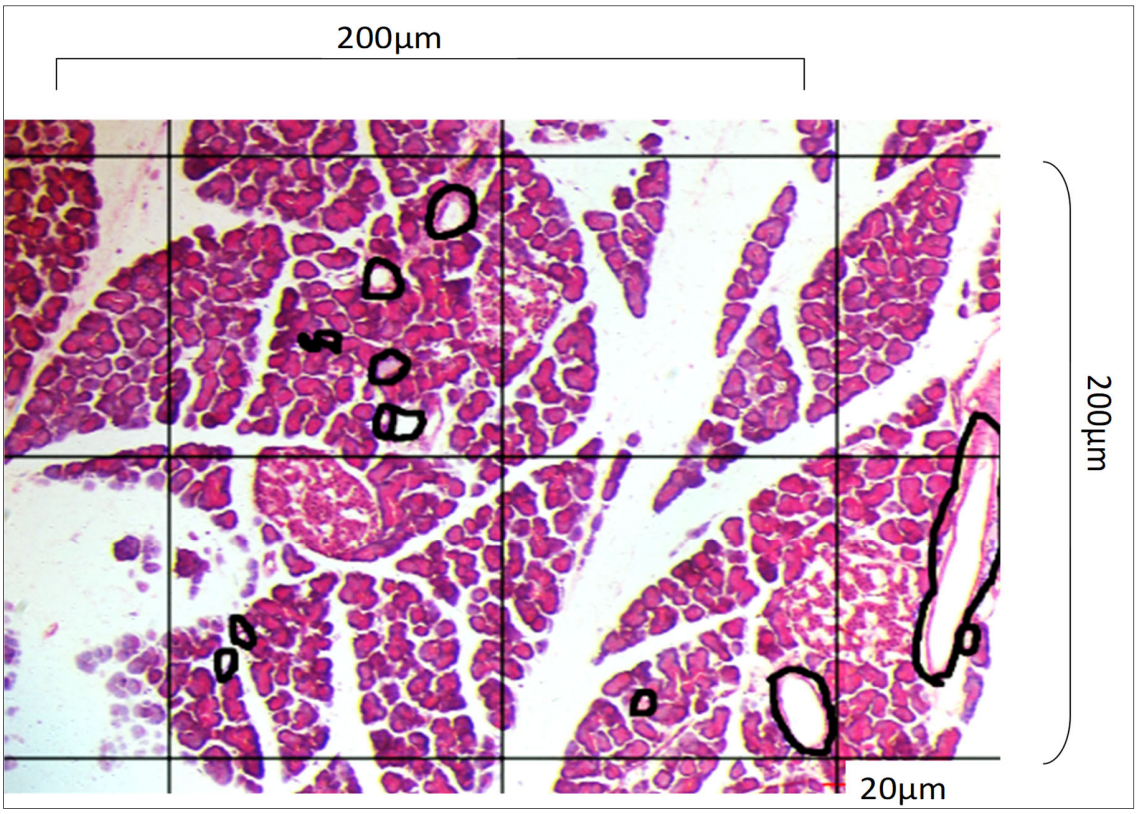

By: E. Ngounou

Figure 0.21: Numerous smaller vessels scattered in the pancreatic tissue section of a normal control animal. (Mag=200X). The vessels were examined and counted under a grid of 1 µm^2 for each square.

Like in the large vessels, arteries had smaller diameters compared to the corresponding veins (Figure 4.20A). Arteriolar walls showed little or no smooth muscle fibres with 2-3 endothelial cells surrounding the lumen in all groups (Figure 4.22) and the two pancreatic regions.

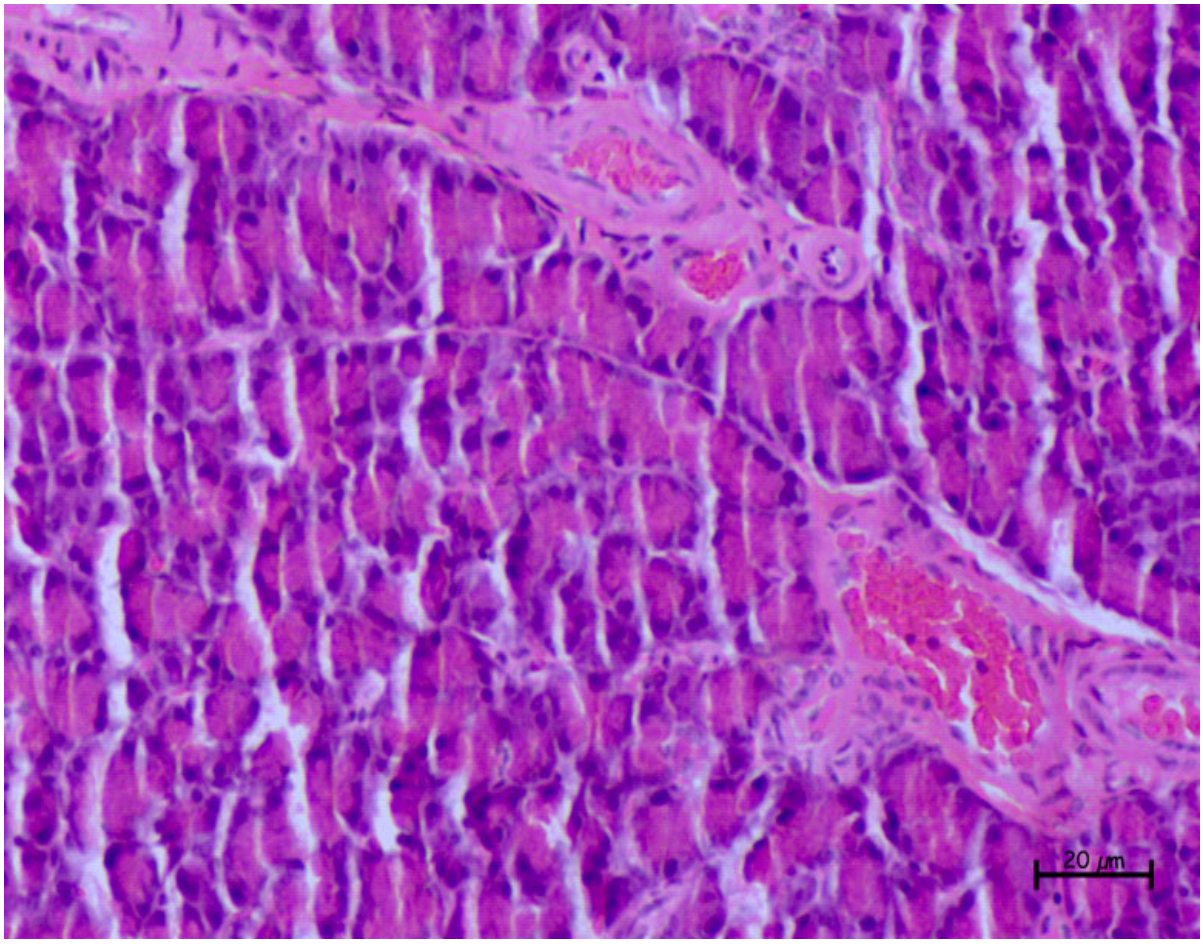

By: E. Ngounou

Figure 0.22: Section of a duodenal pancreatic tissue. Photomicrograph representation of small vessels of the rat (artery and homologous vein) with walls having little smooth muscle fibres. Bar: 20µm.

4.3.2.2 Vascular histomorphology in the streptozotocin-induced type one diabetic group

Micrographs of the duodenal and splenic portions of the pancreatic tissue sections stained with H&E of the RAC / STZ group showing the structure of the large vessels are represented in Figure 4.23. Eight weeks of hyperglycaemia (>15mMol/L) affected the histological features of the pancreatic vessels (arteries and veins) supplying the islet. These vessels had extremely thin walls with less delineated components (tunica adventitia, media and intima). As a result, the lumens were larger and wide open with no perivascular fat deposit found around them (Figure 4.23). Vessels in these sections were characterised by lumens lined by a very disconnected endothelium supported by the thickest BM compared with all the remaining groups.

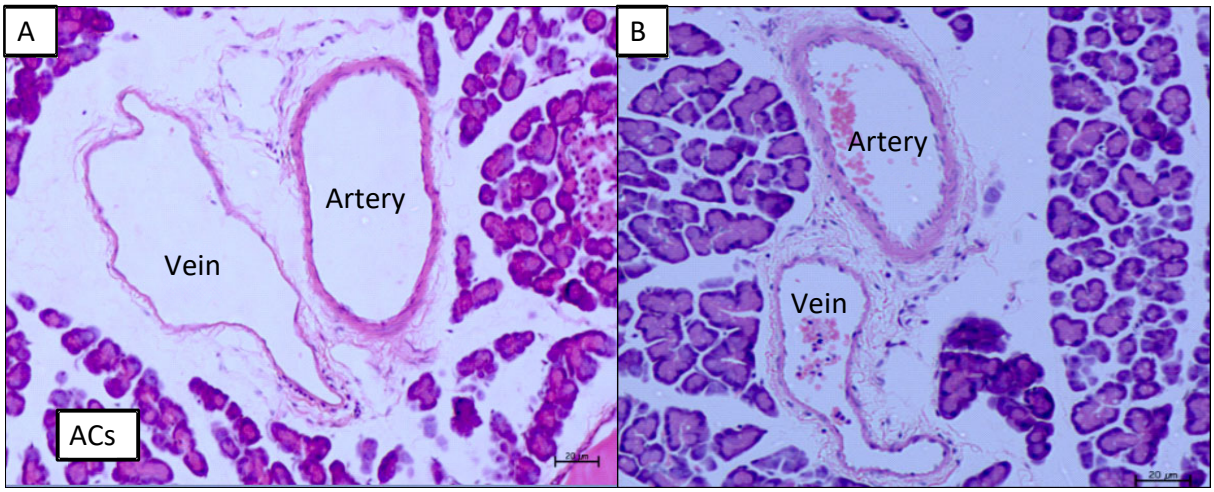

By: E. Ngounou

Figure 0.23: Photomicrographs of histological sections of RAC / STZ rats showing the detailed anatomical characteristics and components of the vessel wall. Bar: 20µm.

A) Duodenal thin-walled vein and artery. B) Splenic thin-walled vein and artery. Mag=200X.

4.3.2.3 Vascular histomorphology in the control to streptozotocin-induced type one diabetic group

Histological sections from C-SSC control groups showed arteries with normal anatomical features in both pancreatic regions as those seen in the NC group.

4.3.2.4 Vascular histomorphology in the streptozotocin-induced type two diabetic group

Tissues sections from the HFD / STZ group maintained the same pattern as those of the obese animals, but with a reduced vascular wall thickness, and less fatty congestion (figure 4.24).

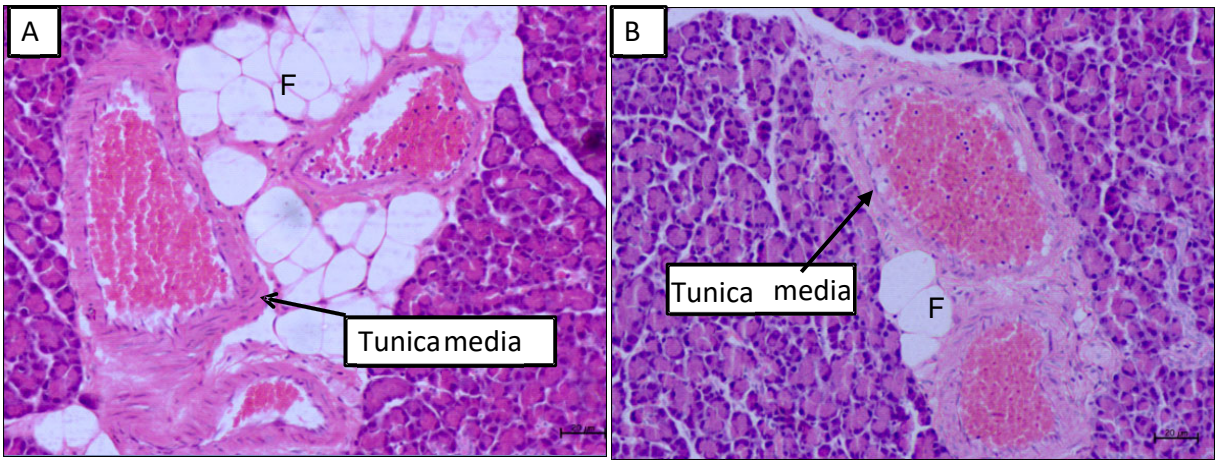

By: E. Ngounou

Figure 0.24: Photomicrographs of histological sections of HFD / STZ rats showing the detailed anatomical characteristics and components of the vessel wall. Bar: 20µm.

A) Connective tissue invaded with fat (F) around blood vessels in a duodenal section B) the same characteristic seen in the artery in the splenic section. Mag=200X.

4.3.2.5 Vascular histomorphology in the control to streptozotocin-induced type two diabetic group

The pancreatic sections stained with H&E of the C-HFD / SSC had the largest vessels (total diameter 85-90µm in arteries and 110-130µm in veins) with a net increase in the wall thickness and a clear reduction of the luminal diameter (Figure 4.25). The structure of the vessel wall in this group maintained the same anatomical pattern as those of the NC group with the exception that 1) the basement membrane (BM) was pronounced especially in the duodenal section (D), supporting a normal endothelium with very flat endothelial cells in the artery and swollen endothelial cells in the vein. The luminal surface of the venous wall was sometimes coated with fatty deposition, 2) a pronounced tunica media, especially in the duodenal section (Figure 4.25D), compared to the splenic section (Figure 4.25A & B}. Bundle of connective tissues (CT) (amyloids) in addition to large fat cells were found around the blood vessel. Smaller arteries had a very small inner diameter as compared to the total diameter (Figure 4.25C).

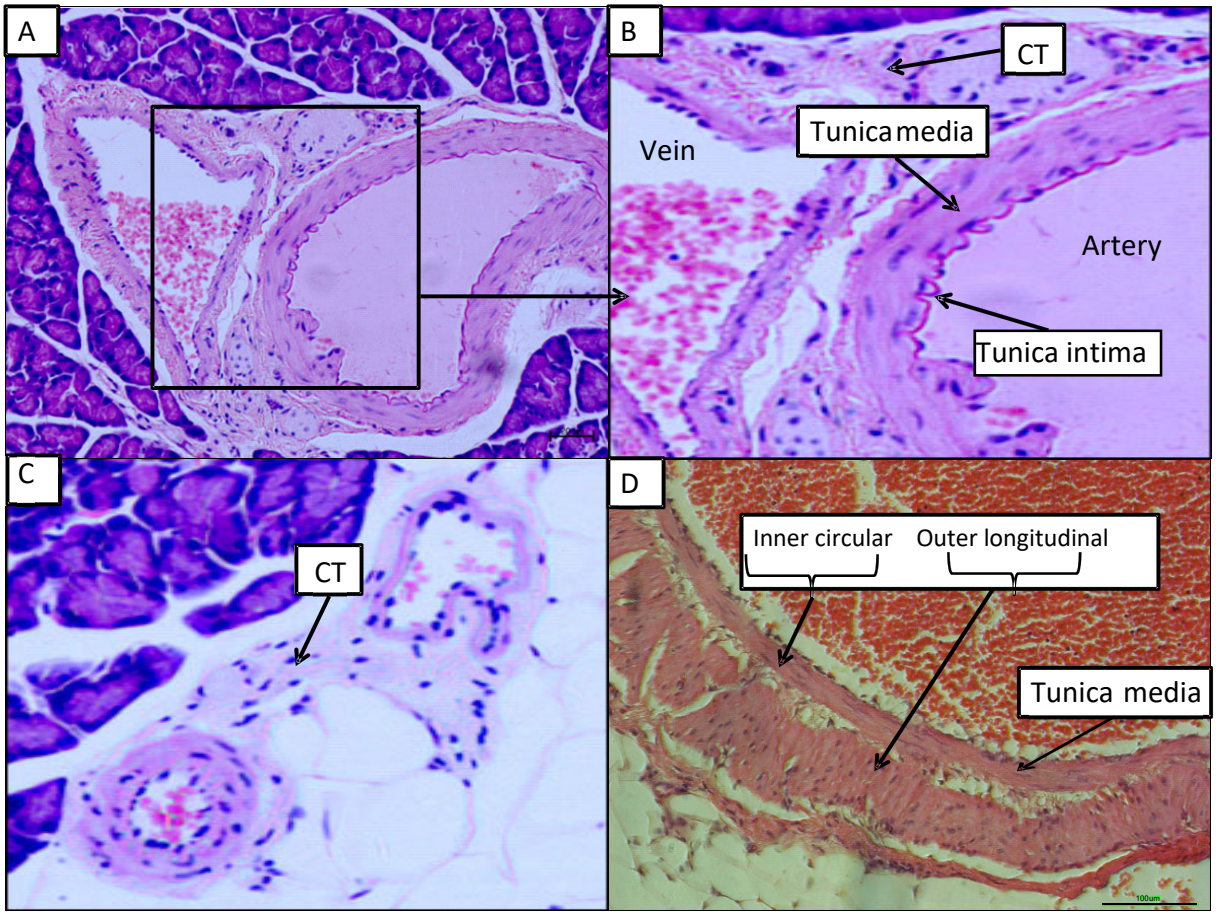

By: E. Ngounou

Figure 0.25: Photomicrographs of histological sections of the C-HFD / SSC animals showing the detailed anatomical characteristics and components of the vessel wall.

A) Vein with a thinner wall on the right and artery with a thicker wall of the left (Mag=200X, Bar: 20µm.). B) Enlarge portion of the artery and vein wall. C) A thick wall medium artery and the homologous thin wall vein surrounded by dense connective and adipose tissues (Mag=400X). D) A portion of a large artery clearly showing the two layers of tunica media separated from the acinus by a thick adventitia and from the lumen by the endothelium (Mag=400X, Bar: 100µm.).

4.3.3 Assessment of the basement membrane distribution in the pancreatic tissue

Basement membrane in the islet and the peri-islet space (Figure 4.26) was demonstrated using the silver staining method. In the islet, the distribution of the BM was not homogeneous and had the profile of CD34 expression as described with the immunological results. In other words, the core of the islet tends to be stronger impregnated with the silver stain than the mantle under all

conditions (Figure 4.26). The capsule of the islet and its invaginations while allowing blood vessels to enter the islet was highlighted. Outside the islet, the BM supporting the acinar cells was highlighted separating one acinus from the other.

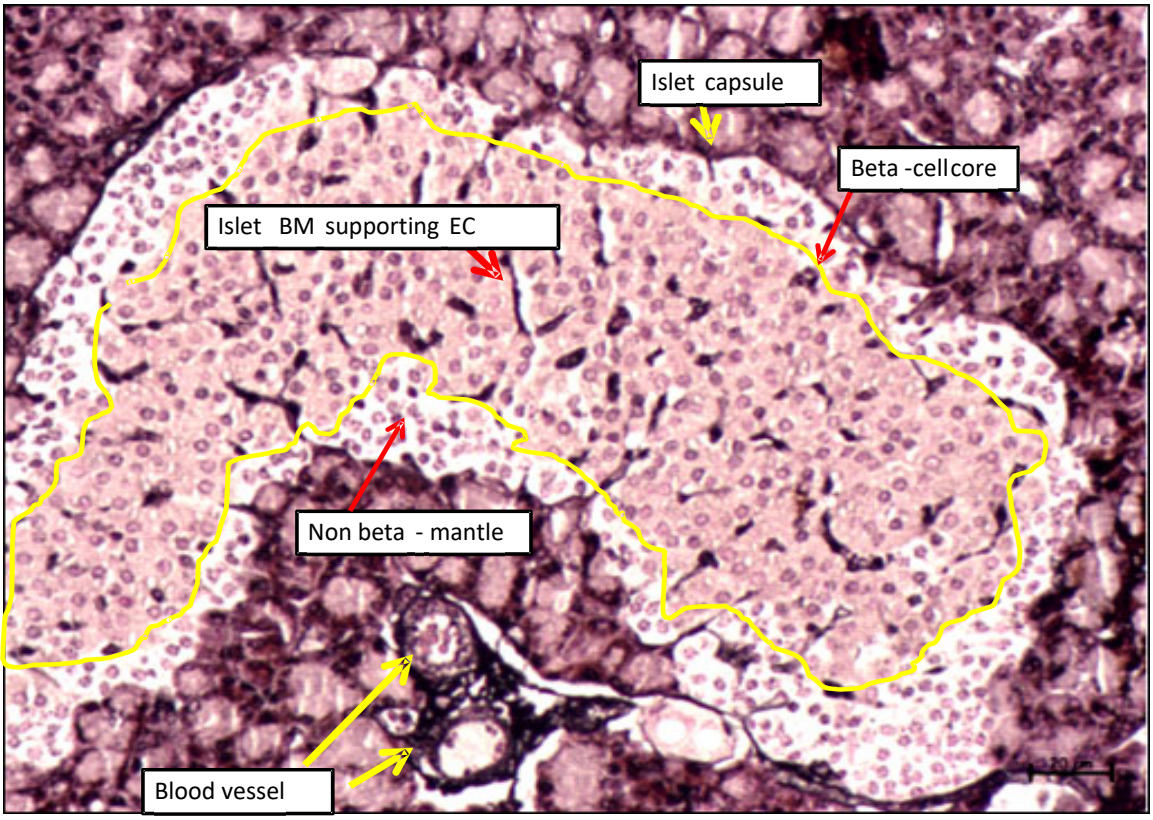

By: E. Ngounou

Figure 0.26: Light photomicrograph of the histological section showing the detailed distribution of the connective tissue in the pancreatic section of a C-HFD / SSC animal focused on the islet of Langerhans. Bar: 20µm.

A section of the C-HFD / SSC group impregnated by the methenamine silver stain delineated the BM and the peri-islet capsule (yellow arrow). The centre (core) of the islet (lined yellow) stained heavily when compared to the periphery (mantle) Mag=400X.

The connective tissue of the pancreas was well demonstrated by the silver staining method in all experimental conditions and both regions. The distribution of the intraislet BM (connective tissue) in the duodenal and splenic pancreatic tissue sections of all groups is summarized in Figure 4.27 (A and C for NC and C-SSC, E and G for C-HFD/ SSC, B and D for RAC / STZ and G and H for HFD / STZ). Although the sections of the two diabetic groups were strongly impregnated compared to the sections of the remaining groups, the HFD / STZ sections (G and H) had the highest silver impregnation. The lowest staining intensity was recorded in the NC and SSC sections.

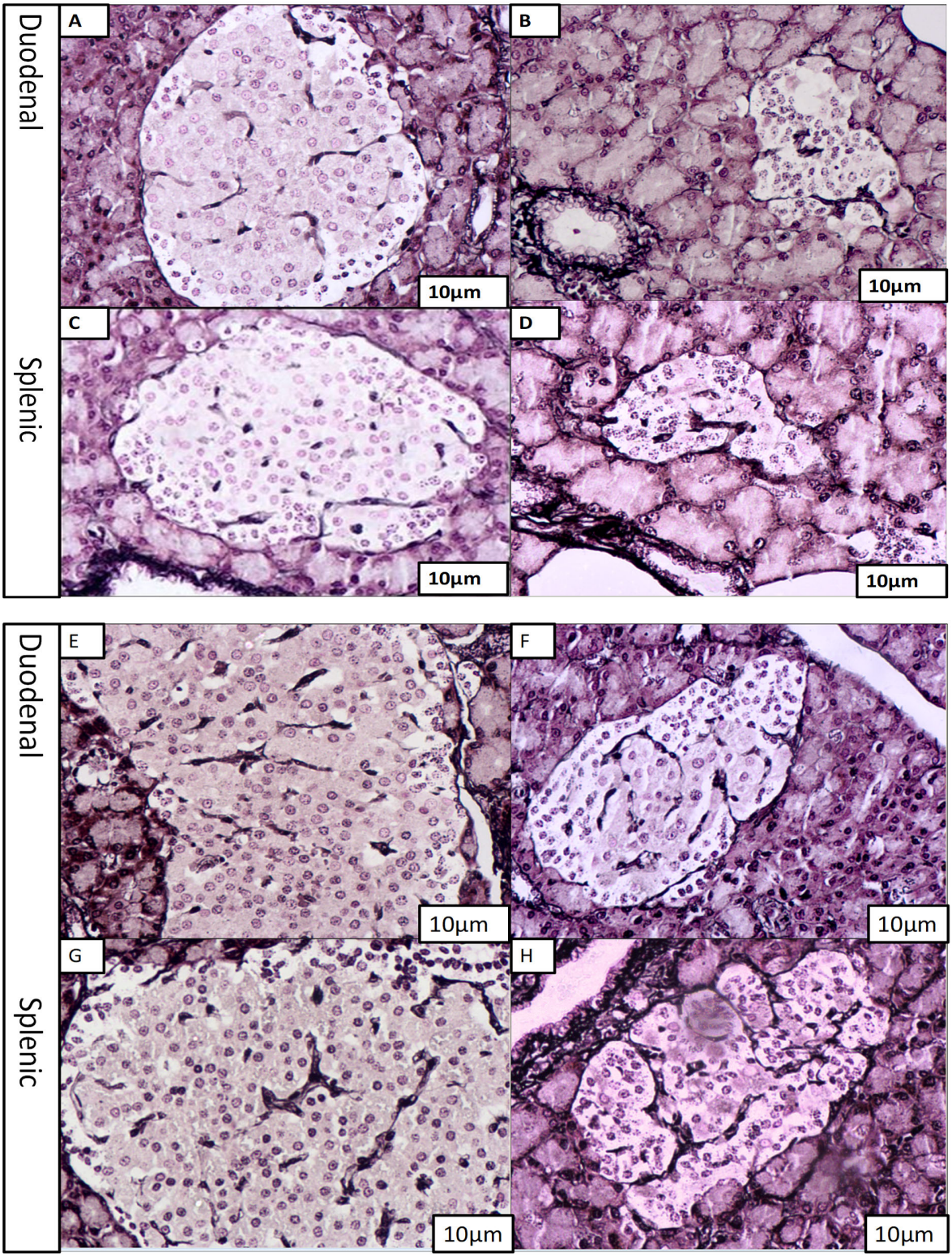

By: E. Ngounou

Figure 0.27: Light photomicrograph of histological sections showing the distribution of the connective tissue supporting the endothelial cells in all conditions. Mag=400X.

.

The distribution and the thickness of BM highlighted by the silver stain were similar for both the NC and C-SSC section and in the two pancreatic regions (Figure 4.27A and C). The C-HFD / SSC (Figure 4.26 and Figure 27E and G) group were heavily impregnated with silver stain in the islet and the exocrine tissue compared to the NC group (Figure 27A and C). In this group (C-HFD / SSC), the silver stain also clearly demonstrated the amount of connective tissue constituting the pancreatic vascular wall (Figure 4.28A and B). The vascular wall in this group was separated into three main layers, the tunica adventitia (c), the tunica media (b) and the tunica intima (a). The tunica media was pronounced, demarcating individual hypertrophied muscle fibres (Figure 4.28).

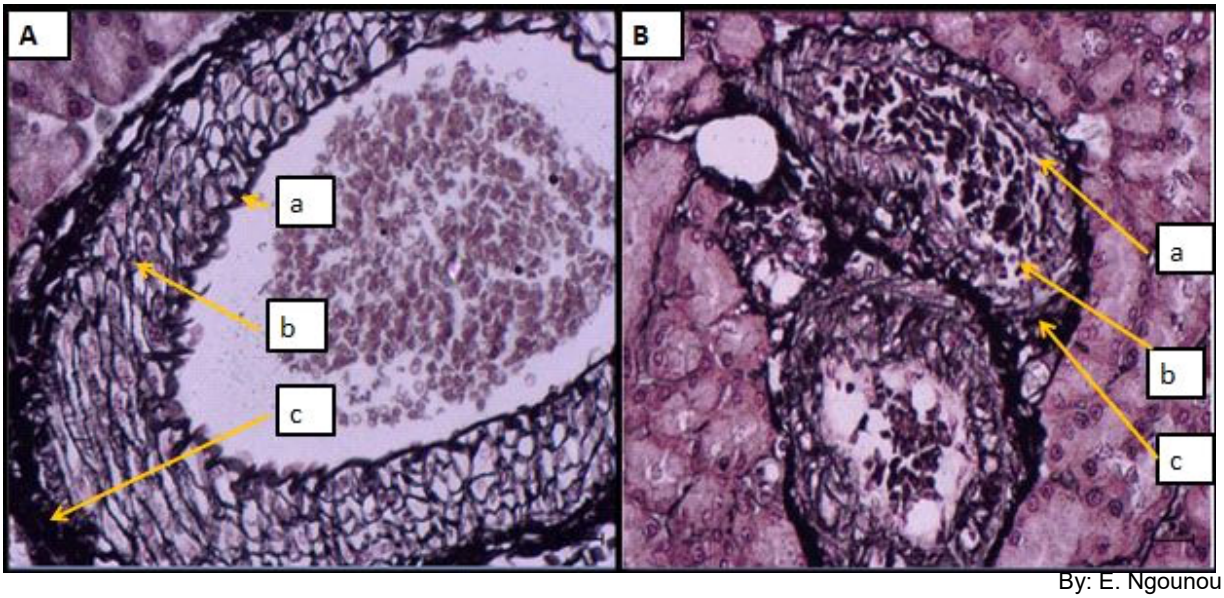

By: E. Ngounou

Figure 0.28: Photomicrograph of the C_HFD / SSC pancreatic section impregnated with the silver stain delineating the connective tissue content of the vascular wall. Bar: 10µm.

A large (A) and a medium (B) vessels, representative of the vascular feature from the two pancreatic regions in this group. Mag-400X.

In conclusion, for each of the pancreatic regions, the characteristic and the thickness of the layers (tunica intima, tunica media and tunica adventitia) and the diameter of the lumen of the vessels were determined not only by the size, type (arteries or veins) of the vessel (large, medium, small, arterioles and venules) but also, and most importantly, by the feeding and the treatment regimen. While the amounts of connective tissue and smooth muscle in the wall of each vessel type (arteries and veins) varied with the size (total diameter), and the experimental condition, the

endothelium (marked by CD34 antibody and evaluated in the islet using ImageJ software) retained the same pattern throughout the pancreatic tissue.

Changes in the structure of the vascular wall in different groups stained with H&E (Figure 29A, B, C, and D) and impregnated with the silver stain (Figure 29E, F, G, and H) are summarised in Figure 4.29 below: in this study, the medium size vessel was representative of the general trend.

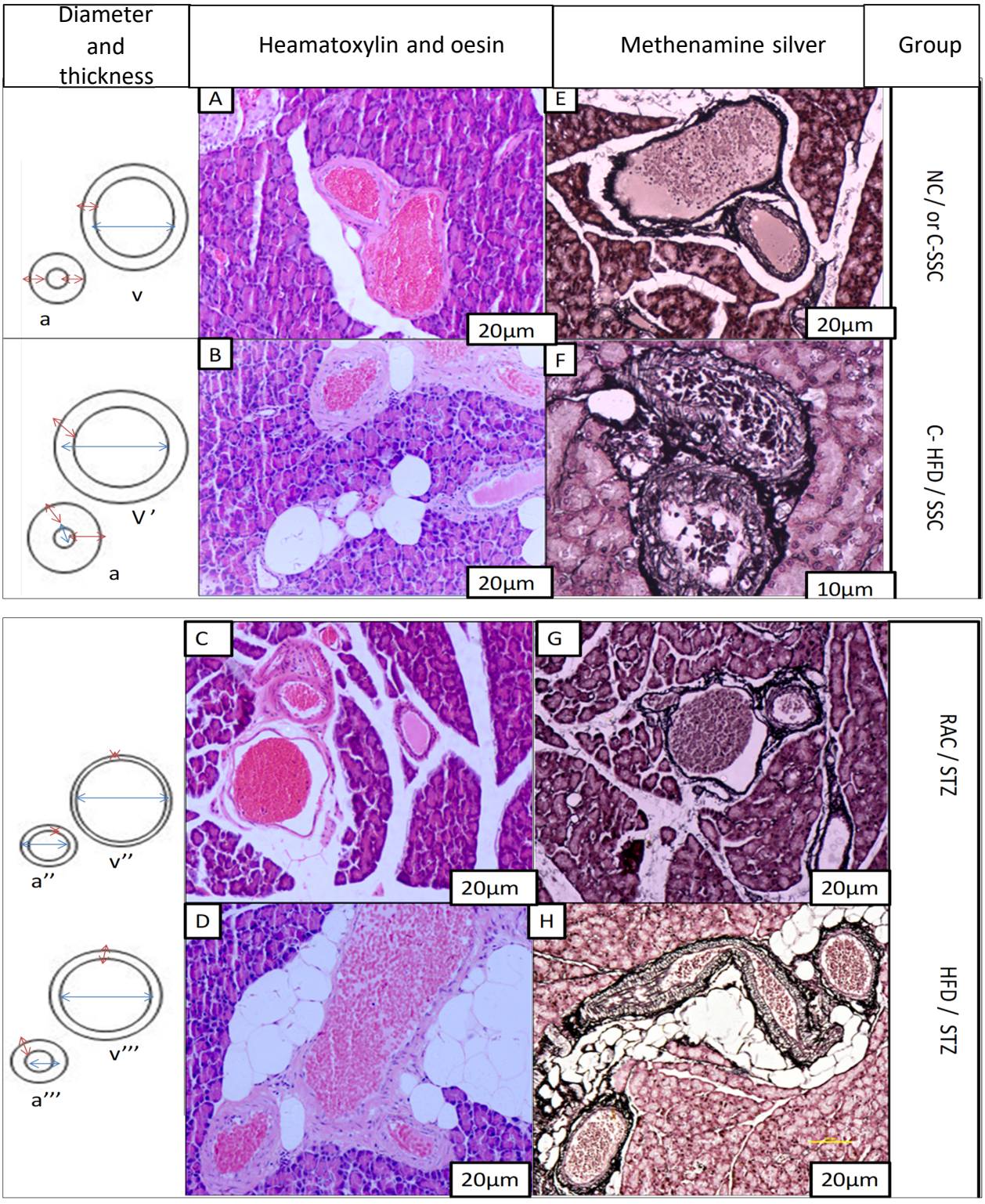

By: E. Ngounou

Figure 0.29: Represents the light micrograph of the tissue sections showing the trend in the anatomical differences of macro vessels of the pancreas in different experimental conditions: case of the medium-size vessels. Mag=200X.

The tendency of the vascular histological characteristic being the same in the two regions, each image of the figure is the representation of the sections of the pancreatic duodenal and splenic tissue. While the H&E stained sections (Figure 4.29A, B, C and D) showed the general

histomorphology of the vessels (details of the intima, tunica media and adventitia), methenamine silver impregnated sections delineated the BM supporting the endothelium and the acini (Figure 4.29E, F (Mag-400X), G, H). Intima, tunica media and adventitia formed the vessels wall components of different thickness and different diameter length according to whether it was an artery (a, a', a'' and a''') or vein (v, v', v'' and v''') and also to the animal group. The extreme left column on figures represents the schematic details of the observed vascular morphological difference (artery and its homologous vein) in each condition. The vessels with an apparently thicker wall (red arrow) were arteries of arteries.

Each large vessel (longer diameter) in the homologous pair was much smaller than that of the smaller vessel (shorter diameter) and hence was considered as vein and the other an artery.

4.3.4 The effect of hyperglycaemia on the expression of CD34 by the pancreatic endothelial cells

The expression of CD34 antibody was varied not only from one group of the animals to the other and from one region of the pancreas to another but also between the islet core and the mantle regions (Figure 4.30). NC and C-SSC sections showed the highest expression which was considered highlighting the normal distribution of the microvasculature within the islets and used to compare all the other groups (figure 4.30A and C). CD34 antibody was poorly expressed (lightly coloured) in the C-HFD / SSC sections but with more representation in each ROI) (Figure 4.30F and G). In RAC / STZ sections, CD34 antibody was expressed similarly to those of the HFD / STZ group and confined mainly to the centre of the islet (Figure 4.30B), the endothelial cells having a degenerative characteristic such as the nuclei pyknotics (arrow).

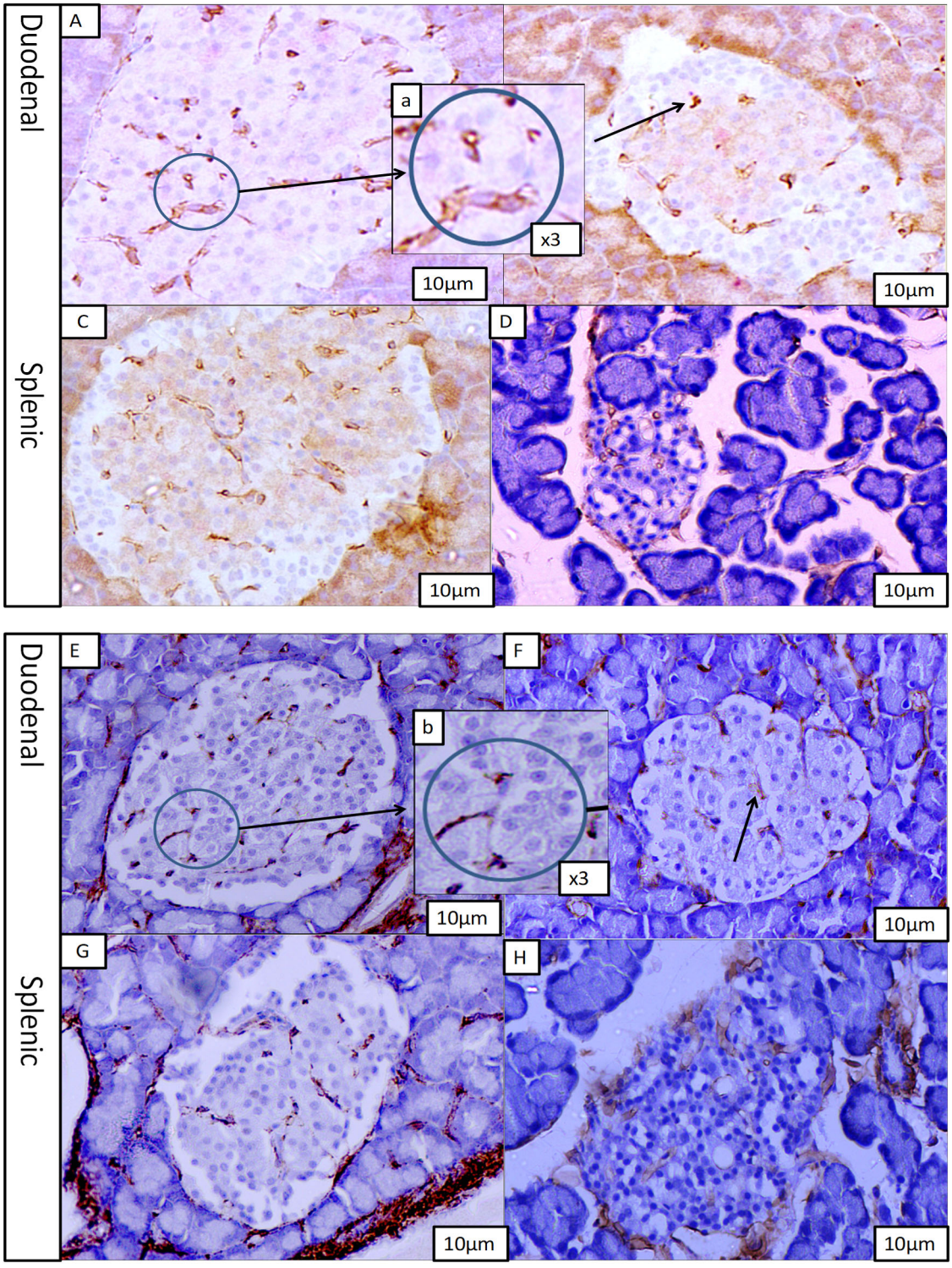

By: E. Ngounou

Figure 0.30: The expression of CD34 on the cell membrane of the endothelial cells.

A and B panels show normal control (NC) sections from the duodenal and splenic pancreas respectively with islet cells nuclei coloured blue in an unstained cytoplasm. The CD34 strongly expressed cells are coloured brown and healthy and are scattered between islet cells. B and D panel present the photomicrograph for the RAC/STZ in the duodenal and splenic pancreas respectively with CD34 staining cells appeared shrunken (arrows). Panels E and G represent

CD34 expressing cells status with the islets appearing compressed (Figure 4.30B). These cells are not arranged around a lumen as in the NC sections (Figure 4.30A) Mag=400X.

4.4 EFFECT OF HYPERGLYCAEMIA ON THE HISTOMORPHOMETRY OF THE PANCREATIC VASCULATURE

This section gives an account of the measured data obtained from 1) the Islet and 2) large pancreatic vessels.

4.4.1 In the Islet

In the islet, the distribution of the endothelial cell and the supporting BM were quantitatively evaluated.

4.4.1.1 The percentage CD34 stained pixel area in the islet

The difference in the ECs expressing CD34 antibody was assessed in each group and for each pancreatic region using ImageJ colourisation method (Figure 4.30A-H). The percentage CD34 pixel area per unit area of the pancreatic tissue section is illustrated in the percentage area in the bar chart graph below (Figure 4.31). The mean values ranged between 5.6±0.3 to 8.0±1% for the RAC / STZ and NC groups respectively in the duodenal islets and 6.0±0.5 to 8±0.6 in the splenic islet. The RAC / STZ groups in both regions therefore always recorded the lowest and significant mean values ($p<0.05$) compared to NC and the SSC groups, which always had the highest value. In addition, within each group, the mean percentage area of the CD34 tends to be higher in the splenic section. Data provided here were taken randomly without considering any islets regionalisation difference and like with the silver impregnation, the expression of CD34 in the islet core was higher than that in the mantle.

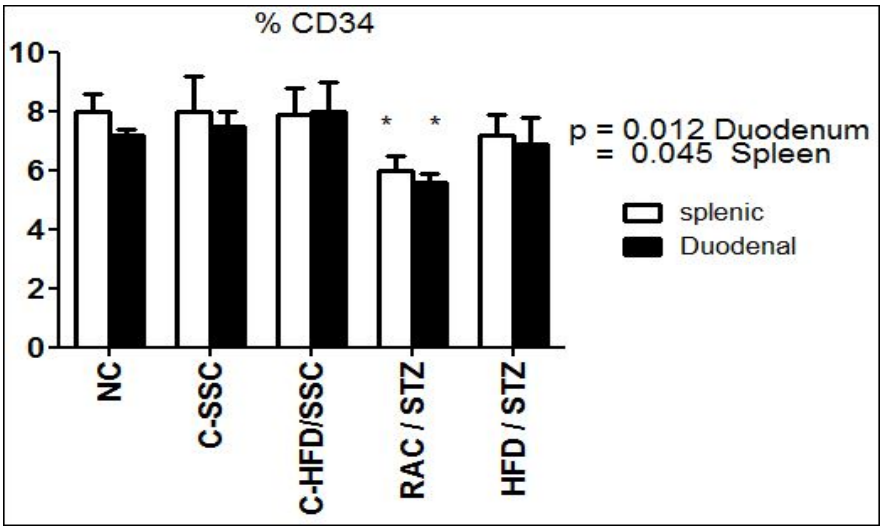

Figure 0.31: Representation of the percentage CD34 pixel area per region of interest within the islet using the ImageJ technique. *p<0.05.

The pixel value of CD34 stained area was thresholded, selected and measured from the total area of interest from five different islets in each group and for each pancreatic region. The mean percentage was calculated in each condition with the RAC / STZ always carrying the lowest values. Data are presented as mean ± SEM * p<0.05.

Relationship between CD34 expression and number of islet cell per unit area

In order to determine whether the size of the islet was associated with the number but not with the size of the islet cell, the fractional islet cell (total islet cell number/section area) was evaluated and data illustrated in Figure 4.32A and B. The mean fractional islet cell was significantly increased in the HFD groups: in the duodenal region, 55.8±5.49 for the C-HFD / SSC group vs 32±4.3 for the NC has recorded p<0.0032 and 39.9±4.3 for HFD / STZ vs 32±4.3 for NC p<0.029, in the splenic region 53±6.3 for the C-HFD / SSC vs 32.6±5.1 for NC p<0.0019 and 38.4±4.3 for HFD / STZ vs 32.6±4.7 for NC p<0.041).

To determine whether the islet cell number was associated with the amount of blood supply, a relationship between the fractional islet cells and mean values CD34 expression was evaluated and illustrated in Figure 4.32C and D. A positive but not significant (r^2=0.041, p=0.24) correlation was recorded for the duodenal sections while a negative and not significant one was observed for the splenic sections (r^2=0.0052, p=0.90).

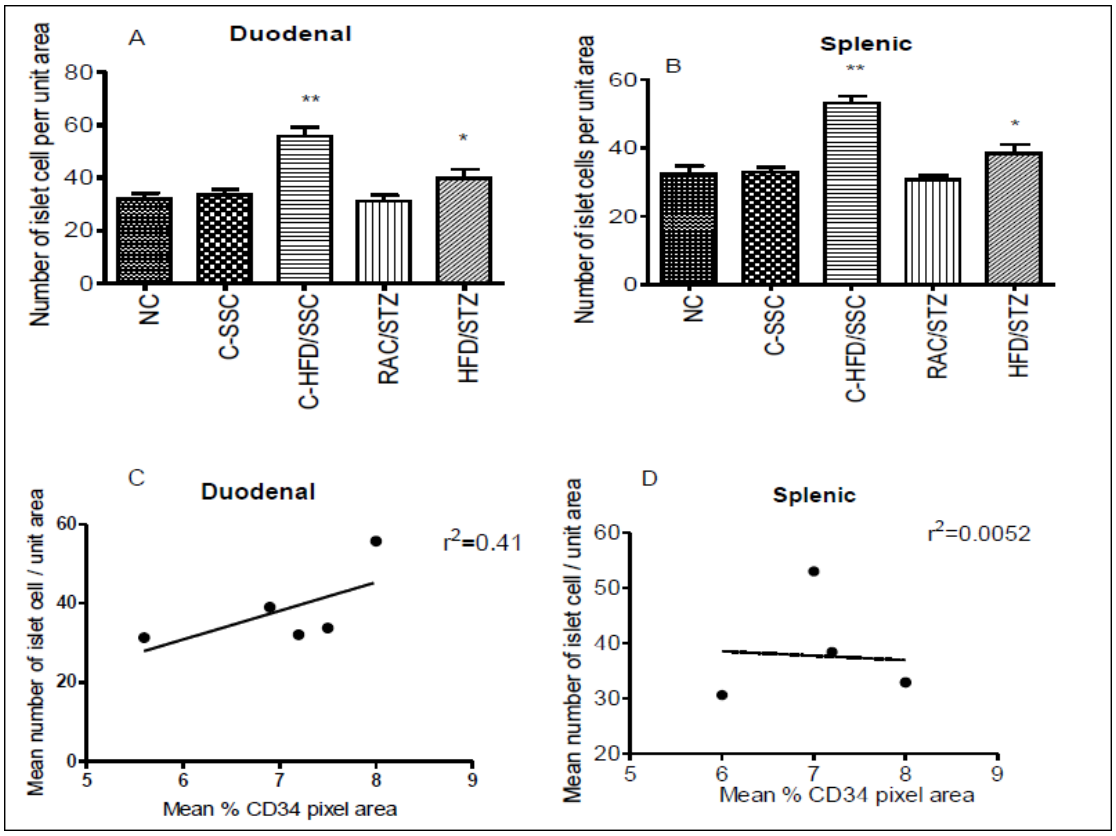

Figure 0.32: A correlation curve showing the relationship between percentage CD34 expression in the islet and mean fractional islet cell. *p<0.05, **p<0.01.

Relationship between CD34 expression and number percentage of CEPC

To determine whether the effect of hyperglycaemia on the vascular integrity was associated with the impairment of the vascular repair, the relationship between percentage CD34 stained pixel area per unit area of the islet in the pancreatic tissue section and the CEPC level in the blood circulation was evaluated. It was observed that the increase in the BGL caused the decrease in the % CEPC in the blood circulation which was in turn accompanied by a decrease in the expression of the CD34 by the islet cells. Therefore, the RAC / STZ and HFD/STZ groups had a mean in BGL raised above 28mMol/L which caused a mean of 0.951% and 1.009% CEPC decrease and finally a mean decrease of 0.6±0.5% and 0.3±0.9% of the CD34 expression in the duodenal islet and 2±07% and 0.8±0.3%±0.02 in the splenic islet respectively.

4.4.1.2 The percentage methenamine silver-stained pixel area in the islet

Basement membranes are the only tissue supporting the islet endothelium whose integrity is well known to maintain the function of the islet cells (Nikolova et al., 2006). The percentage of the methenamine silver-stained pixel area per unit area of the islet was considered as the abundance (thickness) of BM associated with the islet microvasculature and this was best measured by the colourisation method of the image j software and recorded. The mean values of the percentage pixel area obtained ranged between 7.5±0.5 and 13.2±1.026% for the NC and RAC / STZ groups respectively in the duodenal islets and, in the splenic islets, between 8.6±1 to 14.5±1.5% for the same groups (Figure 4.33). RAC / STZ groups in both regions, therefore, always recorded the highest and most significant values ($p=0.037$ for the duodenal and $p=0.047$ for the splenic) compared to the NC group, which always had the lowest values. Moreover, within each group, the percentage pixel area of the silver stain appeared to be higher but never significant in the splenic sections.

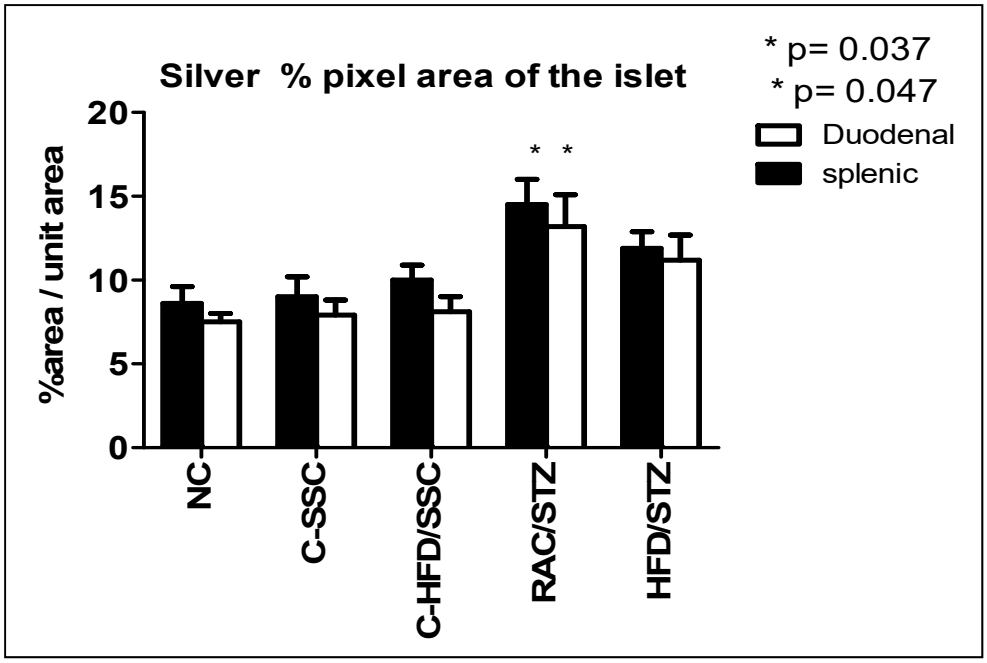

Figure 0.33: Bar chart representing the percentage of the silver stain pixel area calculated in each condition and the two regions of the pancreas. *p<0.05.

The RAC / STZ group always carrying the highest values for both pancreatic regions compared to the other group. Data are presented as mean ± SEM and *p<0.05.

Relationship between methenamine stained pixel areas and pancreatic vessel thickness

The increase in BGL was accompanied with a reduction of the large pancreatic vessel thickness (Table 4.2) which was in turn accompanied with an increase in the percentage of methenamine stain pixel area in the islet (Figure 4.32).

4.4.2 Large vessels

4.4.2.1 Mean vascular diameters and thickness

The outer diameter was used to estimate the total vessel enlargement while the inner diameter (Figure 4.33) was used as the main haemodynamic parameter, which depends on its radius. The wall thickness obtained by measurement and validated by calculating the difference between the OD and the ID (Table 4.2) was used to evaluate the changes of the amount of smooth muscle layer thickness and the supporting connective tissue forming the vascular wall because of any vascular remodelling. In addition, whenever an inadequate chemical exchange between blood and tissue at the capillary endings is suspected, the vessel wall thickness is the best parameter to assess. Also, the ratio between vessel wall thickness and luminal diameter was considered as one of the main factors in evaluating the circumferential stress.

The outer diameter of the pancreatic vessels ranged between 10-130µm. For descriptive purpose in this study, the vessels were classified into four main categories (vein vs their corresponding arteries): large (100-130µm vs 70-90µm), medium (70-100µm vs 40-60µm), and small (50-70µm vs 30-50µm) vessels, and finally, venules and arterioles (20-50µm vs 10-30µm) in both regions of the pancreas.

No significant difference was found between the mean OD of the vessels from the duodenal and that of the splenic sections of the pancreas within each group in all conditions and for all categories. However, the highest mean of OD was recorded in C-HFD / SSC in all vessel categories (veins and arteries) (Figure 4.34 A-I) with a significant difference ($p<0.05$, $p<0.01$) observed between the data obtained from the splenic sections in both regions except in the large vein.

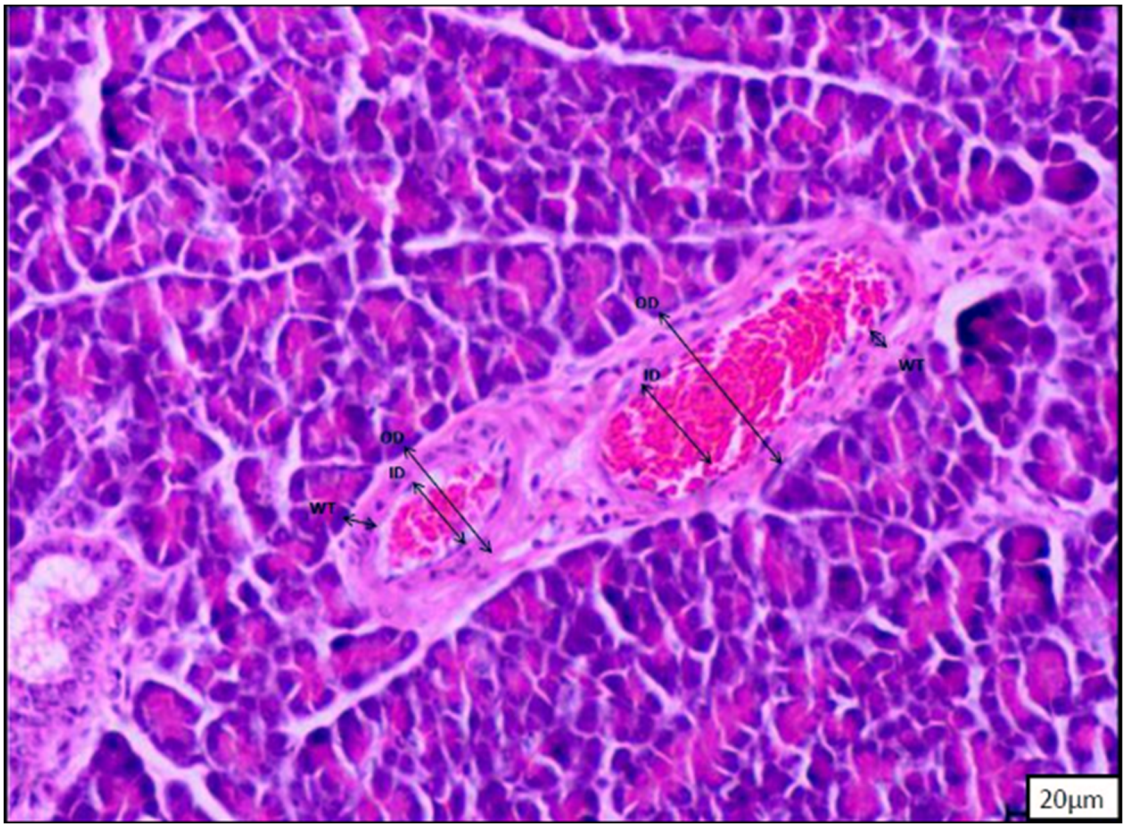

By: E. Ngounou

Figure 0.34: Schematic representation of the measured outer and inner diameters of a medium artery and vein from the normal control group.

Several measurements were taken connecting different two-point of the outer and inner edges of the vessel and the average in each category was considered. In addition, the circularity of each vessel was measured and a single diameter value obtained when the vessels were deformed as described in 3.5.2.1.

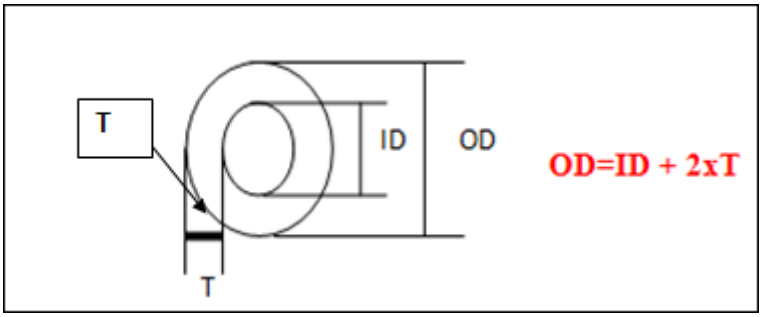

Figure 0.35: Schematic representation of the relationship between the diameters (OD and ID) of a blood vessel and wall thickness.

OD-outer diameter, ID=inner diameter, T=wall thickness

Note that in this study, the above formula was deduced from the data obtained after the measurement of each parameter separately.

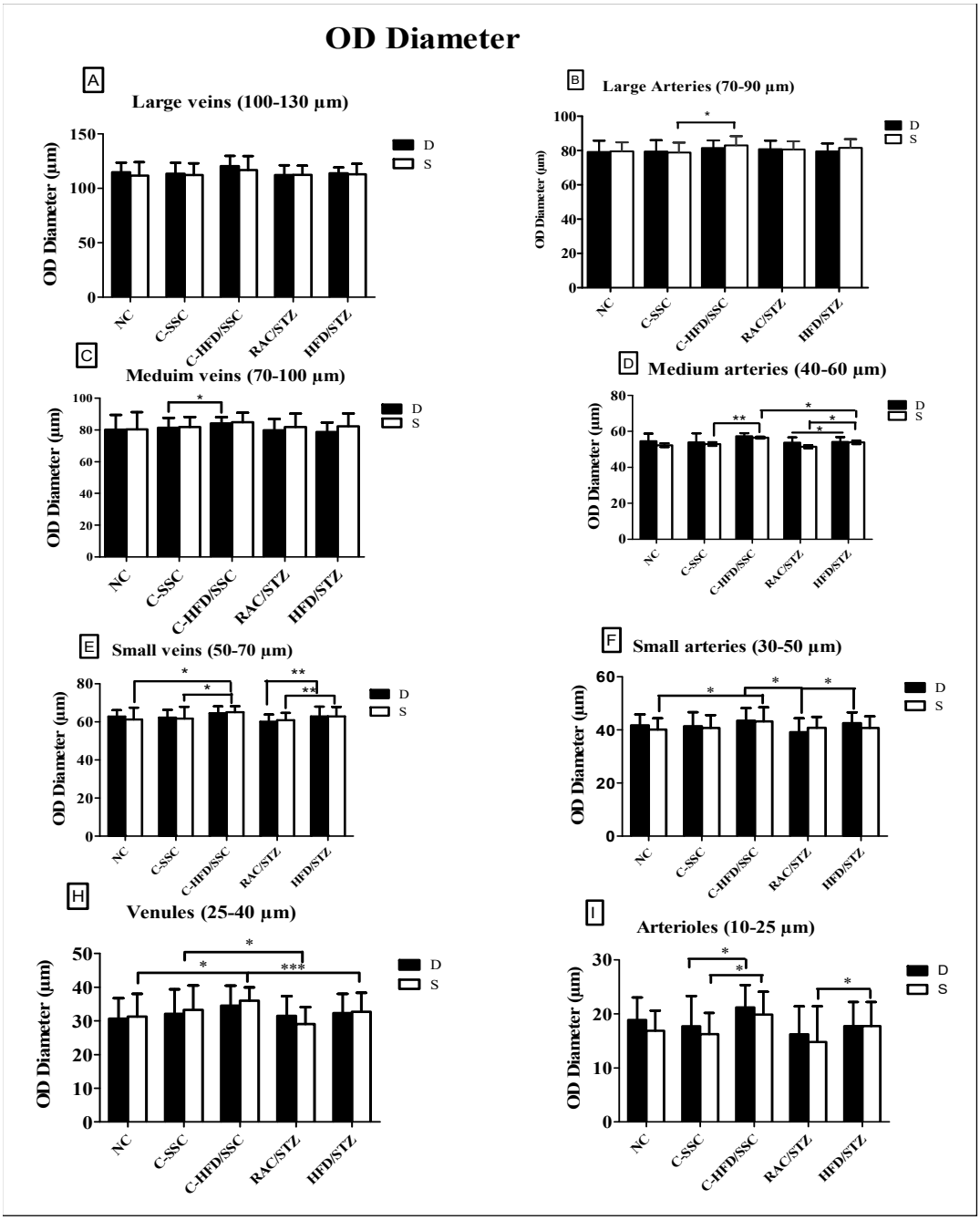

Figure 0.36: Summary of the mean OD: veins (A, C, E, H) and arteries (B, D, F I) in all conditions and both pancreatic regions. *p<0.05, **p<0.01 and ***p<0.001. D=Duodenum, S= Splenic.

Data were obtained from the outer edges of the adventitia. No significant difference was observed between the duodenal (D) and the splenic (S) pancreas in all conditions (p=0.2 NC vs SSC, p=0.07 NC vs C=HFD / SSC, p=0.45 NC vs RAC / STZ and p=0.092 NC vs HFD / STZ). A and B graphs report the mean OD of large vessels (veins and arteries respectively, 100-130µm vs 70-100µm), C and D, medium vessels (70-100 vs 40-60µm), E and F, small vessels (50-70 vs 30-50µm), and G and H venules and arterioles (25-40 vs. 10-25µm) respectively. All data are expressed as mean ± SEM.

The corresponding IDs were smaller than ODs in all classes of vessels and both pancreatic regions (Figure 4.35). However, unlike in OD results, the C-HFD / SSC sections (Figure 4.35 C, H) had the lowest and most significant IDs ($p<0.01$) and therefore the highest and most significant wall thickness values (the difference between outer and inner diameter) (Table 4.2, $p<0.05$, $p<0.001$, Figure 4.37) compare to all other groups. Blood vessels from RAC / STZ sections (Figure 4.35 D, I) had the highest and most significant IDs ($p<0.01$) with a corresponding lowest and most significant wall thickness in all category of vessels compared to all other groups in both regions (Table 4.2 $p<0.05$, $p<0.01$).

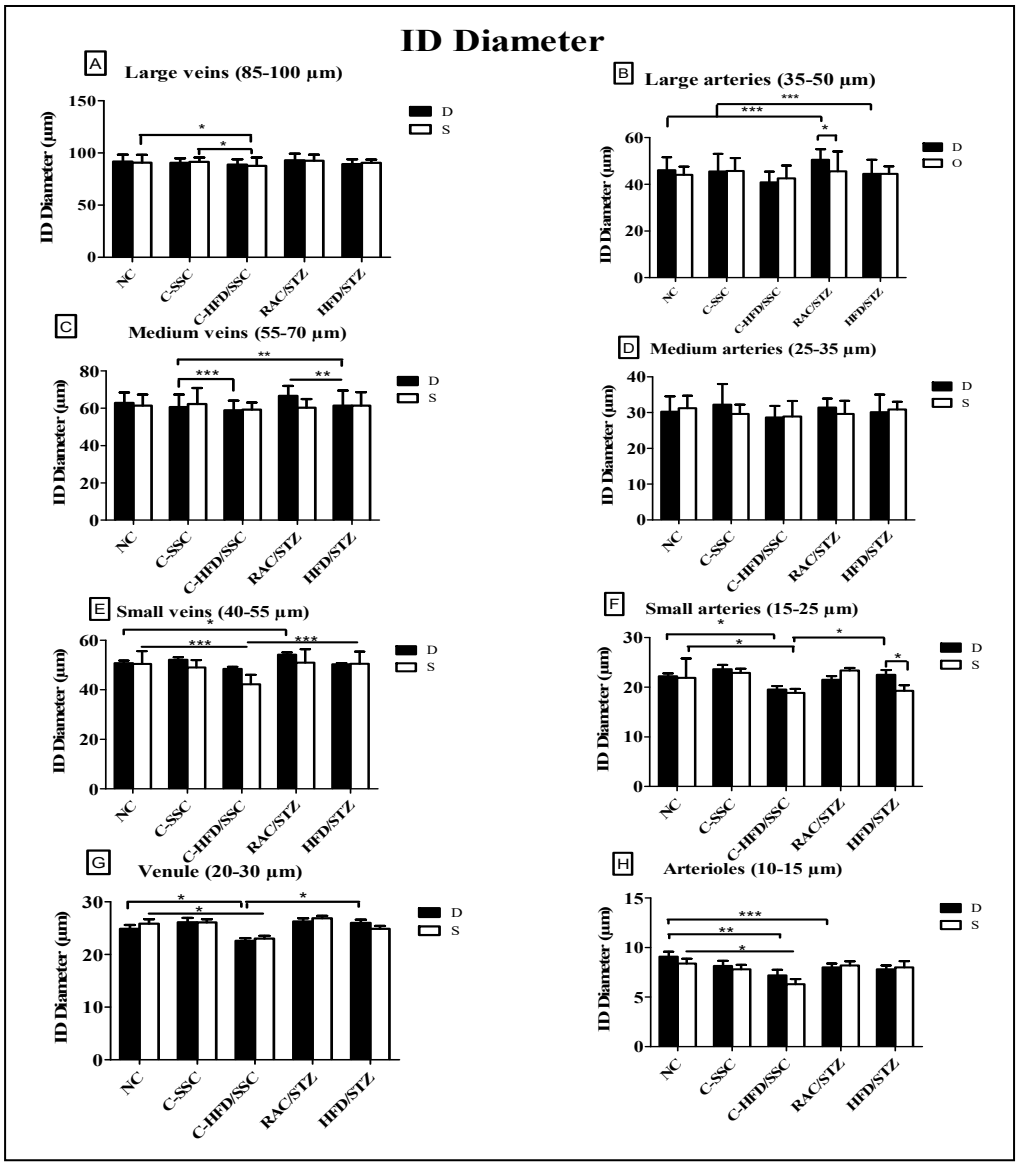

Figure 0.37: Summary of the mean ID: veins (left column) and arteries (right column) in all conditions and both pancreatic regions. *p<0.05, **p<0.01 and ***p<0.001. D=Duodenum, S= Splenic.

Data obtained from two opposite inner edges of the endothelium of each vessel class. No significant difference was observed between the duodenal (D) and the splenic (S) pancreas

in all conditions. A and B report the means ID of large vessels (veins and arteries respectively, 85-100μm vs 35-50μm), C and D, medium vessels (55-70 vs 25-35μm), E and F, small vessels (40-55 vs 15-25μm), and G and H for venules and arterioles (25-40 vs 10-25μm). All data are expressed as mean ± SEM.

Table 0.2: Mean vessel thickness in all conditions in both pancreatic regions

	NC		C-SSC		C-HFD / SSC		RAC / STZ		HFD / STZ	
	D	**S**	**D**	**S**	**D**	**S**	**D**	**S**	**D**	**S**
L.V. (>90µm)	11.04±2.5	10.96±3	11.02±0.9	11.1±21	15.69±2.6**	14.9±1.9**	8.30±0.9*	8.1±0.92*	12.1±2.5	11.91±1.9
M.V. (90-40µm)	9.01±0.8	9.1±1.4	10.01±1.8	9.54±1.4	12.6±1.5*	11.93±2 *	6.04±0.5*	6.28±0.5*	7.66±0.9	9.9±0.835
S.V. (<30µm)	6±0.4	5.44±0.6	5.1.1±0.7	6.39±0.9	8.07±1.9**	8.6.33±1.8**	2.9±0.3*	3.9±0.9*	4.27±0.8	5.3±0.8
Arteriole	4±0.5	3.9±0.9	4.2±0.8	3.5±0.7	5.5±1	6.1±0.9*	2.5±05*	2.2±0.8*	3.05±0.7	2.9±0.9
Venule	2.4±0.2	2.6±0.3	2.8±0.4	3.2±0.6	4.32±0.6**	4.4±0.8**	2.1±0.9	2.5±0.04	2.8±0.5	3.2±0.5

All data are expressed as mean ± SEM. * $p<0.05$ ** $p<0.01$

D= duodenum, S= splenic, L.V.= large vessel, M.V.=medium vessel, S.V.= small vessel

4.4.2.2 Numerical density of the pancreatic blood vessels

We used the numerical density (ND) to validate the occurrence of any form of difference in the number of blood vessels in the pancreatic tissue under the effect of hyperglycaemia, and between duodenal and splenic regions in each condition. Blood vessels per unit area of thin pancreatic sections were counted under the microscope and the total number recorded. Ten different fields representing a total surface area of 4mm^2 were considered as the unit area.

No significant difference was observed between the mean total numbers of blood vessels in all conditions for both pancreatic regions (Figure 4.38). However, the splenic section from HFD / STZ group had the highest number of blood vessels per unit area (39.66±0.42/unit area) followed by that of the C-HFD / SSC group (37.32±1.5/unit area). The number of small vessel size, arterioles and venules accounted for these slight differences (Table 4.3). On the other hand, while the duodenal sections always accounted for a higher number of large vessels, splenic pancreatic sections showed a higher number of medium size, small vessel size, arterioles and venules per unit area in most conditions. A significant difference in the number of these small vessels was recorded between the NC group and all the HFD groups (C-HFD / SSC, p=0.033 and HFD / STZ, p=0.02). There was no significant difference in the distribution of vessel size per unit area in duodenal and splenic regions between NC and the other groups (C-SSC and RAC / STZ) for all categories of vessels (Table 4.3). Note that in the two pancreatic regions, different categories of blood vessels were unevenly distributed in all conditions with larger vessels more present in the duodenal portion.

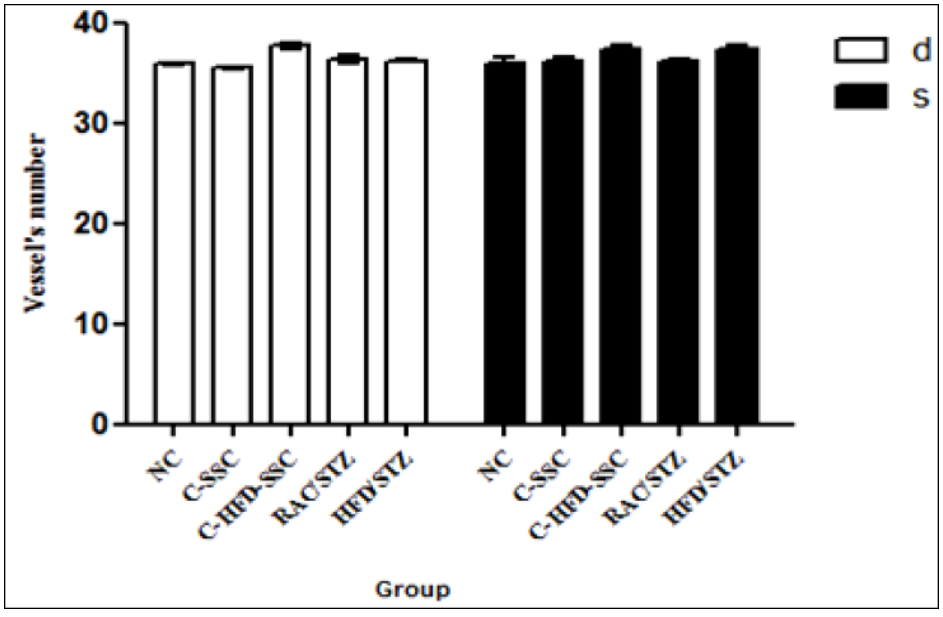

Figure 0.38: Mean total number of blood vessels in all conditions. D=Duodenum, S= Splenic.

No significant difference was observed between groups and between the pancreatic regions per unit area.

Table 0.3: Distribution of vessel size per unit area in the duodenal and splenic regions.

	NC		C-SSC		C-HFD / SSC		RAC / STZ		HFD / STZ	
	D	**S**	**D**	**S**	**D**	**S**	**D**	**S**	**D**	**S**
L.V. (>90µm)	4.16±0.32	3.16±0.29	4.2±0.14	3.04±0.21	4±0.31	3.42±0.26	4.24±0.25	3.44±0.22	4.04±0.35	3.62±0.35
M.V. (90-40µm)	7.64±1.921	8.44±0.32	7.44±2.04	8.52±0.22	7.36±1.85	8.72±0.38	7.44±0.38	9.04±0.32	7.36±0.08	8.96±0.35
S.V. (<30µm)	23.96±1.57	24.24±2.56	23.97±0.17	24.6±0.89	25.32±0.46	25.24±1.39*	24.72±0.83	24.16±0.63	24.88±0.7	26.76±0.69
Total	35.86±0.29	35.84±2.28	35.5±0.3	36.16±1.15	36.68±0.7	37.32±1.5	36.32±1.08	36.16±0.35	36.28±0.5	39.66±0.42

All values are expressed as mean ± SEM * $p<0.05$ LV=large vessels MV=medium vessels SV=mall vessels.

4.4.2.3 Area fraction

The area fraction (AFr) of the vessels was defined as the percentage area covered by blood vessel per unit area of the pancreatic tissue section and was therefore calculated as the sum of all the small areas covered by each vessel within a defined ROI. Two values were considered: the first AFr was measured from the outer diameter (adventitia) (Figure 4.39A), the second from the inner diameter (Figure 4.39B). In the first case, the total duodenal AFr per unit area was always but not significantly higher than that of spleen in all conditions (NC: 25.9±5.36% vs 21.58±4.5%, C-SSC: 23.6±2.5% vs 21.6±5.7%, C-HFD / SSC: 23.2±3.6% vs 20.3±5.2 %, RAC / STZ: 29.6±3.3% vs 26.7±4.2%, HFD / STZ: 24±2.5% vs 21.1±4.4%). In the second case, there was no significant difference between the values of the duodenal AFr and those of the splenic pancreatic sections. However, in both regions, the RAC / STZ group recorded the highest and most significant values (**p<0.01) (20.45±5.2 vs 21.6±4.7) followed by the HFD / STZ groups (18.9±3.9 vs 17.9±5.9) compared with NC and C-SSC animals. This suggests that at each time point, the volume of blood in a unit volume of the pancreatic tissue was not significantly different in the two regions for each condition (Figure 4.40).

It was also observed that in all cases the mean cross-sectional area of the major vein was more than twice that of the artery.

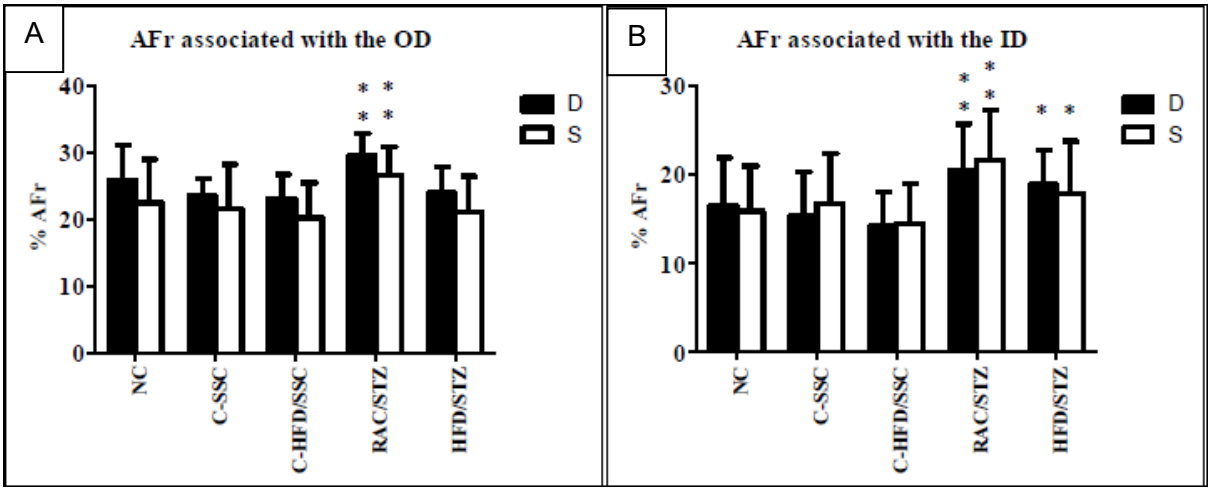

Figure 0.39: Percentage Area Fraction (AFr) of blood vessels on the pancreatic tissue section in each condition. *p<0.05.

In the AFr associated with OD, the two pancreatic regions of the RAC / STZ showed a significant difference compared with the NC animals. In the AFr associated with the ID, both STZ treated groups had significant differences compared to the NC group. Data reported were represented as the mean ± SD Statistical difference versus NC, C-SSC and C-HFD / STZ groups using two way ANOVA followed by Bonferroni posttests.

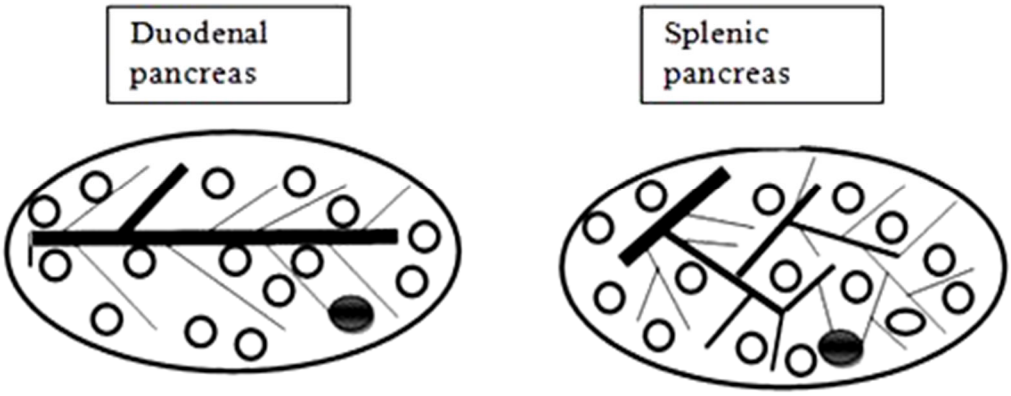

By: E. Ngounou

Figure 0.40: Schematic illustration of the size, distribution and density of vessels (vein or artery) per unit area in the duodenal and splenic pancreas in all conditions.

Large vessels (thick dark lines=large vessels with luminal diameter >90µm) are more represented in the duodenal region than in the splenic region. The medium size (less thick dark lines = medium-size vessels, 90-40µm), small vessels, arterioles and venules (tiny vessels, <30µm) are more represented in the splenic region. However, AFr per unit area remains the same in the two pancreatic regions in each condition. Small empty circles represent the acini within the pancreatic tissue while the filled ones are the islets receiving arterioles.

4.5.2.4 Perfusion time

In section 3.3.2.2 of the Materials and Methods (Chapter 3), we reported that the animal pancreatic vasculature was filled with a urethane-based resin to produce its duplicate. The perfusion time of the resin ranged between 108.3±5.93 and 169.8±8.1 seconds with the C-HFD / SSC group carrying the highest and significant value (Table 4.4, 169.8±8.1 vs NC=123±4.5s p=0.004). Interestingly, under the same pressure, C-HFD / SSC had the smallest and most significant resin volume displaced in the syringe (Table 4.4, 14.63±2 vs NC=18.86±1.8mL, p=0.009), suggesting that the flow rate of blood in this group was very low and therefore more time was needed to fill the vessels. The RAC / STZ group had the fastest perfusion time (108.3±5.93 vs 123±4.5±3.2s) with the highest volume of resin displaced (22.6±1.01mL) followed by the HFD/STZ group (117.6±5.09s and 20.9±0.92mL, p=0.045).

Table 0.4: Mean perfusion time and volume of resin displaced in the syringe in each condition.

Experimental group	Time (Seconds)	Volume (mL)
NC	123±4.5±3.2	18.86±1.8
C-SSC	126.8±5.6	18.2±2
C-HFD / SSC	169.8.1±3.7**	14.63±2*
RAD / STZ	108.5±2.9 **	22.6±1.01*
HFD / STZ	117.6±5.09	18.85±1.8

The casting medium (resin) was perfused at a pressure of 110mm/Hg using a manual mercury manometer connected to a T-piece to the injection line. Data are presented on average ± SEM. * $p<0.05$ and **$p<0.01$.

4.5. RESULTS FROM THE NAN- CT SCAN ANALYSIS

The nano-CT scanner (General Electric V|TomeX L240) was used to generate detailed three-dimensional (3D) images of the complete replica of the pancreatic vascular network, which allowed for morphological and morphometric evaluations. Note that this network represented the true picture of the luminal morphological features and the volume of the vascular tree. Hence, data obtained in this section were compared only with the luminal features from the histological study (ID and AFr evaluation).

4.5.1 Vascular cast morphological feature

Morphologically there was no obvious visible difference in the vasculature of the pancreas between various groups. However, the C-HFD / SSC group appeared to be larger with a denser network (Figure 4.41A) than the cast from other groups (Figure 4.41B, C and D).

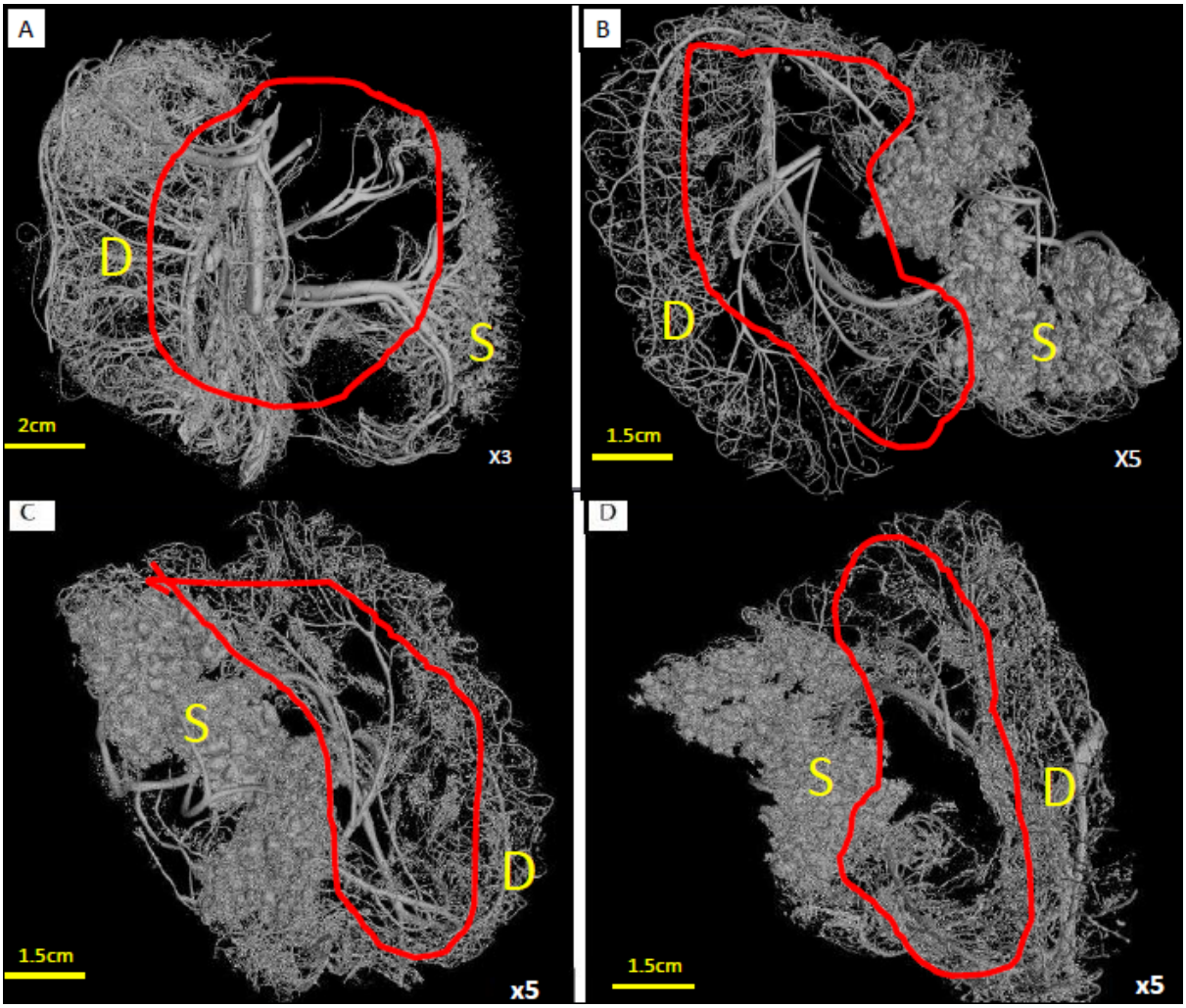

By: E. Ngounou

Figure 0.41: 2D representation of the 3D Nano-CT images of the pancreatic vascular cast of rat pancreas in all groups

A) From the C-HFD/SSC, B) from the NC, C) from the RAC/STZ and the HFD/STZ. The images show fine texture mass of the pancreatic blood vessels (encircle in red) between the vascular network of the duodenum ("D") and that of the spleen, "S". Note that images B, C and D are mainly cast of the arterial tree, the venous network being represented scantily due to some segments that fell off during the manipulation.

All casts showed similar network pattern displaying the major vessels supplying the pancreas and the surrounding organs: mainly the splenic artery, branch of the celiac trunk (by following in a retrograde direction the splenic artery, the celiac trunk could be identified) and their associated veins with a little contribution from superior mesenteric vessels (not shown in Figure 4.42). The network of vessels (Figure 42B) was similar to the pattern seen in human (Figure 4.42 A). It started on the right as that providing blood to the C-shaped portion of the duodenum surrounding the head (duodenal portion) of the pancreas to that supplying the spleen on the left.

The main vessel supplying the pancreas is the splenic branch of the celiac trunk. The vessel runs almost the entire length of the pancreatic portion of the cast, an area occupied by the neck (on the right), body and tail (on the left) (Figure 4.42C). In its course, it gives out a collateral branch the transverse pancreatic artery. The splenic artery terminates by dividing into two main trunks close to the spleen. The vascular cast of the remaining regions of the pancreas (head and uncinate process) consisted of branches from the gastroduodenal artery, and the branch of the common hepatic artery, the second-largest branch of the celiac trunk. Note that each daughter segment was traced to its origin at the node where the parent vessel branches.

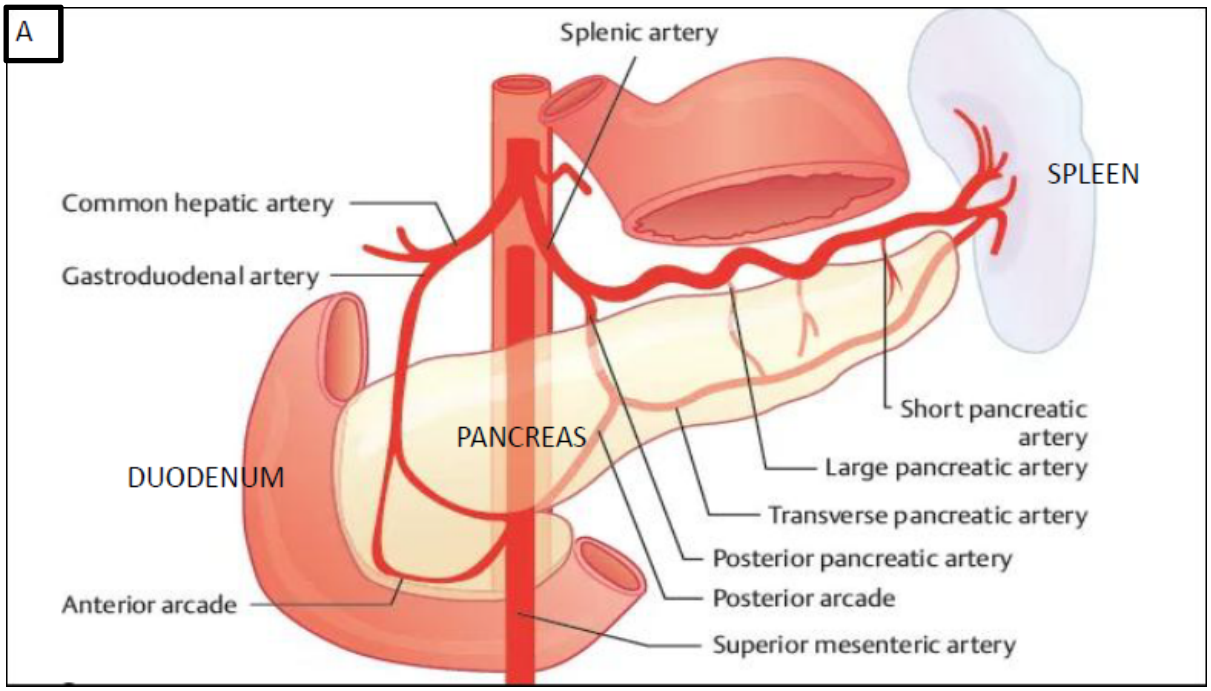

Adapted from https://radiologykey.com/pancreatic-arteries/

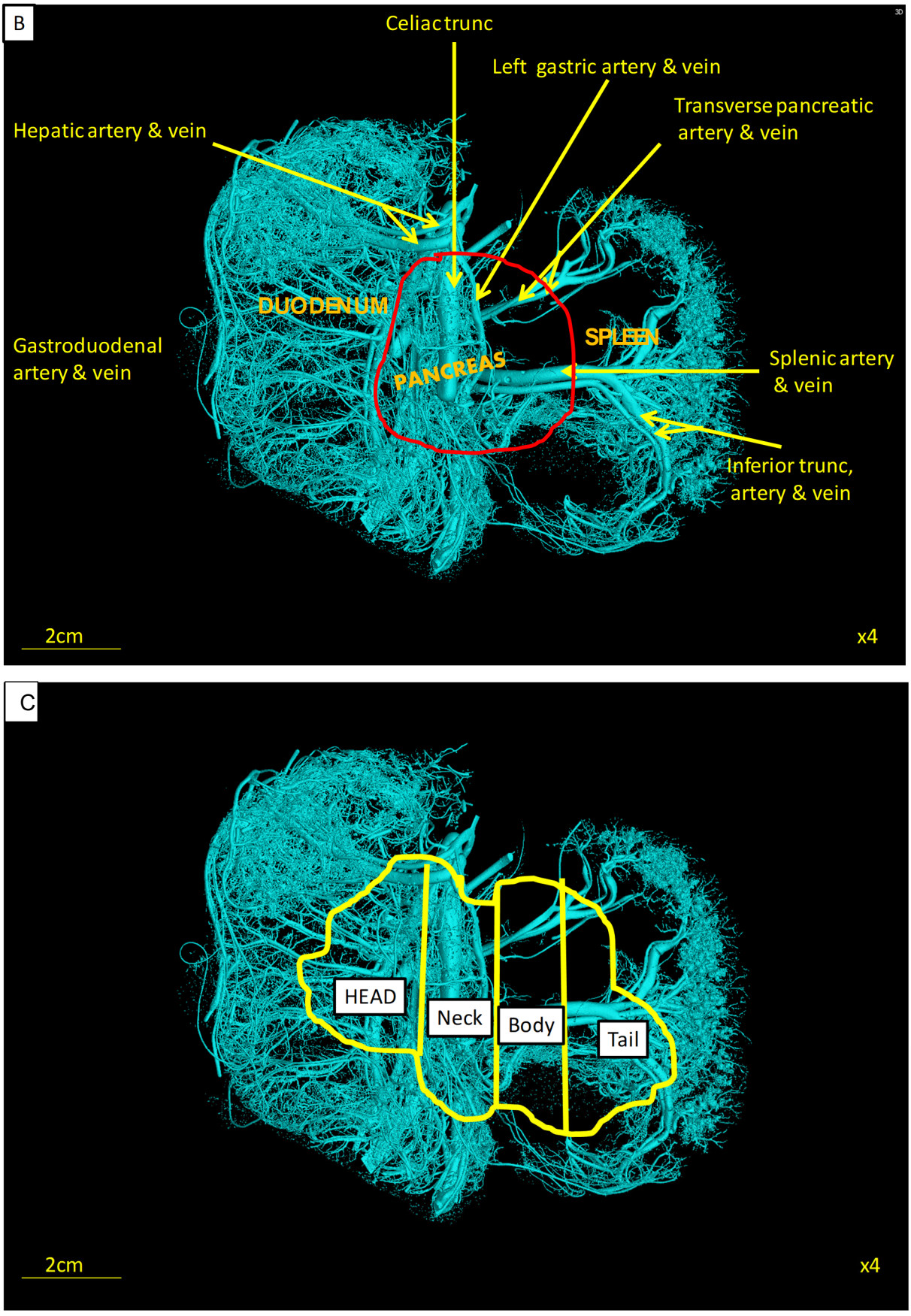

By: E. Ngounou

Figure 0.42: Major vessels supplying the pancreas. Strong similarity between the standard human distribution pattern (A) and that of rat one (B) generated in this study.

A) Major arteries of the human pancreas and surrounding visceral organs B) Nanotomography image of the pancreatic vascular cast showing the pattern of distribution of large vessels (labelled) supplying the rat pancreas (circled red) and the surrounding visceral organs in the C-HFD / SSC group after noise and small vessels have been removed. Representative diagram annotated for all the other groups because they were similar in all group as per the branching pattern. C) Representation of the dispersed rat pancreatic tissue with the associated regions

Elimination of the small vessels from the model by threshold revealed the major vessels of the entire pancreas. The celiac trunk and branches were the prominent features of the 3-D image. Its branches constituted the bulk of the pancreatic arterial network with little contribution from the superior mesenteric artery. Terminal branches of the splenic artery penetrate the hilum of the spleen. All arteries were accompanied by their corresponding veins.
At all levels of the vascular tree, arteries were accompanied by their homologous veins in a very organized manner (Figure 4.43A); veins always had at least twice the diameter of the arteries (Figure 4.43B).

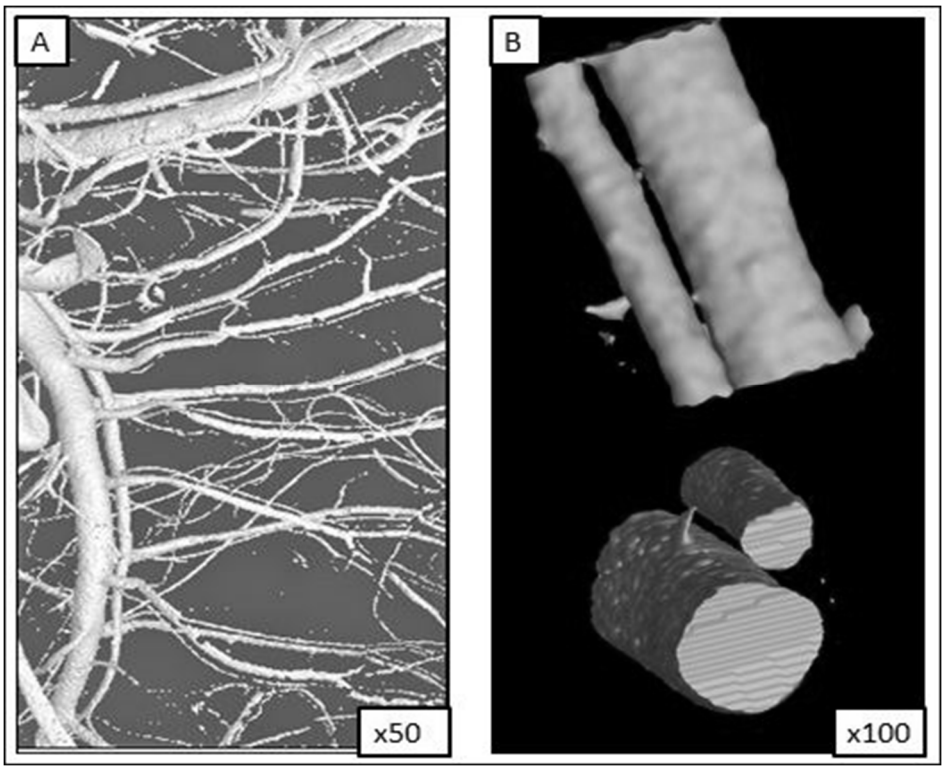

By: E. Ngounou

Figure 0.43: Visualisation of the nanotomography image by surface rendering showing arteries and veins running strictly parallel to each other.

A) A section of the C-HFD / SSC and B) A segment of the splenic artery and its homologous vein: the diameter at least 2 folds that of the artery.

It was observed without any morphometric evaluation that the pancreatic vascular network of the duodenal region showed many more large vessels than the splenic one under all conditions. There were more medium and small vessels in the splenic network confirming results obtained from the histological studies. At this level, no obvious differences were observed between groups and hence morphometric analysis was considered for details morphology.

4.5.2 Geometry of the pancreatic vasculature

The qualitative differences mentioned above in the macroscopic and microscopic arrangement of the vascular cast architecture were analyzed morphometrically. In this study, morphometric differences of the parameters describing the vascular network were obtained using ImageJ and VGStudioMax 3®. The vessel density, vessels lengths per unit volume, vessel diameter, number of segments, number of nodes, inter-branch distances and branch angles were assessed. Results were then used to deduce the possible quantitative data of the islet microvasculature using hemodynamic laws.

4.5.2.1 Vascular density of the cast

The Vascular density (VD) was expressed simply as a ratio of voxels determined to be inside the vessel cast divided by the total number of voxels in the cuboid domain (Figure 4.44). This parameter could be compared which the area fraction in the histological sections but not the number of cell per unit area.

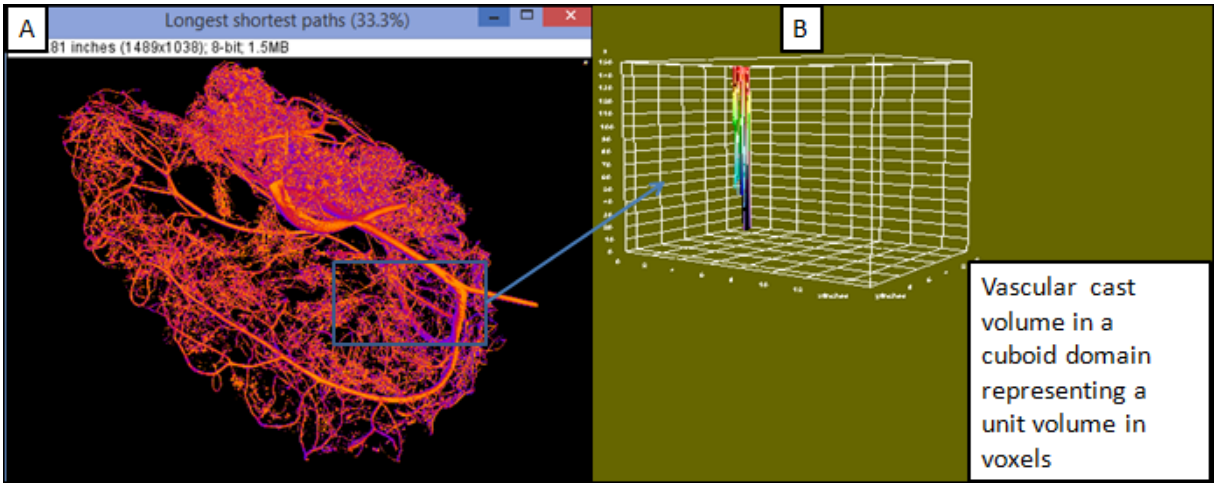

By: E. Ngounou

Figure 0.44: Visual representation of the vascular cast.

(A) volume in votex in a cuboid domain (B) and raw data sheet obtained from this evaluation from which the mean ratio was calculated. (C).

The mean vascular density (VD) obtained from the 3D image in both regions for each group is summarized in (Figure 4.45). Overall, the results were broadly consistent in each group for

both the duodenal (Figure 4.45A) and splenic (Figure 4.45B) pancreatic regions (0.297±0.016 vs 0.307±0.029 for NC, 0.295±0.020 vs 0.298±0.026 for C-SSC, 0.221±0.018 vs 0.2±0.02 for the C-HFD / SSC, 0.336±0.020 vs 0.337±0.025 for RAC / STZ and 0.307±0.020 vs 0.317±0.023). However, results varied considerably between groups with the significance differences recorded only in the splenic regions: NC vs RAC / STZ, p =0.006, C-SSC vs C-HFD / STZ p=0.045 and RAC / STZ vs HFD / STZ, p=0.00003 (Figure 4.45B).

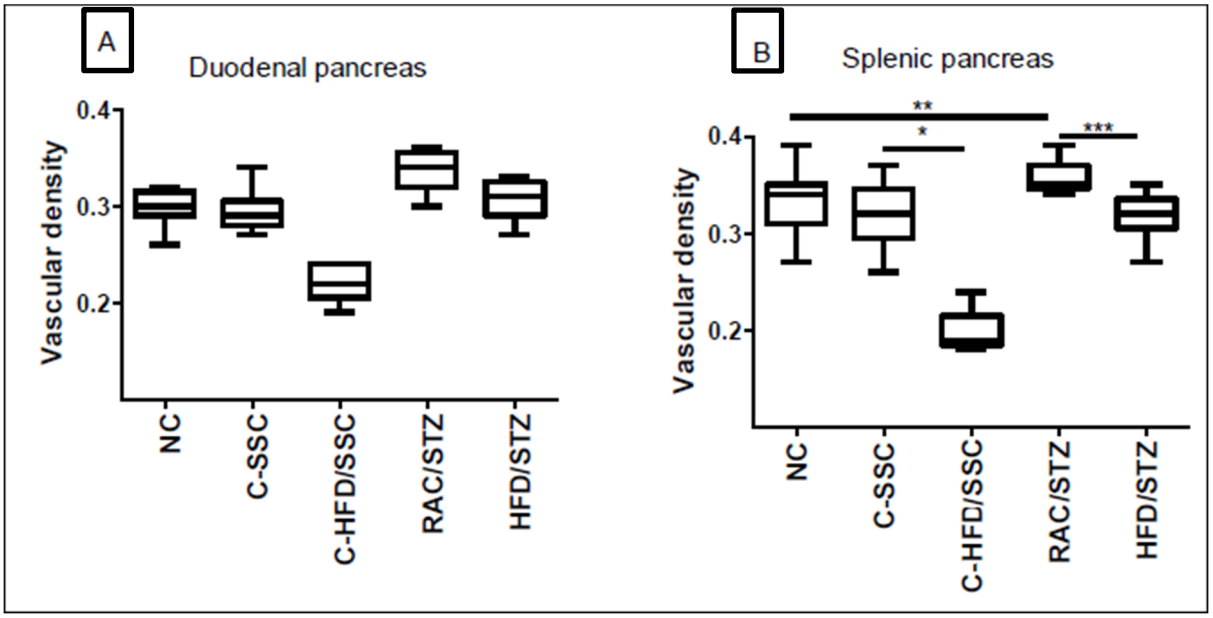

Figure 0.45: Box and whisker plots of the vascular density.

The vascular density of all groups in the (A) duodenal and (B) splenic regions of the pancreas. (NC vs C-HFD / SSC, **p<0.01 RAC / STZ vs HFD / STZ, *** p<0.001). Data expressed as mean ± SEM.

The evaluation of the relationship between the AFr of the pancreatic vasculature obtained from the histological slide and the VD from the corrosion cast is shown in the scatter plot (Figure 4.46) below. The curve graph indicates that there is a moderately strong positive linear relationship between the two variables, which is supported by the correlation coefficient (r=0.7606). The linear equation for predicting from VD= 0.13±1.018 of the AFr, (p=00047).

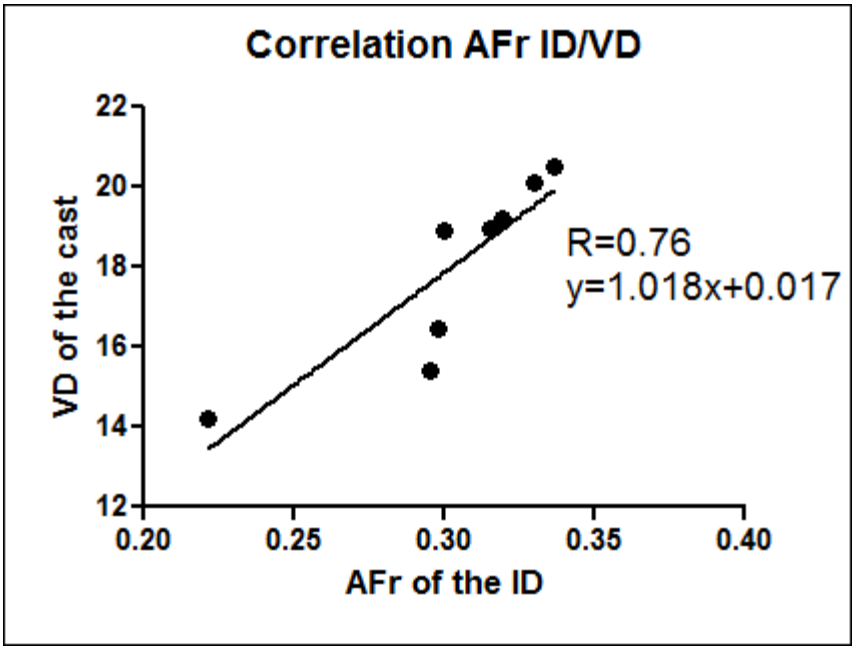

Figure 0.46: Schematic representation of the relationship between the area fractions (AFr) obtained from the ID of vessels from the histological section and the vessel density of the corrosion cast study.

4.5.2.2 Vessels length density

Expressed as the vessel length within a reference volume, the average vessel length density (Table 4.5) was smaller in the duodenal cast as compared to the splenic in all conditions. The venous portion, which was more tortuous, accounted for this difference. The value ranged between 2975±124.3µm/mm^3 of the RAC / STZ to 3708±93.5µm/mm^3 of the C-HFD / SSC animals.

Table 0.5. Mean vessel length density of the duodenum (D) and the splenic vascular per unit volume of the cast in each condition and each pancreatic region

	NC	C-SSC	C-HFD / SSC	RAC / STZ	HFD / STZ
D	3005±83.2	3108.5±78.2	3506.5±125**	3225±96.2	3458±104.6*
S	3205±103.2	3096.4±100.6	3708±104.6**	3356±125.6	3504.2±85.6-

P<0.05, **p<0.01, *** p<0.001. D=Duodenum, S=Splenic

4.5.2.3 Vessel diameter

The diameters of the gastroduodenal and the left gastric artery and vein and their branches were determined for the duodenal region. The diameter of the splenic artery and vein and branches were determined for the splenic region. Measurements of parent and branch vessel diameters were made at least at 100 other branch-points for each of the pancreatic vessels in each condition. The diameter of a vein at any given point in the vascular tree was greater than

that of the artery (at least twice). The major veins had the same as many inflowing tributaries as the major artery had branches. Figure 4.47 shows the distribution of the number of vessel segments and their diameter. More vessels (arterial and venous) were recorded in the smallest diameter group. The number of vessel segments gradually decreased from the smallest to the largest diameter ranges in both regions of the pancreas. Fewer segments were found in the 8–30µm diameter range in the venous, compared to the arterial vessels (p=0.03 for vessels 10-15µm and, p=0.011 for vessels 15-20µm). Within the diameter range 30-110µm, there were more segments, but no significant difference in the venous, compared to the arterial casts. Larger vessels (70-110 µm) were mainly recorded in duodenal regions of the NC and the C-SSC control groups. The highest number of the smallest vessels was recorded in the C-SSC / HFD groups in both regions of the pancreas.

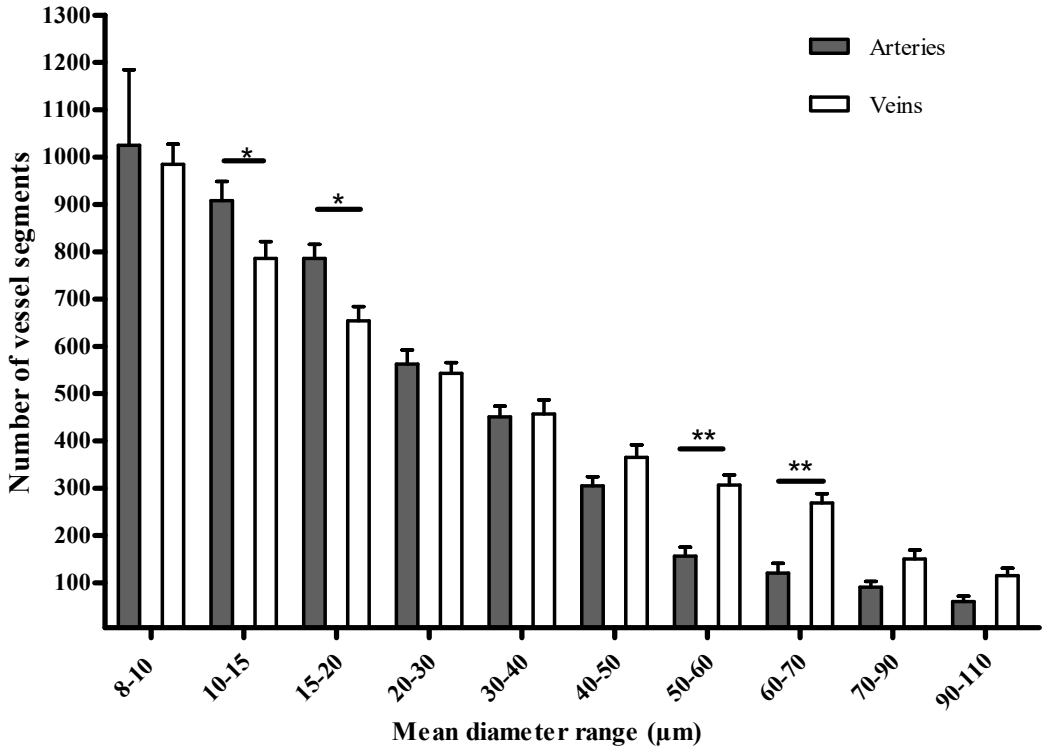

Figure 0.47: The number of vessel segments in different diameter ranges in the normal arterial and venous casts of the pancreas. * p=0.05, **p=0.01.

4.5.2.4 Inter branching distance

In order to compare the vessel network pattern between the duodenal and splenic regions and between-groups, the interbranching distance (distance between a node and the next one on a vessel) was evaluated in for the major vessels of the pancreatic cast. The mean distances between nodes were significantly higher (range 15µm to 256.2µm) in the splenic regions in each group compared to the duodenal regions (10µm - 189µm p=0.025). These ranges were

broadly maintained in all groups for each region. The longest distances were recorded in the large-diameter vessels in all conditions. All these results suggest that diabetes and obesity did not cause major changes in the pattern of distribution of the vessels within the pancreatic tissue.

4.5.2.5 Branching pattern and angle

The duodenal pancreatic cast presented a more asymmetrical branching model (69%) on the 100 randomly selected nodes evaluated compared to the splenic ones (35%). In the duodenal regions, the smallest vessel generally deviated from the axis of the parent vessel by at least 88º (between 88º and 100º), the largest branch tending to continue in the same trajectory (Figure 4.48A). In splenic regions, the parent segments generally divide into two almost equal diameter branches, each of which takes a different direction from the axis of the parent vessel. In addition, few nodes gave more than two branches in the two regions (Figure 4.48B).

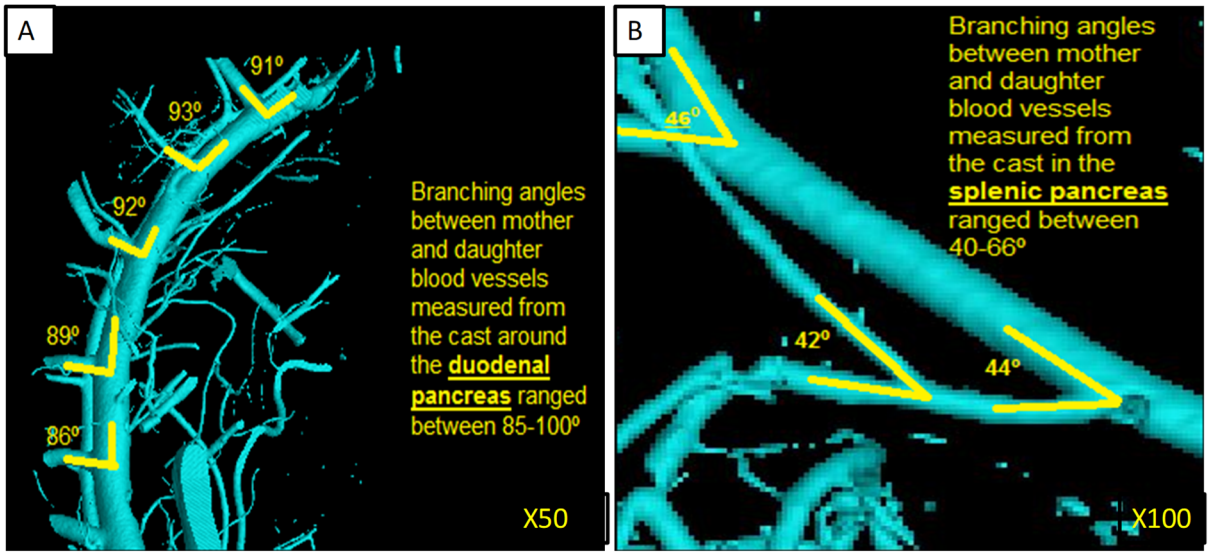

By: E. Ngounou

Figure 0.48: 2D Nano-CT images of the vascular branching pattern and the corresponding angles.

A) A portion of the duodenal and B) splenic pancreatic vascular casts. This pattern was observed in all control and diabetic groups.

A summary of the results includes, for example, a significant increase in the mean body weight was accompanied by a slight increase in mean BGL within 2 weeks in HFD. Streptozotocin caused the development of two diabetic models with all clinical symptoms (polyuria, polyphagia, high BGL (> 28mmol/L) and a significant decrease in body mass in both diabetic groups (26.68% and 15.54% in RAC / STZ and HFD / STZ respectively). The results of the flow cytometry and the Luminex assay validated the presence of islet vascular lesions in animals, which also justified the significant necrosis of endothelial cells, a decrease ($p<0.05$)

in the mean percentage of the stained area of CD34 pixels in islets, and thickening of the basement membrane. The scaling law was used to obtain the relationships between 1) the length and volume of the pancreatic vascular tree up to capillary level ($R^2=0.693\pm0.053$), 2) the diameter of the lumen and the blood flow in each pancreatic vascular branch ($R^2=0.988\pm0.055$), and 3) the diameter and length of the branches of the vessels ($R^2=0.838\pm0.0123$).

CHAPTER 5: DISCUSSION

This study aimed to establish the morphological and morphometric characteristics of islet microvasculature in the duodenal and splenic pancreatic tissues, as well as its modification under the insult of hyperglycaemia. We hypothesised that the size, structure, and pattern of distribution of the duodenal vessels were different from that of the splenic pancreas, a condition that could have affected not only the composition of islet cell types during the intra-uterine life (Tirziu & Simons 2009; Cleaver & Melton 2003), but also be predisposing factors of the duodenal pancreas to diseases such as DM and cancer in some people. Obese, T1DM and the T2DM animal models were successfully developed to achieve this aim. The following facts on the pancreatic tissue prompted this work.

1- The vulnerability of duodenal islets to diseases of the pancreas (Gullo et al., 1994; Hidalgo, 2010; Xiaojun Wang et al., 2013; Daniel et al., 2015).

2- Despite the knowledge of a) the regional cell type's difference in the islet, b) the importance of blood supply on the function of β cells, c) the effect of high blood sugar on the cardiovascular system, and d) finally the regional vulnerability of the duodenal pancreas to diseases such as cancer and diabetes, less is known on the pattern, distribution and the structural morphology of the islet microvasculature under normal and diabetic conditions.

Data from the present study has helped define the structural components of the different classes of the pancreatic vessels under normal and diabetic conditions. The metabolic statuses of the general human population associated with DM were well represented in this study grouping. The normal control animals (NC) for the healthy individual, the group exposed to HFD throughout the experiment (C-HFD/STZ) for the obese individual, the high dose of STZ (50mg/kg BW) treated animals for the T1DM individual and the combined HFD and STZ treated animal for the T2DM individuals. In other words, these animal groups were used to establish the normal distribution and structure of the pancreatic vessels including the islet microvasculature and the alterations of these features in obese and diabetic rats reflected the changes caused by hyperglycaemia.

5.1 DEVELOPMENT OF DIABETES MELLITUS

The two common types of DM, the T1 and T2DM were successfully induced in the animals in this study. While T1DM was induced by a single high dose of STZ, the T2DM was developed following a combination of an HFD and a low dose of STZ. The HFD put the animals in a pre-diabetic state within 14 days while STZ triggered the onset of DM. In addition, both types of DM were successfully maintained (BGL ≥ to 15mMol/L) for 60 days that is about 8 weeks.

Similar studies maintained the diabetic state in the animals for even longer (Ding et al., 2013; Yang et al., 2013; Salie et al., 2014).

5.1.1 The pre-diabetic state: bodyweight and blood glucose level

In the present study, a pre-diabetic condition was successfully induced in animals to prepare them for T2DM induction. The aim was to mimic the pathophysiology of human T2DM. Two weeks of HFD exhibited a significant increase in BW and BGL in the HFD group. The profile of BW during the period of the experiment varied from one study to the other: while De MagalhÃes et al., (2019) did not register any significant increase in the BW within 12 days of HFD, the present study and that of Srinivasan and colleagues (2005) registered a significant increase in this group.

The increase in BW found in HFD animals could simply be due to the rich energy food (fats) consumption and the deposition of fatty acid in various fat pads in the body (Srinivasan et al., 2004). Accumulation of fat in the body subsequently led to the reduction of energy expenditure compared to control animals (Storlien et al., 1986). Under this condition, the animals gradually moved from a healthy to a pre-diabetic state with a mild increase in BGL (Skovsø, 2014) but never became diabetic (BGL>6<8mMol/L). In a study by Salie and colleagues (2014) on the protective effect of the same diet on the heart against ischemia and reperfusion injury, they reported that even after 16 weeks, the animals never became diabetic.

Similar works used the same diet within the same period to induce insulin resistance with the rats showing the characteristics of the metabolic syndrome such as obesity and hyperlipidaemia (Reed et al., 2000; Srinivasan et al., 2005). Insulin resistance was confirmed by an OGTT which was the easiest way to assess the effective function of insulin (De MagalhÃes et al., 2019; Reed et al., 2000; Srinivasan et al., 2005). The composition of the HFD used in the study was previously described by Salie, Huisamen & Lochner, (2014). This high cholesterol-rich diet (13g / 100g) is not far from the food usually consumed in human households and is well established to be used effectively for the induction of insulin resistance (Lozano et al., 2016). However, the amount of lipids contained in the diet is not clearly defined: 10% (Jian-Gang Zhang et al., 2015); 32% (Salie et al., 2014); 45% (Atanasovska et al., 2014); 58% (Srinivasan et al., 2005); and 60% (De MagalhÃes et al., 2019) making the results obtained from these works non-standardised.

In humans, when trying to compensate for the high insulin demand under the prediabetic condition, the secretory capacity of the pancreatic β cells declines, leading to the conversion from the pre-diabetic state to a frank hyperglycaemic condition (Reed et al., 2000, Wortham & Sander, 2016). In rats, the conversion of animals with insulin resistance to T2DM with the presence of insulin in the blood as per that observed in humans was only achieved upon an intraperitoneal injection of a low dose of STZ (35mg/kg BW).

High-fat diet induces insulin resistance by various mechanisms (Srinivasan et al., 2005), the key mechanism is the one associated with glucose–fatty-acid cycle (Range et al., 1963). In fact, HFD increases the level of triglycerides leading to an increased availability of fatty acid for oxidation. The preference of fatty acids in the oxidation mechanism could be due to the reduction of the hepatic production of glycogen and the absorption of glucose in the muscular tissues, alterations which could ultimately lead to an increase in the production of insulin in order to compensate for the increasing demand (Belfiore & Iannello, 1998; Iwanishi & Kobayashi, 1993).

A high-fat diet has also been reported to promote microvascular dysfunction long before atherosclerotic lesions in the large vessels due to a high level of cholesterol (Ishikawa et al., 2004; Koller & Bagi, 2006). Under normal physiological conditions, the role of insulin is to regulate glucose homeostasis, by making glucose available to the skeletal muscle and adipose tissues, inhibiting the gluconeogenesis in the liver (Petersen et al., 2007) and regulating the delivery of nutrients to the target tissues while acting on the microvasculature (Muniyappa et al., 2008). In addition, insulin promotes the production of NO from the vascular endothelium which then leads to an increase in blood flow through dilatation (Koller & Bagi, 2006). The increase in blood flow facilitates the absorption of glucose into the tissues (Vincent et al., 2004). The insensitivity and the non-responsiveness of tissue to insulin causes the reduction in the activity of NO, an increase in oxidative stress, high expression of pro-inflammatory and pro-thrombotic factors, and abnormal vasoreactivity (Barac et al., 2007).

5.1.2 Diabetic state

5.1.2.1 Type one diabetes mellitus

A single intraperitoneal injection of a high dose of STZ (50 mg/kg) successfully induced T1DM in rat chow-fed rats after 4 days. This was justified by a high increase in BGL (20-31mMol/L) which was maintained throughout the 60 days of the diabetic period. The increase in BGL was due to the destruction of β cells by STZ, the cells producing the insulin hormone. Streptozotocin is an antibiotic produced by Streptomyces achromogene and has been extensively used to induce diabetes in laboratory animals due to its toxic effects on pancreatic β cells (Bolzán & Bianchi, 2002; Eleazu et al., 2013). The action of STZ in the β cell is associated with the generation of ROS. In the cytoplasm, ROS cause oxidative damage which leads to the destruction of β cells by inducing apoptosis and suppressing the synthesis of insulin (Szkudelski, 2001; Jun Zhang et al., 2010). Although the toxic action of STZ on β-cells is not yet understood, it is thought to be mediated by the inhibition of free radical scavenger-enzymes. This, in turn, enhances the production of superoxide, the main leading cause of β cell death (Zhang et al., 2010).

In addition to high BGL, the T1 diabetic animal model thus developed presented a gradual decrease in BW; an increase in the food and water consumption and increase urination over time, the characteristic feature of human T1DM. Weight loss is a major characteristic of DM and may be due to protein wasting because of lack of carbohydrate for energy (Chen & Ianuzzo, 1982). The lack of energy in the body triggers the hunger which causes polyphagia. Polyphagia causes an increase BGL which is unfortunately not captured into the various glucose-dependent organs because of the absence of insulin. The accumulation of glucose in the blood causes its elimination by the kidney through excessive urination. Excessive urination leads to dehydration which leads to an increase in water consumption. Many other studies have successfully induced T1DM using similar or higher doses (50-70mmg/kg) in as little as two days (van Dam et al., 1999; Zarros et al., 2009; Chaudhry et al., 2013; Wang-Fischer & Garyantes, 2018). Although the objectives of using STZ in diabetes research is to develop diabetic animal models, the use of different dosages of STZ reported in the literature has not been justified. More studies are needed to be able to critically analyse the results from different investigators.

In our study and several other research protocols, the diabetogenic action of STZ is thought to be improved by fasting the animal overnight prior to injection (Amin et al., 2011; Chaudhry et al., 2013; Atanasovska et al., 2014; Skovsø, 2014; Furman, 2015). Fasting animals for at least 4 to 12 hours before injecting STZ (Eleazu et al., 2013, Wang-Fischer & Garyantes, 2018), prevent postprandial glucose from competing with STZ via the high-affinity GLUT2-transporter in the β cell (Chaudhry et al., 2013). The issue of animal fasting or not fasting is very important and must be carefully considered when developing experimental protocols to reduce animal discomfort and stress (Chaudhry et al., 2013).

During the diabetic period, two animals from the RAC / STZ died, the first on day 34 and the other on day 43. According to the concept of the survival rate evaluation from previous studies, if a mouse or rat died within 5 days of STZ injection, it should be considered as due to the acute toxicity of STZ while the animals that died after 10 days of STZ injection should be due to the complications from severe hyperglycaemia (Deeds et al., 2011). This implies that the death of the two animals in our study was not due to the toxic effect of STZ but more likely due to the complications of hyperglycaemia.

5.1.2.2 Type two diabetes mellitus

The Type 2 DM is a complex metabolic disease characterized by insulin resistance followed by β cell loss while trying to compensate for the insulin demand (Mezza et al., 2019). In the present study, a T2DM animal model was successfully developed using the induced prediabetic animals and a low dose of STZ (35mg/kg). Previous studies have used different types of HFD with different doses of STZ to induce T2DM (Srinivasan et al., 2005; Zhang et

al., 2015). It is interesting to note that the low dose of STZ administered to the HFD animal in the present study would not normally have caused diabetes in a standard fed animal, perhaps just a slight increase in blood glucose level. As mentioned earlier, unlike in humans where excessive nutrition is a major cause of T2DM with increased insulin secretion but impaired metabolic actions in the liver (Petersen et al., 2007), HFD is said to induce only insulin resistance in rats but has never caused diabetes (>15 mMol/L) (Salie et al., 2014). To shift from the prediabetic to the diabetic state, a low dose of STZ (35mg/Kg BW) must be administered to the animals. Hence in this study, the low dose of STZ was able to induce diabetes to HFD animals. This may be because they were already insulin resistant (confirmed by OGTT). Consequently, under these conditions, any slight alteration of β cells function caused by STZ automatically led the HFD animals into the hyperglycaemic state.

In summary, because both insulin resistance and β cell malfunction constitute the key characteristics of the pathogenesis of human type 2 DM (DeFronzo, 2004), in this study, the rat model of HFD treated with STZ (HFD/STZ) was used to establish a nongenetic rat model of T2DM. While HFD induces insulin resistance, the low dose of STZ causes mild impairment in β cell function (Skovsø, 2014). The following sections discuss the effect of obesity and DM on blood and tissues parameters associated with the vascular injury in the body.

5.2 VASCULAR DAMAGE AND REPAIR ASSOCIATED WITH INSULIN RESISTANCE AND HYPERGLYCAEMIA

In the present study, the vascular damage (Navarro-González & Mora-Fernández, 2008; Aziz et al., 2013) and repair potential of the damage (DiMeglio et al., 2010; Yoder, 2012) were assessed using the Magnetic Luminex assay and flow-cytometry respectively while CD34 was used as the biomarker for endothelial cells.

5.2.1 Serum levels of inflammatory cytokines associated with the vascular damage

In this study, the levels of four cytokines associated with vascular injury (IL-6, TNF-α, TIMP-1, and VEGF) were successfully evaluated in the blood serum obtained from each group using magnetic Luminex assay (Figure 4 7-10). These cell-signalling molecules are involved in the normal functions of haematopoiesis, the immune system, metabolism, as well as in the pathogenesis of cardiovascular diseases (Qu et al., 2014). For example, they help in the mediation of the movement among the immune cells (lymphocytes, macrophages, dendritic cells) and other inflammatory cells (Omodanisi et al., 2017). Inflammation is the mechanism by which the body responds to injury and is one of the first markers of oxidative stress leading to a generation of ROS. The generation of ROS causes the up-regulation of pro-inflammatory cytokines reported in the diabetic condition in rats (Azam et al., 2015, Navarro-González & Mora-Fernández, 2008). All four cytokines were elevated in the two STZ treated animals

indicating that hyperglycaemia may have caused some degree of vascular injury in the animals within the 60 diabetes days. Similar studies have also used the level of these cytokines in the body to assess vascular damage. Details are discussed below for individual cytokine description.

5.2.1.1 Role of interleukin-6 in endothelial dysfunction

Our study provided evidence that IL-6 levels increased with DM because the level was significantly higher in the RAC/STZ. The HFD/STZ group also had a high but not significant increased level of IL-6 which may be due to the protective role of hyperlipidaemia sometime observed in cardiovascular ischemia (Salie et al., 2014). This difference may also be because the BGL in this group never increased to the level seen in the RAC/STZ group. Consistent with this study is the experiment done by Klover et al. (2005) who showed that chronic IL-6 treatment to the mice immediately impaired sensitivity of the liver to insulin. However, when IL-6 was neutralised in diet-induced obese mice, this improved the hepatic insulin responsiveness, indicating a direct role of IL-6 in insulin resistance (Duncan et al., 2003; Klover et al., 2005). Another study showed the critical role of IL-6 in the vascular dysfunction: Wassmann et al. (2004) demonstrated that wild mice treated with exogenous IL-6, had endothelial dysfunction in the aorta by up-regulating the angiotensin II type 1 receptor (Wassmann et al., 2004). Schrader et al. (2007) on the other hand reported that the deficiency of IL-6 prevented the endothelial dysfunction induced in carotid arteries (Schrader et al., 2007). Another group of researchers provided evidence that IL-6 is the main contributor to endothelium-derived hyperpolarizing factor (EDHF)-mediated coronary endothelial dysfunction in T2DM (Jonghae Lee et al., 2017).

5.2.1.2 Role of tumour necrosis factor-α in the endothelial dysfunction

Data from the present study showed clearly that TNF was significantly higher in STZ treated animals indicating that hyperglycaemia may have led to multiple tissues inflammation especially in the vascular system. The tumour necrosis factor-α is known to be implicated in diabetes through different biological processes including impairment of insulin secretion and induction of endothelial apoptosis and necrosis (Navarro-González & Mora-Fernández, 2008; Azam et al., 2015). Similar results were obtained by the study from Gao et al., (2007) who reported the pivotal role of the TNF in endothelial dysfunction in T2DM as it was proven that antibody neutralization of TNF prevented endothelial dysfunction of the coronary vessels

Although not clearly defined, there seems to be an interaction between TNF and IL-6 in the development of vascular pathology. Turner et al (2007) reported that the stimulation of IL-6 mRNA expression was achieved through TNF-α receptor I and the p38 mitogen-activated protein kinase, PI3K/Akt, and NF-kB pathway (Jonghae Lee et al., 2017).

5.2.1.3 Role of tissue inhibitor of metalloproteinase 1 in the endothelial dysfunction

Just like the IL-6 and TNF, the inhibitor of metalloproteinase -1 (TIMP-1) is a marker for diabetes and was significantly increased in diabetic animals. This finding is consistent with those of (Papazafiropoulou & Tentolouris, 2009; Usmanova, 2015). TIMP-1 is an endogenous matrix metallopeptidases inhibitor that might be involved in vascular matrix fibrosis (Tayebjee et al., 2003) which has a role in left ventricular hypertrophy and diastolic dysfunction by reducing cardiac collagen type I turnover, thereby increasing cardiac mass and stiffness (Tayebjee et al., 2003). Increased central and peripheral artery stiffness (Van Bortel et al., 2001) occurs with diabetes (Schram et al., 2004), and higher TIMP-1 circulating levels complete the hypothesis that altered TIMP-1 activities can be related to arterial stiffness. The fibrotic area occupying the islet core observed in the diabetic islet may also be associated with an increase in TIMP-1 level in the blood.

5.2.1.4 Vascular endothelial growth factor in endothelial dysfunction

The vascular endothelial growth factor is known to increase the growth of collateral vessels in ischaemia (Bauters et al., 1999) and hence is a potent angiogenic factor that has been identified as a primary initiator of proliferative diabetic retinopathy (Aiello & Wong, 2000). Although no significant difference was recorded in the present study, insulin resistance (C-HFD/STZ) and hyperglycaemia (RAC/STZ HFD/STZ) increased the level of serum VEGF. This suggests that under the present experimental conditions, some degree of new vessels may have been formed in some tissues of the animals. *In vivo* administration of VEGF improve the endothelium-dependent responses in animal models of endothelial dysfunction significantly, leading to collateral circulation and the regeneration of the endothelium (Bauters et al., 1999). While the mechanisms underlying this universal role of VEGF are still to be determined, these results are not yet sufficient to use such factors as a new therapeutic strategy in patients with vascular diseases (Bauters et al., 1999).

There is evidence that VEGF-A plays a major role in vascular wall remodelling (Makurina, 2016; Nemtsova et al., 2019). It is believed that VEGF can serve as an early indicator in serum for the development of endothelial dysfunction even when active intravascular inflammation has not yet been detected (Cubbon et al., 2009). Although VEGF-A is an important bioactive substance involved in the development of vascular pathologies in DM, the present data available showed that its level in DM and associated complications are controversial: Some studies describe both the increase and the decrease in VEGF-A levels in DM. Vural et al (2017) successfully used VEGF-A as a potential treatment of limb ischaemia in DM (He et al., 2016; Vural et al., 2017), while inhibition of the production of VEGF-A by anti-VEGF biologics was used in the treatment of diabetic retinopathy.

In conclusion, although the level of these biomarkers do not specifically indicate whether pancreatic vascular dysfunction has occurred as a result of prolonging insulin resistance and high BGL, these tests validate the severity of these parameters on the vascular system in general.

5.2.2 Impact of insulin resistance and hyperglycaemia on the mechanism of vascular repair

Endothelial progenitor cells (EPCs) play a major role in the repair of endothelial surfaces after injury (Cha et al., 2004). Under all circumstances, a reduced number of EPCs is associated with endothelial dysfunction, suggesting that endothelial lesions in the absence of sufficient repair by circulating endothelial progenitor cells (CEPCs) promote the progression of vascular disorders.

The present study showed that animals with insulin resistance (C-HFD/STZ) and high BGL had a decreased level of CEPCs in the blood circulation. These results are similar to the studies done by (Ling et al., 2012, Wei Zhang & Yan, 2013) performed on STZ induced diabetic rats in which CEPC levels significantly reduced. Additionally, Fadini et al. (2006) reported a relationship between the severity of diabetic peripheral arterial disease and reduced CEPC levels, while suggesting that CEPC could be used as a novel biomarker for peripheral atherosclerosis in DM e.g. low CEPCs counts predicts future cardiovascular pathologies (Sibal et al., 2009) and reduced vascular endothelial function in T2DM (Liao et al., 2010). Furthermore, Chen et al. (2007) reported that hyperglycaemia inhibits the mobilisation of CEPC from the bone marrow, which may justify again the reduced CEPC levels recorded in our study. These findings are contrary to our previous study which showed an increase but not significant of CEPC levels in STZ treated rat (TIDM), justified as due to small sample size (Tchokonte-Nana et al., 2017).

West et al. (2015) showed a relationship between CEPC and TNF-α. Furthermore, cardiovascular research showed that the reduction of CEPC in diabetes is due to the myelosuppressive effect of TNF-α as 3 months after the administration of the TNF-α inhibitory drug to a patient with rheumatoid arthritis, a significant rise in CEPCs was recorded (Spinelli et al., 2013).

Additionally, in the present study, the alterations of vascular repair in STZ treated animals reflected the poor expression of CD34 cells on the pancreatic tissue sections compared to the healthy animals (NC, C-SSC groups).

Studies have shown that the number of CEPCs varies considerably with age with higher values in the T1DM children (<20 years) compared to T1DM adults (>20 years) (Loomans et al., 2004; Sibal et al., 2009; DiMeglio et al., 2010; Palombo et al., 2011,). Interestingly, this trend was maintained even among healthy individuals (Rousseau et al., 2010; Altabas, 2015)

and correlated with impairment in endothelial repair and onset of vascular damage in the adult (Williamson et al., 2012). The animals used in the present study were of the same age group and the age-related factor could not be responsible for any difference in the number of CEPCs between the experimental groups. The differences in the number of CEPCs recorded rather reflected the effect of insulin resistance or hyperglycaemia on the vascular repair system.
This condition could have contributed greatly to the vascular morphological changes observed on the histological sections of obese and diabetic animal models. Cubbon et al. (2009) reported that an effective mechanism of endogenous vascular repair delays the development of vascular diseases (Cubbon et al., 2009). However several investigations have shown that the physiological maintenance of vascular repair is impaired by insulin-resistance due to abnormal cellular insulin signalling at the level of vascular cells (Kahn et al., 2011; Aziz et al., 2013; Sengupta et al., 2014; Kuschnerus et al., 2015).

5.2.3 Impact of insulin resistance and hyperglycaemia on the expression of CD34 in the islet

Endothelial cells (EC) of the blood vessels are adapted to the functional needs of the tissues to which they supply and therefore constitute a heterogeneous group of cells (Mattsson 2004). In addition, ECs differ functionally between large and small blood vessels, as well as between different organs and species (Kuzu et al., 1992). The heterogeneous nature of ECs makes it very difficult to find markers which are specific to all ECs (Mattsson, 2004). It was interesting to observe in this study that, the CD34 marker used to express endothelial cells was greater in the islet core than in the mantle in both pancreatic regions which makes the ECs heterogeneity to be applied even between a different region of the same organ (Simionescu et al., 1981; Ghitescu & Robert, 2002). There are two possible explanations for the different islet CD34 regional expression. First, the fact that in rodents, β cells are more clustered in the islet core than in the mantle and represent the most metabolically active cells in the islet, they need more blood supply than the other islet cells and hence more network of blood vessels. This is the reason for a higher expression CD34 in the islet core. Secondarily, the active metabolic β cells in the core may have influenced the nature of the surrounding ECs. In other words, the distribution (among) of blood vessels serving a unit area between the core and the mantle may be the same but the immunostaining density of the CD34 differs between the two regions.
If the first explanation for these CD34 expression regional differences is true, then the assumption is that blood capillaries in the islet are organised in such a way that a maximum exchange of material between islet cells and blood in the core is performed. And this can only be effective if the incoming blood into the islet flows first to the core and then to the mantle as described by (Stagner et al., 1989; Samols & Stagner, 1990).

Furthermore, the present study confirms that the distribution of ECs in the islet was not the same in different experimental groups: CD34 was significantly higher expressed in the islet of the healthy (NC and C-SSC groups) animals of both pancreatic regions compared to the diabetic groups (RAC/STZ and HFD/STZ). Our previous study (Tchokonte-Nana et al., 2017) on the level of CD34 expression in healthy and STZ induced diabetic animals reported the same findings. Under the study condition could STZ on its own be harmful to the ECs? Although this was not tested, the answer should be: no. Because evidence from the study of Zhang & Lv (2016) on the diabetic patients with diabetic foot ulcer also showed that CD34 was highly expressed in the tissue receiving local insulin treatment compared to the non-treated individuals. Many other works in the literature (Altabas, 2015; Lozano et al., 2016), report that it is clear that high BGL should be the sole cause of vascular endothelial dysfunction.

Lastly, the high distribution but less dense expression of CD34 of ECs in the sections from the obese individual (C-HFD / SSC) seemed to reflect an increase in the new but immature blood vessels circulating in the islets. Maybe if the experimental period were extended for more weeks, new blood vessels could have become more mature and functional.

In conclusion, the distribution of ECs in the islet perhaps reflected the relationship that exists between islet cells' function and the ECs activity and proliferation. Rodents have a higher percentage of β cells (80%) which are confined within the central portion of the islet while in human the distribution is less localised (Cabrera et al., 2006; Kim et al., 2009). This may be the reason why rodent islets contain an extensive network of fine and tortuous capillaries in the core in contrast to human islets which contain fivefold fewer, but larger vessels, which are less tortuous (Hogan & Hull, 2017).

5.3 IMPACT OF INSULIN RESISTANCE AND HYPERGLYCAEMIA ON THE HISTOMORPHOLOGY OF THE PANCREATIC TISSUE

At the end of the experiment, obesity and hyperglycaemia affected the general histomorphology of the pancreatic tissue sections. Three major visibly affected features were recorded in the pancreatic tissue: 1) presence of fatty infiltration, 2) the islet histomorphology and 3) the vasculature. These items are further clarified in the indicated paragraphs.

5.3.1 Fatty infiltration in the pancreatic tissue

Fatty infiltration, particularly around vessels, was the striking feature recorded in the pancreatic sections of the C-HFD / SSC and the HFD / STZ animals (obese and T2DM models). Results consistent which those of Takahashi et al., 2018 who reported that fatty depositions are ectopic adipocytes which infiltrate into the pancreatic tissue mainly in the area between the pancreatic lobules, around the large vessels (interlobular fat) and inside the lobules

themselves (intralobular fat). It should be noted that in this study, the fatty infiltration was maintained in the T2DM model even in the event of chronic hyperglycemia.

In the clinical settings, these fatty infiltrations are considered as non-alcoholic fatty pancreas diseases. Although benign, the condition is known to be a risk factor of insulin resistance, diabetes and pancreatic cancer (Lesmana et al., 2018; Takahashi et al., 2018). In our study, fatty infiltrations were associated with glucose intolerance which usually results from an impaired sensitivity to insulin action.

5.3.2 Islet

In addition to fatty infiltration, the second histomorphological changes in the pancreatic tissues were the presence of many huge islets in obese animals (C-HFD / SSC) compared to the NC group, results consistent with the studies of Hull et al. (2005) and Linnemann et al. (2014). The increase in the size of the islets in the obese group should be the consequence of an increase in the β cells mass in response to the increase in the demand for insulin to prevent diabetes (Dai et al., 2013; Linnemann et al., 2014). Previous studies by Kim et al. (2009) and Kilimnik et al. (2012) demonstrated that islet cytoarchitecture is size-dependent whether found in human or rodent. In this study, large islets (>∼100 μm in diameter) had non-β cells intermingled with β cells. In rodents, large islets of this size are only found in conditions such as pregnancy, obesity, diabetes and inflammation accompanied by increased blood flow (Homo-Delarche et al., 2006) while in humans, smaller islets had the conventional rodent β cells core surrounded by the non-β cell mantle.

The present study has shown that the increase in β cell mass is accompanied by a gain in BW similar to Hull et al. (2005). Their work showed that, in addition to BW gain, the increase in β cells mass is also correlated with the degree of insulin resistance but not with the increase in insulin secretion. This may be due to impaired vascular function. Note that although the expression of CD34 in the pancreatic section from the obese group was poor in our study, it was highly distributed. Increase in β cell mass may have triggered the formation of new blood vessels to ensure a better supply of oxygen and nutrients to proliferative cells (Dai et al., 2013). The reason why there was an increasing level of VEGF in our study, is a response to tissue hypoxia. However, these vessels were not functionally adapted to facilitate the normal secretion of insulin in the blood. The impaired insulin secretion as reported by Hull et al. (2005) in such conditions could also be associated with the new cytoarchitectural arrangement of the islet to adapt to obesity: that is converting the conventional rodent β cells core and non-β cell mantle to an intermingled β cell and non-β cell human islet-like (Xiaojun et al., 2013).

In humans, as time goes by and the condition persists, one can generate the hypothesis that the obesity milieu does not favour the formation of functional ECs (may be due to the absence of functional CEPCs in the blood as confirmed in our study) leading to tissue ischemia and

maybe haemorrhage. While tissue ischemia may lead to β cells necrosis, haemorrhage may expose β cell to immune destruction (macrophages) leading to the onset of DM. However, increased proliferation of local macrophages is reported to cause β cell dysfunction (Ying et al., 2020) but not haemorrhage as hypothesised. Regardless of how β cells become damaged, it remains to be understood how these events do not cause DM in non-genetically obese rodents and other primates. The understanding of how rodents deal with obesity without the onset of T2DM may shed light on the disease pathophysiology and treatment. The duodenal pancreas appears to be more vulnerable to these conditions, perhaps because it receives blood from a higher pressure source. All these analyses are contrary to the study of Dai (2013) reporting that the adaptation of the islet microvasculature to insulin resistance is done by dilation but not angiogenesis. All the animal strains used in the study of Dai (2013) were genetically modified and that may have contributed to these differences in the results. In addition, the animals were exposed to HFD for up to 20 weeks. A longer time compared to our study might have caused more vascular structural changes to occur.

In contrast, sections from both STZ treated animals showed islets with reduced size in the two regions of the pancreatic tissue compared to those of the NC animals. The severe islet shrinkage in T1DM model was due to the toxic effect of the high dose of STZ. (Kumar et al., 2006; Abunasef et al., 2014; Willcox & Gillespie, 2016; Omodanisi et al., 2017). Willcox & Gillespie (2016) reported that T1D becomes clinically evident upon the destruction of up to 70-80 % of β cell mass, with a marked reduction or absence of insulin. Beta cells represent up to 80% of the islet cell mass (Cabrera et al., 2006; Kim et al., 2009) in rodents and therefore any slight toxic effect of STZ on the islet β cells causes a noticeable reduction of the total size and volume of the islet. On the other hand, there was a mild shrinkage of the islets in HFD / STZ (T2DM model) surely due to a moderate loss of β cells mimicking, therefore, the human T2DM characterised with hyperglycaemia and presence of insulin in the blood (Mezza et al., 2019).

The substantial increase in the BGL, BW, food and water intake which confirmed the failure of pancreatic β-cell function (Ding et al., 2013). The absence of β cells led to the absence of insulin which then caused DM. A condition in agreement with the studies demonstrated by many other investigators who used different single high doses of STZ (50 mg/kg (Gajdosik et al., 1999; Ayepola et al., 2013; Wang-Fischer & Garyantes, 2018), 60 mg/kg (Gajdosik et al., 1999; Akbarzadeh et al., 2007; Amin et al., 2011; Abunasef et al., 2014;) and 65 mg/kg (Menger et al., 1992; Wang-Fischer & Garyantes, 2018) to destroy pancreatic β-cells in rats followed by a subsequent reduction of insulin secretion. In addition, polyphagia and polyuria further confirm that in the STZ treated groups, β cells are indeed either absent (T1DM) or not functional.

In addition to β cell loss leading to islet shrinkage, other features of the effects of STZ-induced diabetes on the pancreas tissue sections were recorded such as oedema (Wang et al., 2015), fibrosis of the islet core (Zechner et al., 2014) and lymphocyte infiltration (Pechhold et al., 2001). Oedema and lymphocyte infiltrations perhaps occur as a result of small blood vessels damage in the pancreatic tissue similar to what has been reported in retinopathy (Stitt et al., 2016). In the eye, hyperglycaemia causes the damage of the ECs lining the capillaries, responsible for maintaining the blood-retinal barrier. Consequently, there is an increase in the vascular permeability leading to the accumulation of extracellular fluid in the macula (Yu et al., 2016, Duh et al., 2017). On the other hand, although the cause of fibrosis in the islet is unclear, it is believed to be due to the loss of β cells and inflammation (Hart et al., 2018) and that the vascularisation seems to be the starting point of fibrosis formation in Goto-Kakizaki (GK) rat islets (Homo-Delarche et al., 2006). The GK rat is a substrain Wistar rat that is polygenic non-obese and develops adult onset T2DM early in life.

Note that even with a very high BGL, unlike in the T1DM model, all the above-mentioned data were moderate in T2DM. Consequently, the histomorphology of the pancreatic tissue in this group still maintained a high amount of fatty infiltration in the islet and the perivascular space in both pancreatic regions. This may explain why none of the T2D animal models died during the period of the experiment. With the assumption that all the above-mentioned effects are caused by high BGL, HFD may have had a protective effect on the pancreatic tissue as in the heart against ischaemia/reperfusion injury in a study conducted by Salie et al., in 2014.

In conclusion, under obesity and diabetes, the link between the structures of the pancreas, especially in T2Dm models, does not contribute to the best physiological maintenance of the integrity of the vascular system. This condition may have impaired the secretion and action of insulin leading to DM.

5.3.3 Pancreatic blood vessels

The other visible structures affected by obesity and hyperglycaemia were the blood vessels. The assessment of the detailed morphological features of the large vessels serving the islet microvasculature under the insult of obesity and hyperglycaemia was important in this study. Because the islet functions depend on the structural integrity of the pancreas vasculature, impairment in the integrity of the large vessels could say a lot about that of the intraislet capillaries concomitantly evaluated in this study using CD34 antibody as a biomarker for endothelial cells and supported by a BM delineated by the silver stain. Additionally, if the pattern of larger peripheral vessels abnormality is established under these conditions, then more accessible method such as vascular ultrasonography could be used to predict the severity of their effect on the islet microvasculature.

The vessel size (diameter), structural characteristics of the wall (individual layer thickness) and the relationship of the vessels with the surrounding pancreatic tissue were considered for this histomorphological evaluation: Firstly, the main vessel types found in most tissues were present in the pancreatic tissue: arteries, veins, arterioles, venules and capillaries. In most cases, the vessels were presented in doublet: an artery and a vein. Although different in thickness, the wall of arteries and veins consisted of three main layers; from outside to inside, the tunica adventitia, tunica media and tunica intima. The capillary was mainly made up of a layer of endothelium supported by a BM (Gray et al., 1989). In this study, the visual structural alteration of the vessels between experimental groups was mainly the thickness of the muscularis (tunica media). It was varied not only between the major classes of the vessels but also between groups and may justify the remodelling of the vascular wall to sustain the physiological requirement in the different experimental conditions. The significant increase in the vessels size for example in the obese model was mainly due to the increased thickness of the tunica media layer in obese and in T2DM models. However, other studies with similar results (Chung et al., 2009; Hamburg et al 2010; Kappus et al., 2014) did not specify which of the wall layers brought the difference. In addition, the morphometric analysis confirmed the morphological observations. In the T1DM models, the decrease in the thickness of the tunica media was associated with all the symptoms of a typical chronic diabetic state.

In addition, the vascular remodelling was revealed to a certain degree in the large vessels by the methenamine silver-stained which delineated the connective tissue surrounding the myocytes. In both obesity and diabetes, the connective tissue supported different size range of smooth muscle. The resulting overall increased wall thickness was due mainly to a marked increase in the size of myocytes but not their number.

5.4 IMPACT OF INSULIN RESISTANCE AND HYPERGLYCAEMIA ON THE PANCREATIC VASCULAR CORROSION CAST

In recent years, several different methods, such as microtomography (Aughwane et al., 2019) and confocal microscopy have been used to generate images of the entire microcirculation in a given organ (Blinder et al., 2013). This invited a better understanding of the complex interrelationship between organ function and vascular topology. In the present study, the 3D images of the entire pancreatic vascular casts were successfully obtained using more recent technology, the nano-CT scan.

These images were then used to obtain quantitative and qualitative data from the entire pancreatic vascular system in all experimental groups. This helped to understand the similarities and differences not only between the groups but especially between the duodenal and the splenic pancreas of the luminal characteristics of the pancreatic vascular system. Note that the vascular corrosion cast obtained was a cast of the lumen space of the vessels but not

the entire real vessels (which includes the vascular wall). To our knowledge, this is the first of such a study, as the few studies reported using the nano-CT scan have focused mainly on obtaining the qualitative data of the vessels (Chong et al., 1998, Ibukuro, 2001).

5.4.1 Morphology and large vessel distribution

Visualisation of the pancreas vascular cast was successfully carried out and the established distribution of blood vessels in the duodenal and splenic pancreas up to the level of arterioles corresponded to that described by most authors (Ibukuro, 2001, Kulenović & Sarac-Hadzihalilović, 2010, Dolenšek et al., 2015): the duodenal pancreas being supported by the arcade formed by the anterior and posterior pancreaticoduodenal vessels, branches of the gastroduodenal vessels while the splenic region is supplied exclusively by the branches of the splenic vessels. It was therefore clear that despite the dispersed nature of the anatomy of the rat pancreas, the distribution of its vascular tree obtained from the cast was similar to that of humans.

In addition, the pattern of distribution of the large blood vessels of the pancreas was the same in all study groups. This suggests that obesity and hyperglycaemia did not cause any visible change in the distribution of the vessels at this level of the pancreatic vascular. Therefore, whatever consequence of DM and obesity on the distribution of blood vessels in the pancreas, it would mainly be due to changes in the distribution of the smallest vessels. Unfortunately, the nano-CT scan did not make it possible to visualise the detailed arrangement of the smallest vessels (capillary bed, <8μm in diameter) and the data were only collected histologically. Junaid et al., (2017) conducted a similar study on the entire placental vascular corrosion cast using micro-CT scans and could not visualise vessels beyond the arteriole level. In his case, the placental arteriole was as large as the largest vessels in the present study (80μm) which may have been seen here because of the use of a higher resolution technique, namely the nano-CT scan. Understanding the exact structural component and anatomy of the vessels that supply the duodenal and splenic pancreas under the conditions of this study may have practical value in the cause, treatment and management of DM. This led to the evaluation of morphometric parameters.

5.4.2 Morphometry

The following morphometric parameters were evaluated: vascular density, vascular length, distances between branches, all indicators of angiogenesis and finally vascular diameter as the main indicator of vascular remodelling. Angiogenesis mainly occurs in the smallest vessels (capillaries), hence the results obtained in this study reflected the normal characteristics of each of the regions for large vessels, but not as a result of an angiogenic process. Note also that the evaluation of the vascular density of the vascular cast was considered as a ratio of

the volume of the blood vessels in a cuboid domain but not as the number of blood vessels in the domain. Consequently, the data obtained in this evaluation corresponded to the surface fraction obtained in the histological study.

Examination of the duodenal and splenic regions of the pancreatic cast revealed no significant difference between the two regions. However, C-HFD / SSC consistently had the lowest values for both regions. This indicates that the volume of blood supplying the entire vascular system may be nearly the same in the normal and diabetic animals and both regions. The vascular density in the splenic regions alone significantly varied between one group to the other, indicating that blood circulation in the splenic region seems to be more affected by obesity and hyperglycemia. These results correlated with those obtained from the histological evaluations although they were not significant. Such differences in local blood flow in the same organ have been reported in several studies of the brain (Lazorthes et al 1968; Harrison et al., 2002) and the kidney (Postnov et al 2016). The authors suggested a close coupling between metabolic demand of activated neurons and local changes in hemodynamics. One of these studies (Harrisson, 2002) reported that in core areas of the auditory cortex, the spatial pattern of intrinsic signals related directly not only to the physical position and density of capillary beds but also to the distribution of the myogenic valves that control blood flow to these vessels. Hence, the significances in the vascular density in the splenic pancreas reveals that the blood flow in the splenic region of the pancreas (loaded with a higher percentage of β cells) have different blood flow under different experimental conditions and this may be associated with the metabolic demand.

The reduced vascular density observed in the C-HFD / SSC group (obese animal) correlated with the study carried out by Dai (2013). In this study, the increase in metabolic demand accompanying obesity did not cause an angiogenic process (increase in vascular density) but rather caused the dilation of capillaries. However, since the capillaries could not be visualised in the current study by the nano-CT scan, that is the level of the vascular tree which is likely to undergo the angiogenesis, the results in our study (reduced the density) were not validated by this method and hence might be erroneous.

The length density of the blood vessels was significantly higher in the C-HFD / SSC group with no difference in the branching angle and interbranching distance when compared to the control group. This suggests that in this group, a small volume of blood supplies the tissue but through high tortuous/looping and very long and tiny vessels. Since the vascular cast obtained was a duplicate of the luminal volume of the vascular system, the observed long and tiny vessels may be due to the reduced inner diameters of the vessel characteristics in the obese subject. Reduced vascular diameter leads to increased blood pressure which may, in turn, cause breakage of small vessels. In the pancreas, islets of Langerhans are highly vascularised by

capillaries and very vulnerable to increased blood pressure, a condition which may jeopardise β cells following ischaemia.

5.4.3 Angioarchitecture of the pancreatic tissue and validation of the form and function relationship

The vascular tree is formed by consecutive branching of blood vessels from a stemmed vessel and venous trees by the repeated merging of a blood vessel from smaller vessels (Schreiner et al., 1996) In this study, we have shown the potential of a combination of corrosion casting and nano-CT imaging to achieve a fuller account of rat pancreatic vascular morphology. We achieved resolution of vessels down to ≈10-8 µm (diameter) with a whole cast measuring ~1.8 to 3 cm in its widest diameter. In the pancreas, vessels at this diameter were reported earlier as the terminal arteriole or post-capillary venule level and below this level the capillaries, with a mean level of ≈5.27 µm (Henderson & Moss, 1985). Diameters of stem (parent, mother) vessels and daughter vessels (branches), the density of vessels, number of nodes, interbranching distances and branching angles between mother and daughter vessels finally defined the overall 3D structure of the vascular network of the pancreas as well as the basic transport capacity of the system. In the present study, the above morphometric parameters were evaluated in all groups. A study which to our knowledge has not been done before.

The histological and corrosion cast study results justified the perfusion rate pattern observed in this study. Type one diabetic animal models had the fastest perfusion rate. A similar study done by Menger in 1992 showed that microvascular blood perfusion through islet grafts of diabetic animals models was higher as compared to normoglycaemic age match controls, and this was not on account of an increased capillary density, but on the increased in capillary diameter and lower microvascular hindrance. Experimental studies on blood perfusion of pancreatic islets *in situ* have shown an increase of microvascular blood flow as a result of hyperglycemia (Jansson and Sandler, 1985).

CHAPTER 6: CONCLUSION LIMITATION AND RECOMMENDATIONS

6.1 CONCLUSION

Results of this study lead to two important conclusions:

1- There is still a major challenge in the visualisation of the detailed structure of very small-sized organs such as the islet (in this study, the islet microvasculature) using the nano-CT scan. However, in this study, it was important to combine nano-CT scans and histological approaches to gain a deeper understanding of the role of vascular topology in the islet function. In this regard, our main task was to use the nano-CT scan characteristic of the entire vascular corrosion cast of the large pancreatic vessels and histological findings of the islet microvasculature to reconstitute the entire pancreatic vascular tree in normal and diabetic animals.

2- This investigation provides detailed morphological information on the pancreatic vasculature in normal and diabetic Wistar rat models. There were large differences in the structure of the pancreatic vascular system between the two regions but also between groups. The pancreatic tissue did not escape the principle of form-function relationship confirmed in other tissues such as the brain. The heterogeneity of the cytoarchitecture in the pancreatic tissue correlated with a heterogeneity of the angioarchitecture. In other words, the complexity of the spatial arrangement of the vessels in the duodenal pancreas and islet specifically is different from that in the splenic pancreas and islets. The difference should be related to the regional specific functions of the pancreatic tissues in response to hemodynamics and metabolic stimuli. The vascular topology is optimized to subserve the specific needs of a given organ or tissue. This difference in function poses restrictions on the design of the vascular system in the specific organs and tissues. Many diseases such as hypertension and DM, affect the cardiovascular system, and the associated morbidity and mortality are to a large extent related to effects on the vascular system. The effect of such a disease in a given organ is not only the result of the disease process itself but also depends on the specific topology of the vascular system in the organ (Razavi et al 2018).

6.2 LIMITATIONS AND RECOMMENDATIONS

The strength of this study lies in the establishment of differences in the pancreatic islet microvasculature, between the duodenal and splenic pancreas and how these are altered in DM using a combination of nano-CT scan and histological methods. However, there were some limitations of the current methods employed.

Firstly, although nano-CT allowed for the visualisation of the 3D structure of the vessels up to ~10 µm in diameter, smaller arterioles, capillaries and post-capillary venules constituting the islet microvasculature, could not be seen. Regarding the reconstruction of the pancreatic vascular tree, these missing data were managed through the histological technique. In addition, due to these missing data, the pattern of islet microvasculature reported justifying the paracrine function of the gland could not be revealed. It was therefore not possible to determine the distribution of branching angles and the distance between branches in the islet microvasculature network reported to be tenfold more vascularised than that of the exocrine tissue.

Secondly, with the use of ImageJ and VGStudioMax 3® software, the duodenal and spleen networks of the detailed vascular structure (diameter, branch angles, area fraction) could not be examined instantly. Instead, a return on investment was taken into account for the measurement one after the other and during this process, the parameters had to be adjusted from time to time and could cause bias.

Thirdly, although histological technique and morphometric and hemodynamic data of the large pancreatic vascular cast were used to deduce the islet microvasculature using a computational algorithm, the parity between units of measurement obtained from the 3D cast (µm, μm^2 and μm^3) and those obtained from the histological sections (pixel) remain questionable.

Fourthly the scaling law used in this study for the reconstitution of the pancreatic vascular tree was designed for normal tissue and the abnormality that may have caused DM may not have been expressed effectively.

Lastly, although the animal group studied were relatively tightly defined and statistical differences were observed, more useful information could be obtained if groups of different stages in the disease process were included in the study. Further experiments with a more tightly defined early and late of DM group are planned.

REFERENCES

Abunasef, S.K., Amin, H.A. & Abdel-Hamid, G.A. 2014. A histological and immunohistochemical study of beta cells in streptozotocin-diabetic rats treated with caffeine. *Folia Histochemica et Cytobiologica*. 52(1):42-50.

Adamson, R.H., Lenz, J.F., Zhang, X., Adamson, G.N., Weinbaum, S. & Curry, F.E. 2004. Oncotic pressures opposing filtration across non-fenestrated rat microvessels. *The Journal of Physiology*. 557(3):889–907.

Adamson, R.H., Zeng, M., Adamson, G.N., Lenz, J.F. & Curry, F.E. 2003. PAF- and bradykinin-induced hyperpermeability of rat venules is independent of actin-myosin contraction. *American Journal of Physiology-Heart and Circulatory Physiology*. 285(1): H406–H417.

Adkins, J.N., Varnum, S.M., Auberry, K.J., Moore, R.J., Angell, N.H., Smith, R.D., Springer, D.L. & Pounds, J.G. 2002. Toward a human blood serum proteome: analysis by multidimensional separation coupled with mass spectrometry. *Molecular and Cellular Proteomics*. 1(12):947–55.

Aharinejad, S., MacDonald, I.C., Schmidt, E.E., Böck, P., Hagen, D. & Groom, A.C. 1993. Scanning and transmission electron microscopy and high-resolution intravital video-microscopy of capillaries in the mouse exocrine pancreas, with special emphasis on endothelial cells. *The Anatomical Record*. 237(2):163–177.

Aharinejad, S.H. & Lametschwandtner, A. 1992. *Microvascular corrosion casting in scanning electron microscopy: techniques and applications*. Springer Science and Business Media. Chapter/pg numbers

Ahren, B. 2000. Autonomic regulation of islet hormone secretion–implications for health and disease. *Diabetologia*. 43(4):393–410.

Ahrén, B. & Holst, J.J. 2001. The cephalic insulin response to meal ingestion in humans is dependent on both cholinergic and noncholinergic mechanisms and is important for postprandial glycemia. *Diabetes*. 50(5):1030-1038.

Ahrén, B., Wierup, N. & Sundler, F. 2006. Neuropeptides and the regulation of islet function. *Diabetes*. 55(Supplement 2): S98-S107.

Aiello, L.P. & Wong, J.S. 2000. Role of vascular endothelial growth factor in diabetic vascular complications. *Kidney International*. Supplement. 77:S113-9.

Aird, W.C. 2007. Phenotypic heterogeneity of the endothelium: II. Representative vascular beds. *Circulation Research*. 100(2):174–190.

Akbarzadeh, A., Norouzian, D., Mehrabi, M.R., Jamshidi, S.H., Farhangi, A., Verdi, A.A., Mofidian, S.M.A. & Rad, B.L. 2007. Induction of diabetes by streptozotocin in rats. *Indian Journal of Clinical Biochemistry*. 22(2):60-64.

Alaiti, M.A., Ishikawa, M. & Costa, M.A. 2010. Bone marrow and circulating stem/progenitor cells for regenerative cardiovascular therapy. *Translational Research*. 156(3):112–129.

Alberti, K., Christensen, N.J., Christensen, S.E., Hansen, A.P., Iversen, J., Lundbaek, K., Seyer-Hansen, K. & Orskov, H. 1973. Inhibition of insulin secretion by somatostatin. *The Lancet*. 302(7841):1299–1301.

Alberts, B., Johnson, A., Lewis, J., Raff, M., Roberts, K. & Walter, P., 2007. *Molecular Biology of the Cell*. 5th edition New York. NY: Garland Science.

Alberts, B., Johnson, A., Lewis, J., Raff, M., Roberts, K. & Walter, P. 2002. Blood vessels and endothelial cells. In: *Molecular Biology of the Cell*. 4th edition. Garland Science.

Altabas, V. 2015. Diabetes, endothelial dysfunction, and vascular repair: what should a diabetologist keep his eye on? *International Journal of Endocrinology*. …..vol/page

Amin, A., Lotfy, M., Mahmoud-Ghoneim, D., Adeghate, E., Al-Akhras, M.A., Al-Saadi, M., Al-Rahmoun, S. & Hameed, R. 2011. Pancreas-protective effects of chlorella in STZ-induced diabetic animal model: insights into the mechanism. *Journal of Diabetes Mellitus*. 1(03):36.

Antigenix.com 2019 https://www.antigenix.com/flowcytometry.html

Antonetti, D.A., Klein, R. & Gardner, T.W. 2012. Diabetic retinopathy. *New England Journal of Medicine*. 366(13):1227–1239.

Apte, M., Pirola, R.C. & Wilson, J.S. 2015. Pancreatic stellate cell: physiologic role, role in fibrosis and cancer. *Current Opinion in Gastroenterology*. 31(5):416–423.

Armulik, A., Genové, G. & Betsholtz, C. 2011. Pericytes: developmental, physiological, and pathological perspectives, problems, and promises. *Developmental Cell*. 21(2):193–215.

Asahara, T., Murohara, T., Sullivan, A., Silver, M., van der Zee, R., Li, T., Witzenbichler, B., Schatteman, G & Isner JM. 1997. Isolation of putative progenitor endothelial cells for angiogenesis. *Science* (New York, N.Y.). 275(5302):964–7.

Atanasovska, E., Tasic, V., Slaninka-Miceska, M., Alabakovska, S., Zafirov, D., Kostova, E. & Labacevski, N. 2014. Six-week follow-up of metabolic effects induced by a high-fat diet and streptozotocin in a rodent model of type 2 diabetes mellitus. *Contributions Section of Medical Sciences*. 35(1):169-79.

Atsawarungruangkit, A. & Pongprasobchai, S. 2015. Current understanding of the neuropathophysiology of pain in chronic pancreatitis. *World Journal of Gastrointestinal Pathophysiology*. 6(4):193.

Aughwane, R., Schaaf, C., Hutchinson, J.C., Virasami, A., Zuluaga, M.A., Sebire, N., Arthurs, O.J., Vercauteren, T., Ourselin, S., Melbourne, A. & David, A.L., 2019. Micro-CT and histological investigation of the spatial pattern of feto-placental vascular density. *Placenta*. 88:36-43.

Avogaro, A., Albiero, M., Menegazzo, L., de Kreutzenberg, S. & Fadini, G.P. 2011. Endothelial dysfunction in diabetes: The role of reparatory mechanisms. *Diabetes Care*. 34(Supplement 2): S285–S290.

Ayepola, O.R., Chegou, N.N., Brooks, N.L. & Oguntibeju, O.O. 2013. Kolaviron, a Garcinia biflavonoid complex ameliorates hyperglycemia-mediated hepatic injury in rats via suppression of inflammatory responses. *BMC Complementary and Alternative Medicine*. 13(1):363.

Azam, S., Huda, A.F., Shams, K., Hasan, P.A.M., Mustafa, K.M. & Hasan, M.M. 2015. Anti-inflammatory and anti-oxidant study of ethanolic extract of *Mimosa pudica*. *Journal of Young Pharmacists*. 7(3):234.

Aziz, A., Yuldasheva, N., Smith, J., Haywood, N., Paul, C., Cubbon, R., Kearney, M., Porter, K. & Wheatcroft, S. 2013. 166 Enhancing vascular endothelial repair in the setting of insulin resistance: effects of insulin-like growth factor-binding protein-1. *Heart*. 99(supplement 2): A96-A97.

Balletshofer, B.M., Rittig, K., Enderle, M.D., Volk, A., Maerker, E., Jacob, S., Matthaei, S., Rett, K., & Häring, H.U. 2000. Endothelial dysfunction is detectable in young normotensive

first-degree relatives of subjects with type 2 diabetes in association with insulin resistance. *Circulation*. 101(15):1780–4.

Ballian, N. & Brunicardi, F.C. 2007. Islet vasculature as a regulator of endocrine pancreas function. *World Journal of Surgery*. 31(4):705–714.

Bancroft, J.D. & Gamble, M. eds., 2008. *Theory and Practice of Histological Techniques*. Elsevier Health Sciences.

Barac, A., Campia, U. & Panza, J.A. 2007. Methods for *Evaluating Endothelial Function in Humans*. Hypertension. 49(4):748–760.

Bateman, G.A., Levi, C.R., Schofield, P., Wang, Y. & Lovett, E.C. 2006. Quantitative measurement of cerebral haemodynamics in early vascular dementia and Alzheimer's disease. *Journal of Clinical Neuroscience*. 13(5):563–568.

Bauters, C., Six, I., Meurice, T. & Van, E.B. 1999. Growth factors and endothelial dysfunction. *Drugs.* 59:11-15.

Beckman, J.A., Creager, M.A. & Libby, P. 2002. Diabetes and atherosclerosis: epidemiology, pathophysiology, and management. *Journal of American Medical Association*. 287(19):2570–81.

Beckman, J.A., Goldfine, A.B., Gordon, M.B., Garrett, L.A., Keaney, J.F. & Creager, M.A. 2003. Oral antioxidant therapy improves endothelial function in Type 1 but not Type 2 diabetes mellitus. *American Journal of Physiology-Heart and Circulatory Physiology*. 285(6): H2392–H2398.

Belfiore, F. & Iannello, S., 1998. Insulin resistance in obesity: metabolic mechanisms and measurement methods. *Molecular Genetics and Metabolism.* 65(2), pp.121-128.

Beltrami, A.P., Barlucchi, L., Torella, D., Baker, M., Limana, F., Chimenti, S., Kasahara, H., Rota, M., Musso, E., Urbanek, K. & Leri, A. 2003. Adult cardiac stem cells are multipotent and support myocardial regeneration. *Cell*. 114(6):763-776.

Bennet, H.S., Luft, J.H. & Hampton, J.C. 1959. Morphological classifications of vertebrate blood capillaries. *The American Journal of Physiology.* 196(2):381–390.

Benninger, R.K. & Piston, D.W. 2014. Cellular communication and heterogeneity in pancreatic islet insulin secretion dynamics. *Trends in Endocrinology & Metabolism*. 25(8):399-406.

Berg, A.C., Chernavvsky-Sequeira, C., Lindsey, J., Gomez, R.A. & Sequeira-Lopez, M.L. 2013. Pericytes synthesize renin. *World Journal of Nephrology*. 2(1):11–16.

Bergers, G. & Song, S. 2005. The role of pericytes in blood-vessel formation and maintenance. *Neuro-oncology*. 7(4):452–464.

Betsou, F., Gaignaux, A., Ammerlaan, W., Norris, P.J. & Stone, M. 2019. Biospecimen science of blood for peripheral blood mononuclear cell (pbmc) functional applications. *Current Pathology Reports.* 7(2): 17–27.

Bhupathiraju, S.N. & Hu, F.B. 2016. Epidemiology of obesity and diabetes and their cardiovascular complications. *Circulation Research*. 118(11):1723–35.

Bierhaus, A., Chevion, S., Chevion, M., Hofmann, M., Quehenberger, P., Illmer, T., Luther, T., Berentshtein, E., Tritschler, H., Müller, M. & Wahl, P. 1997. Advanced glycation end product-induced activation of NF-κB is suppressed by α-lipoic acid in cultured endothelial cells. *Diabetes*. 46(9):1481-1490.

Bierhaus, A., Schiekofer, S., Schwaninger, M., Andrassy, M., Humpert, P.M., Chen, J., Hong, M., Luther, T., Henle, T., Klöting, I. & Morcos, M. 2001. Diabetes-associated sustained activation of the transcription factor nuclear factor-κB. *Diabetes*. 50(12):2792-2808.

Blanco, R. & Gerhardt, H. 2013. VEGF and Notch in tip and stalk cell selection. *Cold Spring Harbor Perspectives in Medicine*. 3(1):a006569.

Blinder, P., Tsai, P.S., Kaufhold, J.P., Knutsen, P.M., Suhl, H. & Kleinfeld, D. 2013. The cortical angiome: an interconnected vascular network with noncolumnar patterns of blood flow. *Nature Neuroscience*. 16(7):889.

Bodin, P. & Burnstock, G. 2001. Purinergic signalling: ATP release. *Neurochemical Research*. 26(8–9):959–69.

Bodin, P., Bailey, D. & Burnstock, G. 1991. Increased flow-induced ATP release from isolated vascular endothelial cells but not smooth muscle cells. *British Journal of Pharmacology*. 103(1):1203–5.

Bolzán, A.D. & Bianchi, M.S. 2002. Genotoxicity of streptozotocin. *Mutation Research/Reviews in Mutation Research*. 512(2-3):121-134.

Bonner-Weir, S. & Orci, L. 1982. New perspectives on the microvasculature of the islets of Langerhans in the rat. *Diabetes*. 31(10):883–9.

Bonner-Weir, S. 1993. The microvasculature of the pancreas, with emphasis on that of the islets of Langerhans. In: *The Pancreas: Biology, Pathobiology, and Disease*. Vay Liang W. Go Editor. COMPLETE

Bosco, D., Armanet, M., Morel, P., Niclauss, N., Sgroi, A., Muller, Y.D., Giovannoni, L., Parnaud, G. & Berney, T. 2010. Unique arrangement of α-and β-cells in human islets of Langerhans. *Diabetes*. 59(5):1202-1210.

Breen, E.J., Tan, W. & Khan, A. 2016. The statistical value of raw fluorescence signal in Luminex xmap based multiplex immunoassays. *Scientific Reports. Nature* 6: 26996.

Brendle, T.A. 2010. Preventing surgically induced diabetes after total pancreatectomy via autologous islet cell reimplantation. *Association of PeriOperative Registered Nurses Journal*. 92(2):169–184.

Brissova, M., Aamodt, K., Brahmachary, P., Prasad, N., Hong, J.Y., Dai, C., Mellati, M., Shostak, A., Poffenberger, G., Aramandla, R. & Levy, S.E. 2014. Islet microenvironment, modulated by vascular endothelial growth factor-A signaling, promotes β cell regeneration. *Cell Metabolism* 19(3):498-511.

Brissova, M., Shostak, A., Fligner, C.L., Revetta, F.L., Washington, M.K., Powers, A.C. & Hull, R.L. 2015. Human islets have fewer blood vessels than mouse islets and the density of islet vascular structures is increased in type 2 diabetes. *Journal of Histochemistry & Cytochemistry*. 63(8):637–645.

Brissova, M., Shostak, A., Shiota, M., Wiebe, P.O., Poffenberger, G., Kantz, J., Chen, Z., Carr, C., Jerome, W.G., Chen, J. & Baldwin, H.S. 2006. Pancreatic islet production of vascular endothelial growth factor-A is essential for islet vascularization, revascularization, and function. *Diabetes*. 55(11):2974-2985.

Brocq, M. Le, Leslie, S.J., Milliken, P. & Megson, I.L. 2008. Endothelial Dysfunction: From Molecular Mechanisms to Measurement, Clinical Implications, and Therapeutic Opportunities. *Antioxidants & Redox Signaling*. 10(9):1631–1674.

Brownlee, M. 2005. The pathobiology of diabetic complications: a unifying mechanism. *Diabetes*. 54(6):1615–1625.

Brunicardi, F.C., Stagner, J., Bonner-Weir, S., Wayland, H., Kleinman, R., Livingston, E., Guth, P., Menger, M., McCuskey, R., Intaglietta, M. & Charles. A. 1996. Microcirculation of the islets of Langerhans: Long Beach Veterans Administration Regional Medical Education Center Symposium. *Diabetes*. 45(4):385-392.

Bshouty, Z., 2012. Vascular compromise and hemodynamics in pulmonary arterial hypertension: Model predictions. *Canadian Respiratory Journal*. 19(3):209-215.

Busse, R. & Fleming, I. 2003. Regulation of endothelium-derived vasoactive autacoid production by haemodynamic forces. *Trends in Pharmacological Sciences*. 24(1):24–29.

Caballero, A.E., Arora, S., Saouaf, R., Lim, S.C., Smakowski, P., Park, J.Y., King, G.L., LoGerfo, F.W., Horton, E.S. & Veves, A. 1999. Microvascular and macrovascular reactivity is reduced in subjects at risk for type 2 diabetes. *Diabetes*. 48(9):1856-1862.

Cabrera, O., Berman, D.M., Kenyon, N.S., Ricordi, C., Berggren, P.-O. & Caicedo, A. 2006. The unique cytoarchitecture of human pancreatic islets has implications for islet cell function. *Proceedings of the National Academy of Sciences*. 103(7):2334–2339.

Camussi, G., Deregibus, M.C., Bruno, S., Cantaluppi, V. & Biancone, L. 2010. Exosomes / microvesicles as a mechanism of cell-to-cell communication. *Kidney International.* 78(9):838–848.

Cantaluppi, V., Biancone, L., Figliolini, F., Beltramo, S., Medica, D., Deregibus, M.C., Galimi, F., Romagnoli, R., Salizzoni, M., Tetta, C. and Segoloni, G.P. 2012. Microvesicles derived from endothelial progenitor cells enhance neoangiogenesis of human pancreatic islets. *Cell Transplantation*. 21(6):1305–1320.

Canzano, J.S., Nasif, L.H., Butterworth, E.A., Fu, D.A., Atkinson, M.A. & Campbell-Thompson, M. 2019. Islet microvasculature alterations with loss of beta-cells in patients with type 1 diabetes. *Journal of Histochemistry & Cytochemistry*. 67(1):41–52.

Cao, Z. & Wang, X. 2014. The endocrine role between β cells and intra-islet endothelial cells. *Endocrine Journal*. 61(7):647–54.

Carlsson, P.-O., Palm, F. & Mattsson, G. 2002. Low revascularization of experimentally transplanted human pancreatic islets. *The Journal of Clinical Endocrinology & Metabolism*. 87(12):5418–5423.

Carlsson, P.-O., Sandler, S. & Jansson, L. 1996. Influence of the neurotoxin capsaicin on rat pancreatic islets in culture, and on the pancreatic islet blood flow of rats. *European Journal of Pharmacology*. 312(1):75–81.

Carroll, R.G. & Carroll, R.G. 2007. Endocrine System. In: *Elsevier's Integrated Physiology.* Elsevier p157–176.

Ceradini, D.J., Kulkarni, A.R., Callaghan, M.J., Tepper, O.M., Bastidas, N., Kleinman, M.E., Capla, J.M., Galiano, R.D., Levine, J.P. & Gurtner, G.C. 2004. Progenitor cell trafficking is regulated by hypoxic gradients through HIF-1 induction of SDF-1. *Nature Medicine*. 10(8):858.

Cha, D.R., Kang, Y.S., Han, S.Y., Jee, Y.H., Han, K.H., Han, J.Y., Kim, Y.S. & Kim, N.H. 2004. Vascular endothelial growth factor is increased during early stage of diabetic nephropathy in type II diabetic rats. *Journal of Endocrinology* 183(1):183-194.

Chance, B., Sies, H. & Boveris, A. 1979. Hydroperoxide metabolism in mammalian organs. *Physiological Reviews*. 59(3):527–605.

Chaudhry, Z.Z., Morris, D.L., Moss, D.R., Sims, E.K., Chiong, Y., Kono, T. & Evans-Molina, C. 2013. Streptozotocin is equally diabetogenic whether administered to fed or fasted mice. *Laboratory Animals.* 47(4):257–65.

Cheifetz, S., Bellón, T., Calés, C., Vera, S., Bernabeu, C., Massagué, J. & Letarte, M. 1992. Endoglin is a component of the transforming growth factor-beta receptor system in human endothelial cells. *The Journal of Biological Chemistry.* 267(27):19027–30.

Chen, L., Endler, A. & Shibasaki, F. 2009. Hypoxia and angiogenesis: regulation of hypoxia-inducible factors via novel binding factors. *Experimental and Molecular Medicine*. 41(12):849.

Chen, V. & Ianuzzo, C.D. 1982. Dosage effect of streptozotocin on rat tissue enzyme activities and glycogen concentration. *Canadian Journal of Physiology and Pharmacology*. 60(10):1251-1256.

Chen, Y.H., Lin, S.J., Lin, F.Y., Wu, T.C., Tsao, C.R., Huang, P.H., Liu, P.L., Chen, Y.L. & Chen, J.W. 2007. High glucose impairs early and late endothelial progenitor cells by modifying nitric oxide–related but not oxidative stress–mediated mechanisms. *Diabetes*. 56(6):1559-1568.

Cheng, M.J., Kumar, R., Sridhar, S., Webster, T.J. & Ebong, E.E. 2016. Endothelial glycocalyx conditions influence nanoparticle uptake for passive targeting. *International Journal of Nanomedicine.* 11:3305–15.

Chong, M., Freeny, P.C. & Schmiedl, U.P. 1998. Pancreatic arterial anatomy: depiction with dual-phase helical CT. *Radiology*. 208(2): 537-542.

Christoffersonm, R.H. & Nilsson, B.O. 1988. Microvascular corrosion casting with analysis in the scanning electron microscope. *Scanning*. 10(2):43–63. John Wiley & Sons, Ltd.

Christoffersson, G., Henriksnas, J., Johansson, L., Rolny, C., Ahlstrom, H., Caballero-Corbalan, J., Segersvard, R., Permert, J., Korsgren, O., Carlsson, P.O. & Phillipson M. 2010. Clinical and experimental pancreatic islet transplantation to striated muscle: establishment of a vascular system similar to that in native islets. *Diabetes*. 59(10):2569–2578.

Chu, X., Gao, X., Jansson, L., Skogseid, B. & Barbu, A. 2013. Multiple microvascular alterations in pancreatic islets and neuroendocrine tumors of a Men1 mouse model. *The American Journal of Pathology*. 182(6):2355–2367.

Chung, W.B., Hamburg, N.M., Holbrook, M., Shenouda, S.M., Dohadwala, M.M., Terry, D.F., Gokce, N. & Vita, J.A. 2009. The brachial artery remodels to maintain local shear stress despite the presence of cardiovascular risk factors. *Arteriosclerosis, Thrombosis, and Vascular Biology*. 29(4):606-612.

Churukian, C.J. 1996. Consistent silver methods for demonstrating basement membranes, reticulum, and fungi. *Journal of Histotechniology*. 19(3): 211–217.

Cines, D.B., Pollak, E.S., Buck, C.A., Loscalzo, J., Zimmerman, G.A., McEver, R.P., Pober, J.S., Wick, T.M., Konkle, B.A., Schwartz, B.S. and Barnathan, E.S. 1998. Endothelial cells in physiology and in the pathophysiology of vascular disorders. *Journal of the American Society of Hematology*. 91(15): 3527-3561.

Cirulli, V., Halban, P.A. & Rouiller, D.G. 1993. Tumor necrosis factor-alpha modifies adhesion properties of rat islet B cells. *The Journal of Clinical Investigation*. 91(5):1868–76.

Claesson-Welsh, L. 2015. Vascular permeability--the essentials. *Upsala Journal of Medical Sciences.* 120(3):135–43.

Cleaver, O. & Melton, D.A. 2003. Endothelial signaling during development. *Nature Medicine*. 9(6):661-668.

Clee, S.M., Yandell, B.S., Schueler, K.M., Rabaglia, M.E., Richards, O.C., Raines, S.M., Kabara, E.A., Klass, D.M., Mui, E.T., Stapleton, D.S. and Gray-Keller, M.P. 2006. Positional cloning of Sorcs1, a type 2 diabetes quantitative trait locus. *Nature Genetics*. 38(6):688–693.

Colagiuri, S., Colagiuri, R. & Ward, J. 1998. National diabetes strategy and implementation plan. *Diabetes Australia, Canberra*.1-281.

Costa, M., Brookes, S.J. & Hennig, G.W. 2000. Anatomy and physiology of the enteric nervous system. *Gut*. 47(suppl 4):iv15-iv19.

Crawford, S.E., Stellmach, V., Murphy-Ullrich, J.E., Ribeiro, S.M.F., Lawler, J., Hynes, R.O., Boivin, G.P. & Bouck, N. 1998. Thrombospondin-1 is a major activator of TGF-β1 *in vivo*. *Cell*. 93(7):1159–1170.

Cross, S.E., Vaughan, R.H., Willcox, A.J., McBride, A.J., Abraham, A.A., Han, B., Johnson, J.D., Maillard, E., Bateman, P.A., Ramracheya, R.D., Rorsman, P., Kadler, K.E., Dunne, M.J., Hughes, S.J. & Johnson, P.R. V. 2017. Key matrix proteins within the pancreatic islet basement membrane are differentially digested during human islet isolation. *American Journal of Transplantation*. 17(2):451–461.

Crowther, N.J., Gotfredsen, C.F., Moody, A.J. & Green, I.C. 1989. Porcine islet isolation, cellular composition and secretory response. *Hormone and Metabolic Research*. 21(11):590–595.

Cubbon, R.M., Kahn, M.B. & Wheatcroft, S.B. 2009. Effects of insulin resistance on endothelial progenitor cells and vascular repair. *Clinical Science*. 117(5):173–190.

Curtis, T.M., Gardiner, T.A. & Stitt, A.W. 2009. Microvascular lesions of diabetic retinopathy: clues towards understanding pathogenesis? *Eye*. 23(7):1496–1508.

Dai, C., Brissova, M., Reinert, R.B., Nyman, L., Liu, E.H., Thompson, C., Shostak, A., Shiota, M., Takahashi, T. & Powers, A.C. 2013. Pancreatic islet vasculature adapts to insulin resistance through dilation and not angiogenesis. *Diabetes*. 62(12):4144–53.

Dandona, P., Weinstock, R., Thusu, K., Abdel-Rahman, E., Aljada, A. & Wadden, T. 1998. Tumor necrosis factor-α in sera of obese patients: fall with weight loss. *The Journal of Clinical Endocrinology & Metabolism*. 83(8):2907–2910.

Darwish, A. & Lui, F., 2019. Physiology, Colloid Osmotic Pressure. In: StatPearls [Internet]. StatPearls Publishing.

Dasevcime, N. & King, G. 2007. The role of protein kinase C activation and the vascular complications of diabetes. *Pharmacological Research*. 55(6):498–510.

Davidson, S.M. 2010. Endothelial mitochondria and heart disease. *Cardiovascular Research*. 88(1):58–66.

De Carlo, E., Milanesi, A., Martini, C., Maffei, P., Sicolo, N. & Scandellari, C. 2000. Endothelin-1 and endothelin-3 stimulate insulin release by isolated rat pancreatic islets. *Journal of Endocrinological Investigation*. 23(4):240–245.

De Jongh, R.T., Serné, E.H., IJzerman, R.G., de Vries, G. & Stehouwer, C.D.A. 2004. Impaired microvascular function in obesity: implications for obesity-associated microangiopathy, hypertension, and insulin resistance. *Circulation*. 109(21):2529–2535.

De Koning, E.J.P., van den Brand, J.J.G., Mott, V.L., Chargé, S.B.P., Hansen, B.C., Bodkin, N.L., Morris, J.F. & Clark, A. 1998. Macrophages and pancreatic islet amyloidosis. *Amyloid*. 5(4):247–254.

De la Torre, J.C. & Mussivand, T. 1993. Can disturbed brain microcirculation cause Alzheimer's disease? N*eurological Research.* 15(3):146–53.

De la Torre, J.C. 2002 Alzheimer disease as a vascular disorder: nosological evidence. *Stroke* 33(4): 1152–1162.

De MagalhÃes, D.A., Kume, W.T., Correia, F.S., Queiroz, T.S., Allebrandt Neto, E.W., Dos Santos, M.P., Kawashita, N.H. & De França, S.A. 2019. High-fat diet and streptozotocin in the induction of type 2 diabetes mellitus: A new proposal. *Anais da Academia Brasileira de Ciencias*. 91(1). Pg numbers

Deeds, M.C., Anderson, J.M., Armstrong, A.S., Gastineau, D.A., Hiddinga, H.J., Jahangir, A., Eberhardt, N.L. & Kudva, Y.C. 2011. Single dose streptozotocin-induced diabetes: considerations for study design in islet transplantation models. *Laboratory Animals*. 45(3):131-140.

DeFronzo, R.A. 2004. Pathogenesis of type 2 diabetes mellitus. *Medical Clinics*. 88(4):787-835.

Degenhardt, T.P., Thorpe, S.R. & Baynes, J.W. 1998. Chemical modification of proteins by methylglyoxal. *Cellular and Molecular Biology* (Noisy-le-Grand, France). 44(7):1139–45.

Dejana, E. & Orsenigo, F. 2013 Endothelial adherens junctions at a glance. *Journal of Cell*

Science. 126(Pt 12):2545–2549.

DiMeglio, L.A., Tosh, A., Saha, C., Estes, M., Mund, J., Mead, L.E., Lien, I., Ingram, D.A. & Haneline, L.S. 2010. Endothelial abnormalities in adolescents with type 1 diabetes: a biomarker for vascular sequelae? *The Journal of Pediatrics*. 157(4):540-546.

Dimmeler, S., Fleming, I., Fisslthaler, B., Hermann, C., Busse, R. & Zeiher, A.M. 1999. Activation of nitric oxide synthase in endothelial cells by Akt-dependent phosphorylation. *Nature*. 399(6736):601–605.

Ding, Y., Zhang, Z., Dai, X., Jiang, Y., Bao, L., Li, Y. & Li, Y. 2013. Grape seed proanthocyanidins ameliorate pancreatic beta-cell dysfunction and death in low-dose streptozotocin-and high-carbohydrate/high-fat diet-induced diabetic rats partially by regulating endoplasmic reticulum stress. *Nutrition and Metabolism*. 10(1):51.

Dolenšek, J., Rupnik, M.S. & Stožer, A., 2015. Structural similarities and differences between the human and the mouse pancreas. *Islets*. 7(1):e1024405.

Dorrell, C., Schug, J., Lin, C.F., Canaday, P.S., Fox, A.J., Smirnova, O., Bonnah, R., Streeter, P.R., Stoeckert, C.J., Kaestner, K.H. & Grompe, M. 2011. Transcriptomes of the major human pancreatic cell types. *Diabetologia*. 54(11):2832–2844.

Drel, V.R., Pacher, P., Stavniichuk, R., Xu, W., Zhang, J., Kuchmerovska, T.M., Slusher, B. & Obrosova, I.G. 2011. Poly (ADP-ribose) polymerase inhibition counteracts renal hypertrophy and multiple manifestations of peripheral neuropathy in diabetic Akita mice. *International Journal of Molecular Medicine*. 28(4):629.

Drexler, H. & Hornig, B. 1999. Endothelial Dysfunction in Human Disease. *Journal of Molecular and Cellular Cardiology*. 31(1):51–60.

Du Plessis, A., Broeckhoven, C., Guelpa, A. & Le Roux, S.G. 2017. Laboratory x-ray micro-computed tomography: a user guideline for biological samples. *GigaScience*. 6(6):gix027.

Dubois, S., Madec, A.M., Mesnier, A., Armanet, M., Chikh, K., Berney, T. & Thivolet, C. 2010. Glucose inhibits angiogenesis of isolated human pancreatic islets. *Journal of Molecular Endocrinology*. 45(2):99–105.

Dufrane, D., Goebbels, R.M. & Gianello, P. 2010. Alginate macroencapsulation of pig islets allows correction of streptozotocin-induced diabetes in primates up to 6 months without immunosuppression. *Transplantation*. 90(10):1054–1062.

Duh, E. & Aiello, L.P. 1999. Vascular endothelial growth factor and diabetes: the agonist versus antagonist paradox. *Diabetes*. 48(10):1899–906.

Duh, E.J., Sun, J.K. & Stitt, A.W. 2017. Diabetic retinopathy: current understanding, mechanisms, and treatment strategies. *Journal Clinical of Investigation. Insight*. 2(14). Page numbers

Duncan, B.B., Schmidt, M.I., Pankow, J.S., Ballantyne, C.M., Couper, D., Vigo, A., Hoogeveen, R., Folsom, A.R. & Heiss, G., 2003. Low-grade systemic inflammation and the development of type 2 diabetes: the atherosclerosis risk in communities study. *Diabetes*. 52(7):1799-1805.

Duncan, E.R., Crossey, P.A., Walker, S., Anilkumar, N., Poston, L., Douglas, G., Ezzat, V.A., Wheatcroft, S.B., Shah, A.M., Kearney, M.T. & Kearney, M.I. 2008. Effect of endothelium-specific insulin resistance on endothelial function *in vivo*. *Diabetes*. 57(12):3307–14.

Durand, M.J. & Gutterman, D.D. 2013. Diversity in mechanisms of endothelium-dependent vasodilation in health and disease. *Microcirculation*. 20(3):239–247.

Durbeej, M. 2010. Laminins. *Cell and Tissue Research*. 339(1):259–268.

Eberhard, D. & Lammert, E. 2009. The pancreatic β-cell in the islet and organ community. *Current Opinion in Genetics and Development*. 19(5):469–475.

Eberhard, D., Kragl, M. & Lammert, E. 2010. 'Giving and taking': endothelial and β-cells in the islets of Langerhans. *Trends in Endocrinology and Metabolism.* 21(8):457–463.

Ebner, I. & Anderhuber, F. 1985. Arterial vascularization of the tail of the pancreas with special reference to the relation of the tail and body vessels. *Acta Anatomica*. *121*(2):115-123.

Edlund, H. 2002. Organogenesis: Pancreatic organogenesis — developmental mechanisms and implications for therapy. *Nature Reviews Genetics.* 3(7):524–532.

Einarson, T.R., Acs, A., Ludwig, C. & Panton, U.H. 2018. Prevalence of cardiovascular disease in type 2 diabetes: a systematic literature review of scientific evidence from across the world in 2007-2017. *Cardiovascular Diabetology*. 17(1):83.

Eizirik, D.L., Pipeleers, D.G., Ling, Z., Welsh, N., Hellerström, C. & Andersson, A. 1994. Major species differences between humans and rodents in the susceptibility to pancreatic beta-cell injury. *Proceedings of the National Academy of Sciences*. 91(20):9253-9256.

Ejaz, S., Chekarova, I., Ejaz, A., Sohail, A. & Lim, C.W., 2008. Importance of pericytes and mechanisms of pericyte loss during diabetic retinopathy. *Diabetes, Obesity and Metabolism*. 10(1):53-63.

Eleazu, C.O., Eleazu, K.C., Chukwuma, S. & Essien, U.N. 2013. Review of the mechanism of cell death resulting from streptozotocin challenge in experimental animals, its practical use and potential risk to humans. *Journal of Diabetes and Metabolic Disorders*. 12(1):1.

Erdei, N., Tóth, A., Pásztor, E.T., Papp, Z., Édes, I., Koller, A. & Bagi, Z. 2006. High-fat diet-induced reduction in nitric oxide-dependent arteriolar dilation in rats: role of xanthine oxidase-derived superoxide anion. *American Journal of Physiology-Heart and Circulatory Physiology*. 291(5): H2107-H2115.

Fadini, G.P., Pucci, L., Vanacore, R., Baesso, I., Penno, G., Balbarini, A., Di Stefano, R., Miccoli, R., De Kreutzenberg, S., Coracina, A. & Tiengo, A. 2007. Glucose tolerance is negatively associated with circulating progenitor cell levels. *Diabetologia*. 50(10):2156–2163.

Fadini, G.P., Sartore, S., Albiero, M., Baesso, I., Murphy, E., Menegolo, M., Grego, F., Vigili de Kreutzenberg, S., Tiengo, A., Agostini, C. & Avogaro, A. 2006. Number and function of endothelial progenitor cells as a marker of severity for diabetic vasculopathy. *Arteriosclerosis, Thrombosis, and Vascular Biology*. 26(9):2140-2146.

Jaffe, E.A., Nachman, R.L., Becker, C.G. & Minick, C.R., 1973. Culture of human endothelial cells derived from umbilical veins. Identification by morphologic and immunologic criteria. *The Journal of Clinical Investigation*. *52*(11):2745-2756.

Farack, L., Golan, M., Egozi, A., Dezorella, N., Bahar Halpern, K., Ben-Moshe, S., Garzilli, I., Tóth, B., Roitman, L., Krizhanovsky, V. & Itzkovitz, S. 2019 Transcriptional heterogeneity of beta cells in the intact pancreas. *Development Cel.* 48(1):115-125.e4.

Favaro, E., Bottelli, A., Lozanoska-Ochser, B., Ferioli, E., Huang, G.C., Klein, N., Chiaravalli, A., Perin, P.C., Camussi, G., Peakman, M. & Conaldi, P.G. 2005. Primary and immortalised human pancreatic islet endothelial cells: phenotypic and immunological characterisation. *Diabetologia*. 48(12): 2552-2562.

Favero, G., Paganelli, C., Buffoli, B., Rodella, L.F. & Rezzani, R. 2014. Endothelium and its alterations in cardiovascular diseases: life style intervention. *Biomedical Research International*. ….VOL /pages

Festa, A., D'Agostino, R., Howard, G., Mykkänen, L., Tracy, R.P. & Haffner, S.M. 2000. Chronic subclinical inflammation as part of the insulin resistance syndrome: the Insulin Resistance Atherosclerosis Study (IRAS). *Circulation*. 102(1):42–7.

Figliolini, F., Cantaluppi, V., De Lena, M., Beltramo, S., Romagnoli, R., Salizzoni, M., Melzi, R., Nano, R., Piemonti, L., Tetta, C. & Biancone, L. 2014. Isolation, characterization and potential role in beta cell-endothelium cross-talk of extracellular vesicles released from human pancreatic islets. *Public Library of Science* (1). 9(7):e102521.

Fischer, A.H., Jacobson, K.A., Rose, J. & Zeller, R., 2008. Hematoxylin and eosin staining of tissue and cell sections. C*old Spring Harbor Protocols*. (5): .pdb-prot4986.

Flatt, P.R., Swanston-Flatt, S.K., Tan, K.S. & Marks, V. 1987. Effects of cytotoxic drugs and inhibitors of insulin secretion on a serially transplantable rat insulinoma and cultured rat insulinoma cells. *General Pharmacology*. 18(3):293-297.

Folkman, J., 2002, December. Role of angiogenesis in tumor growth and metastasis. In: *Seminars in oncology*. 29(6):15-18. WB Saunders.

Folli, F., La Rosa, S., Finzi, G., Davalli, A.M., Galli, A., Dick, E.J., Perego, C. & Mendoza, R.G. 2018. Pancreatic islet of Langerhans' cytoarchitecture and ultrastructure in normal glucose tolerance and in type 2 diabetes mellitus. *Diabetes. Obesity and Metabolism*. 20:137–144.

Fransson, M., Brännström, J., Duprez, I., Essand, M., Le Blanc, K., Korsgren, O. & Magnusson, P.U. 2015. Mesenchymal stromal cells support endothelial cell interactions in an intramuscular islet transplantation model. *Regenerative Medicine Research*. 3:1. Page numbers

Fray, J.C. 1980. Stimulus-secretion coupling of renin. Role of haemodynamic and other factors. *Circulation Research*. 47(4):485–92.

Frey, T. & Antonetti, D.A. 2011. Alterations to the blood–retinal barrier in diabetes: cytokines and reactive oxygen species. *Antioxidants and Redox Signaling*. 15(5):1271–1284.

Furman, B.L., 2015. Streptozotocin-induced diabetic models in mice and rats. *Current Protocols in Pharmacology*. 70(1):5-47.

Gajdosik, A., Gajdosikova, A., Stefek, M., Navarova, J. & Hozova, R., 1999. Streptozotocin-induced experimental diabetes in male Wistar rats. *General Physiology and Biophysics*. 18: 54-62.

Gale, N.W. & Yancopoulos, G.D. 1999. Growth factors acting via endothelial cell-specific receptor tyrosine kinases: VEGFs, angiopoietins, and ephrins in vascular development. *Genes and Development.* 13(9):1055–66.

Galley, H.F. & Webster, N.R. 2004. Physiology of the endothelium. *British Journal of Anaesthesia*. 93(1):105–113.

Gannon, M., Ray, M.K., Van Zee, K., Rausa, F., Costa, R.H. & Wright, C. V. 2000. Persistent expression of HNF6 in islet endocrine cells causes disrupted islet architecture and loss of beta cell function. *Development* (Cambridge, England). 127(13):2883–95.

Gao, X., Belmadani, S., Picchi, A., Xu, X., Potter, B.J., Tewari-Singh, N., Capobianco, S., Chilian, W.M. & Zhang, C. 2007. Tumor necrosis factor-a induces endothelial dysfunction in Leprdb mice. Circulation. 115(2):245.

García-Pérez, L.-E., Alvarez, M., Dilla, T., Gil-Guillén, V. & Orozco-Beltrán, D. 2013. Adherence to therapies in patients with type 2 diabetes. *Diabetes Therapy*. 4(2):175–94.

Gerhardt, H., Golding, M., Fruttiger, M., Ruhrberg, C., Lundkvist, A., Abramsson, A., Jeltsch, M., Mitchell, C., Alitalo, K., Shima, D. & Betsholtz, C. 2003. VEGF guides angiogenic sprouting utilizing endothelial tip cell filopodia. *The Journal of Cell Biology*. 161(6):1163–77.

Gerber, H.P., Hillan, K.J., Ryan, A.M., Kowalski, J., Keller, G.A., Rangell, L., Wright, B.D., Radtke, F., Aguet, M. & Ferrara, N. 1999. VEGF is required for growth and survival in neonatal mice. *Development*, *126*(6): 1149-1159.

Ghitescu, L. & Robert, M. 2002. Diversity in unity: the biochemical composition of the endothelial cell surface varies between the vascular beds. *Microscopy research and technique*. 57(5):381-389.

Ghosh, A., Gao, L., Thakur, A., Siu, P.M. & Lai, C.W.K. 2017. Role of free fatty acids in endothelial dysfunction. *Journal of Biomedical Science*. 24(1):50.

Giugliano, D., Ceriello, A. & Paolisso, G. 1996. Oxidative stress and diabetic vascular complications. *Diabetes Care*. 19(3):257–267.

Gökçinar-Yagci, B., Uçkan-Çetinkaya, D. & Çelebi-Saltik, B. 2015. Pericytes: properties, functions and applications in tissue engineering. *Stem Cell Reviews and Reports*. 11(4):549–559.

Goodner, C.J., Ensinck, J.W., Chideckel, E., Palmer, J., Koerker, D.J., Ruch, W. & Gale, C. 1974. Somatostatin, a hypothalamic inhibitor of endocrine pancreas. In vol. 53. *Journal of Clinical Investigation: Diabetes Therapy*. 4(2):175-194.

Gorden, D.L., Mandriota, S.J., Montesano, R., Orci, L. & Pepper, M.S. 1997. Vascular endothelial growth factor is increased in devascularized rat islets of Langerhans *in vitro*1. *Transplantation*. 63(3):436–443.

Gray, H., 1989. Gray's anatomy/edited by Peter L. Williams, 37th ed. C. Livingstone, Edinburgh. Page numbers

Gregersen, S., Thomsen, J.L., Brock, B. & Hermansen, K. 1996. Endothelin-1 stimulates insulin secretion by direct action on the islets of Langerhans in mice. *Diabetologia*. 39(9):1030–5.

Groulx, J.-F., Gagné, D., Benoit, Y.D., Martel, D., Basora, N. & Beaulieu, J.-F. 2011. Collagen VI is a basement membrane component that regulates epithelial cell–fibronectin interactions. *Matrix Biology*. 30(3):195–206.

Guerreiro LH, Da Silva D, Sola-Penna M, Mizurini DM & Lima LMTR (2013) Amylin induces hypoglycemia in mice. *Anais da Adademia Brasileira de Ciencias*. 85(1): 349–354.

Gullo, L., Pezzilli, R., Morselli-Labate, A.M. & Group, the I.P.C.S. 1994. Diabetes and the risk of pancreatic cancer. *New England Journal of Medicine*. 331(2):81–84.

Gustafsson, A.J. & Islam, M.S. 2007. Islet of Langerhans: cellular structure and physiology. In: Ahsan N (ed) Chronic allograft failure: natural history, pathogenesis, diagnosis and management. *Landes Bioscience, Austin*, pp 229–232.

Guzik, T.J., Mussa, S., Gastaldi, D., Sadowski, J., Ratnatunga, C., Pillai, R. & Channon, K.M. 2002. Mechanisms of increased vascular superoxide production in human diabetes mellitus: role of NAD(P)H oxidase and endothelial nitric oxide synthase. *Circulation*. 105(14):1656–62.

Hamburg, N.M., Mott, M.M., Bigornia, S.J., Duess, M.A., Kluge, M.A., Hess, D.T., Apovian, C.M., Vita, J.A. & Gokce, N. 2010. Maladaptive enlargement of the brachial artery in severe obesity is reversed with weight loss. *Vascular Medicine*. 15(3):215-222.

Harrison, R. V., Harel, N., Panesar, J. & Mount, R.J. 2002. Blood capillary distribution correlates with haemodynamic-based functional imaging in cerebral cortex. *Cerebral Cortex*. 12(3):225–233.

Hart, N.J., Aramandla, R., Poffenberger, G., Fayolle, C., Thames, A.H., Bautista, A., Spigelman, A.F., Babon, J.A.B., DeNicola, M.E., Dadi, P.K. & Bush, W.S. 2018. Cystic fibrosis–related diabetes is caused by islet loss and inflammation. *American Society for Clinical Investigation Reference Information*. 3(8). Page numbers

Hauge-Evans, A.C., King, A.J., Carmignac, D., Richardson, C.C., Robinson, I.C., Low, M.J., Christie, M.R., Persaud, & S.J. Jones, P.M. 2009. Somatostatin secreted by islet delta-cells fulfils multiple roles as a paracrine regulator of islet function. *Diabetes*. 58(2):403–411.

He, S., Zhao, T., Guo, H., Meng, Y., Qin, G., Goukassian, D.A., Han, J., Gao, X. and Zhu, Y., 2016. Coordinated activation of VEGF/VEGFR-2 and PPARδ pathways by a multi-component Chinese medicine DHI accelerated recovery from peripheral arterial disease in type 2 diabetic mice. *PloS one*, 11(12), p.e0167305.

Heitzer, T., Finckh, B., Albers, S., Krohn, K., Kohlschütter, A. & Meinertz, T. 2001. Beneficial effects of alpha-lipoic acid and ascorbic acid on endothelium-dependent, nitric oxide-mediated vasodilation in diabetic patients: relation to parameters of oxidative stress. *Free Radical Biology and Medicine*. 31(1):53–61

Hellerstrom, C. and Hellman, B. 1961. The blood circulation in the islets of Langerhans visualized by the fluorescent dye vasoflavine. Studies in normal and obese-hyperglycemic mice. *Acta Societatis Medicorum Upsaliensis.* 66:88.

Henderson, J.R. & Moss, M.C. 1985. A morphometric study of the endocrine and exocrine capillaries of the pancreas. *Quarterly Journal of Experimental Physiology* (Cambridge, England). 70(3):347–356.

Heo, K.-S., Fujiwara, K. & Abe, J. 2014. Shear stress and atherosclerosis. *Molecules and Cells*. 37(6):435–40.

Herold, K.C., Gitelman, S., Greenbaum, C., Puck, J., Hagopian, W., Gottlieb, P., Sayre, P., Bianchine, P., Wong, E., Seyfert-Margolis, V., Bourcier, K. & Bluestone, J.A., 2009. Treatment of patients with new onset Type 1 diabetes with a single course of anti-CD3 mAb teplizumab preserves insulin production for up to 5 years. *Clinical Immunology*. 132(2):166–173.

Hidalgo, M., 2010. Pancreatic cancer. *New England Journal of Medicine.* 362(17):1605-1617.

Himanen, J.-P. & Nikolov, D.B. 2003. Eph signaling: a structural view. *Trends in Neurosciences*. 26(1):46–51

Hirschi, K.K., Ingram, D.A. & Yoder, M.C. 2008. Assessing identity, phenotype, and fate of endothelial progenitor cells. *Arteriosclerosis Thrombosis, and Vascular Biology*. 28(9):1584–1595.

Hogan MF & Hull RL (2017) The islet endothelial cell: a novel contributor to beta cell secretory dysfunction in diabetes. *Diabetologia*. 60(6):952–959.

Holash, J., Maisonpierre, P.C., Compton, D., Boland, P., Alexander, C.R., Zagzag, D., Yancopoulos, G.D. & Wiegand, S.J. 1999. Vessel cooption, regression, and growth in tumors mediated by angiopoietins and VEGF. *Science* (New York, N.Y.). 284(5422):1994–8.

Homo-Delarche, F., Calderari, S., Irminger, J.C., Gangnerau, M.N., Coulaud, J., Rickenbach, K., Dolz, M., Halban, P., Portha, B. & Serradas, P. 2006. Islet inflammation and fibrosis in a spontaneous model of type 2 diabetes. the GK rat. *Diabetes*. 55(6):1625-1633.

Hong, W.X., Hu, M.S., Esquivel, M., Liang, G.Y., Rennert, R.C., McArdle, A., Paik, K.J., Duscher, D., Gurtner, G.C., Lorenz, H.P. & Longaker, M.T. 2014. The role of hypoxia-inducible factor in wound healing. *Advances in Wound Care*. 3(5):390–399.

Hossler, F.E. & Douglas, J.E. 2001 Vascular corrosion casting: review of advantages and limitations in the application of some simple quantitative methods. *Microscopy and Microanalysis*. 7(03):253–264.

Hossler, F.E. & Monson, F.C. 1998 Structure and blood supply of intrinsic lymph nodes in the wall of the rabbit urinary bladder—studies with light microscopy, electron microscopy, and vascular corrosion casting. *The Anatomical Record*. 252(3):477–484.

Huang, A. & Vita, J. 2006. Effects of systemic inflammation on endothelium-dependent vasodilation. *Trends in Cardiovascular Medicine*. 16(1):15–20.

Hull, R.L., Kodama, K., Utzschneider, K.M., Carr, D.B., Prigeon, R.L. & Kahn, S.E. 2005. Dietary-fat-induced obesity in mice results in beta cell hyperplasia but not increased insulin release: evidence for specificity of impaired beta cell adaptation. *Diabetologia*. 48(7):1350-1358.

Huo, Y. & Kassab, G.S. 2012. Intraspecific scaling laws of vascular trees. *Journal of the Royal Society Interface*. 9(66): 190-200.

Ibukuro, K. 2001. Vascular anatomy of the pancreas and clinical applications. *International Journal of Gastrointestinal Cancer*. 30(1-2): 87-104.

Ikeda, U., Ikeda. M., Oohara, T., Kano, S. & Yaginuma. T. 1990. Mitogenic action of interleukin-1 alpha on vascular smooth muscle cells mediated by PDGF. *Artherosclerosis* 84(2–3): 183–8.

In't Veld, P. & Lammert, E. 2015. The dark side of islet vasculature. *Diabetologia*. 58(1):4–6.

In't Veld, P. & Marichal, M. 2010. Microscopic anatomy of the human islet of Langerhans. *Advances in Experimental Medicine and Biology*. 654:1-19.

In't Veld, P. & Smeets, S. 2015. Microscopic anatomy of the human islet of langerhans. In: *Dordrecht: Springer Netherlands Islets of Langerhans*. 19–38.

Inoguchi, T., Battan, R., Handler, E., Sportsman, J.R., Heath, W. & King, G.L. 1992. Preferential elevation of protein kinase C isoform beta II and diacylglycerol levels in the aorta and heart of diabetic rats: differential reversibility to glycemic control by islet cell transplantation. *Proceedings of the National Academy of Sciences*. 89(22):11059–11063.

Irving-Rodgers, H.F., Ziolkowski, A.F., Parish, C.R., Sado, Y., Ninomiya, Y., Simeonovic, C.J. & Rodgers, R.J. 2008. Molecular composition of the peri-islet basement membrane in NOD mice: A barrier against destructive insulitis. *Diabetologia*. 51(9):1680–1688.

Ishikawa, M., Stokes, K.Y., Zhang, J.H., Nanda, A. & Granger, D.N. 2004. Cerebral microvascular responses to hypercholesterolemia: roles of NADPH oxidase and P-selectin. *Circulation Research*. 94(2):239-244.

Islam, M.S. 2010. The islets of Langerhans. Preface. Advances In: *Experimental Medicine and Biology*. 654:8.

Itani, S.I., Ruderman, N.B., Schmieder, F. & Boden, G. 2002. Lipid-induced insulin resistance in human muscle is associated with changes in diacylglycerol, protein kinase C, and Ikappa B-alpha. *Diabetes*. 51(7):2005–11.

Ito, H., Rovira, I.I., Bloom, M.L., Takeda, K., Ferrans, V.J., Quyyumi, A.A. & Finkel, T. 1999. Endothelial progenitor cells as putative targets for angiostatin. *Cancer Research*. 59(23):5875–7.

Iwanishi, M. & Kobayashi, M. 1993. Effect of pioglitazone on insulin receptors of skeletal muscles from high-fat-fed rats. *Metabolism*. 42(8):1017-1021.

Jabs, N., Franklin, I., Brenner, M., Gromada, J., Ferrara, N., Wollheim, C. & Lammert, E. 2008. Reduced Insulin Secretion and Content in VEGF-A Deficient Mouse Pancreatic Islets. *Experimental and Clinical Endocrinology & Diabetes*. 116(S 01):S46–S49.

Jacob, M., Chappell, D. & Becker, B.F. 2016. Regulation of blood flow and volume exchange across the microcirculation. *Critical Care* (London, England). 20(1):319.

Jacob, M.P. 2003 Extracellular matrix remodeling and matrix metalloproteinases in the vascular wall during aging and in pathological conditions. *Biomedicine & Pharmacotherapy*. 57(5–6): 195–202.

Jackson, K.A., Majka, S.M., Wang, H., Pocius, J., Hartley, C.J., Majesky, M.W., Entman, M.L., Michael, L.H., Hirschi, K.K. & Goodell, M.A. 2001. Regeneration of ischemic cardiac muscle and vascular endothelium by adult stem cells. *The Journal of Clinical Investigation*. 107(11):1395-1402.

Jain, R. & Lammert, E. 2009. Cell–cell interactions in the endocrine pancreas. *Diabetes, Obesity and Metabolism*. 11(s4):159–167.

Jansson, L., Barbu, A., Bodin, B., Drott, C.J., Espes, D., Gao, X., Grapensparr, L., Källskog, Ö, Lau, J., Liljebäck, H., Palm, F., Quach, M., Sandberg, M., Strömberg, V., Ullsten, S. & Carlsson, P.O. 2016. Pancreatic islet blood flow and its measurement. *Upsala Journal of Medical Sciences*. 121(2):81–95.

Jansson, L. & Sandler, S. 1985. Pancreatic islet circulation in relation to the diabetogenic action of streptozotocin in the rat. *Endocrinology*. 116(3):896-900.

Jaques, F., Jousset, H., Tomas, A., Prost, A.-L., Wollheim, C.B., Irminger, J.-C., Demaurex, N. & Halban, P.A. 2008. Dual effect of cell-cell contact disruption on cytosolic calcium and insulin secretion. *Endocrinology*. 149(5):2494–2505.

Järvisalo, M.J., Jartti, L., Näntö-Salonen, K., Irjala, K., Rönnemaa, T., Hartiala, J.J., Celermajer, D.S. & Raitakari, O.T. 2001. Increased aortic intima-media thickness: a marker of preclinical atherosclerosis in high-risk children. *Circulation*. 104(24):2943–7.

Jennings, R.E., Berry, A.A., Strutt, J.P., Gerrard, D.T. & Hanley, N.A. 2015. Human pancreas development. *Company of Biologists* Ltd, 3126–3137.

Jiang, F.X., Naselli, G. & Harrison, L.C. 2002. Distinct distribution of laminin and its integrin receptors in the pancreas. *Journal of the Histochemistry Society*. 50(12):1625–1632.

Jiménez, B., Volpert, V., Crawford, S.E., Febbraio, M., Silverstein, R.L. & Bouck, N. 2000. Signals leading to apoptosis-dependent inhibition of neovascularization by thrombospondin-1. *Nature Medicine*. 6(1):41–48.

Jin, Z.W., Yu, H.C., Cho, B.H., Kim, H.T., Kimura, W., Fujimiya, M. & Murakami, G. 2010. Fetal topographical anatomy of the pancreatic head and duodenum with special reference to courses of the pancreaticoduodenal arteries. *Yonsei Medical Journal*. 51(3):398–406.

Johansson, M., Mattsson, G., Andersson, A., Jansson, L. & Carlsson, P.-O. 2006. Islet endothelial cells and pancreatic β-cell proliferation: studies *in vitro* and during pregnancy in adult rats. *Endocrinology*. 147(5):2315–2324.

Johnson, J.D. 2016. The quest to make fully functional human pancreatic beta cells from embryonic stem cells: climbing a mountain in the clouds. Diabetologia. 59(10):2047–2057.

Johnson-Léger, C., Aurrand-Lions, M. & Imhof, B. 2000. The parting of the endothelium: miracle, or simply a junctional affair? *Journal of Cell Science.* 113(6):921–933.

Junaid, T.O., Bradley, R.S., Lewis, R.M., Aplin, J.D. & Johnstone, E.D. 2017. Whole organ vascular casting and microCT examination of the human placental vascular tree reveals novel alterations associated with pregnancy disease. *Scientific Reports*. 7(1): 1-10.

Jung, J., Zheng, M., Goldfarb, M. & Zaret, K.S. 1999. Initiation of mammalian liver development from endoderm by fibroblast growth factors. *Science*. 284(5422): 1998-2003.

Kahn, M.B., Yuldasheva, N.Y., Cubbon, R.M., Smith, J., Rashid, S.T., Viswambharan, H., Imrie, H., Abbas, A., Rajwani, A., Aziz, A. & Baliga, V. 2011. Insulin resistance impairs circulating angiogenic progenitor cell function and delays endothelial regeneration. *Diabetes*. 60(4):1295-1303.

Källskog, Ö. & Jansson, L. 2011. Autoregulation of islet graft blood flow follows the implantation. *Journal of Surgical Research*. 171(2):865–870.

Källskog, Ö., Kampf, C., Andersson, A., Carlsson, P.-O., Hansell, P., Johansson, M. & Jansson, L. 2006. Lymphatic vessels in pancreatic islets implanted under the renal capsule of rats. *American Journal of Transplantation*. 6(4):680–686.

Kappus, R.M., Fahs, C.A., Smith, D., Horn, G.P., Agiovlasitis, S., Rossow, L., Jae, S.Y., Heffernan, K.S. & Fernhall, B. 2014. Obesity and overweight associated with increased carotid

diameter and decreased arterial function in young otherwise healthy men. *American Journal of Hypertension*. 27(4):628-634.

Kars, M., Yang, L., Gregor, M.F., Mohammed, B.S., Pietka, T.A., Finck, B.N., Patterson, B.W., Horton, J.D., Mittendorfer, B., Hotamisligil, G.S. & Klein, S. 2010. Tauroursodeoxycholic Acid may improve liver and muscle but not adipose tissue insulin sensitivity in obese men and women. *Diabetes*. 59(8):1899–905.

Kawai, K. & Rouiller, D. 1981. Evidence that the islet interstitium contains functionally separate “arterial” and “venous” compartments. *Diabetes*. 30(Supplement 1):14A.

Kawamori, D., Kurpad, A.J., Hu, J., Liew, C.W., Shih, J.L., Ford, E.L., Herrera, P.L., Polonsky, K.S., McGuinness, O.P. & Kulkarni, R.N. 2009. Insulin signaling in alpha cells modulates glucagon secretion *in vivo*. *Cell Metabolism*. 9(4):350–61.

Keaney, J.F., Massaro, J.M., Larson, M.G., Vasan, R.S., Wilson, P.W.., Lipinska, I., Corey, D., Sutherland, P., Vita, J.A. & Benjamin, E.J. 2004. Heritability and correlates of intercellular adhesion molecule-1 in the Framingham Offspring Study. *Journal of the American College of Cardiology*. 44(1):168–173.

Keenan, H.A., Sun, J.K., Levine, J., Doria, A., Aiello, L.P., Eisenbarth, G., Bonner-Weir, S. & King, G.L. 2010. Residual insulin production and pancreatic ß-cell turnover after 50 years of diabetes: Joslin Medalist Study. *Diabetes*. 59(11):2846–53.

Keighron, C., Lyons, C.J., Creane, M., O’Brien. T & Liew A. 2018. Recent advances in endothelial progenitor cells toward their use in clinical translation. *Frontiers in Medicine.* 5:354.

Kelly, C, McClenaghan, N.H. & Flatt, P.R. 2011. Role of islet structure and cellular interactions in the control of insulin secretion. *Islets*. 3(2):41–47.

Keelan, J., Chung, E.M. & Hague, J.P. 2016. Simulated annealing approach to vascular structure with application to the coronary arteries. *Royal Society Open Science*. 3(2):150431.

Kibria, G., Heath, D., Smith, P. & Biggar, R. 1980. Pulmonary endothelial pavement patterns. *Thorax*. 35(3):186-191.

Kilimnik, G., Jo, J., Periwal, V., Zielinski, M.C. & Hara, M. 2012. Quantification of islet size and architecture. *Islets*. 4(2):167-172.

Kim, A., Miller, K., Jo, J., Kilimnik, G., Wojcik, P. & Hara, M. 2009. Islet architecture: a comparative study. *Islets*. 1(2):129–136.

Kim, F., Gallis, B. & Corson, M.A. 2001. TNF-α inhibits flow and insulin signaling leading to NO production in aortic endothelial cells. *American Journal of Physiology-Cell Physiology*. 280(5):C1057–C1065.

Kim, J-A, Wei, Y. & Sowers, J.R. 2008 Role of mitochondrial dysfunction in insulin resistance.*Circulation Research* 102(4):401–14.

King, A.J.F. 2012. The use of animal models in diabetes research. *British Journal of Pharmacology*. 166(3):877–894.

King, R.H. 2001. The role of glycation in the pathogenesis of diabetic polyneuropathy. *Molecular Pathology*. 54(6):400–8.

Klover, P.J., Clementi, A.H. & Mooney, R.A. 2005. Interleukin-6 depletion selectively improves hepatic insulin action in obesity. *Endocrinology*. 146(8):3417-3427.

Korpos, É., Kadri, N., Kappelhoff, R., Wegner, J., Overall, C.M., Weber, E., Holmberg, D., Cardell, S., & Sorokin, L. 2013. The peri-islet basement membrane, a barrier to infiltrating leukocytes in type 1 diabetes in mouse and human. *Diabetes*. 62(2):531–542.

Korsgren, E. & Korsgren, O. 2016. An apparent deficiency of lymphatic capillaries in the islets of Langerhans in the human pancreas. *Diabetes*. 65(4):1004–1008.

Kourembanas, S., Marsden, P.A., McQuillan, L.P. & Faller, D. V. 1991. Hypoxia induces endothelin gene expression and secretion in cultured human endothelium. *Journal of Clinical Investigation*. 88(3):1054–1057.

Kouroedov, A., Eto, M., Joch, H., Volpe, M., Lüscher, T.F. & Cosentino, F. 2004. Selective inhibition of protein kinase c 2 prevents acute effects of high glucose on vascular cell adhesion molecule-1 expression in human endothelial cells. *Circulation*. 110(1):91–96.

Kragl, M. & Lammert, E. 2010. Basement membrane in pancreatic islet function. In Springer *The Islets of Langerhans*. pp. 217–234.

Krucker, T., Lang, A. & Meyer, E.P. 2006. New polyurethane-based material for vascular corrosion casting with improved physical and imaging characteristics. *Microscopy Research and Technique*. 69(2):138–147.

Kugelmeier, P., Nett, P.C., Züllig, R., Lehmann, R., Weber, M. & Moritz, W. 2008. Expression and hypoxic regulation of the endothelin system in endocrine cells of human and rat pancreatic islets. *JOP : Journal of the Pancreas*. 9(2):133–49.

Kuiper, E.J., Zijderveld, R. van, Roestenberg, P., Lyons, K.M., Goldschmeding, R., Klaassen, I., Noorden, C.J.F. Van & Schlingemann, R.O. 2008. Connective tissue growth factor is necessary for retinal capillary basal lamina thickening in diabetic mice. *Journal of Histochemistry & Cytochemistry*. 56(8):785–792.

Kulkarni, R.N., Brüning, J.C., Winnay, J.N., Postic, C., Magnuson, M.A. & Kahn, C.R. 1999. Tissue-specific knockout of the insulin receptor in pancreatic beta cells creates an insulin secretory defect similar to that in type 2 diabetes. *Cell*. 96(3):329–39.

Kulenović, A. & Sarač-Hadžihalilović, A. 2010. Blood vessels distribution in body and tail of pancreas-a comparative study of age-related variation. *Bosnian Journal of Basic Medical Sciences.* 10(2):89–93.

Kumar, G.P.S., Arulselvan, P., Kumar, D.S. & Subramanian, S.P. 2006. Anti-Diabetic Activity of Fruits of Terminalia chebula on Streptozotocin Induced Diabetic Rats. *Journal of Health Science*. 52(3):283–291.

Kunnen, S.J., Malas, T.B., Semeins, C.M., Bakker, A.D. & Peters, D.J.M. 2018. Comprehensive transcriptome analysis of fluid shear stress altered gene expression in renal epithelial cells. *Journal of Cellular Physiology*. 233(4):3615–3628.

Kuroda, M., Oka, T., Oka, Y., Yamochi, T., Ohtsubo, K., Mori, S., Watanabe, T., Machinami, R., & Ohnishi, S. 1995. Colocalization of vascular endothelial growth factor (vascular permeability factor) and insulin in pancreatic islet cells. *The Journal of Clinical Endocrinology and Metabolism*. 80(11):3196–3200.

Kuschnerus, K., Landmesser, U. & Kränkel, N. 2015. Vascular repair strategies in type 2 diabetes: novel insights. *Cardiovascular Diagnosis and Therapy*. 5(5):374–86.

Kusuyama, T., Omura, T., Nishiya, D., Enomoto, S., Matsumoto, R., Takeuchi, K., Yoshikawa, J. & Yoshiyama, M. 2006. Effects of treatment for diabetes mellitus on circulating vascular progenitor cells. *Journal of Pharmacological Sciences*. 102(1):96-102.

Kuzu I, Bicknell R, Harris AL, Jones M, Gatter KC & Mason DY. 1992. Heterogeneity of vascular endothelial cells with relevance to diagnosis of vascular tumours. *Journal of Clinical Pathology*.45(2):143-8

Kwon, N.S., Lee, S.H., Choi, C.S., Kho, T. & Lee, H.S. 1994. Nitric oxide generation from streptozotocin. *The Federation American Societies for Experimental Biology Journal*. 8(8):529–533.

Lacraz, G., Giroix, M.-H., Kassis, N., Coulaud, J., Galinier, A., Noll, C., Cornut, M., Schmidlin, F., Paul, J-L., Janel, N., Irminger, J-C., Kergoat, M., Portha, B., Donath, M.Y., Ehses, J.A. & Homo-Delarche, F. 2009. Islet endothelial activation and oxidative stress gene expression are reduced by il-1ra treatment in the type 2 Diabetic GK Rat. *Public Library of Science*. 4(9):e6963.

Lai, A.K.W. & Lo, A.C.Y. 2013. Animal models of diabetic retinopathy: summary and comparison. *Journal of Diabetes Research*. 2013.

Lai, E.Y., Jansson, L., Patzak, A. & Persson, A.E. 2007. Vascular reactivity in arterioles from normal and alloxan-diabetic mice: studies on single perfused islets. *Diabetes*. 56(1):107–112.

Lai, E.Y., Persson, A.E.G., Bodin, B., Källskog, Ö. Andersson, A., Pettersson, U., Hansell, P. & Jansson, L. 2007. Endothelin-1 and pancreatic islet vasculature: studies *in vivo* and on isolated, vascularly perfused pancreatic islets. *American Journal of Physiology-Endocrinology and Metabolism*. 292(6):E1616–E1623.

Lametschwandtner, A., Lametschwandtner, U., Weiger, T. 1990. Scanning electronmicroscopy of vascular corrosion casts—technique and applications: Updated review. *Scanning Microscopy*. 4(4):889–941.

Lammers, W. 2015. Normal and abnormal electrical propagation in the small intestine. *Acta Physiologica*. 213(2):349–359.

Lammert, E., Cleaver, O. & Melton, D. 2001. Induction of pancreatic differentiation by signals from blood vessels. *Science* (New York, N.Y.). 294(5542):564–567.

Lammert, E., Gu, G., McLaughlin, M., Brown, D., Brekken, R., Murtaugh, L.C., Gerber, H.-P., Ferrara, N., & Melton, D.A. 2003. Role of VEGF-A in vascularization of pancreatic islets. *Current Biology*. 13(12):1070–1074.

Lazorthes, G., Espagno, J., Lazorthes, Y. & Zadeh, J.O. 1968. The vascular architecture of the cortex and the cortical blood flow. In: *Progress in Brain Research* 30:27-32.

Le May, C., Chu, K., Hu, M., Ortega, CS., Simpson, E.R., Korach, K.S., Tsai, M-J. & Mauvais-Jarvis, F. 2006. Estrogens protect pancreatic beta-cells from apoptosis and prevent insulin-deficient diabetes mellitus in mice. Proceedings of the National Academy of Sciences of the United States of America. *National Academy of Sciences*. 103(24):9232–7.

Leasher, J.L., Bourne, R.R.A., Flaxman, S.R., Jonas, J.B., Keeffe, J., Naidoo, K., Pesudovs, K., Price, H., White, R.A., Wong, T.Y., Resnikoff, S, Taylor, H.R. & Vision, Loss Expert Group of the Global Burden of Disease Study. 2016. Global estimates on the number of people blind or visually impaired by diabetic retinopathy: A Meta-analysis from 1990 to 2010. *Diabetes Care*. 39(9):1643–1649.

Lee, J., Lee, S., Zhang, H., Hill, M.A., Zhang, C. & Park, Y. 2017. Interaction of IL-6 and TNF-α contributes to endothelial dysfunction in type 2 diabetic mouse hearts. *Public Library of Science* (1). 12(11):e0187189.

Lee, P.S.S. & Poh, K.K. 2014. Endothelial progenitor cells in cardiovascular diseases. *World Journal of Stem Cells*. 6(3):355–66.

Lee, S.W., Song, K.E., Shin, D.S., Ahn, S.M., Ha, E.S., Kim, D.J., Nam, M.S. & Lee, K.-W. 2005. Alterations in peripheral blood levels of TIMP-1, MMP-2, and MMP-9 in patients with type-2 diabetes. *Diabetes Research and Clinical Practice*. 69(2):175–179.

Lenzen, S. 2008. The mechanisms of alloxan-and streptozotocin-induced diabetes. *Diabetologia*. 51(2):216-226.

Lesmana, C.R.A., Gani, R.A. & Lesmana, L.A. 2018. Non-alcoholic fatty pancreas disease as a risk factor for pancreatic cancer based on endoscopic ultrasound examination among pancreatic cancer patients: A single-center experience. *Journal of Gastroenterology and Hepatology*. 2(1):4–7.

Leventhal, C., Rafii, S., Rafii, D., Shahar, A. & Goldman, S.A.1999. Endothelial trophic support of neuronal production and recruitment from the adult mammalian subependyma. *Molecular and Cellular Neuroscience*. 13(6):450–464.

Li, F.-F., Chen, B.-J., Li, W., Li, L., Zha, M., Zhou, S., Bachem, M.G. & Sun, Z.-L. 2016. Islet stellate cells isolated from fibrotic islet of Goto-Kakizaki rats affect biological behavior of beta-cell. *Journal of Diabetes Research*. Vol 2016:1-9.

Li, H., Li, H., Bao, Y., Zhang, X. & Yu, Y. 2011. Free fatty acids induce endothelial dysfunction and activate protein kinase C and nuclear factor-κB pathway in rat aorta. *International Journal of Cardiology*. 152(2):218–224.

Li, X., Zhang, L., Meshinchi, S., Dias-Leme, C., Raffin, D., Johnson, J.D., Treutelaar, M.K. & Burant, C.F. 2006. Islet microvasculature in islet hyperplasia and failure in a model of type 2 diabetes. *Diabetes*. 55(11):2965–73.

Li, W., Yu, G., Liu, Y. & Sha, L. 2019. Intrapancreatic ganglia and neural regulation of pancreatic endocrine secretion. *Frontiers in Neuroscience*. 13:21.

Liao, Y., Chen, L.-L., Zeng, T., Li, Y., Fan Yu, Hu, L. & Ling Yue. 2010. Number of circulating endothelial progenitor cells as a marker of vascular endothelial function for type 2 diabetes. *Vascular Medicine*. 15(4):279–285.

Lin, G., Finger, E. & Gutierrez-Ramos, J.C. 1995. Expression of CD34 in endothelial cells, hematopoietic progenitors and nervous cells in fetal and adult mouse tissues. *European Journal of Immunology*. 25(6):1508–1516.

Ling, L., Shen, Y., Wang, K., Jiang, C., Fang, C., Ferro, A., Kang, L. & Xu, B. 2012. Worse clinical outcomes in acute myocardial infarction patients with type 2 diabetes mellitus: relevance to impaired endothelial progenitor cells mobilization. *Public Library of Science* (1). 7(11):e50739.

Linnemann, A.K., Baan, M. & Davis, D.B. 2014. Pancreatic β-Cell Proliferation in Obesity1,2. *Advances in Nutrition*. 5(3):278–288.

Litwak, K.N., Cefalu, W.T. & Wagner, J.D. 1998 Streptozotocin-induced diabetes mellitus in cynomolgus monkeys: changes in carbohydrate metabolism, skin glycation, and pancreatic islets. Comparative Medicine. *American Association for Laboratory Animal Science*. 48(2): 172–178.

Liu, M.T. & Kirchgessner, A.L. 1997. Guinea pig pancreatic neurons: morphology, neurochemistry, electrical properties, and response to 5-HT. *American Journal of Physiology-Gastrointestinal and Liver Physiology*. 273(6):G1273-G1289.

Liu, X.F., Yu, J.Q., Dalan, R., Liu, A.Q. & Luo, K.Q. 2014. Biological factors in plasma from diabetes mellitus patients enhance hyperglycaemia and pulsatile shear stress-induced endothelial cell apoptosis. *Integrative Biology*. 6(5):511.

Liu, Y.-A., Chung, Y.-C., Shen, M.-Y., Pan, S.-T., Kuo, C.-W., Peng, S.-J., Pasricha, P.J. & Tang, S.-C. 2015. Perivascular interstitial cells of Cajal in human colon. *Cellular and Molecular Gastroenterology and Hepatology*. 1(1):102–119.

Longnecker, D.S., 2014. Anatomy and Histology of the Pancreas. *Pancreapedia: The Exocrine Pancreas Knowledge Ba*se. DOI: 10.3998/panc.2014.3

Loomans, C.J., de Koning, E.J., Staal, F.J., Rookmaaker, M.B., Verseyden, C., de Boer, H.C.,

Verhaar, M.C., Braam, B., Rabelink, T.J. & van Zonneveld, A.J. 2004. Endothelial progenitor cell dysfunction: a novel concept in the pathogenesis of vascular complications of type 1 diabetes. *Diabetes*. 53(1):195–9.

Lotfipour, S. & Smith, M.T. 2018. Morphine hyposensitivity in streptozotocin-diabetic rats: Reversal by dietary l -arginine treatment. *Clinical and Experimental Pharmacology and Physiology*. 45(1): 42–49.

Lou, J., Triponez, F., Oberholzer, J., Wang, H., Yu, D., Buhler, L., Cretin, N., Mentha, G., Wollheim, C.B. & Morel, P. 1999. Expression of -1 proteinase inhibitor in human islet microvascular endothelial cells. *Diabetes*. 48 page numbers.

Love, J.A. & Szebeni, K. 1999. Morphology and histochemistry of the rabbit pancreatic innervation. *Pancreas*. 18(1):53-64.

Lozano, I., Van der Werf, R., Bietiger, W., Seyfritz, E., Peronet, C., Pinget, M., Jeandidier, N., Maillard, E., Marchioni, E., Sigrist, S. and Dal, S. 2016. High-fructose and high-fat diet-induced disorders in rats: impact on diabetes risk, hepatic and vascular complications. *Nutrition & Metabolism*. 13(1):15.

Lüscher, T.F. & Barton, M. 2000. Endothelins and endothelin receptor antagonists: therapeutic considerations for a novel class of cardiovascular drugs. *Circulation*. 102(19):2434–40.

Mahmoud, A.M., Ashour, M.B., Abdel-Moneim, A. & Ahmed, O.M. 2012. Hesperidin and naringin attenuate hyperglycaemia-mediated oxidative stress and proinflammatory cytokine production in high fat fed/streptozotocin-induced type 2 diabetic rats. *Journal of Diabetes and its Complications*. 26(6):483–490.

Mai, J., Virtue, A., Shen, J., Wang, H. & Yang, X.-F. 2013. An evolving new paradigm: endothelial cells-conditional innate immune cells. *Journal of Hematology & Oncology*. 6:61.

Majno, G., Shea, S.M., & Leventhal, M. 1969. Endothelial contraction induced by histamine-type mediators: an electron microscopic study. *The Journal of Cell Biology*. 42(3):647–72.

Makurina, G.I. 2016. Vascular endothelium activation mechanisms study in patients with psoriasis and essential hypertension. *Zaporozhye Medical Journal*. (1):19-24.

Mandriota, S.J., Jussila, L., Jeltsch, M., Compagni, A., Baetens, D., Prevo, R., Banerji, S., Huarte, J., Montesano, R., Jackson, D.G., Orci, L., Alitalo, K., Christofori, G. & Pepper, M.S.

2001. Vascular endothelial growth factor-C-mediated lymphangiogenesis promotes tumour metastasis. *The European Molecular Biology Organization Journa*l. 20(4):672–682.

Mann, E. & Bellin, M.D., 2016. Secretion of insulin in response to diet and hormones. Pancreapedia: *The Exocrine Pancreas Knowledge Ba*se. DOI: 10.3998/panc.2016.3

Manyema, M., Veerman, J.L., Chola, L., Tugendhaft, A., Labadarios, D. & Hofman, K. 2015. Decreasing the burden of type 2 diabetes in South Africa: the impact of taxing sugar-sweetened beverages. *Public Library of Science* (1). 10(11):e0143050.

Marichal, M. 2010. Microscopic anatomy of the human islet of Langerhans. In: *The Islets of Langerhans*. 1–19. Springer

Marín, O., Valiente, M., Ge, X. & Tsai, L.-H. 2010. Guiding neuronal cell migrations. *Cold Spring Harbor Perspectives in Biology*. 2(2):a001834.

Marletta, M.A. 1993. Nitric oxide synthase structure and mechanism. *The Journal of Biological Chemistry*. 268(17):12231–4.

Martin-Orti, R., Stefanov, M., Gaspar, I, Martin, R. & Martin-Alguacil, N. 1999 Effect of anticoagulation and lavage prior to casting of postmortem material with MercoxR and BatsonR 17. *Journal of Microscopy*. 195(2):150–160.

Matsumoto, K., Yoshitomi, H., Rossant, J. & Zaret, K.S. 2001. Liver organogenesis promoted by endothelial cells prior to vascular function. *Science*. 294(5542):559-563.

Mattsson, G. 2004. The Endothelial Cells in Islets of Langerhans. *Upsala Journal of Medical Sciences*. 109:1–16.

Mattsson, G., Danielsson, A., Kriz, V., Carlsson, P.-O. & Jansson, L. 2006. Endothelial cells in endogenous and transplanted pancreatic islets: Differences in the expression of angiogenic peptides and receptors. *Pancreatology*. 6(1–2):86–95.

Mattsson, G., Jansson, L., Nordin, A., Andersson, A. & Carlsson, P.-O. 2004. Evidence of functional impairment of syngeneically transplanted mouse pancreatic islets retrieved from the liver. *Diabetes*. 53(4):948–954.

Mbanya, J.C.N., Motala, A.A., Sobngwi, E., Assah, F.K. & Enoru, S.T. 2010. Diabetes in sub-Saharan Africa. *The Lancet*. 375(9733):2254–2266.

McClung, J.A., Naseer, N., Saleem, M., Rossi, G.P., Weiss, M.B., Abraham, N.G. & Kappas, A. 2005. Circulating endothelial cells are elevated in patients with type 2 diabetes mellitus independently of HbA1c. *Diabetologia*. 48(2):345–350.

McDuffie, R.H., Struck, L. & Burshell, A. 2001. Empowerment for diabetes management: integrating true self-management into the medical treatment and management of diabetes mellitus. *The Ochsner Journal.* 3(3):149–57.

Meda, P. 2013. Protein-mediated interactions of pancreatic islet cells. *Scientifica*. 2013:621249.

Meier, J.J., Butler, A.E., Saisho, Y., Monchamp, T., Galasso, R., Bhushan, A., Rizza, R.A. & Butler, P.C. 2008. Beta-cell replication is the primary mechanism subserving the postnatal expansion of beta-cell mass in humans. *Diabetes*. 57(6):1584–94.

Meigs, J.B., Hu, F.B., Rifai, N. & Manson, J.E. 2004. Biomarkers of endothelial dysfunction and risk of type 2 diabetes mellitus. *Journal of the American Medical Association*. 291(16): 1978-1986

Meigs, J.B., O'Donnell, C.J., Tofler, G.H., Benjamin, E.J., Fox, C.S., Lipinska, I., Nathan, D.M., Sullivan, L.M., D'Agostino, R.B. & Wilson, P.W.F. 2006. Hemostatic markers of endothelial dysfunction and risk of incident type 2 diabetes: the Framingham Offspring Study. *Diabetes*. 55(2):530–7.

Menger, M.D., Vajkoczy, P., Leiderer, R., Jäger, S. & Messmer, K. 1992. Influence of experimental hyperglycemia on microvascular blood perfusion of pancreatic islet isografts. *The Journal of Clinical Investigation*. 90(4):1361–9.

Menon, P.& Fisher, E.A. 2015. Immunostaining of macrophages, endothelial cells, and smooth muscle cells in the atherosclerotic mouse aorta. *Methods in Molecular Biology NIH Public Access* 1339: 131–48.

Mezza, T., Cinti, F., Cefalo, C.M.A., Pontecorvi, A., Kulkarni, R.N. & Giaccari, A. 2019. β-cell fate in human insulin resistance and type 2 diabetes: A Perspective on Islet Plasticity. *Diabetes*. 68(6):1121–1129.

Michiels, C. 2003. Endothelial cell functions. Journal of Cellular Physiology. 196(3):430–443.

Mittal, N., Zhou, Y., Ung, S., Linares, C., Molloi, S. & Kassab, G.S. 2005. A computer reconstruction of the entire coronary arterial tree based on detailed morphometric data. *Annals of Biomedical Engineering*. 33(8):.1015-1026.

Mizutani, M., Kern, T.S. & Lorenzi, M. 1996. Accelerated death of retinal microvascular cells in human and experimental diabetic retinopathy. *The Journal of Clinical Investigation*. 97(12):2883–90.

Montagnani, M., Chen, H., Barr, V.A. & Quon, M.J. 2001. Insulin-stimulated activation of eNOS is independent of Ca 2+ but requires phosphorylation by Akt at Ser 1179. *Journal of Biological Chemistry*. 276(32):30392–30398.

Monti, L.D., Barlassina, C., Citterio, L., Galluccio, E., Berzuini, C., Setola, E., Valsecchi, G., Lucotti, P., Pozza. G., Bernardinelli, L., Casari, G. & Piatti, P. 2003. Endothelial nitric oxide synthase polymorphisms are associated with type 2 diabetes and the insulin resistance syndrome. *Diabetes*. 52(5):1270–5.

Mooradian, A.D. 1988. Diabetic complications of the central nervous system. *Endocrine Reviews*. 9(3):346–356.

Moore, K.L., Dalley, A.F. & Agur, A.M. 2013. Clinically Oriented Anatomy. Lippincott Williams & Wilkins.

Morikawa, S., Baluk, P., Kaidoh, T., Haskell, A., Jain, R.K. & McDonald, D.M. 2002. Abnormalities in pericytes on blood vessels and endothelial sprouts in tumors. *The American Journal of Pathology*. 160(3):985–1000.

Morino, K., Petersen, K.F. & Shulman, G.I. 2006. Molecular mechanisms of insulin resistance in humans and their potential links with mitochondrial dysfunction. *Diabetes*. 55(Supplement 2):S9–S15.

Muniyappa, R. & Sowers, J.R. 2013. Role of insulin resistance in endothelial dysfunction. *Reviews in Endocrine & Metabolic Disorders*. 14(1):5–12.

Muniyappa, R., Hall, G., Kolodziej, T.L., Karne, R.J., Crandon, S.K. & Quon, M.J. 2008. Cocoa consumption for 2 wk enhances insulin-mediated vasodilatation without improving blood pressure or insulin resistance in essential hypertension. *The American Journal of Clinical Nutrition*. 88(6):1685–96.

Munzel, T., Daiber, A., Ullrich, V. & Mülsch, A. 2005. Vascular Consequences of Endothelial Nitric Oxide Synthase Uncoupling for the Activity and Expression of the Soluble Guanylyl Cyclase and the cGMP-Dependent Protein Kinase. *Arteriosclerosis, Thrombosis, and Vascular Biology*. 25(8):1551–1557.

Murakami, T., Fujita, T., Miyake, T., Ohtsuka, A., Taguchi, T. & Kikuta, A. 1993. The insulo-acinar portal and insulo-venous drainage systems in the pancreas of the mouse, dog, monkey and certain other animals: a scanning electron microscopic study of corrosion casts. *Archives of Histology and Cytology*. 56(2):127–47.

Murakami, T., Fujita, T., Taguchi, T., Nonaka, Y. & Orita, K. 1992. The blood vascular bed of the human pancreas, with special reference to the insulo-acinar portal system. Scanning electron microscopy of corrosion casts. *Archives of Histology and Cytology*. 55(4):381–95.

Murphy, J.D., Christman-Skieller, C., Kim, J., Dieterich, S., Chang, D.T. & Koong, A.C. 2010. A dosimetric model of duodenal toxicity after stereotactic body radiotherapy for pancreatic cancer. *International Journal of Radiation Oncology* Biology* Physics 78*(5):1420-1426.

Mutin, M., Canavy, I., Blann, A., Bory, M., Sampol, J. & Dignat-George, F. 1999. Direct evidence of endothelial injury in acute myocardial infarction and unstable angina by demonstration of circulating endothelial cells. *Blood*. 93(9):2951–8.

Narayanan, S., Loganathan, G., Dhanasekaran, M., Tucker, W., Patel, A., Subhashree, V., Mokshagundam, S., Hughes, M.G., Williams, S.K. & Balamurugan, A.N. 2017. Intra-islet endothelial cell and β-cell crosstalk: Implication for islet cell transplantation. *World Journal of Transplantation*. 7(2):117–128.

Nasri, H. & Rafieian-Kopaei, M. 2014. Metformin: current knowledge. *Journal of Research In Medical Sciences:* 19(7):658.

Nathan, D.M., Cleary, P.A., Backlund, J.Y., Genuth, S.M., Lachin, J.M., Orchard, T.J., Raskin, P., Zinman, B., & Group, D.C. 2005. Intensive diabetes treatment and cardiovascular disease in patients with type 1 diabetes. *The New England Journal of Medicine*. 353(25):2643–2653.

Navarro-González, J.F. & Mora-Fernández, C. 2008. The role of inflammatory cytokines in diabetic nephropathy. *Journal of the American Society of Nephrology*. 19(3):433–442.

Nebuloni, L., Kuhn, G.A., Vogel, J. & Müller, R. 2014. A novel in vivo vascular imaging approach for hierarchical quantification of vasculature using contrast enhanced Micro-Computed Tomography. *Public Library of Science* (1): e86562.

Nemtsova, V., Bilovol, O. & Shalimova, A. 2019. Vascular endothelial growth factor as a marker of endothelial dysfunction in poly- and comorbidity: focus on hypertension, type 2 diabetes mellitus and subclinical hypothyroidism. *Arterial Hypertension.* 23(2):98–104.

Nerem, R.M., Levesque, M.J. & Cornhill, J.F. 1981. Vascular endothelial morphology as an indicator of the pattern of blood flow. *Journal of Biomechanical Engineering*. 103(3):172–6.

Nikolova, G., Jabs, N., Konstantinova, I., Domogatskaya, A., Tryggvason, K., Sorokin, L., Fässler, R., Gu, G., Gerber, H-P., Ferrara, N., Melton, D.A. & Lammert, E. 2006. The vascular basement membrane: a niche for insulin gene expression and β cell proliferation. *Developmental Cell*. 10(3):397–405.

Nikolova, G., Strilic, B. & Lammert, E. 2007. The vascular niche and its basement membrane. *Trends in Cell Biology*. 17(1):19–25.

Nishizuka, Y. 1984. The role of protein kinase C in cell surface signal transduction and tumour promotion. *Nature*. 308(5961):693–698.

Nisoli, E., Clementi, E., Paolucci, C., Cozzi, V., Tonello, C., Sciorati, C., Bracale, R., Valerio, A., Francolini, M., Moncada, S. & Carruba, M.O. 2003. Mitochondrial biogenesis in mammals: the role of endogenous nitric oxide. *Science*. 299(5608):896–899.

Nomura, S. 2009. Dynamic role of microparticles in type 2 diabetes mellitus. *Current Diabetes Reviews*. 5(4):245–51.

Nyman, L.R., Ford, E., Powers, A.C. & Piston, D.W. 2010. Glucose-dependent blood flow dynamics in murine pancreatic islets *in vivo*. *American Journal of Physiology, Endocrinology and Metabolism*. 298(4):E807-14.

Nyman, L.R., Wells, K.S., Head, W.S., McCaughey, M., Ford, E., Brissova, M., Piston, D.W. & Powers, A.C. 2008. Real-time, multidimensional *in vivo* imaging used to investigate blood flow in mouse pancreatic islets. *The Journal of Clinical Investigation.* 118(11):3790-3797.

O'Leary, D.H., Polak, J.F., Kronmal, R.A., Kittner, S.J., Bond, M.G., Wolfson, S.K., Bommer, W., Price, T.R., Gardin, J.M. & Savage, P.J. 1992. Distribution and correlates of sonographically detected carotid artery disease in the Cardiovascular Health Study. The CHS Collaborative Research Group. *Stroke*. 23(12):1752–60.

O'Morchoe, C.C.C. 1997. Lymphatic system of the pancreas. *Microscopy Research and Technique*. 37(5–6):456–477.

Ohtani, O. 1987. Three-dimensional organization of the connective tissue fibers of the human pancreas: a scanning electron microscopic study of NAOH treated-tissues. *Archives of Histology and Cytology*. 50(5):557–566.

Olerud, J., Johansson, M., Lawler, J., Welsh, N. & Carlsson, P.O. 2008. Improved vascular engraftment and graft function after inhibition of the angiostatic factor thrombospondin-1 in mouse pancreatic islets. *Diabetes*. 57(7):1870–1877.

Olerud, J., Mokhtari, D., Johansson, M., Christoffersson, G., Lawler, J., Welsh, N. & Carlsson, P.O. 2011. Thrombospondin-1: an islet endothelial cell signal of importance for beta-cell function. *Diabetes*. 60(7):1946–1954.

Olsson, R. & Carlsson, P.-O. 2006. The pancreatic islet endothelial cell: emerging roles in islet function and disease. T*he International Journal of Biochemistry and Cell Biology*. 38(5–6):710–4.

Olsson, R. & Carlsson, P.-O. 2011. A low-oxygenated subpopulation of pancreatic islets constitutes a functional reserve of endocrine cells. *Diabetes*. 60(8):2068–75.

Omodanisi, E.I., Aboua, Y.G., Chegou, N.N. & Oguntibeju, O.O. 2017. Hepatoprotective, antihyperlipidemic, and anti-inflammatory activity of moringa oleifera in diabetic-induced damage in male Wistar rats. *Pharmacognosy Research*. 9(2):182–187.

Orci, L. & Unger, R. 1975. Functional subdivision of islets of Langerhans and possible role of D cells. *The Lancet*. 306(7947):1243-1244.

Orci, L., Malaisse-Lagae, F., Ravazzola, M., Rouiller, D., Renold, A.E., Perrelet, A. & Unger, R. 1975. A morphological basis for intercellular communication between alpha- and beta-cells in the endocrine pancreas. *Journal of Clinical Investigation.* 56(4):1066–1070.

Otani, K., Kulkarni, R.N., Baldwin, A.C., Krutzfeldt, J., Ueki, K., Stoffel, M., Kahn, C.R. & Polonsky, K.S. 2004. Reduced beta-cell mass and altered glucose sensing impair insulin-secretory function in betaIRKO mice. *American Journal of Physiology, Endocrinology and Metabolism*. 286(1):E41-9.

Otonkoski, T., Banerjee, M., Korsgren, O., Thornell, L. & Virtanen, I. 2008. Unique basement membrane structure of human pancreatic islets: implications for β-cell growth and differentiation. *Diabetes, Obesity and Metabolism*. 10(s4):119–127.

Paardekooper, L.M., van Vroonhoven. E., ter Beest. M. & van. den, Bogaart, G. 2019 Radical

stress is more cytotoxic in the nucleus than in other organelles. *International Journal of Molecular Sciences*. 20(17): 4147.

Pace, C.S. & Tarvin, J.T. 1981. Somatostatin: mechanism of action in pancreatic islet beta-cells. *Diabetes*. 30(10):836–42.

Pacini, G., Omar, B. & Ahrén, B. 2013. Methods and models for metabolic assessment in mice. *Journal of Diabetes Researc*h. https://doi.org/10.1155/2013/986906

Palombo, C., Kozakova, M., Morizzo, C., Gnesi, L., Barsotti, M.C., Spontoni, P., Massart, F., Salvi, P., Balbarini, A., Saggese, G. & Di Stefano, R. 2011. Circulating endothelial progenitor cells and large artery structure and function in young subjects with uncomplicated Type 1 Diabetes. *Cardiovascular Diabetology*. 10(1):88.

Papazafiropoulou, A. & Tentolouris, N. 2009. Matrix metalloproteinases and cardiovascular diseases. *Hippokratia*. 13(2):76–82.

Pasricha, P.J. 2012. Unraveling the mystery of pain in chronic pancreatitis. *Nature Reviews Gastroenterology & Hepatology*. 9(3):140.

Pasyk, K.A, & Jakobczak, B.A. 2004 Vascular endothelium: recent advances. *European Journal of Dermatology*. 14(4): 209–13.

Pechhold, K., Patterson, N.B., Blum, C., Fleischacker, C.L., Boehm, B.O. & Harlan, D.M. 2001. Low dose streptozotocin-induced diabetes in rat insulin promoter-mCD80-transgenic mice is T cell autoantigen-specific and CD28 dependent. *Journal of Immunology* (Baltimore, Md. : 1950). 166(4):2531–9.

Peer, N., Kengne, A.-P., Motala, A.A. & Mbanya, J.C. 2014. Diabetes in the Africa region: An update. *Diabetes Research and Clinical Practice*. 103(2):197–205.

Peichev, M., Naiyer, A.J., Pereira, D., Zhu, Z., Lane, W.J., Williams, M., Oz, M.C., Hicklin, D.J., Witte, L., Moore, M.A. & Rafii, S. 2000. Expression of VEGFR-2 and AC133 by circulating human CD34 (+) cells identifies a population of functional endothelial precursors. *Blood*. 95(3):952–8.

Peri, G., Veralli, E. & Trivellini, G., 1969. Vascularization of the pancreas. *Archivio Italiano di Chirurgia*. 95(2), p.287.

Petersen, K.F., Dufour, S., Savage, D.B., Bilz, S., Solomon, G., Yonemitsu, S., Cline, G.W., Befroy, D., Zemany, L., Kahn, B.B. & Papademetris, X. 2007. The role of skeletal muscle

insulin resistance in the pathogenesis of the metabolic syndrome. *Proceedings of the National Academy of Sciences*. 104(31):12587–12594.

Pheiffer, C., Pillay-van Wyk, V., Joubert, J.D., Levitt, N., Nglazi, M.D. & Bradshaw, D. 2018. The prevalence of type 2 diabetes in South Africa: a systematic review protocol. *British Medical Journal Publishing Group* 8(7):e021029.

Phng, L.-K., Stanchi, F., Gerhardt, H. & Fishman, M.C. 2013. Filopodia are dispensable for endothelial tip cell guidance. *Development* (Cambridge, England). 140(19):4031–40.

Piconi, L., Quagliaro, L., Assaloni, R., Da Ros, R., Maier, A., Zuodar, G. & Ceriello, A. 2006. Constant and intermittent high glucose enhances endothelial cell apoptosis through mitochondrial superoxide overproduction. *Diabetes / Metabolism Research and Reviews*. 22(3):198–203.

Pober, J.S. & Min, W., 2006. Endothelial cell dysfunction, injury and death. In: *The Vascular Endothelium II*. Springer, Berlin, Heidelberg. 135-156.

Popov, D. & Simionescu, M. 2006. Cellular mechanisms and signalling pathways activated by high glucose and AGE-albumin in the aortic endothelium. *Archives of Physiology and Biochemistry*. 112(4–5):265–273.

Postnov, D.D., Marsh, D.J., Postnov, D.E., Braunstein, T.H., Holstein-Rathlou, N.H., Martens, E.A. & Sosnovtseva, O. 2016. Modeling of kidney hemodynamics: probability-based topology of an arterial network. *PLoS Computational Biology*. 12(7):e1004922.

Pries, A.R., Reglin, B. & Secomb, T.W., 2005. Remodeling of blood vessels: responses of diameter and wall thickness to hemodynamic and metabolic stimuli. *Hypertension*. 46(4):725-731.

Prokopi, M., Pula, G., Mayr, U., Devue, C., Gallagher, J., Xiao, Q., Boulanger, C.M., Westwood, N., Urbich, C., Willeit, J., Steiner, M. Breuss, J., Xu, Q., Kiechl, S. & Mayr, M. 2009. Proteomic analysis reveals presence of platelet microparticles in endothelial progenitor cell cultures. *Blood*. 114(3):723–732.

Qu, D., Liu, J., Lau, C.W. & Huang, Y. 2014. IL-6 in diabetes and cardiovascular complications. *British Journal of Pharmacology*. 171(15): 3595–603.

Quintero, M., Colombo, S.L., Godfrey, A. & Moncada, S. 2006. Mitochondria as signaling organelles in the vascular endothelium. *Proceedings of the National Academy of Sciences of the United States of America*. 103(14):5379–84.

R&D Systems Luminex High Performance Assays 2017. https://www.rndsystems.com /products/Luminex-high-performance-assays.

Rafii, S. & Lyden, D. 2003. Therapeutic stem and progenitor cell transplantation for organ vascularization and regeneration. *Nature Medicine*. 9(6):702–712.

Rahier, J., Guiot, Y., Goebbels, R.M., Sempoux, C. & Henquin, J.C. 2008. Pancreatic β-cell mass in European subjects with type 2 diabetes. *Diabetes, Obesity and Metabolism*. 10(s4):32–42.

Rajendran, P., Rengarajan, T., Thangavel, J., Nishigaki, Y., Sakthisekaran, D., Sethi, G. & Nishigaki, I. 2013. The vascular endothelium and human diseases. *International Journal of Biological Sciences*. 9(10):1057–1069.

(Range et al., 1963)

Ranjan, A.K., Joglekar, M.V. & Hardikar, A. 2009. Endothelial cells in pancreatic islet development and function. *Islets*. 1(1):2–9.

Rask-Madsen, C. & King, G.L. 2005. Proatherosclerotic mechanisms involving protein kinase c in diabetes and insulin resistance. *Arteriosclerosis, Thrombosis, and Vascular Biology*. 25(3):487–496.

Read, M.A., Whitley, M.Z., Williams, A.J. & Collins, T. 1994. NF-kappa B and I kappa B alpha: an inducible regulatory system in endothelial activation. *The Journal of Experimental Medicine*. 179(2):503–12.

Reed, M.J., Meszaros, K., Entes, L.J., Claypool, M.D., Pinkett, J.G., Gadbois, T.M. & Reaven, G.M. 2000. A new rat model of type 2 diabetes: the fat-fed, streptozotocin-treated rat. *Metabolism-Clinical and Experimental*. 49(11):1390–1394.

Reidy, K., Kang, H.M., Hostetter, T. & Susztak, K. 2014 Molecular mechanisms of diabetic kidney disease. *The Journal of Clinical Investigation. American Society for Clinical Investigation*. 124(6): 2333–40.

Reitsma, S., Slaaf, D.W., Vink, H., van Zandvoort, M.A.M.J. & Oude Egbrink, M.G.A. 2007. The endothelial glycocalyx: composition, functions, and visualization. *Pflügers Archiv-European Journal of Physiology*. 454(3):345–359.

Rennert, R.C., Sorkin, M., Garg, R.K. & Gurtner, G.C. 2012. Stem cell recruitment after injury: lessons for regenerative medicine. *Regenerative Medicine*. 7(6):833–850.

Resnick, N., Collins, T., Atkinson, W., Bonthron, D.T., Dewey, C.F. & Gimbrone, M.A. 1993. Platelet-derived growth factor B chain promoter contains a cis-acting fluid shear-stress-responsive element. *Proceedings of the National Academy of Sciences of the United States of America*. 90(10):4591–5.

Rizzoni, D., Agabiti-Rosei, C. & Agabiti-Rosei, E. 2017. Hemodynamic consequences of changes in microvascular structure. *American Journal of Hypertension*. 30(10):939–946.

Roberts, F.R., Hupple, C., Norowski, E., Walsh, N.C., Przewozniak, N., Aryee, K.-E., Van Dessel, F.M., Jurczyk, A., Harlan, D.M., Greiner, D.L., Bortell, R. & Yang C. 2017. Possible type 1 diabetes risk prediction: Using ultrasound imaging to assess pancreas inflammation in the inducible autoimmune diabetes BBDR model. *Public Library of Science* (1). 12(6):e0178641.

Roberts, W.G. & Palade, G.E. 1995. Increased microvascular permeability and endothelial fenestration induced by vascular endothelial growth factor. *Journal of Cell Science*. 108 (Pt 6):2369–79.

Rodriguez-Diaz, R., Abdulreda, M.H., Formoso, A.L., Gans, I., Ricordi, C., Berggren, P.-O. & Caicedo, A. 2011. Innervation patterns of autonomic axons in the human endocrine pancreas. *Cell Metabolism*. 14(1):45–54.

Rossi, R., Cioni, E., Nuzzo, A., Origliani, G. & Modena, M.G. 2005. Endothelial-dependent vasodilation and incidence of type 2 diabetes in a population of healthy postmenopausal women. *Diabetes Care*. 28(3):702–7.

Rossi, J., Santamäki, P., Airaksinen, M.S. & Herzig, K.H. 2005. Parasympathetic innervation and function of endocrine pancreas requires the glial cell line–derived factor family receptor α2 (GFRα2). *Diabetes*. 54(5): 1324-1330.

Rousseau, A., Ayoubi, F., Deveaux, C., Charbit, B., Delmau, C., Christin-Maitre, S., Jaillon, P., Uzan, G. and Simon, T. 2010. Impact of age and gender interaction on circulating endothelial progenitor cells in healthy subjects. *Fertility and Sterility*. 93(3):843–846.

Roy, S., Ha, J., Trudeau, K. & Beglova, E. 2010. Vascular basement membrane thickening in diabetic retinopathy. *Current Eye Research*. 35(12):1045–1056.

Roy, S., Trudeau, K., Roy, S., Behl, Y., Dhar, S. & Chronopoulos, A. 2010. New insights into hyperglycaemia-induced molecular changes in microvascular cells. *Journal of Dental Research*. 89(2):116–127.

Rubbia-Brandt, L., Terris, B., Giostra, E., Dousset, B., Morel, P. & Pepper, M.S. 2004. Lymphatic vessel density and vascular endothelial growth factor-c expression correlate with malignant behavior in human pancreatic endocrine tumors. *Clinical Cancer Research*. 10(20):6919–6928.

Ryan, E.A., Lakey, J.R.T., Rajotte, R. V., Korbutt, G.S., Kin, T., Imes, S., Rabinovitch, A., Elliott, J.F., Warnock, G.L., Larsen, I. & Shapiro, A.M.J. 2001. Clinical outcomes and insulin secretion after islet transplantation with the Edmonton protocol. *Diabetes*. 50(4):710–719.

Salie, R., Huisamen, B. & Lochner, A. 2014. High carbohydrate and high fat diets protect the heart against ischaemia/reperfusion injury. *Cardiovascular Diabetology*. 13:108–109.

Sabry, D. & Olfat Noh, M.S. 2016. Comparative evaluation for potential differentiation of endothelial progenitor cells and mesenchymal stem cells into endothelial-like cells. *International Journal of Stem Cells*. 9(1):44.

Samols, E. & Stagner, J.I. 1988. Intra-islet regulation. *The American Journal of Medicine*. 85(5):31–35.

Samols, E. & Stagner, J.I. 1990. Islet somatostatin--microvascular, paracrine, and pulsatile regulation. *Metabolism: Clinical and Experimental*. 39(9 Supplement 2):55–60.

Samols, E. 1972. Glucagon-insulin interrelationships. Glucagon. Molecular physiology, clinical and therapeutic implications.151-172. Pergamon Press.

Samols, E., Marri, G. & Marks, V. 1966. Interrelationship of glucagon, insulin and glucose. The insulinogenic effect of glucagon. *Diabetes*. 15(12):855–866.

Samols, E., Tyler, J.M. & Kajinuma, H. 1970. August. Influence of the sulfonamides on pancreatic humoral secretion and evidence for an insulin-glucagon feedback system. In: *Proceedings Seventh International Diabetes Federation Congress*. Excerpta Medica Berlin, Heidelberg. pp636-655

Samols, E., Tyler, J.M., Marks, V. & Mialhe, P. 1969. The physiological role of glucagon in different species. *Proc. III International Congress Endocrinol. Mexico, Progress in Endocrinol. ICS*. 184:206–219.

Sandoo, A., van Zanten, J.J.C.S.V., Metsios, G.S., Carroll, D. & Kitas, G.D. 2010. The endothelium and its role in regulating vascular tone. *The Open Cardiovascular Medicine Journal*. 4:302–12.

Sanlioglu, A.D., Altunbas, H.A., Balci, M.K., Griffith, T.S. & Sanlioglu, S. 2013. Clinical utility of insulin and insulin analogs. *Islets*. 5(2):67–78.

Satomi, J., Mount, R.J., Toporsian, M., Paterson, A.D., Wallace, M.C., Harrison, R.V. & Letarte, M. 2003. Cerebral vascular abnormalities in a murine model of hereditary hemorrhagic telangiectasia. *Stroke*. 34(3):783–9.

Savari, O., Zielinski, M.C., Wang, X., Misawa, R., Millis, J.M., Witkowski, P. & Hara, M. 2013. Distinct function of the head region of human pancreas in the pathogenesis of diabetes. *Islets*. 5(5):226–228.

Scharpfenecker, M., Fiedler, U., Reiss, Y. & Augustin, H.G. 2005. The Tie-2 ligand Angiopoietin-2 destabilizes quiescent endothelium through an internal autocrine loop mechanism. *Journal of Cell Science*. 118(4):771–780.

Schatten, H. 2012. *Scanning Electron Microscopy for the Life Sciences*. Cambridge University Press.

Schrader, L.I., Kinzenbaw, D.A., Johnson, A.W., Faraci, F.M. & Didion, S.P. 2007. IL-6 deficiency protects against angiotensin II induced endothelial dysfunction and hypertrophy. *Arteriosclerosis, Thrombosis, and Vascular Biology.* 27(12):2576–81.

Schram, M.T., Henry, R.M., van Dijk, R.A., Kostense, P.J., Dekker, J.M., Nijpels, G., Heine, R.J., Bouter, L.M., Westerhof, N. & Stehouwer, C.D. 2004. Increased central artery stiffness in impaired glucose metabolism and type 2 diabetes: the Hoorn Study. *Hypertension.* 43(2):176–81.

Schwartz, T.W., Holst, J.J., Fahrenkrug, J., Jensen, S.L., Nielsen, O.V., Rehfeld, J.F., De Muckadell, O.S. & Stadil, F. 1978. Vagal, cholinergic regulation of pancreatic polypeptide secretion. *The Journal of Clinical Investigation*. 61(3):781-789.

Secomb, T.W. 2016. Haemodynamics. *Comprehensive Physiology*. 6(2):975.

Semrock.com 2018. Flow Cytometry-Semrock. https://www.semrock.com/flow-cytometry.aspx

Sengupta, A., Yuldasheva, N., Gage, M., Viswambharan, H., Aziz, A., Ali, N., Galloway, S., Mercer, B., Kearney, M. & Cubbon, R. 2014. Role of vascular endothelial insulin sensitisation in vascular repair in systemic insulin resistance. *The Lancet*. 383:S97.

Sergi, D., Naumovski, N., Heilbronn, L.K., Abeywardena, M., O'Callaghan, N., Lionetti. L & Luscombe-Marsh, N. 2019. Mitochondrial (Dys)function and insulin resistance: from pathophysiological molecular mechanisms to the impact of diet. *Frontiers in Physiology.* 10:532.

Sha, L., Ou, L.L., Miller, S.M., Ma, R. & Szurszewski, J.H. 1996. Cat pancreatic neurons: morphology, electrophysiological properties, and responses to 5-HT. *Pancreas*. 13(2): 111-124.

Sha, L., Miller, S.M., & Szurszewski, J.H. 1995. Nitric oxide is a neuromodulator in cat pancreatic ganglia: histochemical and electrophysiological study. *Neuroscience letters. 192*(2): 77-80.

Shah, P., Lueschen, N., Ardestani, A., Oberholzer, J., Olerud, J., Carlsson, P.-O. & Maedler, K. 2016. Angiopoietin-2 signals do not mediate the hypervascularization of islets in type 2 diabetes. *Public Library of Science* (1). 11(9):e0161834.

Shah, V.N. & Garg, S.K. 2015. Managing diabetes in the digital age. *Clinical Diabetes and Endocrinology*. 1(1):16.

Shantsila, E., Watson, T. & Lip, G.Y.H. 2007. Endothelial progenitor cells in cardiovascular disorders. *Journal of the American College of Cardiology*. 49(7):741–752.

Shao, J., Iwashita, N., Ikeda, F., Ogihara, T., Uchida, T., Shimizu, T., Uchino, H., Hirose, T., Kawamori, R. & Watada, H. 2006. Beneficial effects of candesartan, an angiotensin II type 1 receptor blocker, on β-cell function and morphology in DB/db mice. *Biochemical and Biophysical Research Communications*. 344(4):1224–1233.

Shaul, P.W., Smart, E.J., Robinson, L.J., German, Z., Yuhanna, I.S., Ying, Y., Anderson, R.G. & Michel, T. 1996. Acylation targets endothelial nitric-oxide synthase to plasmalemma caveolae. *The Journal of Biological Chemistry*. 271(11):6518–22.

Shoelson, S.E., Lee, J. & Goldfine, A.B. 2006. Inflammation and insulin resistance. *Journal of Clinical Investigation*. 116(7):1793–1801.

Sibal, L., Aldibbiat, A., Agarwal, S.C., Mitchell, G., Oates, C., Razvi, S., Weaver, J.U., Shaw, J.A. & Home, P.D. 2009. Circulating endothelial progenitor cells, endothelial function, carotid intima-media thickness and circulating markers of endothelial dysfunction in people with type 1 diabetes without macrovascular disease or microalbuminuria. *Diabetologia*. 52(8):1464–1473.

Silver, A.E. & Vita, J.A., 2006. Shear stress-mediated arterial remodeling in atherosclerosis: Too much of a good thing? *Circulation*. 113 (24):2787-2789

Simionescu, M., Popov, D., Sima, A., Hasu, M., Costache, G., Faitar, S., Vulpanovici, A., Stancu, C., Stern, D. & Simionescu, N. 1996. Pathobiochemistry of combined diabetes and atherosclerosis studied on a novel animal model: The hyperlipemic-hyperglycemic hamster. *American Journal of Pathology.* 148(3):997–1014.

Simionescu, N., Simionescu, M. & Palade, G.E. 1981. Differentiated microdomains on the luminal surface of the capillary endothelium. I. Preferential distribution of anionic sites. *The Journal of Cell Biology*. 90(3):605–613.

Singh, H., Bishen, K.A., Garg, D., Sukhija, H., Sharma, D. and Tomar, U. 2019 Fixation and Fixatives: Roles and Functions—A Short Review. *Dental Journal of Advance Studies*. 07(02):051–055.

Skeie, J.M., Aldrich, B.T., Goldstein, A.S., Schmidt, G.A., Reed, C.R. and Greiner, M.A. 2018. Proteomic analysis of corneal endothelial cell-descemet membrane tissues reveals influence of insulin dependence and disease severity in type 2 diabetes mellitus. *PLoS One*. 13(3):p.e0192287.

Skovsø, S. 2014. Modeling type 2 diabetes in rats using high-fat diet and streptozotocin. *Journal of Diabetes Investigation*. 5(4):349–358.

Slavin, B.G., Zarow, C., Warden, C.H. & Fisler, J.S. 2010. Histological, immunocytochemical, and morphometrical analyses of pancreatic islets in the bsb mouse model of obesity. *The Anatomical Record: Advances in Integrative Anatomy and Evolutionary Biology*. 293(1):108–116.

Sowers, J.R., Epstein, M. & Frohlich, E.D. 2001. Diabetes, hypertension, and cardiovascular disease: an update. *Hypertension* (Dallas, Tex. : 1979). 37(4):1053–9.

Spinelli, F.R., Metere, A., Barbati, C., Pierdominici, M., Iannuccelli, C., Lucchino, B., Ciciarello, F., Agati, L., Valesini, G. & Di Franco, M. 2013. Effect of therapeutic inhibition of TNF on circulating endothelial progenitor cells in patients with rheumatoid arthritis. *Mediators of Inflammation*. 2013:1–8.

Sprague, A.H. & Khalil, R.A. 2009. Inflammatory cytokines in vascular dysfunction and vascular disease. *Biochemical Pharmacology*. 8(6):539–52.

Squires, P.E., Hauge-Evans, A.C., Persaud, S.J. & Jones, P.M. 2000 Synchronization of Ca2+-signals within insulin-secreting pseudo islets: Effects of gap-junctional uncouplers. *Cell Calcium*. 27(5):287–296.

Srinivasan, K., Patole, P.S., Kaul, C.L. & Ramarao, P. 2004. Reversal of glucose intolerance by pioglitazone in high fat diet-fed rats. *Methods and Findings in Experimental and Clinical Pharmacology*. 26(5):327.

Srinivasan, K., Viswanad, B., Asrat, L., Kaul, C.L. & Ramarao, P. 2005. Combination of high-fat diet-fed and low-dose streptozotocin-treated rat: A model for type 2 diabetes and pharmacological screening. *Pharmacological Research*. 52(4):313–320.

Stagner, J.I. & Samols, E. 1986. Retrograde perfusion as a model for testing the relative effects of glucose versus insulin on the A cell. *The Journal of Clinical Investigation*. 77(3):1034–1037.

Stagner, J.I., Samols, E. & Marks, V. 1989. The anterograde and retrograde infusion of glucagon antibodies suggests that A cells are vascularly perfused before D cells within the rat islet. *Diabetologia*. 32(3):203–6.

Steiner, D.J., Kim, A., Miller, K. & Hara, M. 2010. Pancreatic islet plasticity: Interspecies comparison of islet architecture and composition. *Islets*. 2(3):135–145.

Stendahl, J.C., Kaufman, D.B. & Stupp, S.I. 2009. Extracellular matrix in pancreatic islets: relevance to scaffold design and transplantation. *Cell Transplantation*. 18(1):1–12.

Stitt, A.W., Curtis, T.M., Chen, M., Medina, R.J., McKay, G.J., Jenkins, A., Gardiner, T.A., Lyons, T.J., Hammes, H.P., Simo, R. & Lois, N. 2016. The progress in understanding and treatment of diabetic retinopathy. *Progress in Retinal and Eye Research*. 51:156–186.

Stitt, A.W., Li, Y.M., Gardiner, T.A., Bucala, R., Archer, D.B. & Vlassara, H. 1997. Advanced glycation end products (AGEs) co-localize with AGE receptors in the retinal vasculature of diabetic and of AGE-infused rats. *The American Journal of Pathology*. 150(2):523–31.

Stocker, R. & Keaney, J.F. 2004. Role of Oxidative modifications in atherosclerosis. *Physiological Reviews*. 84(4):1381–1478.

Stokes, R.A., Cheng, K., Lalwani, A., Swarbrick, M.M., Thomas, H.E., Loudovaris, T., Kay, T.W., Hawthorne, W.J., O'Connell, P.J. & Gunton, J.E. 2017. Transplantation sites for human and murine islets. *Diabetologia*. 60(10):1961–1971.

Storlien, L.H., James, D.E., Burleigh, K.M., Chisholm, D.J. & Kraegen, E.W. 1986. Fat feeding causes widespread *in vivo* insulin resistance, decreased energy expenditure, and obesity in rats. A*merican Journal of Physiology-Endocrinology and Metabolism*. 251(5):E576–E583.

Strell, C. & Entschladen, F. 2008. Extravasation of leukocytes in comparison to tumor cells. *Cell Communication and Signaling*. 6(1):10.

Su, D., Zhang, N., He, J., Qu, S., Slusher, S., Bottino, R., Bertera, S., Bromberg, J., Bromberg, J. & Dong, H.H. 2007. Angiopoietin-1 production in islets improves islet engraftment and protects islets from cytokine-induced apoptosis. *Diabetes*. 56(9):2274–2283.

Suckale, J. & Solimena, M. 2008. Pancreas islets in metabolic signaling-focus on the beta-cell. *Frontiers in Bioscience*.13:7156–7171.

Suh, J.H. & Miner, J.H. 2013. The glomerular basement membrane as a barrier to albumin. Nature reviews. *Nephrology*. 9(8):470–7.

Sumagin, R., Brown, C.W., Sarelius, I.H. and King, M.R., 2008. Microvascular endothelial cells exhibit optimal aspect ratio for minimizing flow resistance. *Annals of Biomedical Engineering*. 36(4):580-585.

Sung, C.P., Arleth, A.J., Storer, B.L. & Ohlstein, E.H. 1994. Angiotensin type 1 receptors mediate smooth muscle proliferation and endothelin biosynthesis in rat vascular smooth muscle. *The Journal of Pharmacology and Experimental Therapeutics.* 271(1):429–37.

Surat, P. 2019. *Flow Cytometry Methodology, Uses, and Data Analysis*, https://www.news-medical.net/life-sciences/Flow-Cytometry-Methodology-Uses-and-Data-Analysis.aspx.

Suto, K., Yamazaki, Y., Morita, T. & Mizuno, H. 2005. Crystal structures of novel vascular endothelial growth factors (vegf) from snake venoms. *Journal of Biological Chemistry*. 280(3):2126–2131.

Van Dam, P.S., Van Asbeck, B.S., Bravenboer, B., Van Oirschot, J.F., Marx, J.J. and Gispen, W.H., 1999. Nerve conduction and antioxidant levels in experimentally diabetic rats: effects of streptozotocin dose and diabetes duration. *Metabolism*, *48*(4), pp.442-447.

Szkudelski, T. 2001. The mechanism of alloxan and streptozotocin action in B cells of the rat pancreas. *Physiological Research*. 50(6):537–546.

Tabit, C.E., Chung, W.B., Hamburg, N.M. & Vita, J.A. 2010. Endothelial dysfunction in diabetes mellitus: molecular mechanisms and clinical implications. *Reviews in Endocrine and Metabolic Disorders*. 11(1):61–74.

Taborsky, G.J., Ahrén, B. & Havel, P.J. 1998. Autonomic mediation of glucagon secretion during hypoglycemia: implications for impaired alpha-cell responses in type 1 diabetes. *Diabetes*. 47(7):995-1005.

Takahashi, M., Hori, M., Ishigamori, R., Mutoh, M., Imai, T. & Nakagama, H. 2018. Fatty pancreas: A possible risk factor for pancreatic cancer in animals and humans. *Cancer Science*. 109(10):3013–3023.

Tal, M.G. 2009. Type 2 diabetes: Microvascular ischemia of pancreatic islets? *Medical Hypotheses*. 73(3):357–358.

Tang, S.C., Baeyens, L., Shen, C.N., Peng, S.J., Chien, H.J., Scheel, D.W., Chamberlain, C.E. & German, M.S. 2018. Human pancreatic neuro-insular network in health and fatty infiltration. *Diabetologia*. 61(1):168-181.

Tanner, M., Kent, N., Smith, B., Fletcher, S & Lewer M 2008 Stability of common biochemical analytes in serum gel tubes subjected to various storage temperatures and times pre-centrifugation. *Annals of Clinical Biochemistry*. 4:375–9.

Tarbell, J.M., Simon, S.I. & Curry, F.-R.E. 2014. Mechanosensing at the Vascular Interface. *Annual Review of Biomedical Engineering*. 16(1):505–532.

Tayebjee, M.H., MacFadyen, R.J. & Lip, G.Y. 2003. Extracellular matrix biology: a new frontier in linking the pathology and therapy of hypertension? *Journal of Hypertension*. 21(12):2211–8.

Tchokonte-Nana, V., 2011. Cellular mechanisms involved in the recapitulation of endocrine development in the duct ligated pancreas (Doctoral dissertation, Stellenbosch: University of Stellenbosch).

Tchokonte-Nana, V., Le-Roux, D.J., Kotze, P.C. & Ngounou, E. 2017. Immunohistomorphology of pancreatic islet microvasculature and the immunophenotypic analysis of cepc in adult diabetic rats. *International Journal of Morphology*. 35(4):1560–1567.

Teitelman, G., Guz, Y., Ivkovic, S. & Ehrlich, M. 1998. Islet injury induces neurotrophin expression in pancreatic cells and reactive gliosis of peri-islet Schwann cells. *Journal of Neurobiology*. 34(4):304–318.

Tepper, O.M., Galiano, R.D., Capla, J.M., Kalka, C., Gagne, P.J., Jacobowitz, G.R., Levine, J.P. & Gurtner, G.C. 2002. Human endothelial progenitor cells from type II diabetics exhibit impaired proliferation, adhesion, and incorporation into vascular structures. *Circulation*. 106(22):2781–6.

Tesauro, M., Rizza, S., Iantorno, M., Campia, U., Cardillo, C., Lauro, D., Leo, R., Turriziani, M., Cocciolillo, G.C., Fusco, A., Panza, J.A., Scuteri, A., Federici, M., Lauro, R. & Quon, M.J. 2007. Vascular, metabolic, and inflammatory abnormalities in normoglycemic offspring of patients with type 2 diabetes mellitus. *Metabolism*. 56(3):413–419.

Tesch, G.H. & Allen, T.J. 2007. Rodent models of streptozotocin-induced diabetic nephropathy (Methods in renal research). *Nephrology*. 12(3):261–266.

Tesfamariam, B., Brown, M.L. & Cohen, R.A. 1991. Elevated glucose impairs endothelium-dependent relaxation by activating protein kinase C. *Journal of Clinical Investigation*. 87(5):1643–1648.

Thomas, F.T., Ricordi, C., Contreras, J.L., Hubbard, W.J., Jiang, X.L., Eckhoff, D.E., Cartner, S., Bilbao, G., Neville Jr, D.M. & Thomas, J.M. 1999. Reversal of naturally occurring diabetes in primates by unmodified islet xenografts without chronic immunosuppression. *Transplantation*. 67(6):846-854.

Timpl, R. & Brown, J.C. 1996. Supramolecular assembly of basement membranes. *BioEssays*. 18(2):123–132.

Tirziu, D. & Simons, M. 2009. Endothelium as master regulator of organ development and growth. *Vascular Pharmacology*. 50(1–2):1–7.

To, M., Goz, A., Camenzind, L., Oertle, P., Candiello, J., Sullivan, M., Henrich, P.B., Loparic, M., Safi, F., Eller, A. & Halfter, W. 2013. Diabetes-induced morphological, biomechanical, and compositional changes in ocular basement membranes. *Experimental Eye Research*. 116:298–307.

Tong, X., Evangelista, A. & Cohen, R.A. 2010. Targeting the redox regulation of SERCA in vascular physiology and disease. *Current Opinion in Pharmacology*. 10(2):133–138.

Torrallardona, D., Harris, C.I. & Fuller, M.F. 1996. Microbial amino acid synthesis and utilization in rats: the role of coprophagy. *British Journal of Nutrition*. 76(5):701–710.

Tortora, G.J. & Derrickson. B.H. 2018. *Principles of Anatomy and Physiology*. John Wiley & Sons.

Tuomilehto, J., Lindström, J., Eriksson, J.G., Valle, T.T., Hämäläinen, H., Ilanne-Parikka, P., Keinänen-Kiukaanniemi, S., Laakso, M., Louheranta, A., Rastas, M. & Salminen, V. 2001. Prevention of type 2 diabetes mellitus by changes in lifestyle among subjects with impaired glucose tolerance. *New England Journal of Medicine.* 344(18):1343-1350.

Turner, N., Mughal, R., Warburton, P., Oregan, D., Ball, S. & Porter, K. 2007. Mechanism of TNFα-induced IL-1α, IL-1β and IL-6 expression in human cardiac fibroblasts: Effects of statins and thiazolidinediones. *Cardiovascular Research*. 76(1):81–90.

Tuttle, J.L., Nachreiner, R.D., Bhuller, A.S., Condict, K.W., Connors, B.A., Herring, B.P., Dalsing, M.C. & Unthank, J.L. 2001. Shear level influences resistance artery remodeling: wall dimensions, cell density, and eNOS expression. *American Journal of Physiology-Heart and Circulatory Physiology*. 281(3):H1380–H1389.

Twig, G., Elorza, A., Molina, A.J.A., Mohamed, H., Wikstrom, J.D., Walzer, G., Stiles, L., Haigh, S.E., Katz, S., Las, G., Alroy, J., Wu, M., Py, B.F., Yuan, J. Deeney, J.T., Corkey, B.E. & Shirihai, O.S. 2008. Fission and selective fusion govern mitochondrial segregation and elimination by autophagy. *The European Molecular Biology Organization Journal*. 27(2):433–446.

Tyrberg, B., Andersson, A. & Borg, L.H. 2001. Species differences in susceptibility of transplanted and cultured pancreatic islets to the β-cell toxin alloxan. *General and Comparative Endocrinology*. 122(3):238-251.

Urbich, C. & Dimmeler, S. 2004. Endothelial progenitor cells: Characterization and role in vascular biology. *Circulation Research*. 343–353.

Usmanova, Z. 2015. Relationship between the Levels of MMP-9, TIMP-1, and Zinc in biological samples of patients with carotid atherosclerosis. *International Journal of Biomedicine*. 5(2):60–64.

Vågesjö, E., Christoffersson, G., Waldén, T.B., Carlsson, P.-O., Essand, M., Korsgren, O. & Phillipson, M. 2015. Immunological shielding by induced recruitment of regulatory T-lymphocytes delays rejection of islets transplanted in muscle. *Cell Transplantation*. 24(2):263–276.

Van Belle, T.L., Coppieters, K.T. & Von Herrath, M.G. 2011. Type 1 diabetes: etiology, immunology, and therapeutic strategies. *Physiological Reviews*. 91(1):79–118.

Van Bortel, L.M., Struijker-Boudier, H.A. & Safar, M.E. 2001. Pulse pressure, arterial stiffness, and drug treatment of hypertension. *Hypertension*. 38(4):914-921.

Van Deijnen, J.H.M., Hulstaert, C.E., Wolters, G.H.J. & van Schilfgaarde, R. 1992. Significance of the peri-insular extracellular matrix for islet isolation from the pancreas of rat, dog, pig, and man. *Cell and Tissue Research*. 267(1):139–146.

Vasir, B., Jonas, J.-C., Steil, G.M., Hollister-Lock, J., Hasenkamp, W., Sharma, A., Bonner-Weir, S. & Weir, G.C. 2001. Gene expression of VEGF and its receptors flk-1/kdr and flt-1 in cultured and transplanted rat islets1. *Transplantation*. 71(7):924–935.

Vasqtec.com 2018 https://vasqtec.com/wp_live/wp-content/uploads/2015/05/procedure_ download version.pdf. https://www.rndsystems.com/products/luminex-high-performance-assays.

Velican, C. & Velican, D. 1977. Histogenetic differences between parent and daughter vessels of human coronary arteries. *Atherosclerosis*. 26(3):273-287.

Vella, R.K., Jackson, D.J. & Fenning, A.S. 2017. Δ^9-Tetrahydrocannabinol Prevents Cardiovascular Dysfunction in STZ-Diabetic Wistar-Kyoto Rats. *Biomedical Research International*: 1–10.

Venkatesan, V., Madhira, S.L., Malakapalli, V.M., Chalasani, M., Shaik, S.N., Seshadri, V., Kodavalla, V., Bhonde, R.R., & Nappanveetti, G. 2013. Obesity, insulin resistance, and metabolic syndrome: a study in WNIN/Ob rats from a pancreatic perspective. Biomedical Research International. doi.org/10.1155/2013/617569.

Verli, F.D., Rossi-Schneider, T.R., Schneider, F.L., Yurgel, L.S. & de Souza, M.A.L. 2007. Vascular Corrosion Casting Technique Steps. *Scanning*. 29(3):128–132.

Verma, S. 2003. Endothelial function testing as a biomarker of vascular disease. *Circulation*. 108(17):2054–2059.

Verma, S., Wang, C.-H., Li, S.-H., Dumont, A.S., Fedak, P.W.M., Badiwala, M. V, Dhillon, B., Weisel, R.D., Li, R-K., Mickle, D.A.G. & Stewart, D.J. 2002. A self-fulfilling prophecy: C-reactive protein attenuates nitric oxide production and inhibits angiogenesis. *Circulation*. 106(8):913–9.

Villela, N.R., Aguiar, L.G.K., Bahia, L., Bottino, D. & Bouskela, E. 2006. Does endothelial dysfunction correlate better with waist-to-hip ratio than with body mass index or waist circumference among obese patients? *Clinics*. 61(1):53–57.

Vincent, M.A., Clerk, L.H., Lindner, J.R., Klibanov, A.L., Clark, M.G., Rattigan, S. & Barrett, E.J. 2004. Microvascular recruitment is an early insulin effect that regulates skeletal muscle glucose uptake *in vivo*. *Diabetes*. 53(6):1418–1423.

Vissarion, B., Malliarou, M., Theofilou, P. & Zyga, S. 2014. Improvement of Diabetic Patients Nursing Care by the Development of Educational Programs. *Health* Psychology Research. 2(1):931.

Vozarova, B., Weyer, C., Hanson, K., Tataranni, P.A., Bogardus, C. & Pratley, R.E. 2001. Circulating interleukin-6 in relation to adiposity, insulin action, and insulin secretion. Obesity *Research*. 9(7):414–417.

Vural, P., Kabaca, G., Firat, R.D. & Degirmencioglu, S. 2017. Administration of selenium decreases lipid peroxidation and increases vascular endothelial growth factor in streptozotocin induced diabetes mellitus. *Cell Journal*. 19(3):452–460.

Wallner, K., Pedroza, R.G., Awotwe, I., Piret, J.M., Senior, P.A., Shapiro, A.M.J. & McCabe, C. 2018. Stem cells and beta cell replacement therapy: a prospective health technology assessment study. *Biomedical Central Endocrine Disorders*. 18(1):6.

Wang, D., Zhang, X., Lu, L., Li, H., Zhang, F., Chen, Y. & Shen, J. 2015. Assessment of diabetic peripheral neuropathy in streptozotocin-induced diabetic rats with magnetic resonance imaging. *European Radiology*. 25(2):463-471.

Wang, R., Li, J. & Rosenberg, L. 2001. Factors mediating the transdifferentiation of islets of Langerhans to duct epithelial-like structures. *The Journal of Endocrinology*. 171(2):309–318.

Wang, S., Chennupati, R., Kaur, H., Iring, A., Wettschureck, N. & Offermanns, S. 2016. Endothelial cation channel PIEZO1 controls blood pressure by mediating flow-induced ATP release. *Journal of Clinical Investigation*. 126(12):4527–4536.

Wang, X., Misawa, R., Zielinski, M.C., Cowen, P., Jo, J., Periwal, V., Ricordi, C., Khan, A., Szust, J, & Shen, J. 2013. Regional Differences in Islet Distribution in the Human Pancreas-Preferential Beta-Cell Loss in the Head Region in Patients with Type 2. Diabetes. *Public* Library *of Science* (1). 8(6):e67454.

Wang, X., Zielinski, M.C., Misawa, R., Wen, P., Wang, T.-Y., Wang, C.-Z., Witkowski, P. & Hara, M. 2013. Quantitative Analysis of Pancreatic Polypeptide Cell Distribution in the Human Pancreas. *Public Library of Science (1*). 8(1):e55501.

Wang-Fischer, Y. & Garyantes, T. 2018. Improving the reliability and utility of streptozotocin-induced rat diabetic model. Journal of Diabetes Research. doi.org/10.1155/2018/8054073

Wassmann, S., Stumpf, M., Strehlow, K., Schmid, A., Schieffer, B., Böhm, M. & Nickenig, G. 2004. Interleukin-6 induces oxidative stress and endothelial dysfunction by overexpression of the angiotensin II type 1 receptor. *Circulation Research*. 94(4):534–41.

Wei, L., Lu, Y., He, S., Jin, X., Zeng, L., Zhang, S., Chen, Y., Tian, B., Mai, G. & Yang, G. 2011. Induction of diabetes with signs of autoimmunity in primates by the injection of multiple-low-dose streptozotocin. *Biochemical and Biophysical Research Communications*. 412(2):373–378.

West, D.J., Campbell, M.D., Gonzalez, J.T., Walker, M., Stevenson, E.J., Ahmed, F.W., Wijaya, S., Shaw, J.A. & Weaver, J.U. 2015. The inflammation, vascular repair and injury responses to exercise in fit males with and without Type 1 diabetes: an observational study. *Cardiovascular Diabetology* .14(1):71.

Wheatcroft, S.B., Shah, A.M., Li, J.-M., Duncan, E., Noronha, B.T., Crossey, P.A. & Kearney, M.T. 2004. Preserved glucoregulation but attenuation of the vascular actions of insulin in mice heterozygous for knockout of the insulin receptor. *Diabetes*. 53(10):2645–52.

Widlansky, M.E., Gokce, N., Keaney, J.F. & Vita, J.A. 2003. The clinical implications of endothelial dysfunction. *Journal of the American College of Cardiology*. 42(7):1149–60.

Willcox, A. & Gillespie, K.M. 2016. Histology of type 1 diabetes pancreas. *Methods in Molecular Biology* (Clifton, N.J.). 1433:105–17.

Williamson, K., Stringer, S.E. & Alexander, M.Y. 2012. Endothelial progenitor cells enter the aging arena. *Frontiers in Physiology*. 3:30.

Wootton, D.M. & Ku, D.N. 1999. Fluid mechanics of vascular systems, diseases, and thrombosis. *Annual Review of Biomedical Engineering*. 1(1):299–329.

Wortham, M. & Sander, M. 2016. Mechanisms of β-cell functional adaptation to changes in workload. *Diabetes, Obesity and Metabolism*. 18:78–86.

Xu, X., D'Hoker, J., Stange, G., Bonne, S., De Leu, N., Xiao, X., Van De Casteele, M., Mellitzer, G., Ling, Z., Pipeleers, D. and Bouwens, L. 2008. Beta cells can be generated from endogenous progenitors in injured adult mouse pancreas. *Cell*. 132(2):197–207.

Yagihashi, S., Mizukami, H. & Sugimoto, K. 2011 Mechanism of diabetic neuropathy: Where are we now and where to go? *Journal of Diabetes Investigation*. 2(1):18–32.

Yang, H., Fan, S., Song, D., Wang, Z., Ma, S., Li, S., Li, X., Xu, M., Xu, M. & Wang, X. 2013. Long-term streptozotocin-induced diabetes in rats leads to severe damage of brain blood vessels and neurons via enhanced oxidative stress. *Molecular Medicine Reports*. 7(2):431–440.

Yao, V.J., Ozawa, M.G., Trepel, M., Arap, W., McDonald, D.M. & Pasqualini, R. 2005. Targeting pancreatic islets with phage display assisted by laser pressure catapult microdissection. *The American Journal of Pathology.* 166(2):625–636.

Ying, W., Fu, W., Lee, Y.S. & Olefsky, J.M. 2020. The role of macrophages in obesity-associated islet inflammation and β-cell abnormalities. N*ature reviews. Endocrinology*. 16(2):81–90.

Yoder, M.C. 2012. Human endothelial progenitor cells. *Cold Spring Harbor Perspectives in Medicine*. 2(7):a006692.

Yousef El-Gohary, G.G. 2018. Structure of islets and vascular relationship to the exocrine pancreas. Pancreapedia: The Exocrine Pancreas Knowledge Base. DOI:10.3998/panc. 2017.10

Yessoufou, A., Moutairou, K. & Khan, N.A. 2011. A model of insulin resistance in mice, born to diabetic pregnancy, is associated with alterations of transcription-related genes in pancreas and epididymal adipose tissue. *Journal of Obesity*. doi:10.1155/2011/654967.

Yu, CG, Zhang, N, Yuan, SS, Ma, Y, Yang, LY, Feng, YM, & Zhao, D. 2016. Endothelial progenitor cells in diabetic microvascular complications: friends or foes? Stem Cells International. doi.org/10.1155/2016/1803989

Zampetaki, A., Kirton, J.P. & Xu, Q. 2008. Vascular repair by endothelial progenitor cells. *Cardiovascular Research*. 78(3):413–421.

Zanone, M.M., Favaro, E., Doublier, S., Lozanoska-Ochser, B., Deregibus, M.C., Greening, J., Huang, G.C., Klein, N., Cavallo, P.P., Peakman, M. & Camussi, G. 2005. Expression of nephrin by human pancreatic islet endothelial cells. *Diabetologia*. 48(9):1789–1797.

Zarros, A., Liapi, C., Galanopoulou, P., Marinou, K., Mellios, Z., Skandali, N., Al-Humadi, H., Anifantaki, F., Gkrouzman, E. & Tsakiris, S. 2009. Effects of adult-onset streptozotocin-induced diabetes on the rat brain antioxidant status and the activities of acetylcholinesterase, (Na +,K+)- and Mg2+-ATPase: Modulation by L-cysteine. *Metabolic Brain Disease*. 24(2):337–348.

Zatz, R., Dunn, B.R., Meyer, T.W., Anderson, S., Rennke, H.G. & Brenner, B.M. 1986. Prevention of diabetic glomerulopathy by pharmacological amelioration of glomerular capillary hypertension. *The Journal of Clinical Investigation*. 77(6):1925–1930.

Zechner, D., Knapp, N., Bobrowski, A., Radecke, T., Genz, B. & Vollmar, B. 2014. Diabetes increases pancreatic fibrosis during chronic inflammation. *Experimental Biology and Medicine*. 239(6):670–676.

Zha, M., Li, F., Xu, W., Chen, B. & Sun, Z. 2014. Isolation and characterization of islet stellate cells in rat. *Islets*. 6(2):e28701.

Zhang, J., DeFelice, A.F., Hanig, J.P. & Colatsky, T. 2010. Biomarkers of endothelial cell activation serve as potential surrogate markers for drug-induced vascular injury. *Toxicologic Pathology*. 38(6): 856-871.

Zhang, J., Patel, J.M., Li, Y.D. & Block, E.R. 1997. Proinflammatory cytokines downregulate gene expression and activity of constitutive nitric oxide synthase in porcine pulmonary artery endothelial cells. *Research Communications in Molecular Pathology and Pharmacology*. 96(1):71–87.

Zhang, J.-G., Liu, Q., Liu, Z.-L., Li, L. & Yi, L. 2015. Antihyperglycemic activity of *Anoectochilus roxburghii polysaccharose* in diabetic mice induced by high-fat diet and streptozotocin. *Journal of Ethnopharmacology*. 164:180–185.

Zhang, N., Richter, A., Suriawinata, J., Harbaran, S., Altomonte, J., Cong, L., Zhang, H., Song, K., Meseck, M., Bromberg, J. & Dong, H. 2004. Elevated vascular endothelial growth factor production in islets improves islet graft vascularization. *Diabetes*. 53(4):963–970.

Zhang, W. and Yan, H. 2013. Dysfunction of circulating endothelial progenitor cells in type 1 diabetic rats with diabetic retinopathy. *Graefe's Archive for Clinical and Experimental Ophthalmology*. 251(4):1123-1131.

Zhang, Z. & Lv, L. 2016. Effect of local insulin injection on wound vascularization in patients with diabetic foot ulcer. *Experimental and Therapeutic Medicine*. 11(2):397–402.

Ziemińska, K., Butler, D.W., Gleason, S.M., Wright, I.J. & Westoby., M. 2013. Fibre wall and lumen fractions drive wood density variation across 24 Australian Angiosperms. *AoB Plants* 5 plt046.

Zou, M-H., Shi, C. & Cohen, R.A. 2002. Oxidation of the zinc-thiolate complex and uncoupling of endothelial nitric oxide synthase by peroxynitrite. *Journal of Clinical Investigation*. 109(6):817–826.

Zweier, J.L., Samouilov, A. & Kuppusamy, P. 1999. Non-enzymatic nitric oxide synthesis in biological systems. Biochimica et Biophysica Acta (BBA) - *Bioenergetics*. 1411(2–3):250–262.

APPENDICES

APPENDIX 1: MATERIALS AND METHODS- INDIVIDUAL ANIMAL RECORD SHEET

Individual animal record Sheet (Group name)
Study: Hyperglycaemia and its implication in the pancreatic islet microvasculature in diabetic rat models

Group:_____ Animal's Identity: 1
Cage:_____
BY:__PI_

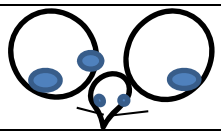

Day	Date	Body Weight/g	Blood glucose level/ mmol/L	Comments
-10				
-8				
-6				
-4				
-2				
Start of the experiment (introduction of dietary regimen / initial oral glucose tolerance test)				
0				
3				
6				
9				
12				
14				
15		Final oral glucose tolerance tests followed by IP STZ injection 50mg/kg BW (RAC/STZ group) and Sodium citrate (control) for C SSC and C-HFD/SSC groups and 35mg/kg BW (HFD/STZ group)		
19		Diabetic day 1		
21				
24				
27				
30				
33				
23				
27				
30				
33				
36				
39				
42				
45				
48				
51				
54				
57				
60				
63				
66				
69				
72				
75				
78		Tissues harvesting		

APPENDIX 2: MATERIALS AND METHODS- ANIMAL MONITORING SHEET- NAME OF THE GROUP (CAGE NUMBER)

	Date	Food (g)		Water (mL)		Cage Wet		Cage Cleaned	
		Before	After	Before	After				
1						Y / N		Y / N	
2						Y / N		Y / N	
3						Y / N		Y / N	
4					-	Y / N		Y / N	
5					-	Y / N		Y / N	
6						Y / N		Y / N	
7						Y / N		Y / N	
8						Y / N		Y / N	
9						Y / N		Y / N	
10						Y / N		Y / N	
11						Y / N		Y / N	
12						Y / N		Y / N	
13						Y / N		Y / N	
14						Y / N		Y / N	
15						Y / N		Y / N	
16						Y / N		Y / N	
17						Y / N		Y / N	
18						Y / N		Y / N	
19						Y / N		Y / N	
20						Y / N		Y / N	
21						Y / N		Y / N	
22						Y / N		Y / N	
23					-	Y / N		Y / N	
24						Y / N		Y / N	
25						Y / N		Y / N	
26						Y / N		Y / N	
27						Y / N		Y / N	
28						Y / N		Y / N	
29						Y / N		Y / N	
30						Y / N		Y / N	
31						Y / N		Y / N	
32						Y / N		Y / N	
33						Y / N		Y / N	

APPENDIX 3: MATERIALS AND METHODS-RECORDS OF BODY WEIGHT AND BLOOD GLUCOSE LEVEL

a. Materials:

1. Wistar rat
2. Blood glucose meter (ACCU-CHEK Aviva) for glucose quantification
3. GlucoPlus Glucose Test Strip (GlucoPlus, Montreal, CA)
4. Sterile lancet
5. Electric scale
6. 70% alcohol
7. Hand gloves
8. Plastic bowl

b. Methods: Blood glucose test

1. The plastic bowl was placed on the scale and tare to 0g. The plastic bowl was used to help hold the animal on the scale and keep the scale clean.
2. Each animal was then placed into the plastic bowl and the weight displayed on the scale screen recorded.
3. With the animal in the same position, the tip of the tail was cleaned with 70% alcohol and rubbed for better circulation.
4. The tip of the animal's tail was pricked with a sterile lancet to collect a small blood sample.
5. The glucose test strip already inserted into the glucometer collected the small drop of blood.
6. The Glucoplus Meter quantified the level of blood glucose and displayed the result on the screen.
7. The result was recorded for each animal at a given time.

APPENDIX 4 NUTRIENT CONTENT OF STANDARD RAT CHOW AND HFD

Standard rat chow

	% Carbohydrate	% Protein	% Total fat (g/100)	% saturated fat (g/100)	Cholesterol (mg/100)	Sucrose (g/100g)	KJ/100g
RAC (contro)	34.6	17.1	4.8	0.9	2.2	5.3	1272
HFD	42	8.3	11.5	7.6	13	20.4	1354

APPENDIX 5: ORAL GLUCOSE TOLERANCE TEST

a Materials

1. D-glucose (AnalaR, chemicals Ltd, BDH, poole England)
2. Distilled water
3. Glass bottle
4. A bulb tipped gastric gavage needle
5. Timer
6. Blood glucose meter (ACCU-CHEK Aviva)

b Methods

1. A 30% D-glucose was prepared and stored in a glass bottle by adding 30g of D-glucose to 100ml of distilled water.
2. Each animal was weighed and the amount of D-glucose calculated. The bulb tipped plastic gavage needle was used to collect the appropriate amount of solution before being inserted to the stomach via the mouth and the oesophagus. The solution was then discharged slowly so as not to cause a pressure-induced “dumping syndrome”.
3. Blood collection and glucose level were quantified by tail bleed at the following time point 0, 3, 5, 10, 20, 30, 90 and 120min using a Blood glucose meter (ACCU-CHEK Aviva) for glucose quantification.

APPENDIX 6: MATERIALS- DIABETES INDUCTION

a Materials

1. Streptozotocin (STZ) (Sigma-Aldrich, Missouri, USA) (always stored at -20°C
2. Sodium citrate buffer, pH 4.5, 10 mM (Kimix Chemicals, Cape Town, RSA)
3. Syringe
4. Aluminium foil
5. Eppendorf tube
6. Needles, 27 G, BD Microlance 3 (Beckman Dickinson SA, Gauteng, RSA)

b Methods: Intraperitoneal injection

1. An appropriate amount of STZ was weighed so that the final concentration of the solution is 10% and stored in the Eppendorf tube and cover with the aluminium foil (STZ is light sensitive).
2. The appropriate volume of sodium citrate buffer was added to the content of the Eppendorf tube and mixed well just prior to the injection (Drug degenerate within 15-20minute in solution).
3. Base on individual animal weight, a specific volume of STZ solution was now drawn into the syringe and injected intraperitoneally.

APPENDIX 7: MATERIALS AND METHODS- BLOOD SAMPLE COLLECTION, SERUM SEPARATION AND STORAGE

a Materials:

1. Syringe 5ml (Neomedic Pty Ltd., Durban, RSA)
2. 25 G needle (Neomedic Pty Ltd., Durban, RSA)
3. 4 ml serum separator tube (SST) (Greiner Bio-one, Kremsmunster, Austria)
4. Micropipette
5. Centrifuge
6. Cryovials, 1.5 ml
7. -80°C Freezer
8. Styrofoam racks

b Methods: Sample collection and storage

1. Collect blood sample from the jugular vein
2. Blood sample was allowed to clot for 30 minutes at room temperature
3. Blood sample was then taken for centrifugation for 15 minutes at 1000 x g
4. Serum lying on the blood clot in the tube was pipetted and aliquot store at -80°C till further use.

c Method Sample and reagent preparation

1. Reagents were all brought to room temperature before use. All standards were assayed in duplicate.
2. All reagents, standards, and samples were prepared as directed by the manufacturer.
3. 100µL Serum samples were diluted with the diluent provided by the manufacturer
4. The diluted microparticle cocktail was resuspended by inversion or vortexing before added 50µL of the
5. microparticle cocktail to each well of the microplate
6. 50 µL of standard or sample* was added per well (Securely cover with a foil plate sealer) and incubated for 2 hours at room temperature on a horizontal orbital microplate shaker (0.12” orbit) set at 800 ± 50 rpm).
7. A magnetic device was used designed to accommodate a microplate, washed by applying the magnet to the bottom of the microplate and allowed 1 minute before removing the liquid, filling each well with Wash Buffer (100 µL) and allow 1 minute before removing the liquid again. Removal of liquid is essential for good performance. The wash procedure was performed three times.

8. 50 µL of diluted Biotin Antibody Cocktail was added to each well and securely covered with a foil plate sealer and incubated for 1 hour at room temperature on the shaker set at 800 ± 50 rpm. The wash was repeated 3 times as in step 4.
9. 25 µL of diluted Streptavidin-PE was added to each well and was securely cover with a foil plate sealer and incubated for 30 minutes at room temperature on the shaker set at 800 ± 50 rpm. The wash was repeated 3 times as in step 4.
10. The microparticles were resuspended by adding 80 µL of Wash Buffer to each well and Incubate for
11. 2 minutes on the shaker set at 800 ± 50 rpm.
12. Luminex or Bio-Rad analyser was used to read the microparticles within 90 minutes.
13. The Standard concentrations on the Certificate of Analysis were used to calculate 3-fold dilutions for the remaining levels. The duplicate readings were averaged for each standard and sample and subtracted from the average blank Median Fluorescence Intensity (MFI).
14. A standard curve was created for each analyte by reducing the data using computer software capable of generating a five parameter logistic (5-PL) curve-fit.

APPENDIX 8: MATERIALS AND METHODS- BLOOD SAMPLE COLLECTION AND PREPARATION FOR CRYOPRESERVATION

a **Materials:** Blood sample collection and cryopreservation

1. Syringe 5ml (Neomedic Pty Ltd., Durban, RSA)
2. 25 G needle (Neomedic Pty Ltd., Durban, RSA)
3. 4 ml Lithium Heparin blood tubes (Greiner Bio-one, Kremsmunster, Austria)
4. Micropipette
5. Centrifuge
6. Cryovials, 1.5 ml
7. -80°C Freezer
8. Liquid Nitrogen storage container
9. Phosphate-buffered saline (PBS)
10. Fetal bovine serum (FBS)
11. 15 ml centrifuge tubes
12. Ficoll-Paque Plus (density medium) (Pharmacia, New Jersey, USA)
13. Basal Medium Eagle Modification (DMEM)
14. Dimethyl sulfoxide (DMSO)
15. Styrofoam racks

b **Methods: PBMC isolation**

1. Dilute blood sample 1:1 with PBS and 5% FBS
2. 3 ml blood + 2.85 ml PBS + 0.15ml FBS
3. Pipette 3 ml density medium into 15 ml centrifuge tubes
4. Pipette diluted blood over density medium
5. Centrifuge at 400xg for 30 minutes
6. After centrifugation aspirate plasma layer
7. Carefully remove PBMC layer with micropipette and place in 15ml centrifuge tube
8. Fill tube with 10ml DMEM
9. Centrifuge at 250xg for 20 minutes.
10. Aspirate supernatant
11. Add 1ml of DMEM and re-suspend carefully
12. Transfer PBMC to a cryovial

c **Method: Cryopreservation protocol**

1. Prepare freezing medium:
2. 50% FBS

3. 40% DMEM
4. 10% DMSO
5. Centrifuge cryovial containing samples at 2500 rpm for 5 minutes
6. Aspirate supernatant
7. Add 1.5ml of freezing medium to a cryovial
8. Place cryovials in Styrofoam racks and place another Styrofoam rack on top
9. Place Styrofoam rack in -80°C freezer for 24 hours and then transfer to a liquid nitrogen storage container for long term storage

APPENDIX 9: MATERIALS AND METHODS: STANDARD HISTOLOGICAL PROCEDURE

a Materials:

1. Dissecting kit
2. Tissue processor
3. Tissues cassette
4. Embedding machine
5. Embedding moulds
6. Paraffin wax

a. Xylene

b. 70%, 80%, 95%, 99% ethanol

c. 10% formalin

b Methods: Tissue processing

1. Section the pancreata and place the head and the tail portions into two different cassettes
2. Label the cassettes

I. Fix tissue in 10% formalin for 48 hours

II. Process the tissue in an automatic processor using protocol in table below

Tissue processing protocol

III Embedded tissue in paraffin and block

Step	Solution	Time (min)	Temperature (ºC)	
1	10% Formalin	30	Room Temperature	
2	70% Ethanol	30	Room Temperature	
3	96% Ethanol	30	Room Temperature	
4	96% Ethanol	30	Room Temperature	
5	99.9% Ethanol	30	Room Temperature	
6	99.9% Ethanol	30	Room Temperature	
7	99.9% Ethanol	30	Room Temperature	
8	Xylene	30	Room Temperature	
9	Xylene	30	Room Temperature	
10	Paraffin	60	60	
11	Paraffin	60	60	
12	Paraffin	60	60	

c Materials- Routine histological staining

1. 10% Formalin
2. Surgical blade
3. Embedding cassettes (SPL Life Science, Pocheon, Korea)
4. Paraffin wax
5. Leica EG 1160 Embedder (Leica Biosystems, Wetzlar, Germany)
6. Leica Autostainer XL, ST5010 (Leica Biosystems, Wetzlar, Germany)
7. Leica RM 2125 RT microtome (Leica Biosystems, Wetzlar, Germany)
8. Leica Bond Autostainer (Leica Biosystems, Wetzlar, Germany)
9. BondTM Software 2009, v4.0 (Leica Biosystems, Wetzlar Germany)
10. Xylene (Kimiz Chemicals, Cape Town, RSA)
11. 99% & 96% Ethanol
12. Acid alcohol (1%)
13. Mayer's Haematoxylin (Kimix Chemicals, Cape Town, RSA)
14. Eosin Yellowish (Kimix Chemicals, Cape Town, RSA)
15. Plastic slide rack
16. Ammonia (0.2%)
17. Bio-Scan Microscope slides frosted (Trifal Imaging, Chatsworth, USA)
18. Bio-Scan Microscope slides positive charge (Trifal Imaging, Chatsworth, USA)
19. Coverslips
20. PDX Mountant (Kimix Chemicals, Cape Town, RSA)

d Methods: H&E staining protocol

1. Program autostainer according to the procedure below and place plastic rack containing slides into autostainer
2. After completion of the staining procedure, mount a coverslip on the glass slides with PDX

H&E staining protocol

Step	Solution	Time	Repetitions
1	Oven (60˚C)	2 min	x1
2	Xylene	5 min	x2
3	Ethanol (99%)	2 min	x2
4	Ethanol (96%)	2 min	x1
5	Ethanol (70%)	2 min	x1

6	Tap water	2 min	x1
7	Haematoxylin	8 min	x1
8	Running water	5 min	x1
9	Eosin	4 min	x1
10	Running water	1 min	x1
11	Ethanol (70%)	30 sec	x1
12	Ethanol (96%)	30 sec	x2
13	Ethanol (99%)	30 sec	x1
14	Xylene	1 min	x1

APPENDIX 10: CASTING PROCEDURE

I Pre-casting solution

A Phosphate buffer saline (PBS)

Materials and method

1. For 1 litre of 1X PBS, prepare as follows:
2. Start with 800 ml of distilled water:
3. Add 8 g of NaCl.
4. Add 0.2 g of KCl.
5. Add 1.44 g of Na2HPO4.
6. Add 0.24 g of KH2PO4.
7. Adjust the pH to 7.4 with HCl.
8. Add distilled water to a total volume of 1 litre.

B 2% Glutaraldehyde

Purchased at that concentration

II Preparation of the casting medium

a Materials

1. PUii resin: 20g (VasQtec)
2. 2-Butanone (Sigma): 12g
3. Pigment: 20mg
4. PUii hardener: 2.4g
5. Scintillation vial (20ml) with a screw cap
6. Preparation
7. Use scintillation vial
8. Weigh the 2-butanone
9. Add the pigment and dissolve.
10. Then add the resin mix. This mixture may be kept for several minutes to hours when tightly covered.
11. Shortly before casting.
12. Add 0.8g of hardener, stir well. Hardener has a short shelf life and should be covered with drt gas XTEND-IT from SMOOTH-ON (www.smooth-on.com) after each opening.
13. Remove air bubbles in the resin.
14. Fill into the perfusing syringe and inject immediately.
15. Curing time is 3-5 days but might be longer when more Butanone was used.

APPENDIX 11: MATERIALS AND METHODS- FLOW-CYTOMETRY CELL LABELLING

1. Materials:
2. 15 ml centrifuge tubes
3. 100 ml tubes
4. Micropipette
5. Beckman Coulter 5 ml flow cytometry sample tubes (Beckman Coulter Inc., California, USA)
6. Roswell Park Memorial Institute medium (RPMI)
7. Fetal Bovine Serum (FBS)
8. Phosphate-buffered saline (PBS)
9. Waterbath
10. Centrifuge
11. Beckman Coulter Navios, 10 colours, 3 lasers (5+3+2 configuration) (Beckman Coulter Inc., California, USA)
12. Beckman Coulter Kaluza Software v1.3 (Beckman Coulter Inc., California, USA)
13. Navios Software v1.3 (Beckman Coulter Inc., California, USA)
14. Markers:
15. PROM-1 polyclonal antibody/CD133 (Abnova, Taipei City, Taiwan)
16. Anti-CD31 antibody-FITC (Abcam, Cambridge, UK)
17. Anti-CD34 antibody-PE (Abcam, Cambridge, UK)
18. Anti-CD45 antibody-AF700 (BioLegend, California, USA)
19. Zombie Violet™ Fixable Viability Kit (BioLegend, California, USA)
20. APC Conjugation Kit (Abcam, Cambridge, UK) Add 20 µl modifier (purple cap) with 200 µl CD45 antibody and mix
21. Method: conjugation of CD133 withAPC67
22. Add the previous mix into conjugation vial and re-suspend gently
23. Incubate at room temperature in dark for 3 hours
24. Add 20 µl quencher (blue cap) to the solution and mix gently.
25. After 30 minutes the conjugated antibody is ready to use
26. Method: Thawing of PBMC samples
27. Prepare Zombie violet solution
28. Dilute 1 µl of zombie violet with 100 µl of DMSO (included with Zombie violet kit) and mix gently
29. Prepare wash buffer
30. Add 5 ml FBS in 45 ml RPMI and mix gently
31. Prepare staining buffer

32. Add 2.5 ml of FBS to 47.5 ml of PBS and mix gently
33. Thaw cells
34. Heat water bath to 37°C
35. Swirl cryovial containing frozen PBMC until a small amount of ice is left in the tube
36. Transfer PBMC to 15 ml tube
37. Add 1 ml of warm wash buffer drop-wise
38. Centrifuge tube at 2500 rpm for five minutes
39. Remove supernatant
40. Resuspend cells in 10 µL zombie violet solution
41. Incubate solution 10-15min at room temperature in the dark
42. Add remaining antibodies
43. CD31: 0.5 µL
44. CD34: 1 µL
45. CD133: 2 µL
46. CD45: 2 µL
47. Incubate solution 10-15min at room temperature in the dark

APPENDIX 12 FLOW CYTOMETRY TECHNIQUES

Method: Creating a new protocol on Navious software v1.3

1. Select *File>New Protocol*
2. Save or discard the current protocol to clear the workspace
3. Select *Cytometer>Cytometer Control* to select the parameters for this protocol
    I. Click on the *Parameters* button
    II. Click on the Shutters to enable/disable the respective lasers
    III. Select the following parameters:
        -FS – Integral Lin, Peak Lin
        -SS – Integral Lin
        -TIME
        -Integral Log for FL parameters
    IV. Deselect the parameters, not in use and select *OK*
    V. Type in a new name for your protocol and select *Save*
4. Create Dotplots
    I. To change X and Y parameters, move the cursor to the lower right of the plot until it changes to the >>> icon
    II. Click to change the desired parameters
    III. Create as many dotplots as is required
    IV. Use *CTRL + D* to duplicate a plot
    V. Use *CTRL + T* to arrange the plots
    VI. Drag and drop in the desired order
    VII. Use the new row symbol before each plot that starts a new row
5. Adjust Cytosettings
    I. Select *Cytometer>Cytometer Control* and then *Acquisition Setup* tab (default)
    II. Select Setup Mode
    III. Select Quick Set
    IV. Select the desired discriminator parameter and then use the slider bar to adjust the channel values
        -Only FS between 100 and 150
        -This allows you to exclude debris from your analysis
6. Adjusting target voltages and gains with a specific sample
    I. Keep the Cytometer control window open
    II. Place a sample in the system (position 21)
    III. Select the □□icon to run the sample
    IV. Adjust the voltage first (try not to go above 700 for FS and SS)
        -Use the sliders on each plot (the Quick Set option)

- Or use the sliders in the *Cytometer Control* window
- You will see that the voltage will need to go higher than is desirable.

V. Now adjust the Gain

-You should see good separation of subpopulations

-It is better to have lower voltage and higher gain

7. Create regions and quadrants

I. If you get stuck while creating a region/gate, press ESC

II. Create a Flow Page if desired

III. Save the Protocol

APPENDIX 13: IHC STAINING PROTOCOL AND MANUAL REHYDRATION

No heat retrieval was used Modified F protocol staining steps

Step	Solution	Incubation time	Temperature
1	Bond Wash Solution	0 min	72˚C
2	Bond Wash Solution	0 min	72˚C
3	Bond Wash Solution	0 min	Ambient
4	Alcohol	0 min	Ambient
5	Alcohol	0 min	Ambient
6	Alcohol	0 min	Ambient
7	Bond Wash Solution	0 min	Ambient
8	Bond Wash Solution	0 min	Ambient
9	Bond Wash Solution	0 min	Ambient
10	Bond ER Solution 1	0 min	Ambient
11	Bond ER Solution 1	0 min	Ambient
12	Bond ER Solution 1	20 min	100˚C
13	Bond ER Solution 1	12 min	Ambient
14	Bond Wash Solution	0 min	35˚C
15	Bond Wash Solution	0 min	35˚C
16	Bond Wash Solution	0 min	35˚C
17	Bond Wash Solution	3 min	Ambient
18	Peroxide Block	5 min	Ambient
19	Bond Wash Solution	0 min	Ambient
20	Bond Wash Solution	0 min	Ambient
21	Bond Wash Solution	0 min	Ambient
22	Primary Antibody 1	30 min	Ambient
23	Bond Wash Solution	0 min	Ambient
24	Bond Wash Solution	0 min	Ambient
25	Bond Wash Solution	0 min	Ambient
26	Post Primary	8 min	Ambient
27	Bond Wash Solution	2 min	Ambient
28	Bond Wash Solution	2 min	Ambient
29	Bond Wash Solution	2 min	Ambient
30	Polymer	8 min	Ambient
31	Bond Wash Solution	2 min	Ambient
32	Bond Wash Solution	2 min	Ambient
33	Deionized Water	0 min	Ambient
34	Mixed DAB Refine	0 min	Ambient
35	Mixed DAB Refine	10 min	Ambient
36	Deionized Water	0 min	Ambient
37	Deionized Water	0 min	Ambient
38	Deionized Water	0 min	Ambient
39	Haematoxylin	5 min	Ambient
40	Deionized Water	0 min	Ambient
41	Bond Wash Solution	0 min	Ambient
42	Deionized Water	0 min	Ambient
43	Primary Antibody 2	15 min	Ambient
44	Bond Wash Solution	0 min	Ambient

45	Bond Wash Solution	0 min	Ambient
46	Bond Wash Solution	0 min	Ambient
47	Post Primary AP	20 min	Ambient
48	Bond Wash Solution	2 min	Ambient
49	Bond Wash Solution	2 min	Ambient
50	Bond Wash Solution	2 min	Ambient

Rehydration steps

Step	Solution	Time	Repetitions
1	Ethanol (70%)	5 dips	1
2	Ethanol (96%)	5 dips	1
3	Ethanol (99%)	5 dips	1
4	Xylene	1 min	2

IHC- Antibody

Antibody	Source	Antibody ID	Clonality	Raised in	Volume	Dilution
Anti-CD34 antibody	Abcam	AB81289	Monoclonal	Rabbit		100

APPENDIX 14: IMAGEJ FLOWCHART FOR CELL DENSITY

Particle counting was done either automatically or by the “Point Picker”. The chart below presents the main steps in the automatic procedure.

1-Original image (Tiff) transported to Fiji (ImageJ)	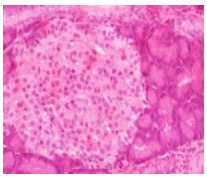
2-Select a ROI in the islet core, clear outside the ROI, magnify for better viewing then measure the surface area (optional)	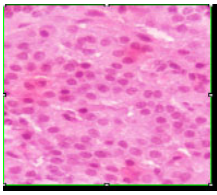 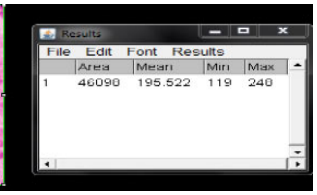
3-Change the image to type/8-bit	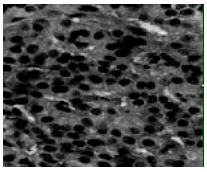
4-Convert the image to a binary image with the “Threshold “command,Separate overlapped nuclei using watershed button	 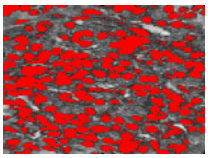
5-Menu command:Analyze	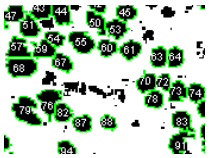
6-Analyze particles (size and number)	
7-Caculate cell density: ratio of cell number vs surface area	

APPENDIX 15 PREPARATION OF METHENAMINE STAIN SOLUTION

a Solutions

Periodic acid, 0.5% aqu.

Yellow gold chloride, 0.2% aqu.

Sodium thiosulphate, 2.5% aqu.

Neutral red, 1% aqu.

Stock Methenamine silver

Methenamine, 3% aqueous 100mL shake until the precipitate redissolves.

Silvering of the container indicates deterioration.

Silver nitrate, 5% aqu. 5mL

Working Methenamine silver

Stock Methenamine silver 50mL Make just before use and preheat to 50°C.

Borax, 5% aqu. 5mL

Tissue sample

3µL paraffin sections of neutral buffered formalin.

b Method

1. Bring sections (Duodenal and splenic) to water via xylene and ethanol.
2. Oxidise with 0.5% periodic acid for 15 minutes.
3. Rinse well with tap water.
4. Rinse with distilled water.
5. Treat with methenamine silver solution at 50°C. until impregnated (up to 3 hours)
6. Wash with distilled water.
7. Tone with 0.2% gold chloride solution for 2 minutes.
8. Rinse with distilled water.
9. Fix in 2.5% sodium thiosulphate for 3 minutes.
10. Wash well with running tap water.
11. Counterstain with, neutral red.
12. Rinse with tap water.
13. Dehydrate with ethanol, clear with xylene and mount with a resinous medium.

Expected results

Basement membranes – black

Oxidisable carbohydrates – black

Background – as counterstained